ELECTRONIC EVALUATION OF ORGANIC SEMICONDUCTORS TOWARDS ELECTRONIC DEVICES

Saadeldin Elamin Taher Elmasly
May 2013

ELECTRONIC EVALUATION OF ORGANIC SEMICONDUCTORS TOWARDS ELECTRONIC DEVICES

Submitted by

SAADELDIN ELAMIN TAHER

Thesis report submitted to the Department of Pure and Applied Chemistry, University of Strathclyde, in part fulfilment of the regulations for the degree of PhD.

2013

Signed:

Date:

بسم الله الرحمن الرحيم

(وقل ربى زدنى علما)

صدق الله العظيم

الى اعز انسان على قلبى الى **روح أمى** الحبيبة الغالية ..... مبروكة أحمد بشير بوحويش

الى ابى الغالى ..... الحاج لامين طاهر

الى روح خالى العزيز.....الدكتور رضوان أحمد بشير بوحويش

الى زوجتى والى بناتى مبروكة وماريا و جيهان

الى جميع افراد اسرتى أخوتى أسامة و محمد و أخواتى

الى جميع اقربائى و اصدقائى

أهدى ثمرة جهدى

Acknowledgments

First of all, I would like to express my highest gratitude and thanks to my supervisor Professor Peter J Skabara for his help, guidance, encouragement and excellent advice throughout this study. I would also like to express my deep thanks to Dr Alexander Kanibolotsky, Dr Neil Findlay, Dr Anto Regis Inigo and Andrew McCrone for their help in the lab with the equipment and chemistry.

I would also like to thank other members of the group for their assistance in the lab Clara Orofino, Diego Cortizo Lacalle, Gary Conboy, Sandeep Kaur, Neil Thomson, Joseph Cameron, Ewan Cameron, Sasikumar Arumugam, Enrico Angioni,

Finally, I take this opportunity to express my profound gratitude to my beloved parents and my wife for their patience, help, encouragement, advice, support, care.

Abstract

Organic π-conjugated macromolecules, (polymers and oligomers) are an important class of semiconductor which are used in applications such as: field effect transistors, photovoltaics, organic light emitting diodes and electrochromic devices. The π-conjugated systems have tuneable band gaps (E_g) and redox properties, whilst offering the potential for flexibility and low cost.

In this thesis, the macromolecular compounds and their low molecular weight precursors were characterised by determining their electrochemical and optical properties which were measured using a series of techniques such as: cyclic voltammetry; UV/vis spectroscopy; emission spectroscopy; spectroelectrochemistry; Raman spectroscopy and thermal analyses.

Chapter 2 Presents thiophene copolymers with electroactive nitrogen heterocycles. In section 1, a series of monomers containing heteropentalene mesomeric betaine derivatives were characterized. In particular the 3,4-ethylenedioxythiophene (EDOT) derivative (**9)** was successfully electropolymerised, yielding a polymer with small optical and electrochemical E_g. In Section 2 the characterisation of EDTT, 3-hexylthiophene and EDOT units (**17**, **18** and **19** respectively) along with their benzothiadiazole (BT) copolymers are shown. Interesting changes in planarity were observed between the PEDOT and PEDTT compounds.

Section 3 and 4 produced many EDOT/thiophene derivatives from phenanthroline and [$Ru(bpy)_2$]) as the core unit. (**20-26)** All polymers exhibited lower electrochemical E_g when compared to their monomers. Compound **26** was polymerised with high oxidative stability to anodic conditions, however, monomer

25 did not polymerise, due to the domination of the strong Ru^{II}/Ru^{III} oxidation process. Section 5 shows bis-EDOT pyridine based monomers (**27** and **28**). Monomer **28** displayed significant effect of the intramolecular charge transfer (ICT) process and lower electrochemical E_g. Three are new compounds **29**, **30** and **31** in the section 6, BODIPY cores with two EDOT, thiophene and EDTT units respectively. When all were compared, Compound **29** showed red shift in the absorption spectra, due to stronger electron donating effect of EDOT.

Chapter 3 In section 1 the optical and electrochemical properties of three oligofluorene substituted DPP macromolecules (**32**, **33**, **34**) and the core precursors (**35**, **36**, **37** and **38**) were investigated. The absorption spectra of all compounds in CH_2Cl_2 revealed two peaks attributed to π–π* transition of quaterfluorene arms and the absorption of DPP core. Compound **33** exhibited a higher LUMO level compared to the other compounds, which was attributed to the effects of the hexyldecyl and phenyl groups. Section 2 describes six new C_3-symmetric compounds containing BT units and truxene core (**41-46)**. The UV-absorption spectra of compounds **41-45**, reveal an ICT band which is hypsochromically shifted in the case of compound **41** and is not resolved for compound **46**. Compounds **41-44** exhibited a good agreement between electrochemical and optical E_g, while a significant difference between those of compound **46** indicates the poor HOMO-LUMO overlap.

C**hapter 4** A novel processing methodology was used to fabricate multi-layer organic electronic devices by employing electropolymerisation to form a PEDOT/PEDTT bi-layer. The fabricated device did not exhibit any distinctive photo-response when it was assessed in a diode configuration. This was due to inefficient charge separation at the donor- acceptor interface.

Symbols and Abbreviations

BODIPY	4,4-difluoro-4-borata-3a-azonia-4a-aza-s-indacene
Bu	butyl
cm	centimetre
CV	cyclic voltammetry
e	electron
EDOT	ethylenedioxythiophene
EDST	ethylenediselenathiophene
EDTT	ethylenedithiathiophene
E_p	voltage peak max
E_{pa}	anodic current peak
E_{pc}	cathodic voltage peak
eV	electron volt
Fc	ferrocene
Fc^+	ferrocenium
g	gram
h	hour
HOMO	highest occupied molecular orbital
ICT	intramolecular charge transfer
I_p	current peak max
I_{pa}	anodic current peak
I_{pc}	cathodic current peak
iR	internal resistance

ITO	indium tin oxide
IUPAC	international union of pure and applied chemistry
L	litre
LUMO	lowest unoccupied molecular orbital
M	molar
Me	methyl
min	minute
mol	mole
mV	millivolt
n	number of electrons / non-bonding orbital
n-doping	negative doping
nm	nanometre
n-type	negative type
OFET	organic field effect transistor
OLED	organic light emitting diode
OSO	ethylenedioxythiophene-ethylenedithiathiophene-ethylenedioxythiophene
OPV	organic photovoltaic
p-doping	positive doping
PEDOT	poly(ethylenedioxythiophene)
PEDTT	poly(ethylenedithiathiophene)
Ph	phenyl
PPV	polyphenylene vinylene
p-type	positive type

R	substituent group
RT	room temperature
s	second
SCE	standard calomel electrode
SEC	spectroelectrochemistry
SHE	standard hydrogen electrode
SOS	ethylenedithiathiophene-ethylenedioxythiophene-ethylenedithiathiophene
THF	tetrahydrofuran
TTF	tetrathiafulavalene
UV	ultraviolet
V	volt
V_1	starting voltage
V_2	finishing volatge
vis	visible
vs	versus
X	counter anion
ΔE_{pc-pa}	difference in potential between cathodic and anodic peaks
θ	torsion angle
λ	wavelength
λ_{max}	maximum absorption wavelength
π	pi bonding orbital
π^*	pi anti-bonding orbital / polarizability
σ	sigma bonding orbital

σ^*	sigma anti-bonding orbital
A	surface area / absorbance
c	concentration / speed of light
D	diffusion coefficient
D_i	diffusion coefficient
E	electrode potential
E^0	standard electrode potential
$E_{1/2}$	reversible wave
$E_{1/2}^{1ox}$	first reversible oxidation wave
$E_{1/2}^{1red}$	first reversible reduction wave
$E_{1/2}^{2ox}$	second reversible oxidation wave
$E_{1/2}^{2red}$	second reversible reduction wave
E^{1ox}	first irreversible oxidation wave
E^{1red}	first irreversible reduction wave
E^{2ox}	second irreversible oxidation wave
E^{2red}	second irreversible reduction wave
E_F	Fermi energy level
E_g	band gap / energy gap
E^{Int}	intramolecular and interchain interactions
E_R	potential of reduction reaction
E^{Res}	aromatic resonance
E^{Sub}	the push / pull effect of the substituent group
E^{θ}	degree of planarity
$E^{\sigma r}$	bond length alternation

F	Faraday constant
h	Planck's constant
i	current density
I	current / light intensity
T	temperature / transmission
v	scan rate
V_D	drain voltage
V_g	gate voltage

Contents

Table of Figures

Chapter 1

1. Introduction and background

1.1. Historical introduction

The last few decades have shown an increase in research on organic semiconductors due to their advantageous properties such as low weight, resistance against corrosion, low cost, processability and large area applications.[1,2] Organic semiconductors have a potential to substitute inorganic analogues in everyday life and are key materials in the development of many fields of modern science and technology.[1] The semiconducting properties originate from the overlap of π-molecular orbitals. The vast variety of organic semiconducting materials can be classified into two main groups: small molecule π-functional compounds and macromolecular conjugated systems. The most numerous among the latter is the group of conjugated polymers. Traditionally, organic polymers were considered as insulators until it was found that polymers possessing conjugated architectures were able to conduct electricity when doped by the removal or injection of electrons.[1, 3] Organic semiconductors have semiconducting properties arising from the overlap of molecular orbitals in the polymer conjugated chain. They can be used in numerous technological applications such as field effect transistors, organic light emitting diodes, solar cells and lasers, for their tunable redox properties and band gaps, processablity, flexibility and potential low cost.[4,5,6,7] Conjugated polymers have also been used in electrochromic devices and they have advantages over their analogous inorganic counterparts due to improvements in certain properties such as stability, high colouration efficiency and fast switching.[7]

1.2 History

Organic semiconducting materials have been investigated for five decades. In the 1950s the semiconducting behaviour of anthracene crystals was identified through photoconductivity measurement.[8,9,10] The electrical conductivity of the complexes between polycyclic aromatic compounds such as perylene and halogen in the solid state was discovered in 1954.[11] Natta *et al.* synthesised polyacetylene in 1958 as the simplest type of the conjugated polymer.[12] Later, in the 1960s, many salts of tetracyano-p-quinodimethane (TCNQ) were found to exhibit semiconducting behaviour, and in 1973 metallic behaviour was observed in the donor-acceptor charge transfer (CT) complex tetrathiafulvalene (TTF)/TCNQ.[13] In the year 1977, conductive organic polymers were discovered, where very high electrical conductivity was measured for doped states.[1] In the early 1980s, organic superconductivity was reported in the charge transfer (CT) salt tetramethyl tetraselenafulvalene (TMTSF)-$PF_{6.}$[13,14] The Nobel prize in chemistry was awarded in 2000 to Alan. J. Heeger, Alan. G. McDiarmid and Hideki Shirakawa for the discovery and development of conducting polymers.[15,16]

1.3. Band Theory

Band theory explains how electrons move in semiconducting materials. The materials can be divided into three groups; (i) metals, (ii) semiconductors and (iii) insulators, depending on the band gap. The band originated from the splitting of

HOMO levels is known collectively as the valence band, whereas that composed of LUMOs represent the conduction band. Figure 1.1 describes the different types of materials and their band structures.

The number of electrons that can be promoted into the conduction band depends on the energy gap ($E_{g)}$ or band gap, which is the difference in energies between the top of the valence and the bottom of conduction bands. The top of the valence and the bottom of the conduction bands are also known as the highest occupied molecular orbital (HOMO) level and the lowest unoccupied molecular orbital (LUMO) level, respectively, and the energy of the state, which is half occupied, called the Fermi level (E_f).

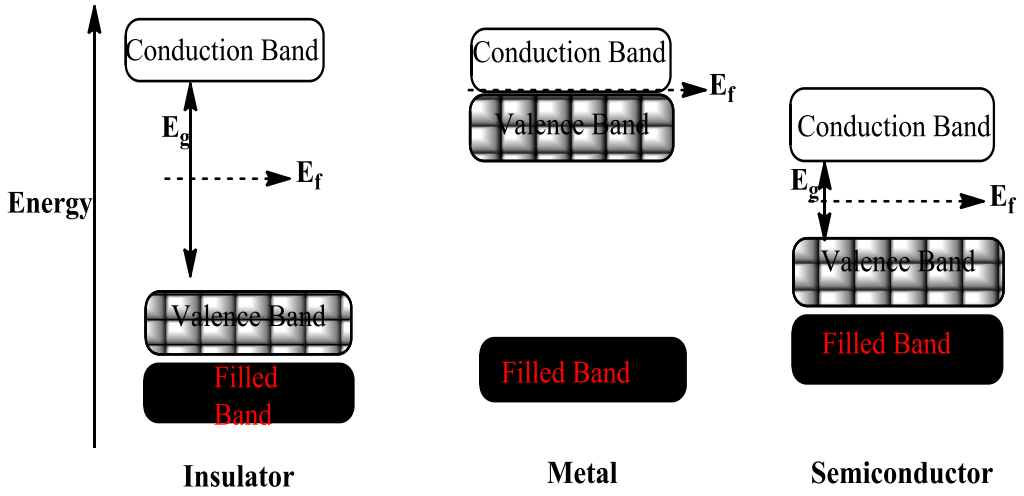

Figure 1.1. Band theory diagram

When the energy gap between the valence band and the conduction band is too large for reasonable thermal excitation then the material is an insulator. In semiconductors, the band gap is small enough for electrons from the valence band to be thermally excited into conduction band. In a metal, the energy levels of the valence and conduction bands are adjacent to each other, hence there is no band gap and electrons can adopt any energy within half filled band.[13,17]

A semiconductor can be doped by adding a small portion of impurity atoms to the pure crystal structure, producing p- and n-doped semiconductors. p-Doping creates deficiencies of valence electrons in the valence band and these deficiencies are termed ‘holes. When a voltage is applied, an electron moves into a nearby hole, leaving behind another electron deficiency (hole) in its place. p-Doping creates vacant states at so called acceptor level (E_a) just above the valence band (Figure 1.2a), which accept electrons from the valence band. In p-doped semiconductor Fermi level moves towards valance band.

n-Doping is a result of excess electrons in the valence band and results in the creation of a new energy level called the energy donor level (E_d), which sits just below the conduction band as depicted in Figure 1.2b. Which lead to an excess of electrons in the valence band, therefore the electrons in this band can be moved into the conduction band more easily, because of the reduced energy gap, resulting in increased conductivity.[17,18]

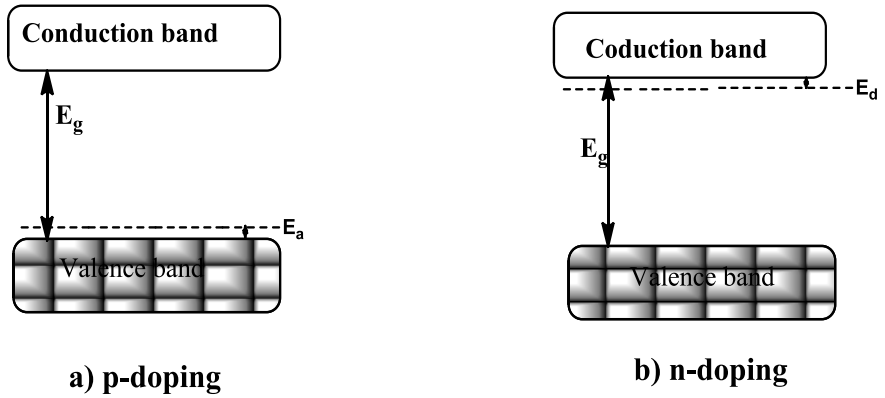

Figure1. 2. p-Doping and n-doping in semiconductors

The simple electrochemical technique can be used to estimate the HOMO and LUMO levels of organic materials through the oxidation and reduction in an electrochemical cell. An electrochemical cell provides the possibility to carry out an oxidation and reduction processes by aligning HOMO and LUMO levels of the analyte with the Fermi level of the working electrode material at external potential. In an oxidation process positive potential is applied to the working electrode of an electrochemical cell so the material (A) loses electrons. The electrons are transferred from the HOMO of the analyte to the working electrode, creating an anodic current. The Fermi level of the working electrode material in the oxidation process has to be lower than the HOMO level of the analyte to provide an easy passage of electrons. On reduction a negative potential is applied, and electrons migrate from the electrode into the analyte, the cathodic current being produced.[19,20] The oxidation and reduction processes are illustrated in Figure 1.3.

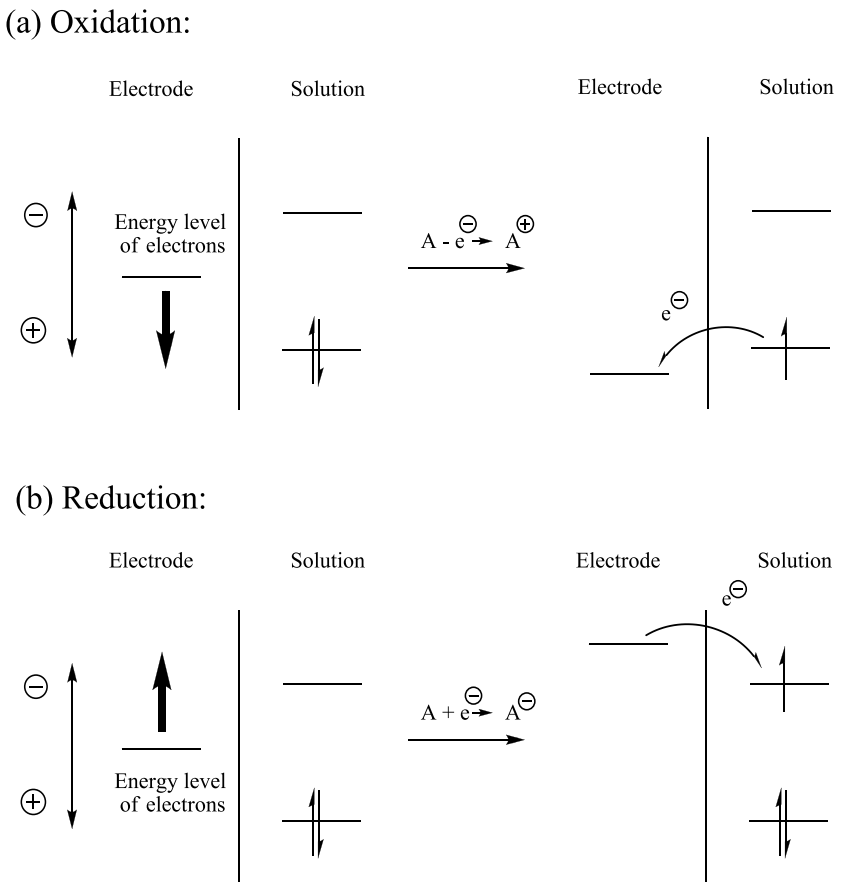

Figure 1. 3. Oxidation and reduction in an electrochemical cell[19]

1.4 Conjugated Polymers

Conjugated materials are an important type of organic semiconductors, which can be further classified into two major sets;[21] oligomers and polymers. Conjugated polymers contain numerous monomeric repeat units that are bonded together in an extended chain, whereas the oligomers consist of a limited number of repeat units. Organic conjugated polymers with an extended π-bonding system show unique

physical properties, which are not present in conventional polymers. They are of great interest due to low cost, easy processing, tunable for optical and electronic properties, high conductivity in doped state and stability.[22] The dopant is required in the conjugated polymer to increase the conductivity by way of altering the bonding structure, therefore holes and electrons will be created and electrical transport along the polymer backbone will occur. Polyacetylene is considered as the simplest case of the conjugated polymer structure; electrical transport characteristics (hole or electron mobility) will be result of an alternating double and single bond structure along the chain of the polymer, which produces unique optical and electronic properties of the polymer.[12] (Figure 1.4).

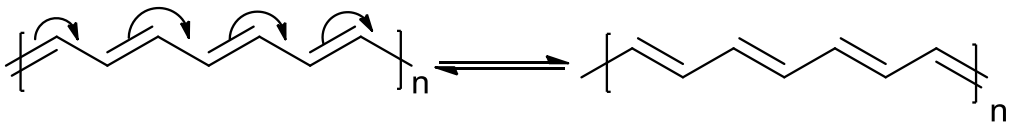

Figure 1. 4. Polyacetylene structure as resonance of the electronic states

Thus, organic conjugated polymers exhibit semiconducting behaviour and electroactivity in the main chain of the conjugated material.[23] The π- and the π*-orbitals (bonding and antibonding orbitals, respectively) support the transport of charges (electrons and holes) from the delocalised valence and conduction bands through the backbone.[24,25] Common classes of organic conjugated polymers include polyacetylene, polythiophene, polypyrrole, polyaniline, polyfluorenes and polyparaphenylenevinylenes and they can exhibit very high electrical conductivity in both p-doped and n-doped states (although they are insulators in their neutral

state).[25,26,27,28] Organic conjugated polymers can be quite stable in their doped states and can be termed stable charge carriers with efficient electron and hole transport properties. Therefore, they have found use in many applications such as light emitting diodes, thin film transistors and solar cells.[28,29]

1.5 Mechanism of Electrical Conduction

Organic conjugated materials, such as polythiophene, polyfuran, polyaniline, polypyrrole and poly-p-phenylene.[1,30,31,32] as shown in Figure 1.5, can be produced by several techniques.

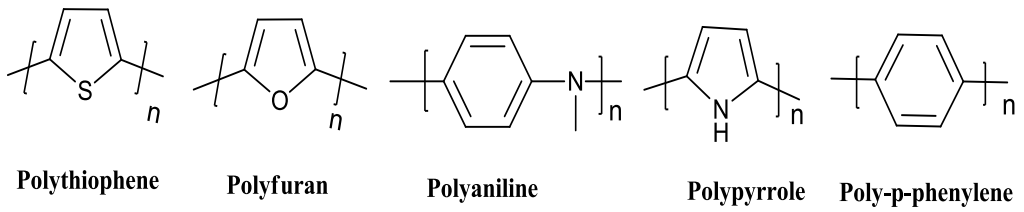

Figure 1. 5. Structures of the most widely studied conducting polymers.

Hence a variety of techniques have been employed to produce organic conjugated materials, including chemical and electrochemical techniques. The chemical technique can produce organic conjugated polymers by using catalytic oxidation in which the control over polymer morphology is very limited and processing is virtually impossible for non-derivatised materials.[1] However, the electrochemical technique of organic conjugated polymers shows many advantages compared to chemical techniques, including the deposition of the polymeric film on an electrode

surface, controlled film thickness, morphology, and polymer growth without any catalyst.[1,33,34] The electropolymerisation process is achieved by the electro-oxidation of a suitable monomer in an organic solvent containing a supporting electrolyte. Figure 1.6 shows the combination of cation radicals of a heterocyclic monomer through general electropolymerisation.[35]

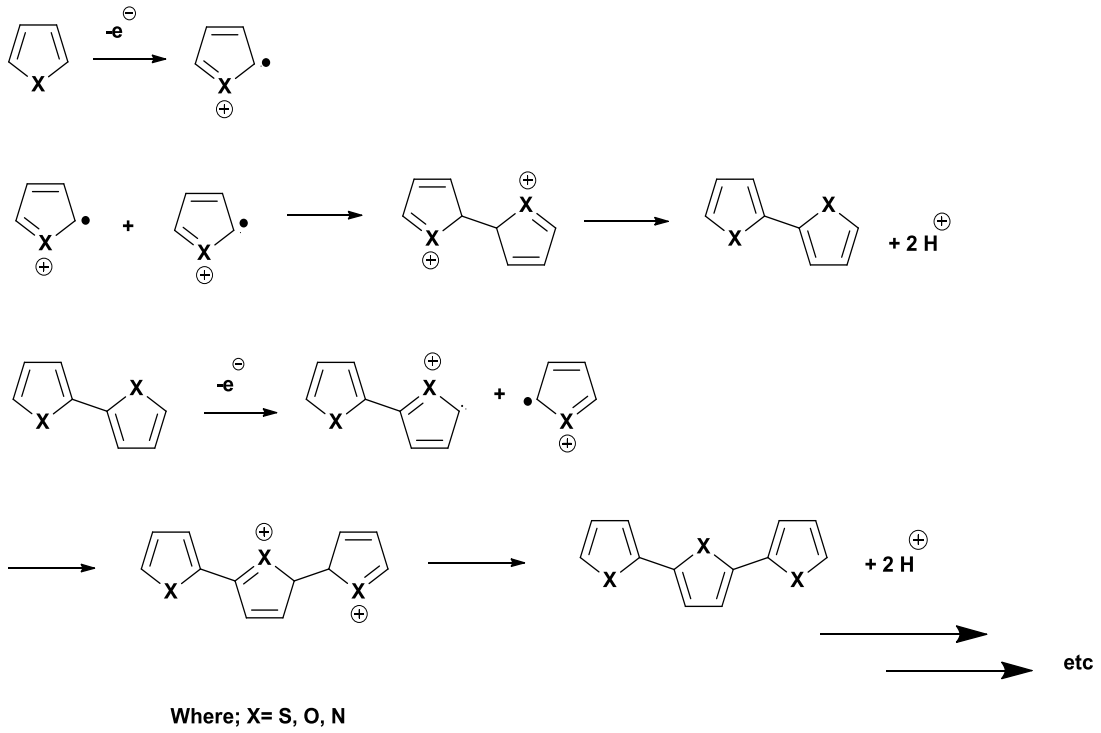

Figure 1. 6. Mechanism of the electrochemical polymerisation of 5-membered aromatic heterocycles [1,36]

In the first step, the heterocyclic ring of the monomer loses an electron to the electrode surface to form a radical-cation. The second step involves the reaction of two radical-cation species to form a dication dimer, which then undergoes the loss of

two protons and rearomatisation to form the dimer in the third step.[36,1] In the fourth step the dimer form is oxidised and combines with another radical-cation to give a trimer, which in turn expels two protons to form a conjugated trimer species as exhibited in the fifth step.[1] The oligomer chain must be oxidised for chain growth and the addition of extra monomer units results in the loss of solubility and deposition on the electrode surface.[1]

Polythiophene (PT) is a commonly used material in electrochromic and electronic devices, such as organic light emitting diodes (OLEDs), organic field effect transistors (OFETs) and organic solar cells (OSCs), due to its high electrical conductivity in the doped state and high stability. Electrochemical growth can be performed by the cyclic voltammetry (CV) technique via repetitive scanning over the oxidation wave of the monomer.[37] Polythiophene growth begins with the oxidation of the monomer and then through to the dimer, trimer and higher oligomer units (Figure 1.7) to produce an electroactive film of the polymer.[36,38]

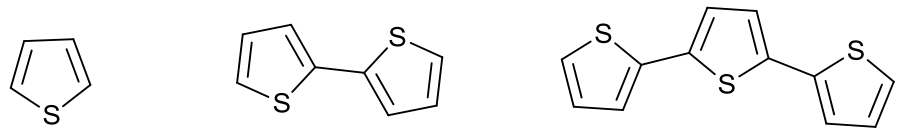

Thiophene Bithiophene Terthiophene

Figure 1. 7. Chemical structure of thiophene and its oligomeric derivatives

Electroactivity is exhibited in both oxidation and reduction processes for terthiophene, by creation of either a cation radical or an anion radical on the terminal

thiophene unit. The radical cation through the oxidation process of terthiophene (Figure 1.8) can react with other oxidised monomers and this process is irreversible.[7,39]

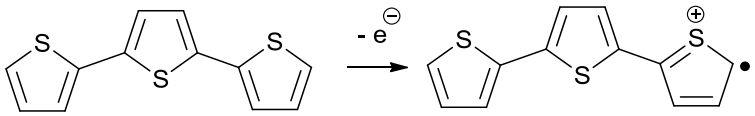

Figure 1. 8. . Oxidation of terthiophene

The produced polymer film has a lower oxidation potential and higher conductivity compared to the monomer.[7,38,40] The electroactivity is represented by the oxidation and reduction processes, which are reversible in some cases. With regard to the electronic absorption spectra (UV-Vis), the polymer exhibits a bathochromic shift for the π-π^* transition in comparison with the monomer, which is due to the increase of conjugation along the polymer chain.[40,41] During electrochemical or chemical oxidation, the conjugated polymers are doped with counter anions. However, in the doped state, the polymer grows on the electrode surface by repetitive cycling over the first oxidation wave; therefore, the positive charges will balance the counter anions of the electrolyte.[42]

The polymer can be de-doped by repetitive cycling in an electrochemical range close to 0 V, where no redox activity takes place and the polymer is obtained free from the counter ions. Figure 1.9 shows the doped and de-doped states of polythiophene as an example.

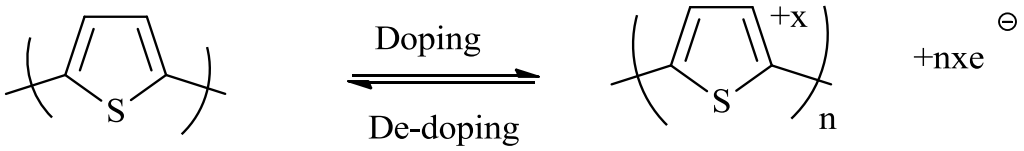

Figure 1. 9. Doping and de-doping of polythiophene

In both doped and de-doped states, the polymers exhibit different colours. For example, poly 3,4-ethylenedioxythiophene (PEDOT) as a thin film is dark blue when neutral (de-doped) and transparent blue when doped. [36,41,35,43]

1.5.1 Substituted Heterocycles

Many side chains and conjugated groups have been attached to the periphery of generic monomers to overcome the low solubility and poor processability of the resulting polymer.[41] For instance, thiophenes substituted at the 3- or 4-position (also known as the β-position) maintain their ability to electropolymerise, due to the fact that the 2- and 5-positions (also known as the α-positions) remain available for monomer coupling. Attaching substituent side-chain groups onto the backbone of polythiophenes provides possibility to vary materials' properties due to inductive or mesomeric effects of the substituent.[41,44,45] As such, attaching side-groups with electron-donating groups, such as methyl, alkoxy or amino functionalities, gives an increase in electron density in the thiophene ring and causes a decrease in the oxidation potential of the material.[1, 41] Electron-withdrawing groups, on the other hand, such as halogens and nitro groups, provide an increase in the oxidation

potential and such monomers are difficult to electropolymerise and result in poorly conducting polymers.[1]

In addition to electronic effects, steric hindrance also influences the properties of the polymers. Steric hindrance arises between head-to-head dimers and causes the thiophene rings to be forced out of coplanarity. This results in poor π-orbital overlap and distortion of conjugation in the backbone.[1, 41] This effect is magnified in 3,4-dialkyl substituted polythiophenes and causes a decrease in conductivity and an increase of the optical band gap of the polymer.[41] The substitution of thiophenes has been investigated with both alkyl and alkoxy groups. Poly-(3-alkoxythiophene) exhibited a lower oxidation potential, smaller band gap and higher absorption maximum than the corresponding poly-(3-alkylthiophene). This indicates the greater electron-donating ability of the oxygen atoms in the alkoxy chain and lesser degree of coplanarity in poly-(3-alkylthiophene). However, poly-(3-alkoxythiophene)s will also suffer steric hindrance, lack of coplanarity and loss of conductivity to a certain degree.[41,46] One method of reducing this effect is through cyclisation of the alkoxy 3,4-positions in the material.

3,4-Ethylenedioxythiophene (EDOT) and 3,4-ethylenedithiothiophene (EDTT) (Figure 1.10) are excellent examples for such a monomer design, where the fused 1,4-dioxane (dithiane) cycle decreases the steric effect and increases the donor ability.[41,44] The electropolymerisation of EDOT and EDTT compounds produces poly3,4-ethylenedioxythiophene (PEDOT) and poly3,4-ethylenedithiothiophene (PEDTT), which have shown high conductivity and good stability.[41, 43]

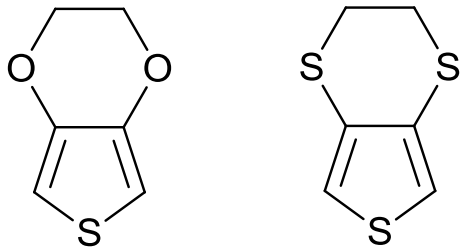

Figure 1. 10. Structures of EDOT and EDTT

PEDOT is one of the best known conducting polymers due to its exceptional electronic properties, such as low band gap, low oxidation potential, high electronic conductivity and outstanding environmental stability in the oxidised (p-doped) state.[44] Furthermore, PEDOT exhibits a stark colour change between the neutral and doped states; it is dark blue in the neutral state and light blue (and highly transparent) when oxidised.[43, 45] PEDOT is used in many fields such as OLEDs, OFETs, photovoltaic cells, batteries, display devices, smart windows and biosensors, particularly since it is also a good hole-injection material in some of these devices.[41, 43-45] Comparing the redox and optical properties of EDTT and EDOT, the monomer of EDTT has a higher oxidation potential than EDOT, but possesses a lower HOMO-LUMO gap. Conversely, in the polymer case, PEDTT has shown a higher oxidation potential and wider band gap than PEDOT owing to an increase in the number of sulfur atoms in the PEDTT chain, which greatly affects the inter-ring conjugation.[47,39] This is a result of the extensive chalcogen---chalcogen steric interactions between the sulfur atoms (S···S interactions) leading to a twisted geometry, whilst the chalcogen---chalcogen interactions (O···S interactions) in PEDOT lead to a highly planar polymer, with a low band gap and oxidation

potential. Therefore, the O···S contact provided the degree of rigidification and consequently increased effective conjugated length along the polymer chain.[41, 43] In addition, the stronger electron-withdrawing effect from the oxygen atoms in PEDOT will decrease the reduction potential.[43]

Spencer *et al.* [43] investigated the effect of the replacement of oxygen by sulfur atoms in PEDOT structure via the synthesis of two new compounds called EDOT-EDTT-EDOT (OSO) and EDTT-EDOT-EDTT (SOS) as shown in Figure 1.11. Thus, more effect have been shown from strong intermolecular (O···S) and (S···S) contacts and interchain interaction that cause to persistent conformers of (OSO) and (SOS) in both solid and solution states. Under electropolymerisation, it was difficult to obtain a suitable film for **SOS**, while **OSO** showed a good growth trace forming a neat film. **POSO** has a lower optical and electrochemical band gap (1.64 and 1.47 eV, respectively) than in the **PSOS** case (2.14, and 1.89 eV). [43]

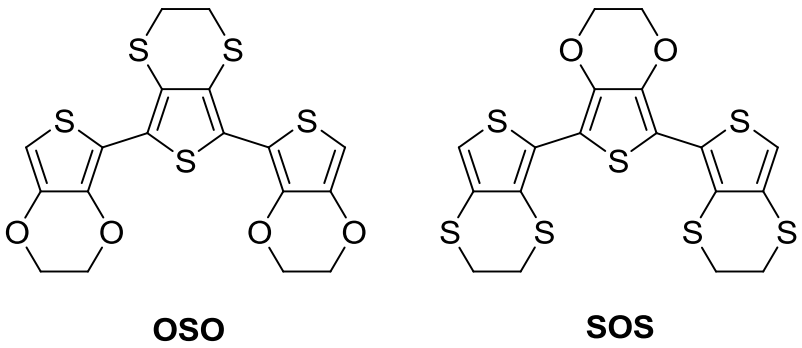

Figure 1. 11. Structure of OSO and SOS[43]

Additionally, **POSO** shows a bathochromic shift by exhibiting a longer wavelength absorption maxima compared to **PSOS**. This is a result of the increase in the

effective conjugation length and planarity in **POSO**. Therefore, the difference in the electrochemical and optical properties of these materials is attributed to the resonance contribution effect of oxygen atoms in **POSO** in comparison to sulfur atoms in **PSOS** and the effect of S-O non-covalent interactions on the polymer backbone planarity.[43] **POSO** also has a higher electrochemical band gap and a small decrease in planarity compared to PEDOT (the electrochemical band gap is 1.35 eV) due to the sterical hindrance of S···S interactions in **POSO** chain.[43] The expected intramolecular interactions of PEDOT, **POSO** and **PSOS** are illustrated in Figure 1.12.

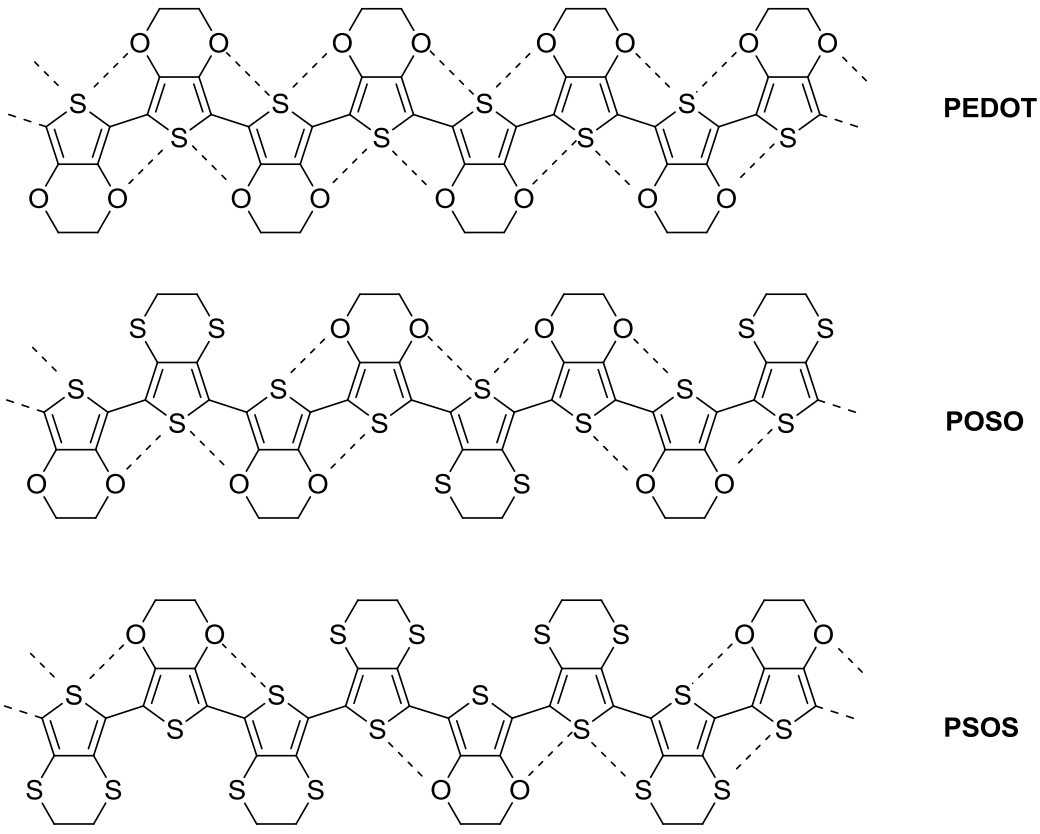

Figure 1. 12. . Expected O···S interactions for PEDOT, **POSO** and **PSOS**.

The sulfur atoms in the PEDTT units can be replaced by selenium atoms to give poly(3,4-ethylenediselena) thiophene (PEDST)[48]. The structure of PEDST is depicted in Figure 1.13. PEDST has been shown higher stability and more planar conformation compared to those of PEDTT. Stronger interchain contacts between Se atoms are another factor, which defines the band gap of the polymer. The electrochemical and UV absorption data of PEDST show agreement between an electrochemical and optical band gap value, which are 1.55 and 1.79 eV respectively. For PEDTT the corresponding values of bandgap were 2.19 and 2.15 eV respectively. The discrepancy in bandgaps between PEDST and PEDTT is likely to be attributed to the stronger interchain Se···Se interactions in addition to substituent and planarity effect.PEDST energy gap values were closer to the electrochemical and optical band gaps of PEDOT (1.35 and 1.63 eV respectively).[48]

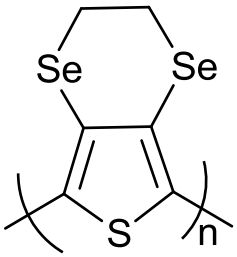

Figure 1. 13. Structure of PEDST.

EDOT and EDTT units can also be attached to many heterocycles, leading to copolymers of various structures. As such, these materials can be studied to evaluate the effects of the EDOT (or EDTT) units to the overall electrochemical and electronic properties of the polymers. As an example of this case, Tanaka *et al.*

synthesised and polymerised 4,7-bis(2,3-dihydrothienodioxin-5-l)benzothiadiazole[16, 17,48,49,50,51]compound to obtain narrow band gap PBDT polymer containing benzothiadiazole (BT) acceptor and 3,4-ethylenedioxythiophene (EDOT) donor electroactive units (Figure 1.14). This polymer exhibited high stability under redox cycling and low band gap value of 1.30 eV.[50] Thus, the alternation of donor and acceptor moiety in the polymer backbone creates the polymer due to donor-acceptor interactions. [50,52,53]

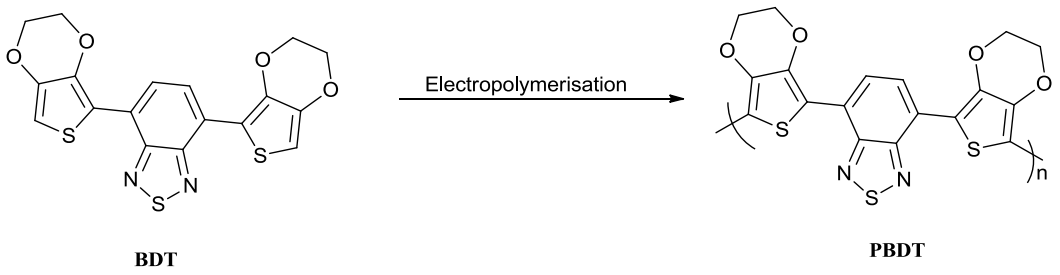

Figure 1. 14. Electropolymerisation of BDT

BDT shows reversible redox processes at low potential and polymerises to PBDT on an indium tin oxide (ITO) working electrode. PBDT is green in the neutral state and its colour changes to a highly transparent light blue when doped. Polymers with donor-acceptor units typically show small band gaps and the value for PBDT was estimated as about 1.19 eV. PBDT can be used as a polymer for many colour applications, for example alongside poly(3-methylthiophene) (red) and PEDOT (blue) as the active layers in organic light emitting diodes and electrochromic devices owing to easy change of colour between states by structure alternations, and high optical contrasts.[54,55,56] Moreover other electron donor groups based on thiophene derivatives have also been associated with BT acceptor units to produce conjugated

polymers with small band gaps, which were used in organic photovoltaic devices.[56,57,58]

The conductivity of conjugated materials can be increased by incorporating materials such as tetrathiafulvalene (TTF) into the polythiophene backbone. The electropolymerisation process of these materials cannot be accomplished directly from the corresponding monomer due to the TTF group's higher sensitivity to the oxidation conditions compared to the thiophene group. Bryce *et al.* [37] have described an electropolymerisation of the polymer film of thiophene unit incorporated with TTF redox active centre by the association of an ester link., Therefore small conjugation lengths have been shown in produced material owing to steric hindrance between TTF groups that would be caused distortion in polythiophene backbone, however in this case the electropolymerisation process has not done because presence of the disruption in the aromaticity of the dicationic TTF followed by the oxidation of thiophene units.[37] In recent years Skabara *et al.*[23] have succeeded to solve this problem by using nonconjugated chemical coupling (saturated spacer groups) to attach TTFs to polythiophene units, and hence TTF units showed independent electroactivity.[23] TTF is easily converted by reversible oxidation, forming two stable states (TTF^{+} and TTF^{++})[59,60,61,62] as shown in Figure 1.15.

TTF and its derivatives have been employed in superconductor materials as charge transfer salts, and recently have been incorporated into conjugated polymers[27] for use in several different application such as organic semiconductors and sensors.[63]

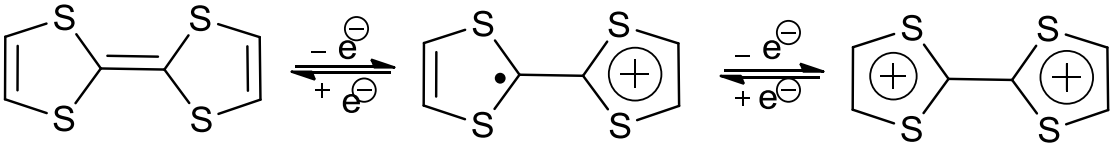

Figure 1.15. Oxidation of TTF [60]

Oligo and polyfluorenes are another class of conjugated materials that exhibit unique properties for several applications, due to their electroluminescence quantum efficiency and highly tunable properties through copolymerisations.[64] Fluorene derivatives emit light in the violet–to-blue colour region; as a consequence, the band gap, *i.e.* the difference between the valance and conduction bands, is generally large. However this material can be used in novel applications such as multicolour displays applications and can be modified to obtain a lower band gap when associated with electron-deficient units, such as the benzothiadiazole unit. Moreover, fluorene (Figure 1.16) based materials have been shown to be highly fluorescent and are also used in organic light emitting diodes and photovoltaic devices.[65,66]

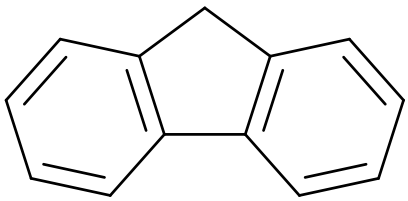

Figure 1. 16. Structure of fluorene

1.6. Cyclic Voltammetry

The cyclic voltammetry (CV) is one of the common electrochemical technique used to investigate the electrochemical behaviour of a material.[67] This technique is used for measuring the oxidation and reduction potentials. When referencing against standard compound with a known energy level (HOMO or LUMO) the data can be used for estimation of the HOMO and LUMO level of the analyte.
In CV experiment a conventional three electrodes electrochemical cell with reference (RE), counter (CE) and working (WE) electrodes is used.[68] The working electrode can have various shaped (cylinder, spade, or disc) and is usually made of gold, glassy carbon, platinum or indium tin oxide (ITO). The counter electrode is typically a platinum wire or gauze, to match the surface areas of the working electrode. The reference electrode is conventionally non-polarisable electrode such as saturated calomel (SCE) or Ag/AgCl aqueous electrodes. For non-aqueous solution a silver wire can be used as a quasireference electrode. An electrolyte is used to allow conduction through the solution in the electrochemical cell. The electrochemical behaviour of the analyte depends on the kinetics of its oxidation or reduction and further transformations of oxidised and reduced species.[1,55,69] In three electrode scheme, the potential is applied between the working electrode and reference electrode and the current response is measured between the working electrode and counter electrode.[69] The data are measured with internal resistance (iR) compensation to avoid any potential drop between working and reference electrodes, that can yield in a serious error.[37] In cyclic voltammetry experiment a triangular shape potential waveform used to rump the voltage linearly from initial voltage to

particular value of end potential at forward scan and backwards from the end potential to its initial value at reverse scan. At this reverse scan the product of oxidation (reduction) that formed at the forward scan reduces (oxidises) back to the neutral analyte. These potential sweeps are kept at constant scan rate (V/s) and can be run continuously multiple times between two potentials in a single experiment. This potential triangular waveform[67] is shown in Figure 1.17.

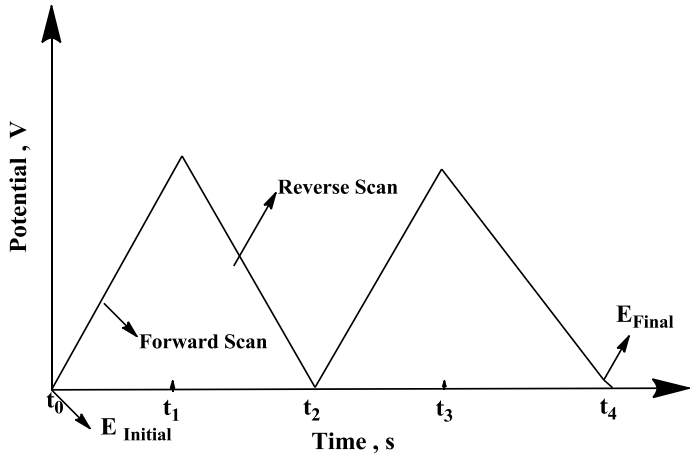

Figure 1.17. Variation of potential as a linear function of time

The current response is plotted against potential giving a cyclic voltammogram plot.[55,37,70] CV can be employed to determine the diffusion characteristics of analyte Where, the scan rate test is employed to show if the redox response of a material (polymer) (charge transport through the polymer) is limited by diffusion or not. Consequently; the CV of polymeric film is usually recorded at various scan rates (from 25 mVs^{-1} to 500 mVs^{-1}) and the values of peak current (I_p) is plotted against the scan rates. The linear relationship between peak current and scan rate confirms that the charge transport through the polymeric film is not diffusion limited.[36,41,45,43]

CV experiment can distinguish reversible, irreversible and quasi-reversible processes.[71,72] Let us consider a simple reversible reaction of analyte (A), described by the flowing equation:

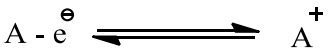

Where, the analyte **(A)** is oxidised to **(A^+)** at forward scan in positive direction. This process results in an anodic current, which reaches its maximum value I_{pa} at the potential E_{pa}. At the backwards scan the oxidised species (**A^+**) is reduced back to (**A**) producing a cathodic current that reaches its maximum value I_{pc} at the potential E_{pc}.[19] For a reversible system the current response should have similar heights for anodic and cathodic peaks (I_{pa}/I_{pc}=1), and the areas, which these curves circumvent, should be roughly equal (Figure1.18), the difference between potential of anodic and cathodic peaks ($\Delta E_p = E_{pc} - E_{pa}$) is close to 59 mV /n at 25 C° and independent of scan rate, where **n** is the number of electrons in oxidation and reduction processes.[71]

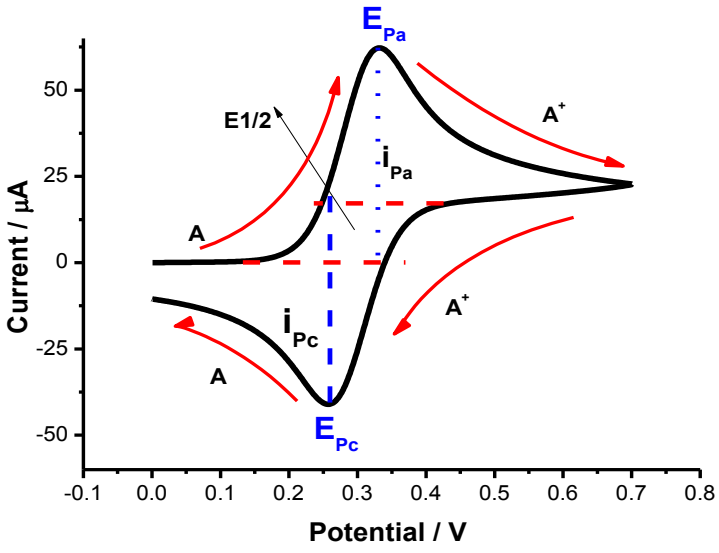

Figure 1.18. Typical cyclic voltammogram graph of reversible redox process

In an electrochemical reaction, there can be the three types of mass transport, which can influence the kinetics of the electrochemical experiment; those are migration, convection and diffusion.

In the reversible system at any reasonable scan rate the electrochemical kinetics will be defined by diffusion of an analyte to the electrode surface, the rate of the electron transfer would be fast, so that the concentration of oxidized and reduced form of the redox couple at the electrode surface would be governed by Nernst equation-.

$$\boldsymbol{E = E^{0} + \frac{RT}{nF} \ln \frac{[O]}{[R]}}$$

Where **E** is the electrode potential, $\boldsymbol{E°}$ the standard electrode potential, $\boldsymbol{R}$ is the universal gas constant: $R = 8.314\,472(15)\ \mathrm{J\,K^{-1}\,mol^{-1}}$, T is the absolute temperature, **[O]** and **[R]** are the concentration of the oxidised and reduced species respectively.[71,67]

For a totally irreversible oxidation or reduction process only one forward reaction is considered to contribute into the electrochemical kinetics, so there is no any observable peak current on the backwards scant due to either instability and further transformations of oxidised or reduced species. or extremely sluggish rate of their reverse transformations.[67] For quasi reversible reactions the both forward and reverse reaction are considered but with electron transfer kinetic limitations. Consequently, the redox process might look like reversible at low sweep rates and become quasi reversible at faster scans. For quasi reversible system, the current peaks for an

oxidation and reduction will lose their steep and become more apart compared to reversible case. [71] In quasi-reversible process the current peak (I_p) increases with the scan rate but is not proportional to it. Moreover the peak in quasi-reversible case does not show reverse scan as reported in reversible case.

Diffusion is a mass transfer that is generated by the difference in the concentration of the dissolved species. Where, the rate of movement of solute on diffusion can be illustrated precisely by Fick's first law as given in the following equation:

$$\boldsymbol{J_0 = -D_0(\frac{\partial c_0}{\partial_x})}$$

Where $\boldsymbol{J_o}$ is the diffusion flux (the rate of the movement multiplied by the concentration of a solute or the quantity of a solute which crosses the unit area per unit time), $\boldsymbol{D_o}$ is diffusion coefficient, the negative sign (-) means that the solute moves from high to low concentration region and ($\partial c_o / \partial x$) is the change of the species $\boldsymbol{o}$ concentration per distance $\boldsymbol{x}$.[73,74]

The peak current (I_p) is controlled by diffusion of analyte its concentration and scan rate as shown in Randle-Sevcik equation:

$$\boldsymbol{I = (2.69\ x10^5)\ n^{3/2}AD^{1/2}Cv^{1/2}}$$

Where **n** is number of the electrons transferred per mole, **A** is the electrode surface area in cm^2, **D** is the diffusion coefficient in cm^2/s ,**C** is solution concentration in mole/L and **ν** is scan rate of the potential in V/s.[75]

The results of the electrochemical experiment are referenced against a stable reversible redox couple with known position of HOMO (LUMO) level. Since, ferrocene exhibit reversible oxidation wave and HOMO level for this compound is conventionally known, it is generally a good practice to use the redox couple of ferrocene/ferrocenium (Fc/Fc^+) as a standard for the study of organic semiconductors.[38]

Fc/Fc^+ was recommended by IUPAC more than 20 years ago.[76] Many other species have also been proposed as a reference redox system, such as $Rb^+/Rb(Hg)$ due to their large ionic radius and small change in the free energy of solvation of Rubidium ion. However, this free energy change was too big to be ignored. For this reason, there are many studies by Strehlow and co-workers on a range of organometallic complexes to find a suitable reference redox system.[77] Therefore, ferrocene/ferricenium ion (Fc/Fc^+)[77] is extensively used as a redox system due to the following properties of these ions:

i) The redox couple of both components should be stable.

ii) The ions have low charges.

iii) The molecules of redox couple are spherical and have large radius.

iv) The components of the redox system are soluble, and the redox potential takes place within the potential range of several solvents.

v) There is a rapid and reversible equilibrium at the electrode surface.

vi) No change occurs in the geometry of the ion or molecule.

Moreover, the kinetics and mechanism of the electrochemical reaction in cyclic voltammetry experiments should be monitored throughout for several factors such as; (i) number of peaks in the forward and reverse scan, (ii) potentials and current densities of each peak and (iii) shape of the peaks.

In addition, cyclic voltammetry has been used as a simple method to determine the location of both the highest occupied molecular orbital (HOMO) and lowest unoccupied molecular orbital (LUMO) levels, and as such, the electrochemical band gap of monomers and polymers.[51] The change in oxidation and reduction potentials of CV indicating the corresponding change in the HOMO and LUMO levels values.

1.7. Band gap control and characterisation

The band gap is one of the most important characteristics of organic semiconductor and defines the electronic and photonic property of organic conjugated materials, which contribute to performance of the material in a number of applications such as organic field effect transistor, solar cell and organic light emitting diodes. There are five factors (Figure 1.19) which affect the band gap value:

(i) The degree of planarity (E^{θ})

(ii) Bond length alternation ($E^{\sigma r}$)

(iii) Aromatic resonance energy effect (E^{Res})

(iv) The substituent effect (E^{Sub})

(v) Intermolecular or interchain interactions (E^{Int})

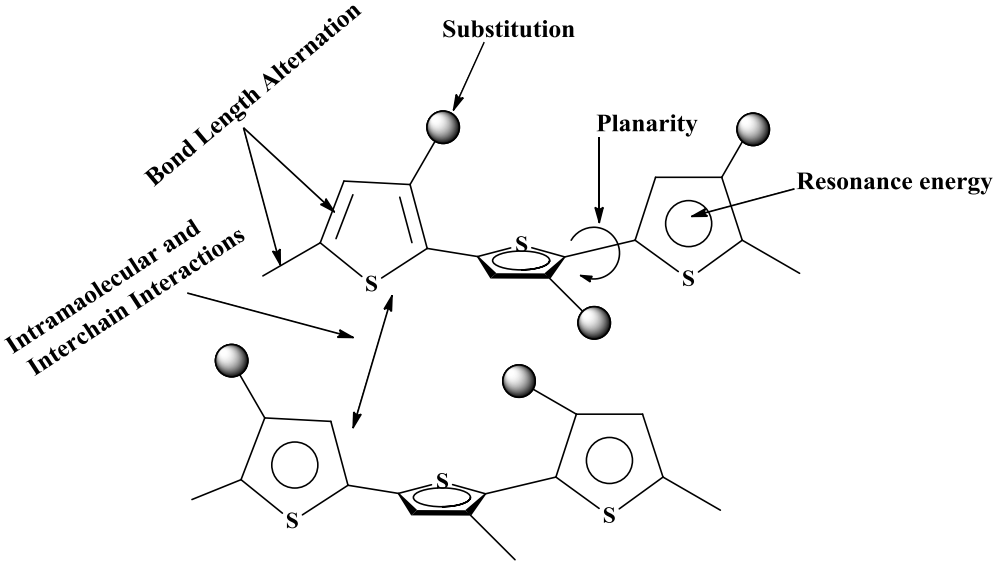

Figure 1.19. Parameters influencing band gap.

(i) The degree of planarity (E^{θ}) is characterised by the twist angles between adjacent rings. The higher degree of planarity and the lesser the torsion angles, the more narrow the band gap due to better overlap between the π-system of adjacent rings and consequently better conjugation.

(ii) Bond length alternation ($E^{\sigma r}$) is a result of π-electrons localisation within two centred bonds instead of being delocalised over the whole conjugated system, which lead to the appearance of single-double bond alternation all over the polymeric conjugated back-bone. It represents the main contribution to the value of band gap and originates from Peierls instability of one-dimensional organic semiconductor. Consequently the structure modifications leading to reduced bond length alteration are expected to produce decrease in band gap. The most reduced BLA exhibit polyacetylene (structure III) in comparison to polyaromatic system such as polythiophene and poly pyrrole (structures I and II respectively).

On of the way to decrease BLA of polyaromatic system is to increase contribution of corresponding quinoidal resonance structure to the wave function of the ground state.

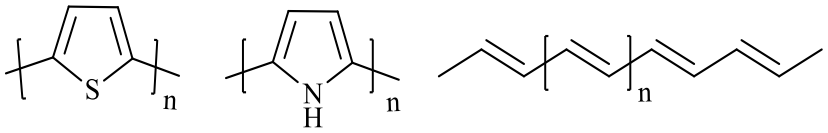

I II III

An illustrative example of the conjugated system with increased quinoidal resonance contribution to the ground state is polyisothianaphthene IV, which has narrow band gap of about 1 eV compared to polythiophene (about 2 eV).

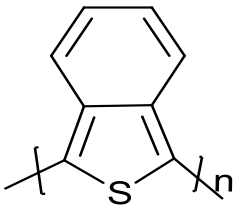

IV

(iii) Aromatic resonance energy effect (E^{Res}). The effect of the aromatic resonance energy of the rings located within the conjugated chain of the polymer prevents delocalisation of π-electrons due to confining them within the aromatic systems of the rings, which lead to increase the band gap.

(iv) The substituent groups (E^{Sub}): The ring substituents can have a large effect on the band gap by influencing the electron density of the polymer through either electron-withdrawing or donating effects. Substitution will affect the HOMO and LUMO levels and the substituent groups can also

cause steric hindrance to intra- and inter-chain interactions that will affect the distance between adjacent polymer chains.

(v) Intermolecular or interchain interactions (E^{Int}) provide further decrease of the band gap due to intermolecular (π-π) interaction or involve non-covalent or electrostatic (dipole-dipole, qudrupole-quadrupole) interactions, which usually leads to aggregation with various affect on band gap.[78]

Using CV experiment, the electrochemical HOMO-LUMO gap of a monomer or a polymer can be determined providing that the oxidation and reduction graphs are referenced to the ferrocene/ferrocenium redox couple as a reference. Firstly, the onsets of the first oxidation and reduction peaks of the materials can be converted the HOMO and LUMO energy levels of monomer or polymer by subtracting them from the HOMO of ferrocene, which has a known value of -4.8 eV. Finally, the difference between HOMO and LUMO energy levels provide band gap value.[40]

1.8. Electronic Absorption Spectroscopy

The ultraviolet and visible absorption spectra of materials are associated with the transitions between electronic energy levels. When the material absorbs energy, then the electronic structure of the molecule is excited from its ground state to an excited state. However, there are three types of electronic transitions, involving σ, π and n

orbitals, which can occur between bonding (filled) and anti-bonding (vacant) orbitals. Thus, there are four possible electronic transitions for heteroatoms, which are σ→σ*, n→σ*, n→π* and π→π* transitions as shown in Figure 1. 20.

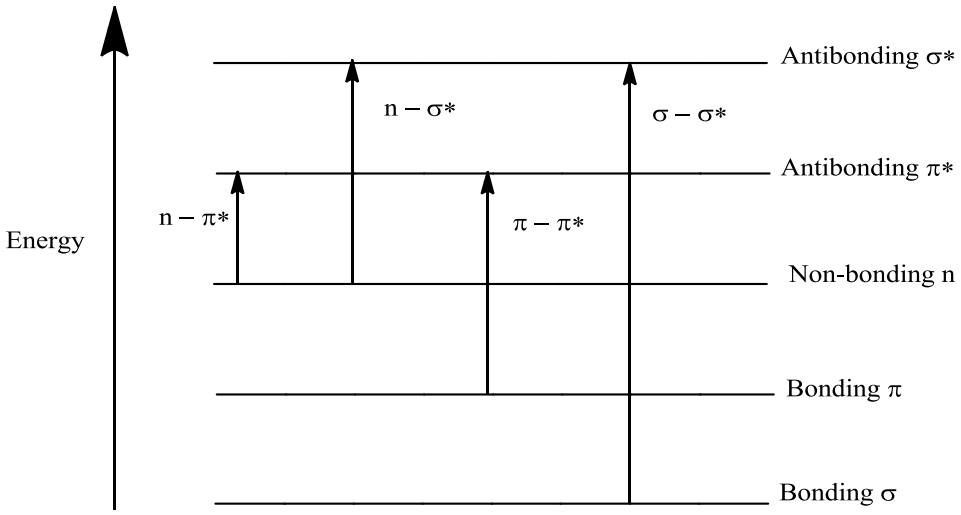

Figure 1.20. The possible electronic transitions for an organic molecule

In σ→σ* transitions an electron is promoted from a bonding (σ) orbital to an anti-bonding orbital (σ*). These transitions require a relatively large amount of energy and show an absorbance maximum normally between 100 – 200 nm. Thus, an absorption maximum representing a σ→σ* transition is not shown in a typical UV-vis spectrum, which is normally registered in the range between 200 to 700 nm.[7,79] Heteroatoms with non-bonding electrons (lone pairs) are able to undergo n→σ* transitions that is occurring at 150 – 250 nm, therefore, the organic functional groups with these transitions show small peaks in this UV region. The n→π* and π→π* electronic transitions have absorption maxima at wavelength between 200 and 700

nm. These transitions require an unsaturated group in the molecule to provide the π electron orbitals.[7,41,68] The absorption maxima of conjugated polymers in the UV-Visible range occur at longer wave than for small molecules due to an increase in the conjugation length within the polymer chains. Thus, the π→π* transitions at higher wavelength is observed for single molecules with long conjugation.[7,39] The longer the conjugation in the molecule, the higher wavelength of the absorption maxima of the π→π* transitions.[7, 39, 40,41,80] The absorption spectrum of terthiophene derivatives shows an absorption maximum at 357 nm, corresponding to the π-π* transition, however this peak is shifted bathochromically in the corresponding polymer to 467 nm,[7] and the bathochromic shift can be observed on the alkyl and alkylsulfanyl substitution in the terthiophenes.[39]

Lambert-Beer law which has been used to quantify the absorption of materials is shown below:

$$\mathbf{A = Log_{10}} \, {}^{I_0}\!/_{I} = \boldsymbol{\varepsilon . l . c}$$

Where **A** is the absorbance, $\mathbf{I_0}$ and **I** are the intensities of the incident and transmitted light, respectively, **l** is the path length of the absorbing solution in centimetres, **c** is the concentration in moles per litre, and **ε** is known as the molar extinction coefficient (also called molar absorptivity).[68]

The ratio $\mathbf{(I_0 / I)}$ is called transmittance **(T)**. The optical density can be found from transmittance by the formula:

$$\mathbf{A = -\log (\%T)}$$

The optical band gap of materials can be calculated from the onset of the longest wave absorption band edge[7] by using the following equation:

$$\mathbf{Eg} = \frac{\boldsymbol{hc}}{\boldsymbol{e\lambda}}$$

Where, $\mathbf{E_g}$ is the optical energy gap (**eV**), **h** is Planck constant = 6.626068 x 10^{-34} Js, **c** is the speed of light = 299,792,458 m/s, **λ** is the wavelength (nm) and **e** charge of an electron = 1.602x10^{-19}C.

1.9 Spectroelectrochemistry

The spectroelectrochemistry (SEC) is an experiment that combines two methods, which are spectroscopic technique, for instance UV-Visible spectroscopy or Infrared (IR), and an electrochemical technique, such as CV. SEC of polymers thin-film is carried out by growing the solid film of a polymer onto a piece of indium tin oxide (ITO) coated glass. SEC experiment can also be carried out for a solution of electroactive compound, where the analyte is dissolved in the solvent. The SEC data can be plotted in three- dimensional graph with absorbance, wavelength and potential axes as shown in Figure 1.21.

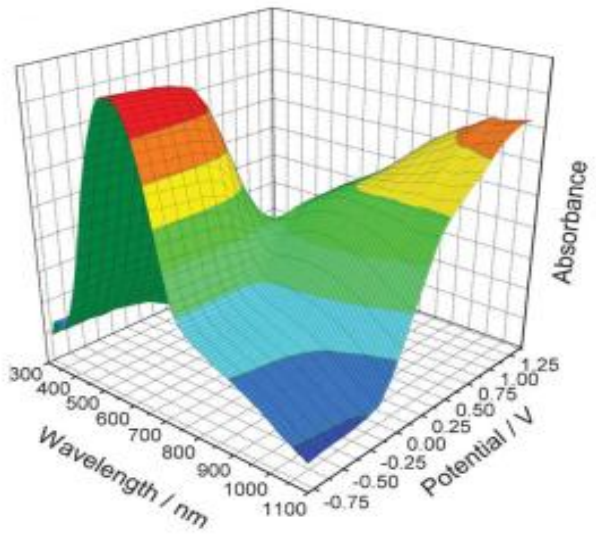

Figure 1. 21. Spectroelectrochemical plot graphs

The spectroelectrochemistry technique shows the evolution of various spectra as the substrate becomes p- or n-doped through the oxidation or reduction processes respectively. This is achieved by applying a positive or negative voltage. In a spectroelectrochemical experiment a polymer oxidation can be revealed as decrease in the intensity of the π-π* transitions of a neutral polymer and the generation of new bands at longer wavelengths. These are attributed to the formation of radical cations (polarons) and dications (bipolarons) and usually appeared in the visible and near IR region. Figure 1.22 is depicted the polaron and bipolaron quasi-particles throughout the polybenzene as an example. It is useful to consider other important examples of polarons in conjugated oligomers and polymers.

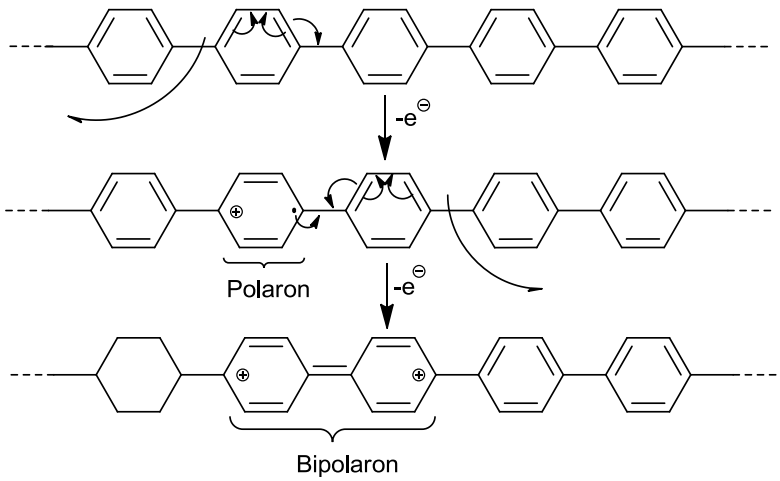

Figure 1. 22. Polarons and bipolarons in oxidised polybenzene

The polaronic signature of oxidised PEDOT is observed between the range of 850 to 860 nm, yet it is difficult to observe in the doped PEDTT.[43] The spectroelectrochemical studies of TTF derivatives exhibit two new absorption peaks at 800 and 390 nm, which are corresponding to the formation of radical cation ($TTF^{+\cdot}$) and dication (TTF^{2+}) respectively.[23,28] However, the hybrid electroactive system poly(DPP-TTF) shows additional new broad band between 890 and 1100 nm, which can be attributed to the charge transfer from TTF unit to the conjugated polymer chain.[81] Polarons and bipolarons are shown as two separate peaks in the spectroelectrochemical graph, but in some cases they can be close together or combined into one peak.[35] Spectroelectrochemical measurements can also be used to study the switching rates of the polymer between two colour states (neutral and doped states). The switching rate measurements by UV-Vis spectroscopy and CV shows the ability of the polymer, (which was grown on ITO coated glass slide) to switch continuously between neutral and doped states of the polymer. In such an

experiment, the absorbance is monitored at the wavelength corresponding to the longest wavelength absorption maximum of the polymer (the greatest difference in transmittance (absorbance) at neutral and doped states) and then determine the change percentage in transmittance of the polymer at specific switching times values.[27,43,82]

1.10. Applications

Organic semiconductors are employed in several electronic devices due to their distinctive properties such as high mechanical flexibility, good performance, low cost, high colouration efficiency and high stability. [83] Examples include thin film and organic field effect transostors (OFETs), organic light emitting diodes (OLEDs), photovoltaic cells (OPVs),[83] switches, smart windows and displays.[43] Organic semiconductors can be key components in everyday applications such as electronic displays, smart cards, identification tags and electrochromic sunglasses.[24]

1.10.1. Electrochromism

Electrochromic materials display a reversible and highly stable change in their optical properties during the application of a voltage. Many types of organic materials show electrochromism.[16,38,43,84] Generally, the difference between the electronic absorption bands in the visible region that generates the electrochromic behaviour corresponds to a change in the oxidation and reduction processes.[85] For utilization in electrochromic devices, the organic electrochromic materials must

exhibit or possess multiple colours, rapid switching times, high contrast, high colouration efficiency, and good stability. Electrochromic polymers are an interesting class of conjugated polymers, since they have the ability to change colour and possess high optical contrasts, stability, fast switching times, and tunable band gaps.[7,24] Electrochromic polymers can be used in many applications such as smart windows, multi-coloured displays and image generation.[24] The common electrochromic device can be constructed from a number of layers as displayed in Figure 1. 23.

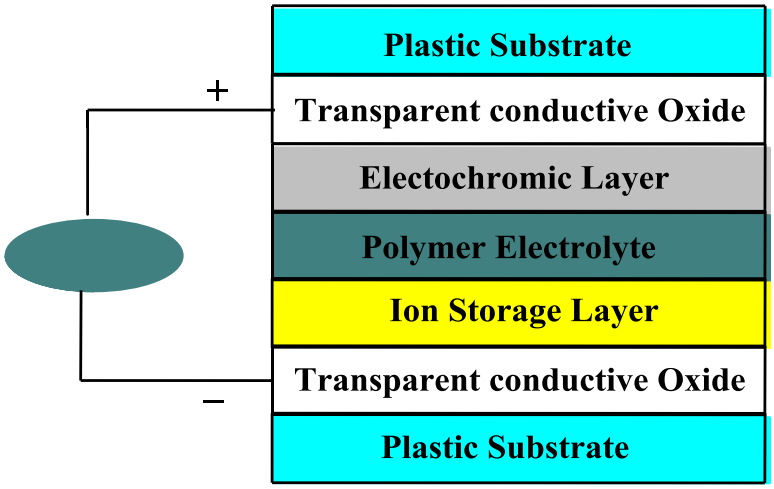

Figure 1.23. Design and working principle of the electrochromic device.[86,85]

Conjugated materials such as blue PEDOT, red poly(3-hexylthiophene) (P3HT) and green poly (aniline-N-butylsulfonate) (PANBS) absorb the three primary colours red, green and blue (RGB) for use in electrochromic devices.[87] Additionally, in PEDOT, the chromatic contrast appears in the visible region with a wavelength maximum at 650 nm.[86] Therefore, PEDOT is considered highly suitable for electrochromic

applications due to its easy processability and high degree of electrochromic contrast in the visible region of the spectrum. It has low energy band gap and is switched between dark blue colour in neutral state and transparent blue colour in oxidised state. On the other hand, polythiophene has a red colour in the neutral state and is blue when p-doped.[7,45,43,88] Excellent electrochromic behaviour has been observed in poly(3,4-ethylenedioxythiophene):poly(styrenesulfonate) (PEDOT:PSS) due to its high conductivity, high stability and high contrast at low potential.[89] Several types of conducting polymers including polypyrrole, polyselenophene and their derivatives exhibit electrochromic behaviour and stability of their optical and electrical properties in both oxidised and neutral states. Such polymers have been used in many applications such as smart windows, electrochromic sunglasses and displays.[82]

1.10.2. Organic field effect transistor

Organic semiconductor materials are highly important components in field effect transistors due to their characteristics such as simple structures, cheap production, ease of purification, high performance, high mobility and capability to be deployed in large-area electronic products. OFETs can be used in several applications such as control elements for displays and sensors.[90] A typical structure of an organic field effect transistor device contains several layers, including the gate electrode, dielectric layer (silicon dioxide), semiconductor layer and source and drain electrodes. The source and drain electrodes are in contact with a semiconductor layer, and a conductive substrate acts as the gate electrode .[76,91] The structure of an OFET device is shown in the Figure 1.24.

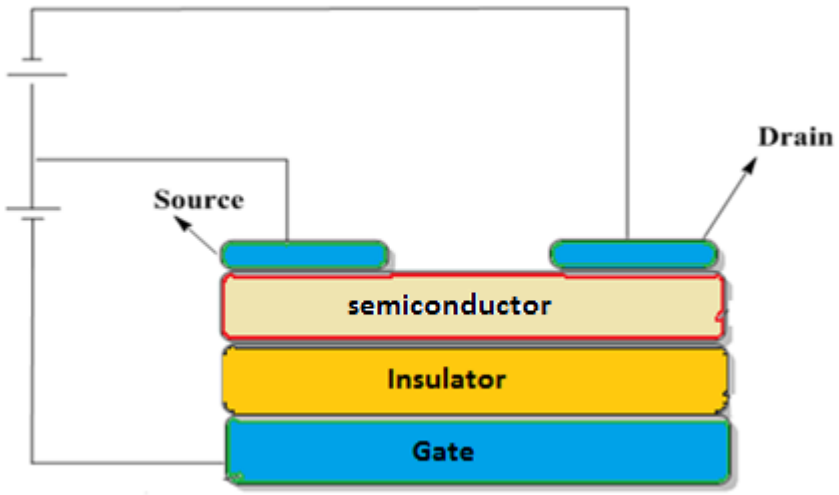

Figure 1.24. Structure of an OFET device

Insulating polymers can be used as the insulator layer coated on the gate electrode. In the off state of the OFET, where $V_G = 0$, there is a negligibly current flowing through the semiconductor layer between the source and drain electrodes. When a voltage is applied to the gate electrode, an electrical field is created in the dielectric layer and this causes an increase in the number of holes and electrons at the semiconductor/dielectric interface. This in turn results in a shift in the molecular orbital energy levels of the semiconductor (change in HOMO and LUMO levels). Consequently the charges (holes and electrons) can be transported between the source and drain electrodes, thus the electrical current pass through the OFET device. Based on the type of charge carriers, organic semiconductors can be divided into two types; p-type and the n-type. In p-type OFET the negative voltage of the gate leads to rising HOMO level of the semiconductor and after aligning it to the Fermi level of the electrode the holes can be injected from the source. In n-type device it is the

LUMO level of the semiconductor that should be aligned with Fermi level of the electrodes at positive voltage of the gate before electron will be injected from the source electrode.[88,92] The operating principle of OFETs based on organic semiconductors is presented by the simplified energy level diagram on the Figure 1. 25.

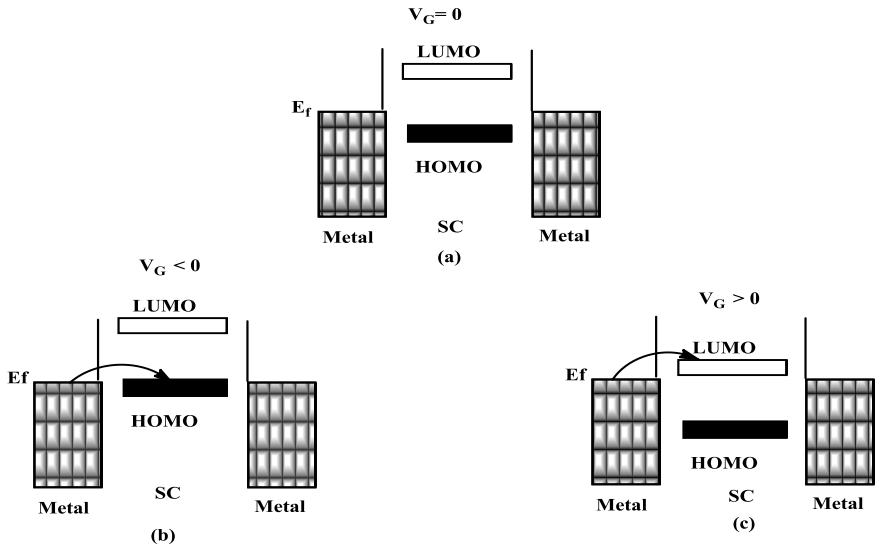

Figure 1.25. Illustration of a principle of an OFET with respect to applied V_G. (a) When VG= 0, (b) VG < 0 and (c) VG > 0.

Organic conjugated materials are used in thin film field effect transistors (OFET) because they can possess high mobility and stability.[91] Many organic electroactive compounds such as pentacene, rubrene, thiophene derivatives, and tetrathiafulvalene can be used as semiconductor materials with high mobility in organic field effect transistors.[91,93]

1.10.3. Organic light emitting diodes

Semiconducting and luminescent π-conjugated materials are used in organic light emitting diodes (OLEDs). They are suitable for such applications due to their processability, flexibility and large-area coverage, which are advantages over conventional semiconductor materials.[64] Electroluminescent materials emit light in the visible spectrum when an electric field is applied.[91,64,94] Organic semiconductors suitable for OLEDs require many key characteristics such as a fast response, low drive voltage, full-colour emission and large thin film area.[95]

In multilayer LED device there are hole-conducting (p-type) and electron-conducting (n-type) layers. Under an applied electric potential the holes and the electrons are injected from the anode and cathode respectively into organic semiconductor layers. Where, the injected holes and electrons will travel through the adjacent organic semiconductor layers, and then create electronically excited states by recombination of charge carriers, which results in generation the huge depletion region between p and n organic semiconductor layers, accompanied by decrease of its resistance, consequently, the excited state, formed on recombination can relax to the ground state to emit a photon of visible light.[96,97,95] A typical single layer OLED with a thin film of conjugated polymer between two electrodes is shown in the Figure 1. 26.

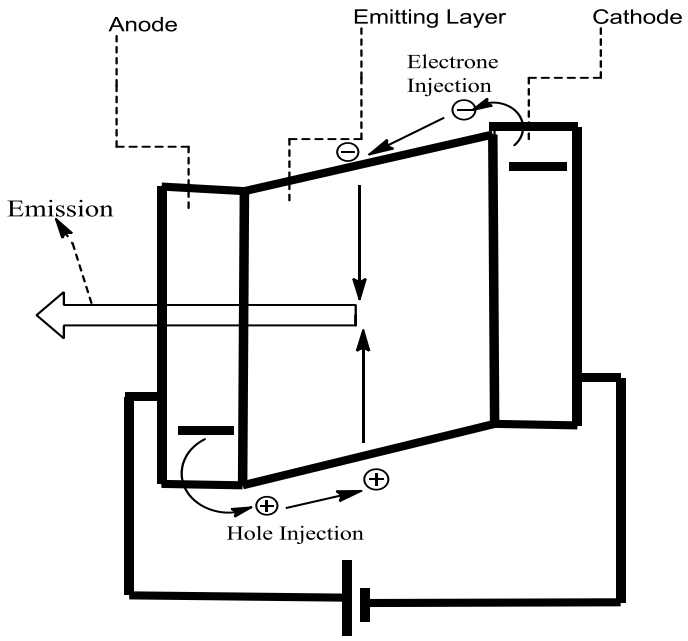

Figure 1.26. Operation principles of organic light emitting diode device[95]

Conjugated polymers such as polyphenylene vinylene (PPV) derivatives and polyfluorenes are used as green and blue electroluminescent materials respectively in organic light emitting diodes.[64,98]

1.10.4 .Photovoltaics

In recent years, organic photovoltaic devices have been developed to provide unique properties that are different from their inorganic based solar cells. These properties are flexibility, low cost fabrication and light weight.[99]

In a solar cell (or organic photovoltaic), the molecules or polymers can absorb photons from sunlight and convert them to electrical energy. In these devices the band gap and the energy positions of HOMO-LUMO energy levels have a large influence in the efficiency of the devices.[100,101,102,95]

The structure of a typical organic photovoltaic device includes donor and acceptor phase sandwiched between anode (usually tin-doped indium oxide - ITO) and metal cathode often with additional layer for instance PEDOT: poly(styrene sulfonic acid (PSS), which is localised between anode and donor phase to improve hole conduction. On the other hand, the pn- heterojunction cell contains double layers of organic thin films, connected with two electrodes, the electrons and holes between p-type and n-type organic semiconductors layers would be played an essential role in device performance.[95] The set-up of pn-heterojunction photovoltaics cell is shown in Figure 1.27.[99]

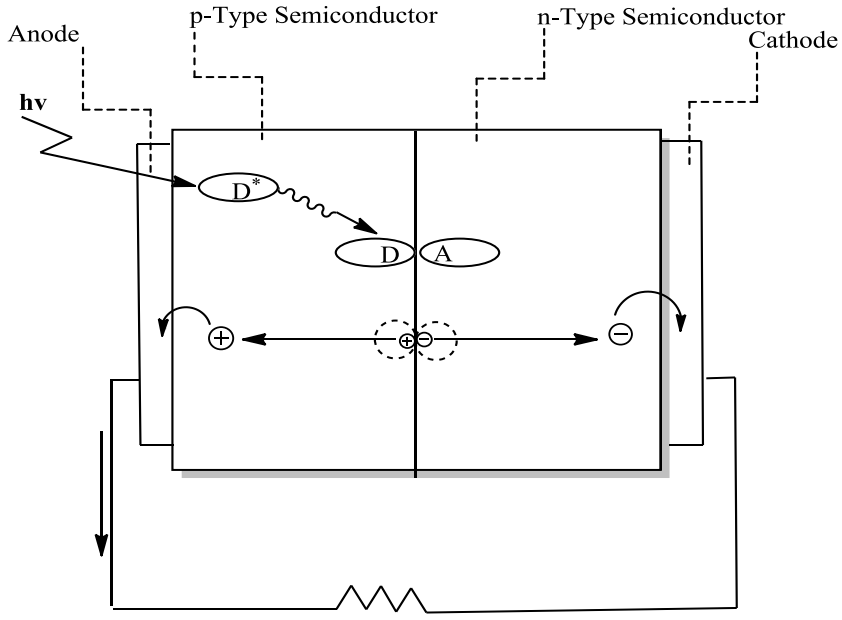

Figure 1.27. Operation principles of pn-heterojunction organic photovoltaics[95]

The operating principle of pn-heterojunction organic photovoltaics can be described through absorption of the sunlight by the conjugated semiconductor material (for instance donor-acceptor polymer) that will lead to generation of an excited state or

exciton. The exciton diffuses to the pn-heterojunction and dissociate, creating electrons and holes in donor and acceptor phases respectively.[102,103,104,95] Electrons and holes will travel away from the donor/acceptor organic interface to their corresponding electrodes resulting in a current flow and generation of electric potential across the device. This process is the opposite to the operation process of organic light emitting diodes device, where the charges injected from anode and cathode form an excited states and then they emit the photons out of OLEDS.[100,95] Semiconductor copolymers materials such as poly(3-hexylthiophene) and tetrathienoanthracene can be used in efficient solar cells due to their exceptional properties for instance broad optical absorption and high charge mobility.[105,106,107]

Chapter 2

2. Thiophene Copolymers with Electroactive Nitrogen Heterocycles.

2.1. Electropolymerisation of a Novel Heteropentalene Mesomeric Betaine: Preparation of a Novel low Band Gap Conjugated Polymer.

2.1.1 Introduction

Many studies have focused on polythiophene and its derivatives. Their synthesis and properties continue to attract considerable interest, particularly when studied as conducting polymers.[30,108,109,110] One of the fundamental challenges of polythiophene chemistry is lowering the band-gap of parent system to prepare more useful materials. This is often achieved by introducing pendant substituents onto the polymer backbone in order to increase the energy of the highest occupied molecular orbital (HOMO) or to reduce the energy of the lowest unoccupied molecular orbital (LUMO). The band-gaps in polythiophenes are typically in the region of 2 eV although some polymers have been reported with significantly lower values. For example, the band-gap of regioregular polyalkylthiophenes was determined as 1.7 eV.[111,112] Larger changes in the band-gap can be achieved by adding stronger electron-donating or withdrawing side groups. Tanaka and Yamashita[113] have prepared and electro-polymerised thienyl-substituted thienothiadiazole[51,113] (compound **1**) giving the polymer (**2),** which has a band gap of E_g = 0.9 eV. The heterocycles of compound (**1)** can be represented by either a dipolar structure **1a** or a non-classical structure **1b**. The parent thienothiadiazole[51,113] system (**3)** is a representative of a Type A heteropentalene mesomeric betaine (HMB) as categorised by Ramsden.[114] Type A HMBs are associated with the general core structure (**4)** in which the heteroatoms X and Y formally contribute a pair of electrons to the

π-system. An important feature of the Type A HMB structure (**4)** is that the HOMO is topologically and energetically similar to a non-bonding molecular orbital (NBMO) whose electron-density distribution is depicted in structure (**5**).[114] Accordingly, the HOMO–LUMO energy separation in these systems is relatively small. In the same way, the thiophene substituted HMB (**1)** is expected to have a relatively small HOMO–LUMO energy separation, which is reflected in the energy gap of the polymer (**2)** and related systems.[115] Other extended Type A HMB derivatives (**6)** and (**7)** have also been prepared and electropolymerised to yield polymers with E_g in the range between 0.5 to 0.8 eV.[116,117,118,119,120] The structures of Type A heterocycles are depicted in Scheme 2.1.

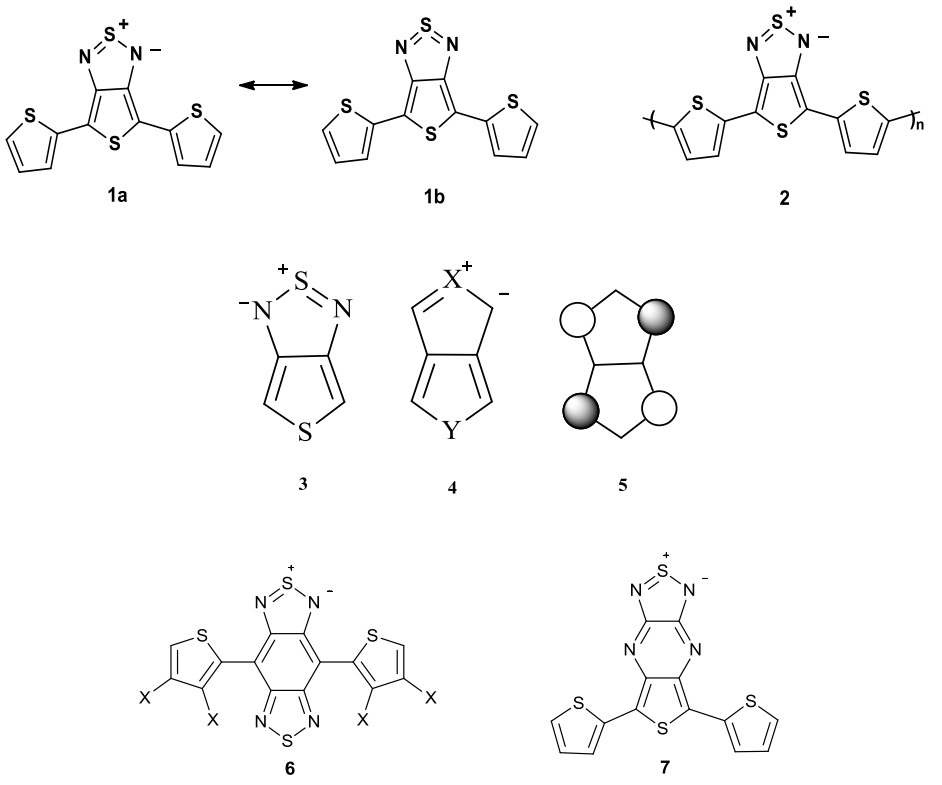

Scheme 2.1. Structures of compounds **1-7**

In Type B HMBs, the heteroatoms X and Y are located at the bridgehead positions as shown in structure (**8**).[114] Type B HMBs are similarly associated with a HOMO that is topologically and energetically similar to a non-bonding molecular orbital and consequently might also provide a convenient core for the construction of novel low band gap polymers.

This chapter describes the electro-polymerisation of the 3,4-ethylenedioxoythiophene (EDOT)-containing monomer (**9**) based upon the core dibenzo-Type B HMB system (**10**). The pendant EDOT group was chosen in view of its widespread recent use in advanced functional π-conjugated systems and its high tendency for promoting electro-polymerisation in multi-aryl monomers.[121] Heterocycle (**10**) was prepared in several steps from ortho-phenylenediamine as reported previously.[122] Bromination[123] of compound (**10**) as described in the literature gave the dibromo-derivative (**11**) as the major product, together with a significant quantity of the tribromo-compound (**12**). This mixture was subjected to a Stille coupling reaction with the stannane (**13**),[124] yielding the required thiophene-containing monomer **9** after purification. The structure of compounds **8** to **13** are illustrated in Scheme 2.2.

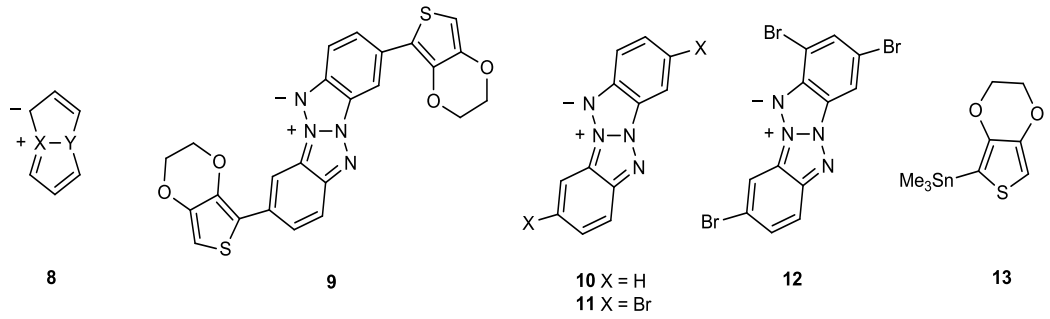

Scheme 2.2.The structure of compounds **8** to **13**

2.1.2 Experimental

The monomer was prepared synthetically by Alexander Gehre, Stephen P. Stanforth (University of Northumbria) and Filipe Vilela (University of Strathclyde). Cyclic voltammetry experiments were carried out using a CH 660A Instruments potentiostat with iR compensation. The electrochemical cells consisted of three electrodes: a glassy carbon electrode, a platinum wire counter electrode and a silver wire as the reference electrode. All cyclic voltammetry experiments were referenced to the Fc/Fc^{+} redox couple as an internal standard. Using dichloromethane as the monomer and monomer-free solvents, Argon gas (Ar) was used to degas solutions for cyclic voltammetry. Monomer concentration is ca. 10^{-4} M, with 0.1 M *n*-Bu_4NPF_6 as supporting electrolyte at a 'scan rate of $0.1Vs^{-1}$.

All electronic absorption spectra were recorded at room temperature on a UNICAM UV 300 spectrophotometer operating between 190 to 1100 nm and between 300 and 1100 nm for the monomer and polymer respectively. For solution spectra, a 1 cm^3 path length quartz cell was used and the baselines were measured before analysis.

2.1.3. Absorption Spectroscopy and Electrochemistry of Monomers

Compound **9** showed two major peaks at 308 and 467 nm, and three shoulders at 345, 442 and 488 nm. The peak at 308 nm is attributed to the n-π* transition of the nitrogen lone pairs, the shoulder at 345 nm corresponds to the lone pairs of the oxygen atom in the EDOT units and the peak at 467nm is due to the π-π* transition from the conjugated portion of the compound.

Compound **11** shows three peaks at 268, 403 and 426 nm. The first peak at 268 nm is the λ_{max} corresponding to the n-π* transition from the lone pairs of the nitrogen atoms. The second peak occurring at 403 nm and the final peak at 426 nm is assigned to π-π* transition from the conjugated part of the compound. The peak at 403 nm in compound **11** has shifted to 442 nm in compound **9,** a difference of 39 nm. The π-π* transition is bathochromically shifted from 426 nm in compound **11** to 467 nm in compound **9**.

The onset of the absorption edge at 529 nm of compound **9** allowed the optical HOMO-LUMO gap (2.35 eV) to be determined; this is lower than that of compound **11** (2.82 eV), which is expected due to the addition of the EDOT units in compound **9**. The absorption spectra of heterocycles **9** and **11** are illustrated in Figure 2.28.

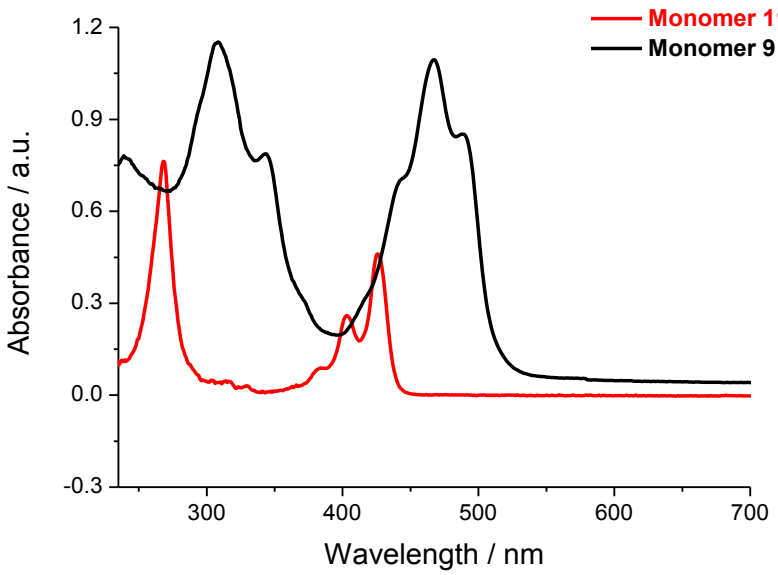

Figure 2.28. UV-Vis spectra of compounds **9** and **11** measured in dichloromethane

The oxidation of dibromo-derivative **11** gives an irreversible peaks at +1.02 and +1.49 V, while the peak maximum for the oxidation of the bis-EDOT compound **9** occurs at a lower oxidation potential (+0.46V). The oxidation gives rise to a radical cation on one or both of the EDOT units as shown in Figure 2.29.

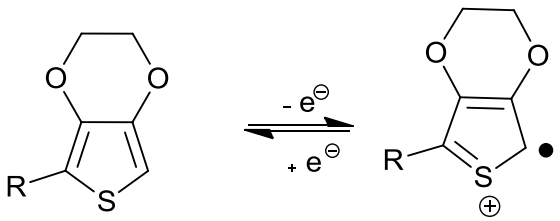

Figure 2. 29. Oxidation of EDOT unit in compound **9**

The reduction of monomer **9** showed an irreversible wave at -2.3V and this has been attributed to reduction of the central core unit producing the dianion (structure**14**), which is isoelectronic with the cyclooctatetraene dianion.

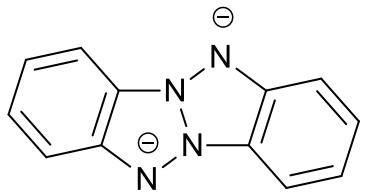

14

Under identical conditions, two irreversible reduction peaks were observed at -1.88 and 2.15V for compound **11**. All oxidation and reduction processes of two monomers are displayed in Figure 2.30.

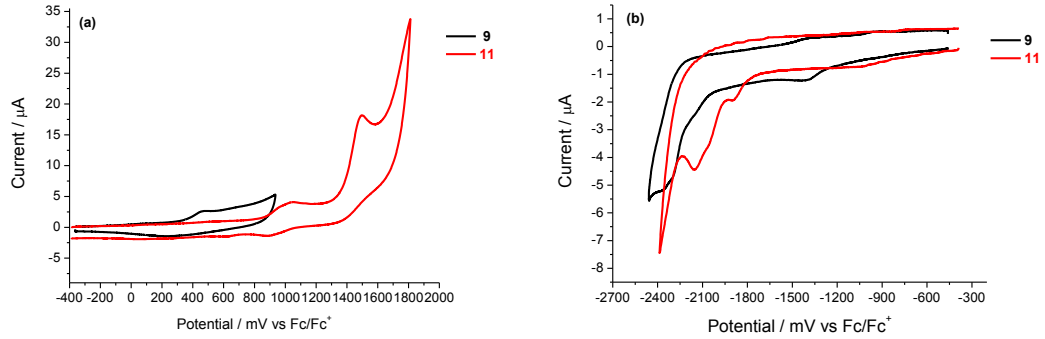

Figure 2. 30. Monomer (**a**) oxidation and (**b**) reduction of monomers **9** and **11** in CH_2Cl_2 using a glassy carbon working electrode, Ag wire reference electrode and Pt counter electrode; the monomer concentration was ca. 10^{-4}M, with 0.1 M $TBAPF_6$ as supporting electrolyte. The scan rate was 0.1V s^{-1}, and the data are referenced to the Fc/Fc^+ redox couple.

The electrochemical HOMO–LUMO gaps of monomer **9** and **11** are 2.34 and 3.28 eV, which were determined from the difference in the onsets of the first oxidation

(+0.32 V) and reduction (-2.02 V) peaks for monomer **9** and from the difference in the onsets of first oxidation (+0.846 V) and reduction (-1.79 V) (using the oxidation and reduction peaks in Figure. 2.30).

HOMO and LUMO levels are calculated by subtracting the onsets from the HOMO of ferrocene, which has an identified value of -4.8 eV. These results are indicative of the electron-donating contribution of the EDOT units, which raise the LUMO and HOMO of compound **9** closer to vacuum. It has to be noted that compound **11** exists as a mixture with the tribromo derivative **12**, but it is anticipated that the redox properties of the two compounds will not differ greatly. All the electrochemical data of both monomers is illustrated in Table 2.1.

Table 2.1. Electrochemical data for monomer **9** and **11** HOMO and LUMO values calculated from the onset of the first peak of the corresponding redox wave and referenced to ferrocene, which has a HOMO of -4.8 eV.

Monomer	Onset oxidation / V	HOMO/eV	Onset reduction / V	LUMO/eV	HOMO-LUMO / eV
9	+0.32	-5.12	-2.02	-2.78	2.34
11	+0.846	-5.64	-1.92	-3.01	2.62

2.1.4. Electropolymerisation of Compound 9

Electropolymerisation of compound **9** was achieved through repetitive cycling over the first oxidation peak of the monomer. Therefore the polymer was grown between -400 to +700 mV referenced to Fc/Fc^{+}. The growth of the polymer was monitored through the increase in current with each cycle and the development of a new peak at lower potential (Figure. 2.31).

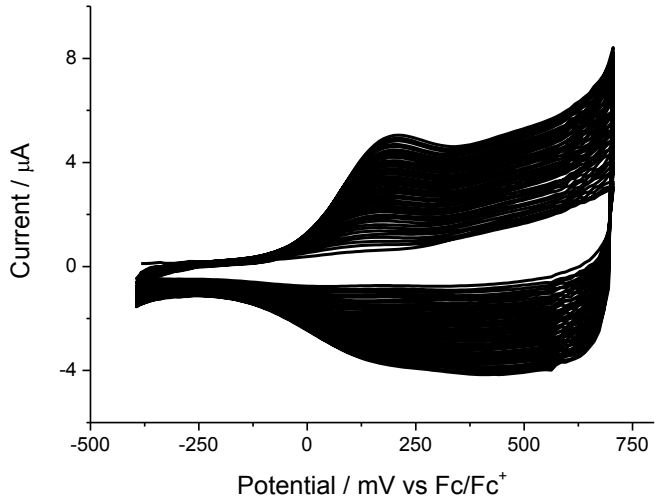

Figure2.31. Polymer growth of compound **9**.The substrate concentration was ca.10^{-4} M and $TBAPF_6$ was used as the supporting electrolyte (0.1 M). A glassy carbon working electrode and scan rate of 100 mV s^{-1} were used**.**

The electrochemical band-gap of poly**9** was determined once again by cyclic voltammetry from the onsets of the oxidation (-0.11 V) and reduction (-2.04 V) waves. The reduction of the polymer showed an irreversible peak at -2.3 eV, which was attributed to the reduction of the central core unit in a similar fashion to the reduction of monomer **9** described above. Both the oxidation and reduction cycles of the polymer are shown in Figure 2.32.

The data allow the electrochemical band gap to be calculated by subtracting the onsets of the first oxidation and reduction peaks from the known HOMO of ferrocene (-4.8 eV) to give a value of 1.93 eV as revealed in Table 2.2.

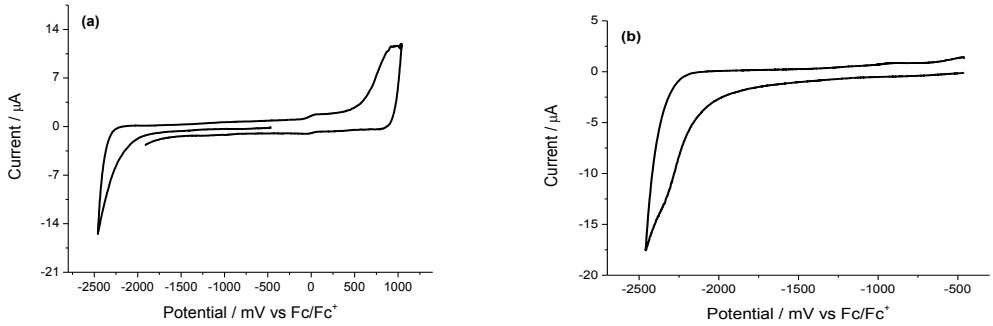

Figure 2.32. (**a**) Cyclic voltammogram and (**b**) reduction of poly**9** using a glassy carbon working electrode in monomer-free CH_2Cl_2 (0.1 M $TBAPF_6$ as supporting electrolyte, at a scan rate of 100mVs^{-1})

Table 2.2. Electrochemical data for poly**9,** HOMO and LUMO values were calculated from the onset of the first peak of the corresponding redox wave and were referenced to ferrocene, which has a HOMO of -4.8 eV.

Polymer	Onset oxidation/V	HOMO/eV	Onset reduction/V	LUMO/eV	HOMO-LUMO/eV
9	-0.11	-4.69	-2.04	-2.76	1.93

2.1.5. Oxidation Stability, Scan Rate and Optical properties of the Polymer

The stability of the polymer towards p-doping was established by repetitive cycling over the oxidation wave of the polymer.

The polymer was found to be reasonably stable under oxidative conditions, with only an 11% decrease in the current response over 80 cycles (Figure. 2.33).

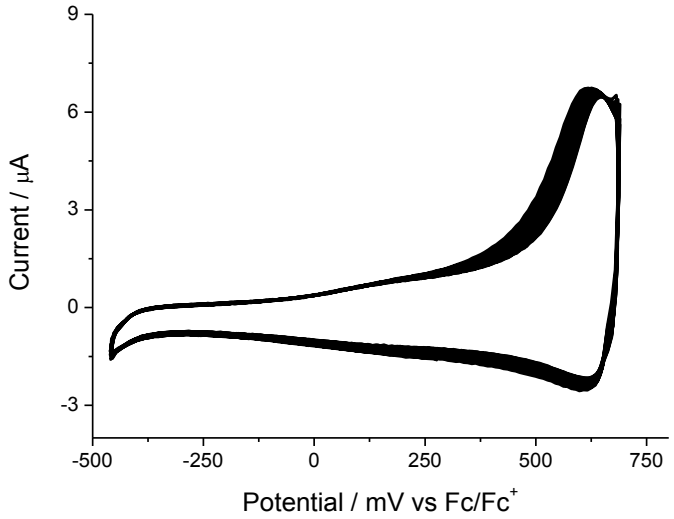

Figure 2. 33. Oxidation stability of poly**9**, in monomer free CH_2Cl_2, at a scan rate of 100mVs^{-1}, over 80 cycles, using glassy carbon working electrode, Ag wire reference electrode and Pt counter electrode and 0.1 M $TBAPF_6$ as supporting electrolyte. The data is referenced to the Fc/Fc^+ redox couple.

To determine if the oxidation of the polymer was limited by diffusion, the oxidation of the polymer was recorded at various scan rates as shown in Figure 2.34. A plot of scan rate versus peak current (Figure 2.35) provides a straight-line graph (R^2 = 0.9977), indicating the presence and stability of the polymer on the working electrode, and it is not diffusion limited.

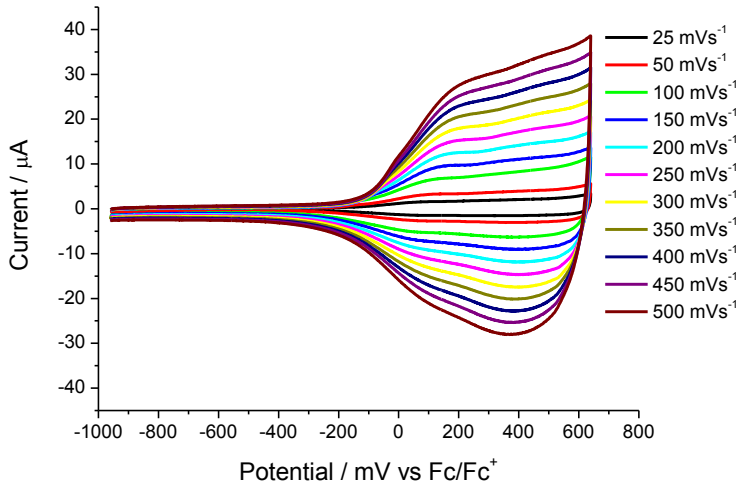

Figure 2.34. Cyclic voltammograms of poly**9** at varying scan rates

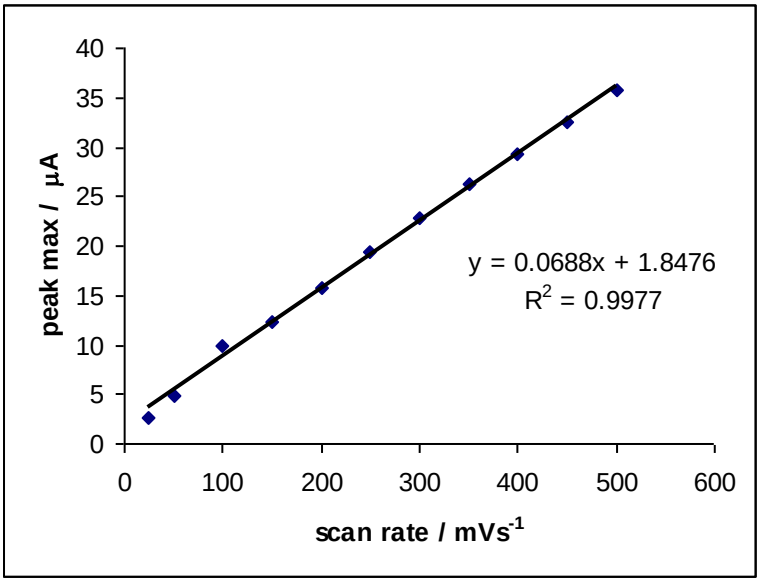

Figure 2.35. Scan rate vs. peak current maxima of poly**9**

The optical band gap of the polymer **9** was determined by growing the polymer onto a piece of ITO-coated glass slide. The polymer was grown by cycling between 0 and 1100 mV vs. Fc/Fc^+ then de-doped between -0.4 and -0.2 V. The spectrum shows an

absorption maxima peak of 547 nm, which corresponds to a shift of 80 nm for the π-π* transition when compared to the monomer (467nm). The absorption spectrum for this polymer is shown in Figure. 2.36. Estimation of the onset of the highest absorption edge after de-doping the polymer (ca. 707 nm) gives an optical band gap of 1.75 eV, that is marginally lower than the band gap determined electrochemically (1.93 eV).

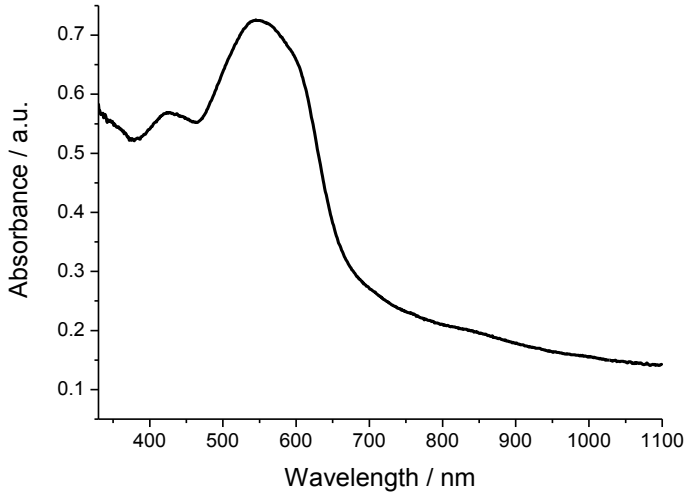

Figure 2.36. Solid state absorption spectrum of poly**9** on ITO-coated glass

2.1.6. UV-vis Spectroelectrochemistry of Polymer 9

To test the p-doping and n-doping effects on poly**9**, oxidation and reduction spectroelectrochemical measurements were performed. The p-doping of the polymer in Figure 2.37a shows that from 200 mV onwards, polarons start to form in the polymer chain and this can be seen from the development of new absorption band between 650 and 900 nm along with a decrease in the π-π* band at 500 nm. At 800 mV a bipolaron band can be observed to form with the formation of a new absorption

band at 900 nm. From 1600 mV onwards, there is a drop in absorbance corresponding to the breakdown of the polymer into soluble material. There is very little change in the reduction features in spectroelectrochemical graph; there is a small increase in the absorption at 700 nm and -1000 mV as shown in Figure 2.37b.

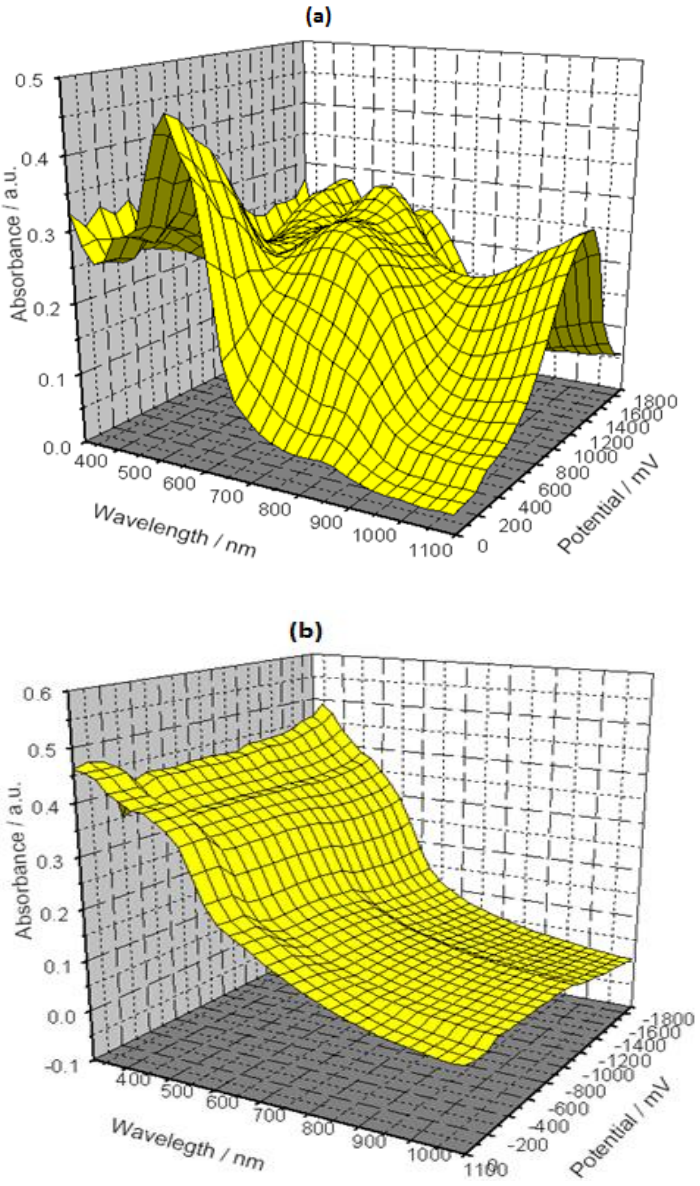

Figure 2.37. UV-vis spectroelectroelectrochemical plot of upon (**a**) p-doping and (**b**) n-doping of poly**9** deposited on ITO glass, Ag wire reference electrode and Pt counter electrode. Experiments were run in monomer-free dichloromethane solution in the presence of $TBAPF_6$ (0.1 M)

2.1.7. Polymer Switching

The ability of the polymer to switch between colour states was tested by measuring the absorbance at 1100 nm and switching the potential between (-0.4 V and +1.3 V) at different rates, as shown in Figure 2.38.

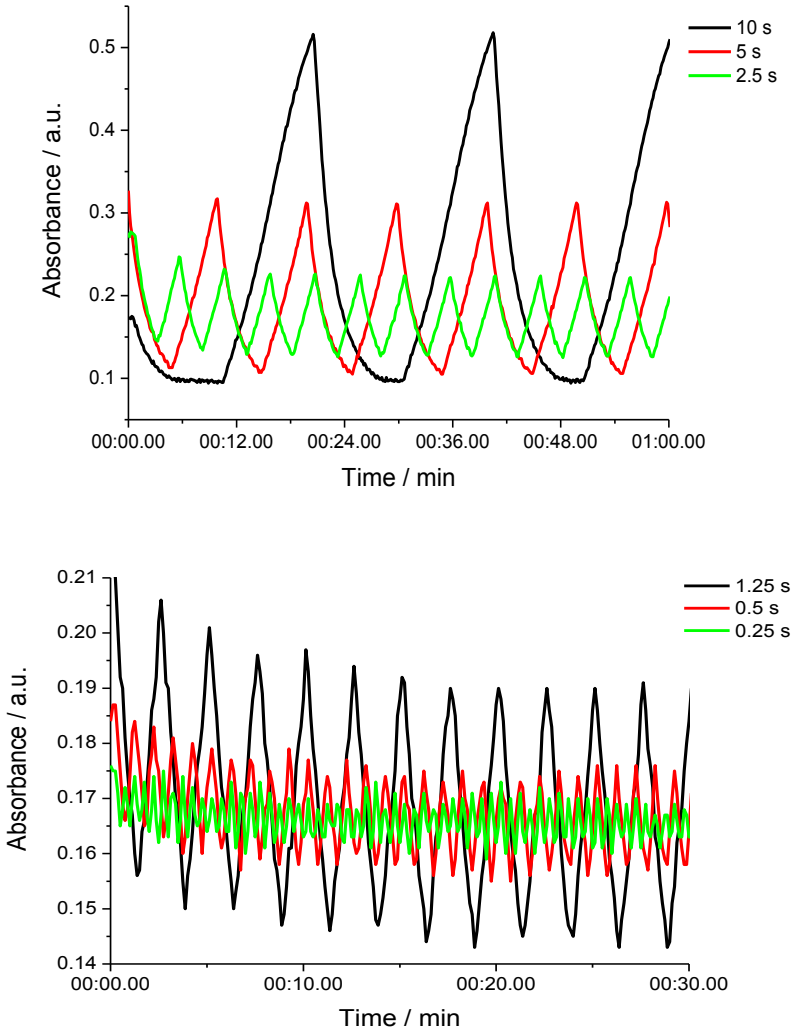

Figure 2.38. Change in optical absorbance at 1100 nm for poly**9** on ITO glass as a function of switching rate between -0.4 and +1.3 V, at varying times: 10, 5, and 2.5 seconds (top graph) and 1.25 ,0.5 , and 0.25 seconds (bottom graph)

The switching times used for these measurements were 10, 5, 2.5, 1.25, 0.5, and 0.25 seconds. The % change in absorbance for each experiment is shown in Table 2.3.

Table 2.3. Switching times and % change in absorbance for poly**9**.

Switching Time / s	**% Change**
10	80.8
5	65.4
2.5	47.15
1.25	21.95
0.5	9.8
0.25	4.0

The switching experiments show that with a 10 second switch there is an 80.8% change in absorbance, which is a slow change but with high contrast. However, with a 0.25 second switching rate, the change in absorbance was only 4.0%.

2.1.8. Other work

A further two compounds (**15** and **16**) have been analysed by UV spectroscopy and cyclic voltammetry and their properties compared with compounds **9** and **11**. Compounds **15** and **16** are similar to the central core units of compounds **9, 10, 11** and **12** as illustrated in Figure 2.39.

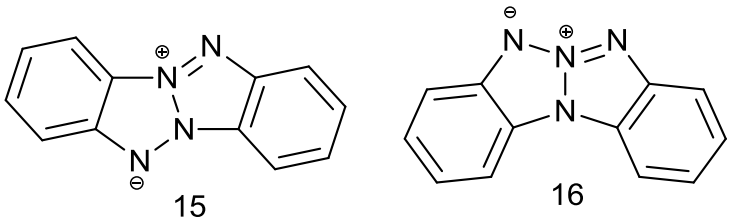

Figure 2.39. Chemical structures of compounds **15** and **16**

2.1.8.1 Absorption Spectroscopy and Electrochemistry of Monomers 15 and 16

The absorption spectrum of compound **15** shows three peaks at 258, 386, and 406 nm. The first peak at 258 nm correspond to the n-π* transition from the lone pairs of the nitrogen atoms. The second peak occurs at 386 nm and the final peak occurs at 406 nm, which is π-π* transition from the conjugation of the compound. However, the absorption spectrum of compound **16** also shows three peaks at 238 nm, 281 nm and 362 nm. These peaks were hyposchromically shifted compared to compound **11**. The optical HOMO-LUMO gaps of compound **15** and **16** were 2.96 and 3.3 eV respectively; these are higher than the values of compound **9** and **11** (2.38 and 2.82 eV respectively). Figure 2.40 shows the absorption spectra of compounds **15** and **16**.

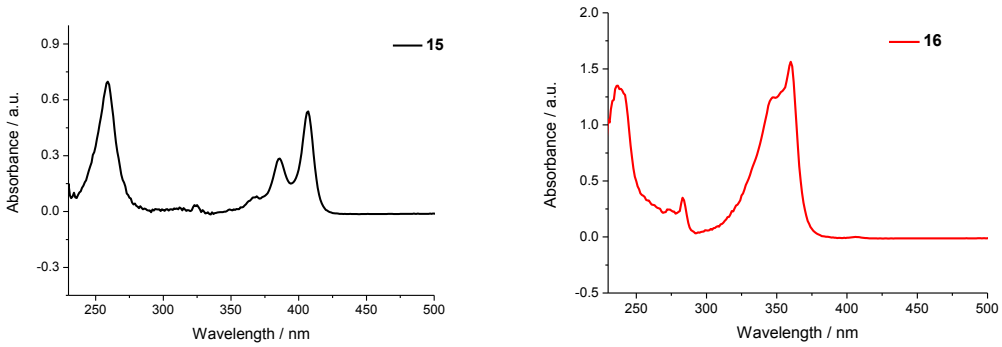

Figure 2.40. UV/ Vis spectra of compound **15** and **16** measured in dichloromethane

Cyclic voltammetry experiments performed on compounds **15** and **16** have shown the oxidation processes are reversible, but the reduction processes of these

compounds were irreversible (Figure 2.41). Compounds **15** and **16** have exhibited reversible oxidation peaks at (+0.78/+0.70V), and (+0.92/+0.86V) respectively, but the reduction processes gave irreversible peaks at -2.17 and -2.43 V for compounds **15** and **16** respectively, which are similar values to the reduction peaks in compounds **9** and **11**.

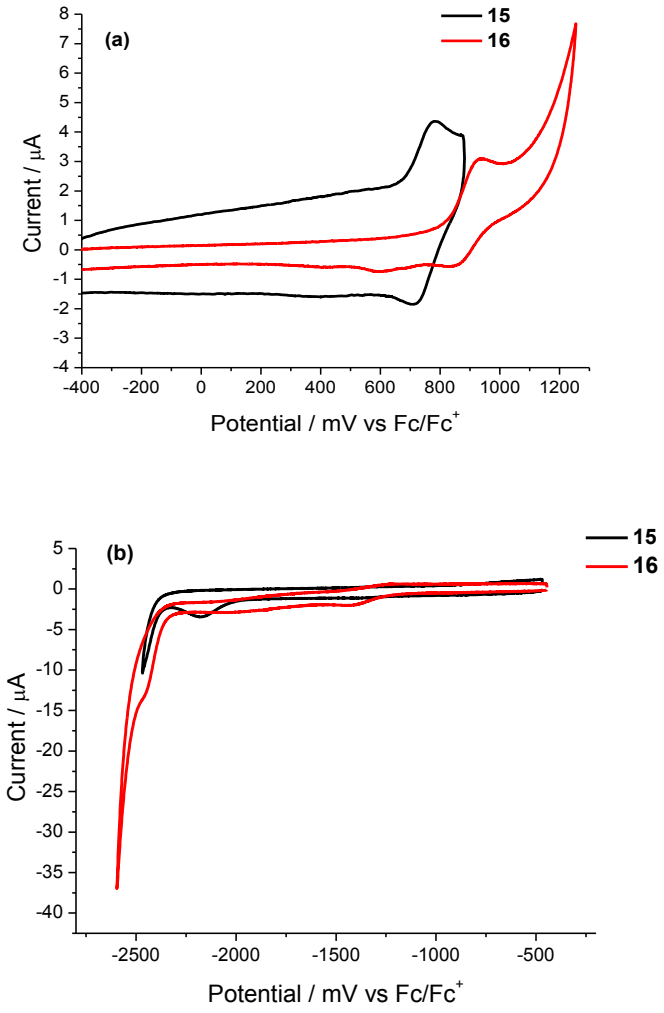

Figure 2.41. (**a**) Oxidation and (**b**) reduction of compound **15** and **16** on a glassy carbon working electrode, Ag wire reference electrode and Pt counter electrode in dichloromethane, concentration ca. 10^{-4} M , with 0.1 M $TBAPF_6$ as supporting electrolyte at a scan rate of $100mVs^{-1}$. The data is referenced to the Fc/Fc^+ redox couple.

The difference between the HOMO and LUMO values gave an electrochemical HOMO-LUMO gap for compounds **15** and **16** that is almost the same value as the optical band gap (2.96 and 3.3 eV respectively), but there are slight differences when compared to the electrochemical HOMO-LUMO gap values of compound **11** and **9** (3.28 eV and 2.34 eV respectively). Table 2.4 represents the electrochemical data for compounds **15** and **16**.

Table 2.4. Electrochemical data for monomer **15** and **16.** HOMO and LUMO values were calculated from the onset of the first peak of the corresponding redox wave and referenced to ferrocene, which has a HOMO of -4.8 eV.

Monomer	Onset oxidation / V	HOMO/eV	Onset reduction / V	LUMO/eV	HOMO-LUMO / eV
15	+0.68	-5.48	-2.0	-2.8	2.68
16	+0.82	-5.62	-2.36	-2.44	3.18

2.1.9. Conclusions

In conclusion the 3,4-ethylenedioxythiophene (EDOT) containing heteropentalene mesomeric betaine (**9**) has been prepared and successfully electropolymerised when coated onto an indium tin oxide (ITO) covered glass slide yielding a polymer with a band-gap of 1.75–1.93 eV. The polymer of compound **9** is reasonably stable to anodic conditions and the scan rate test proves that the polymer is not diffusion limited. Polymer **9** has shown fast switching rate between doped and de-doped states, when a 10 second switch is applied there is an 80.8% change, but a 0.25 second

switching rate afforded only a 4.0% change. This is the first example of a polymer possessing a type B heteropentalene mesomeric betaine core. UV spectroscopy and cyclic voltammetry techniques of monomers **15** and **16** have revealed similar properties when compared to compounds **9** and **11**.

2.2. Electrochemistry, Spectroscopy and Spectroelectrochemistry of novel organic conjugated molecule based on the benzothiadiazole unit.

2.2.1 Introduction

The donor-acceptor structure in conjugated polymers has been introduced in recent years to afford polymers with narrow band gaps that have proven to be highly efficient in several electronic applications.[125,126,127] In addition these groups in the polymer chain have exposed high stability to the doping process with different charge carriers during the redox process that is considered to be one of the main processes to decrease the distance between conduction and valance bands values.[128] The benzothiadiazole (BT) unit is considered to be one of the best units to introduce a low band gap value. When BT is incorporated with electron-rich units, the extension of the conjugated length appears, due to the occurrence of intarmolecular charge transfer (ICT) in donor-acceptor structure.[129] Donor-acceptor polymers exhibited remarkable properties such as fast and reversible colour changing. This has pushed them to be employed in electrochromic applications for instance smart windows and mirrors.[125,130] Wald *et al.* and Toppare *et al.* have investigated donor-acceptor materials based on 3,4-ethylenedioxythiophene (EDOT) and benzothiadiazole (BT) as donor and acceptor units respectively, that exhibited an extremely low band gap and high stability under redox cycling.[50] Therefore these materials are candidates for electrochromic applications owing to their fast switching and reversible change between green and transmissive light blue in the neutral and doped states, respectively.[125,131,54,132] Similarly, Elshehawy *et al* investigated a series

of donor-acceptor alternating conjugated copolymers based on hexylthiophene and BT units. From these studies, broader absorption bands and small highest occupied and lowest unoccupied molecular orbital values have been demonstrated.[129] Thiophene derivatives have been studied previously and they have shown exceptional electroactive behaviour in both monomer and polymer cases. These materials acted as a conducting polymer due to its properties such as low oxidation potential and high conductivity. Therefore, these materials were used in several applications such as organic field effect transistors, light emitting diodes, solar cells and electrochromic materials.[133] Materials based on electron-donor (p-type conjugated polymer) and an electron-acceptor (n-type) were used as an active layer between two electrodes in photovoltaic devices, hence numerous researchers have focused their attention on these materials due to their light weight, large area, low cost and flexibility. An electron-deficient benzothiadiazole (BT) molecule has been attached to electron rich molecules such as thiophene derivatives have unique optical and electrochemical properties due to its conjugated nature.[134,135] These conjugated materials have been synthesised and characterised to enhance the electrochemical and optical properties for instance low HOMO-LUMO gap values, fast switching time, high optical contrast and high conductivity.[133]

In this section of this chapter, three monomers (**17**-**19**) and their polymers have been characterised. Poly**17**, poly**18** and Poly**19** have been prepared electrochemically and studied using electrochemical and spectroelectrochemical experiments. Monomers **17**-**19** contain a benzothiadiazole core, attached to two EDTT, 3-hexylthiophene or bis EDOT units respectively.

2.2.2 Synthesis and experimental

Benzothiadiazole was dibrominated using HBr and Br_2. 3,4-Ethylenedioxythiophene (EDOT), 3,4-ethylenedithiothiophene (EDTT) and 3-hexylthiophene were stannylated *via* lithiation followed by the addition of Me_3SnCl at -78°C. Compounds **17**, **18** and **19** were obtained in good yield (78, 82 and 67% respectively) using microwave assisted Stille cross coupling at 160°C and $Pd(PPh_3)_4$ as the catalyst.[49] All monomers were prepared synthetically by Filipe Vilela and Neil Findlay (University of Strathclyde). The synthesis and structures of the three compounds are illustrated in scheme 2.3 and Figure 2.42.

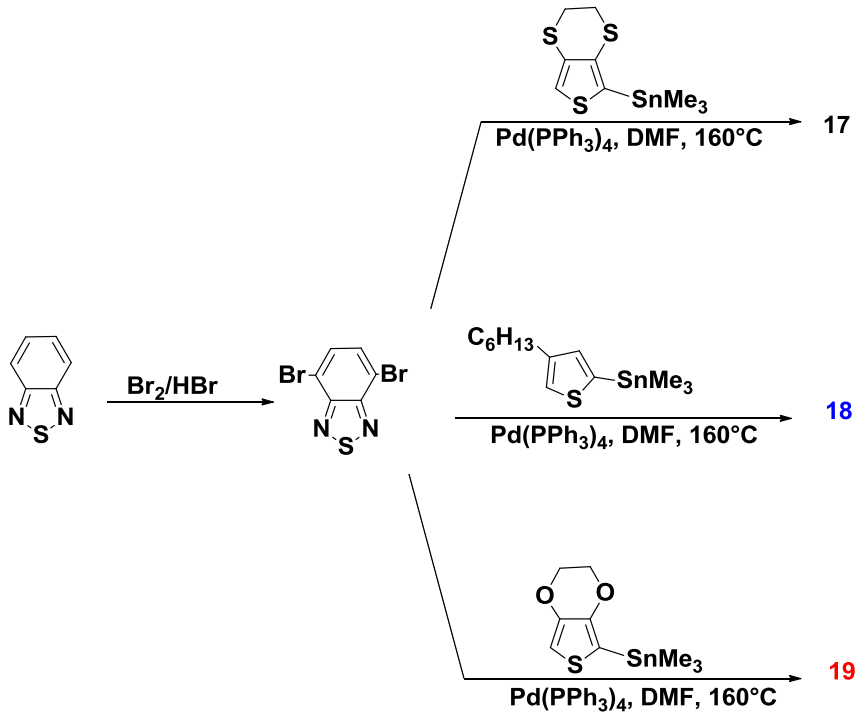

Scheme 2.3. The synthesis of compounds **17** to **19**

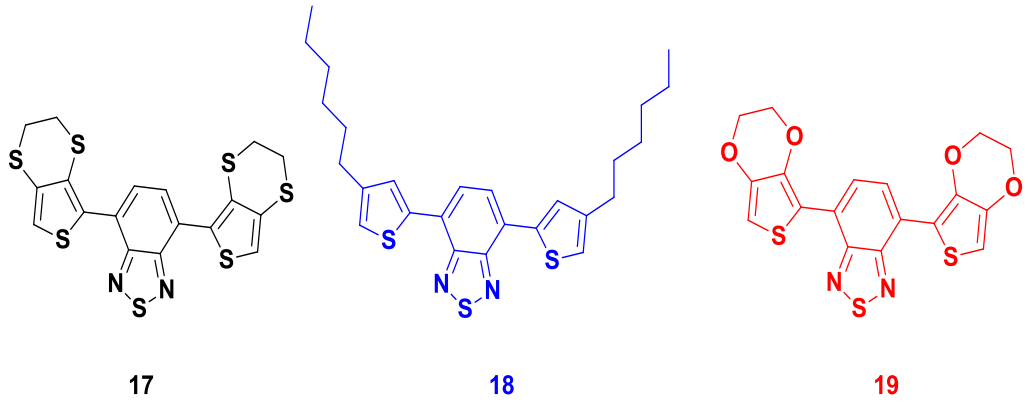

Figure 2.42. Structures of monomer **17**, **18** and **19**

The electrochemical measurements were investigated by cyclic voltammetry using a CH Instruments 660A electrochemical workstation with *iR* compensation and dichloromethane or acetonitrile as the monomer and monomer-free solvents, respectively. Glassy carbon or gold was used as the working electrode, with platinum wire and silver wire as the counter and reference electrode, respectively. All solutions were degassed with (Ar) and contained monomer substrates of ca. 10^{-4} M concentration. Tetrabutylammonium hexafluorophosphate ($TBAPF_6$) 0.1 M was used as the supporting electrolyte. All measurements are referenced against the $E^{1/2}$ of the Fc/Fc^+ redox couple. Spectroelectrochemical on ITO glass slide, spectroscopic and switching experiments have been achieved by using UNICAM UV300 spectrophotometer.

2.2.3 Absorption Spectroscopy and Electrochemistry of Monomers

The absorption spectra of monomers **17, 18** and **19** were performed in acetonitrile solution.

The absorption spectrum exhibits two peaks at 299 and 448 nm for monomer **17** (Figure 2.43). The peak at 299 nm corresponds to the π-π* transition from the conjugated chain of compound and the second peak at 448 nm can be assigned to intramolecular charge transfer interactions (ICT) of the monomer. The absorption spectrum of monomer **18** shows two peaks at 311 and 457 nm, which have shifted bathochromically compared to the peaks in the monomer **17**. For monomer **19**, three peaks at 262, 321, and 492 nm were observed. The highest absorption band at 492 nm exhibits a red shift compared to the peaks in monomers **17** and **18**, which is a arising from the intramolecular chalcogen– chalcogen interactions observed in the crystal structures of the monomers, therefore resulting an extended conjugation form of the two EDOT groups in monomer **19**, and increased number of sulfur atoms in the rest of monomers. [43]

The onset of the absorption edge gives the optical HOMO-LUMO gaps for the monomers. The optical HOMO-LUMO gap values calculated were found to be 2.37, 2.35 and 1.98 eV for monomers **17**, **18** and **19** respectively, indicating that the different side groups in the monomers had a significant effect on the electronic transitions. The higher band gap value in monomer **17** compared to monomer **19** can be attributed to the different effect of EDOT and EDTT units in these monomers.[43]

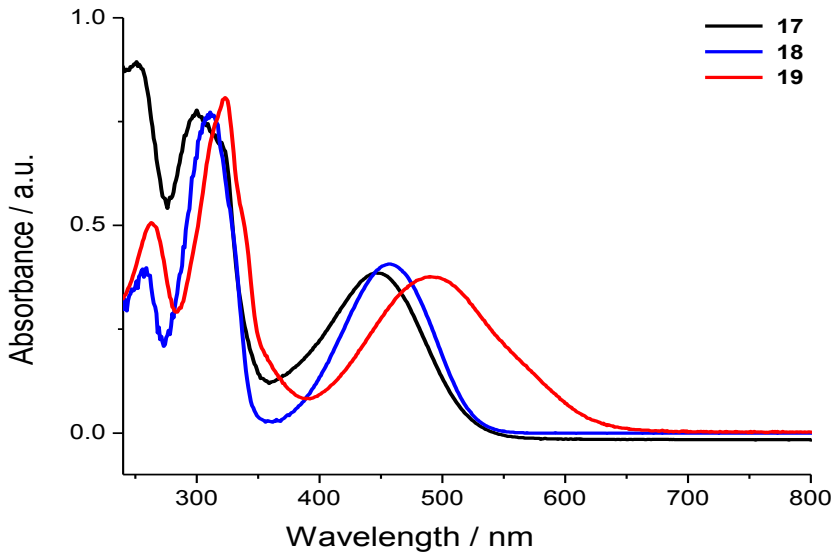

Figure 2.43. Solution state electronic absorption spectrum monomers **17**, **18** and **19** in acetonitrile.

The electrochemistry of the monomers was achieved by cyclic voltammetry in an acetonitrile solution with a gold disc electrode for **17** and in dichloromethane solvent with a glassy carbon working electrode for **18** and **19** (silver wire was used as the reference electrode in all cases). Monomer **17** has two quasi-reversible peaks at +0.58 and +0.75V, these peaks could be attributed to the sequential removal of two electrons from the EDTT units to give a radical cation and then dication (Figure 2.44).

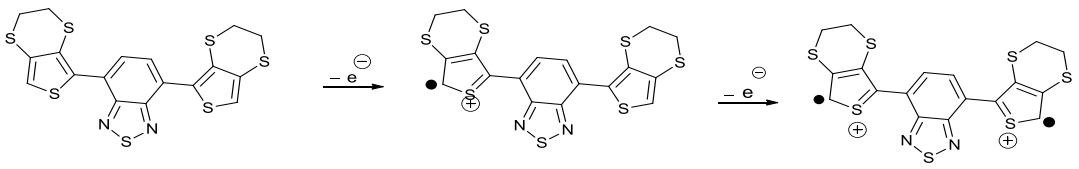

Figure 2. 44. Schematic representation of the electrochemical oxidation for **17**

The oxidation of monomers **18** and **19** shows one quasi reversible peak at +0.71 and +0.46V where each is losing electrons to result in a dication centred on the thiophene and EDOT groups. The difference of oxidation potential values in the monomers is attributed to the different side group structures. Monomer **19** has a lower potential compared with other monomers because of the EDOT units in its structure. The oxidation graphs of the monomers are illustrated in Figure 2.45.

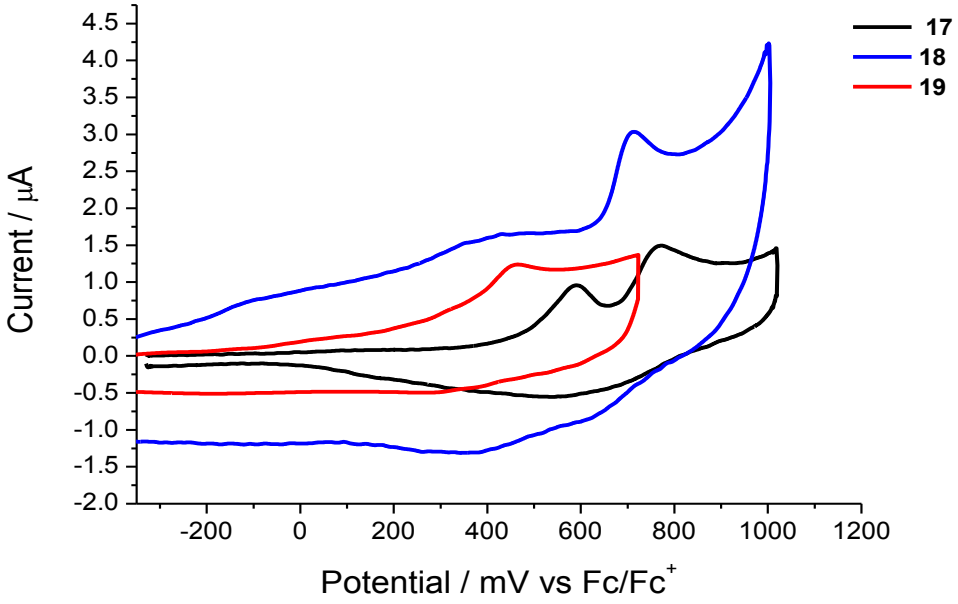

Figure 2.45. Cyclic voltammograms of oxidation of **17**, **18** and **19**, in an acetonitrile solution with a gold disc electrode for **17** and in dichloromethane solvent with a glassy carbon working electrode for **18** and **19,** Ag wire reference electrode and Pt counter electrode, the concentration was ca. 10^{-4} M, with 0.1 M $TBAPF_6$ as supporting electrolyte at a scan rate of $100mVs^{-1}$. The data is referenced to the Fc/Fc^+ redox couple

A reversible reduction of the monomers occurs at -1.75/-1.73 V, -1.76/-1.72 V and -1.81/-1.73 V for monomers **17**, **18** and **19** respectively. Each is attributed to the

reversible reduction of the BT unit since it is known to be an electron acceptor,[136] giving an anion radical. The reduction graphs of the three monomers are illustrated in Figure 2.46.

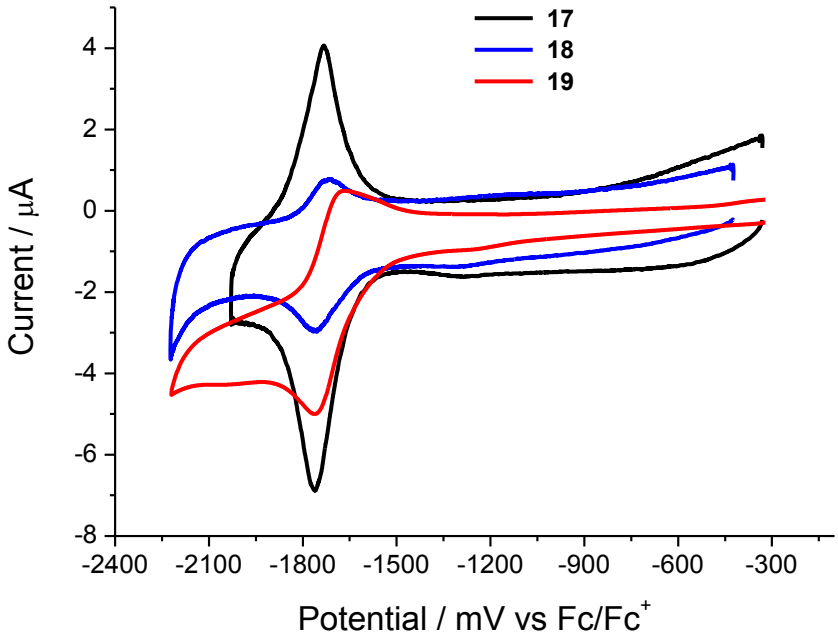

Figure 2.46. Cyclic voltammograms of reduction of **17**, **18** and **19**, in an acetonitrile solution with a gold disc electrode for **17** and in dichloromethane solvent with a glassy carbon working electrode for **18** and **19,** Ag wire reference electrode and Pt counter electrode, the concentration was ca. 10^{-4} M, with 0.1 M $TBAPF_6$ as supporting electrolyte at a scan rate of $100mVs^{-1}$. The data is referenced to the Fc/Fc^+ redox couple

The electrochemical HOMO-LUMO gaps of the three monomers were calculated from the difference in the onsets of the first oxidation and reduction peaks in the Figure 2.47, and then subtracting them from the HOMO of ferrocene. Table 2.5 summarises the data of the three monomers. In the cyclic voltammetry trace of the

three monomers, there is a slight difference in the electrochemical HOMO-LUMO gaps of the three monomers. Monomer **19** has a values of 2.04 eV; this value is lower than the electrochemical HOMO-LUMO gap of monomers **17** and **18** (2.18 and 2.29 eV) respectively. Additionally, there is a difference in the electrochemical HOMO-LUMO gap values when compared with their optical HOMO-LUMO gap values (2.37, 2.35 and 1.98 eV for monomer **17**, **18** and **19**, respectively)

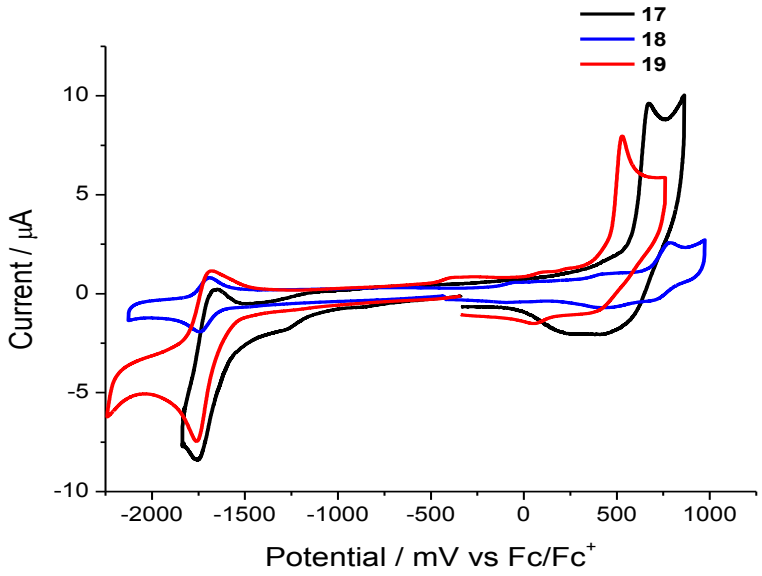

Figure 2.47. Cyclic voltammograms of **17**, **18** and **19** for energy level determination, in an acetonitrile solution with a gold disc electrode for **17** and in dichloromethane solvent with a glassy carbon working electrode for **18** and **19,** Ag wire reference electrode and Pt counter electrode, the concentration was ca. 10^{-4} M, with 0.1 M $TBAPF_6$ as supporting electrolyte at a scan rate of $100mVs^{-1}$. The data is referenced to the Fc/Fc^+ redox couple

Table 2.5 Electrochemical data for compounds **17**, **18** and **19**.

Monomer	Onset oxidation / V	HOMO/eV	Onset reduction / V	LUMO/eV	HOMO-LUMO / eV
17	+0.59	-5.39	-1.60	-3.2	2.18
18	+0.67	-5.47	-1.62	-3.18	2.29
19	+0.47	-5.27	-1.57	-3.23	2.04

HOMO and LUMO values are calculated from the onset of the first peak of the corresponding redox wave and referenced to ferrocene, which has a HOMO of -4.8 eV.

2.2.4 Electrochemistry of the Polymers

The three monomers were polymerised electrochemically by repetitive cycling over both redox-active peaks. All the monomers polymerised and the growth of their polymers is represented in Figure 2.48.

The electropolymerisation process of all three compounds was probed in monomer-free acetonitrile and over 100 scans with the same conditions as illustrated in Figure 2.48. Poly**18** exhibited slow growth on the electrode surface due to the presence of the solubilising hexyl chains.

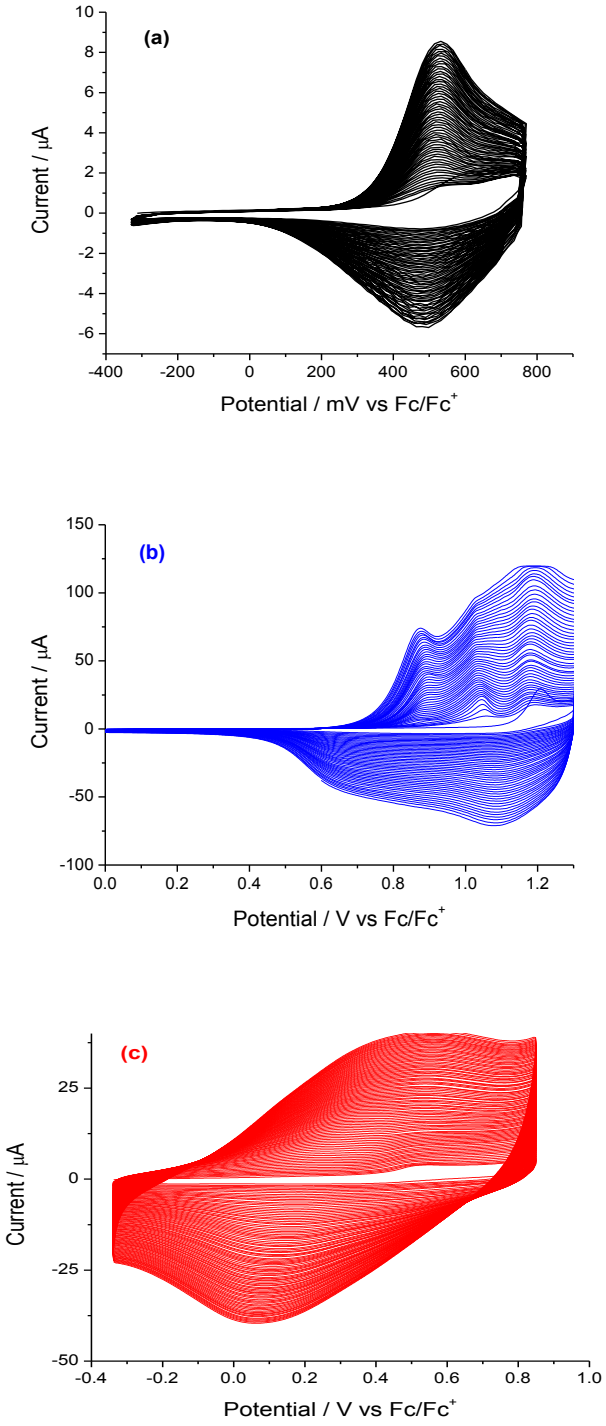

Figure 2.48. Electrochemical growth of (a) poly**17**, (b) poly**18** and (c) poly**19**, using gold for poly**17** and glassy carbon for poly**18** and poly**19** as working electrodes, Ag wire reference electrode and Pt counter electrode in monomer-free MeCN (0.1 M $TBAPF_6$ as supporting electrolyte). At a scan rate of $0.1Vs^{-1}$, over 100 cycles.

Quasi reversible oxidation waves have appeared in all three polymer cases at +0.57, +0.59 and +0.11V for poly**17**, poly**18** and poly**19** respectively, as shown in Figure 2.49a. The oxidation peak at +0.57 V in poly**17** is quite narrow for a conjugated polymer, which is constrained within the bis(EDTT) repeat units of the polymer. The other oxidation waves of poly**18** and poly**19** represent a localised oxidation of the hexyl thiophene or EDOT side groups. The oxidation potential of the three polymers is observed at different values, where poly **19** has given lower oxidation potential than the other polymers that can be attributed to the effect of the interchain interactions (O···S contact) between the EDOT units[43] in poly**19** and the (S···S) contact in rest of polymers. The polymer reduction peaks are illustrated in Figure 2.49b; however in each case, the polymers give an almost identical reversible reduction wave at -1.70 /-1.60 V, -1.58 /-1.42V and -1.94/-1.69V for poly**17**, poly**18** and poly**19** respectively. This can be ascribed to the addition of the electrons to the benzothiadiazole units.[136]

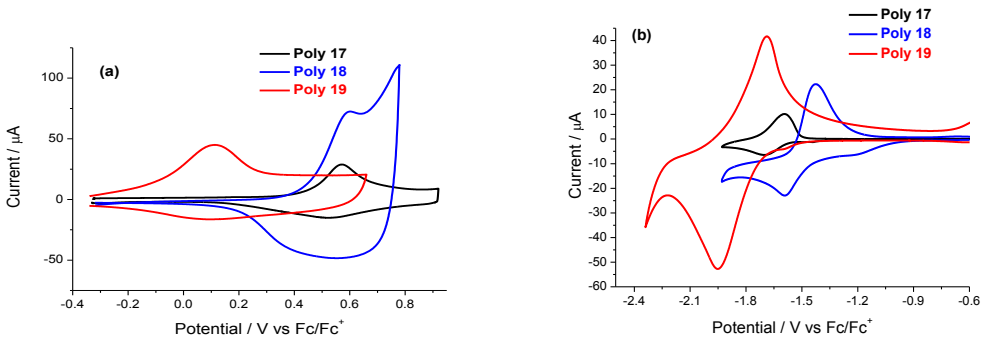

Figure 2.49. Cyclic voltammograms for (**a**) oxidation and (**b**) reduction of poly**17**, poly**18** and poly**19**

The electrochemical band gaps of the polymers were calculated from the difference in the onset of the first oxidation and reduction peaks from the full cycle for energy level determination (Figure 2.49 a and b), and HOMO and LUMO levels are calculated by subtracting the onsets from the HOMO of ferrocene. The difference between the HOMO and LUMO values of the polymers gave an electrochemical HOMO-LUMO gaps are 1.70, 1.80 and 1.41 eV for poly**17**, poly**18** and poly**19** respectively. The data are shown in Table 2.6.

Table 2.6 Electrochemical data for polymers **17**, **18** and **19**.

Polymer	E_{1ox}/V	E_{1red}/V	HOMO/eV	LUMO/eV	E_g/eV
17	+0.57	-1.70 / -1.60	-5.22	-3.52	1.70
18	+0.59	-1.58 / -1.42	-5.25	-3.37	1.80
19	+0.11	-1.94/-1.69	-4.51	-3.10	1.41

HOMO and LUMO values are calculated from the onset of the first peak of the corresponding redox wave and referenced to ferrocene, which has a HOMO of -4.8 eV.

2.2.5. Scan Rate and Stability of the Polymers

The oxidation stability of the three polymers (Figure 2.50) on the working electrode surface was measured on gold electrode for poly**17** and on glassy carbon electrode for poly**18** and poly**19**, in monomer-free acetonitrile solution by repetitive cycling over the first redox active peak. Comparing all three, it is clear that poly**19** is more stable to anodic conditions, with only a 6% decrease in the current response over 140 segments compared to a 12% decrease for Poly**17** and 16% decrease for poly**18**.

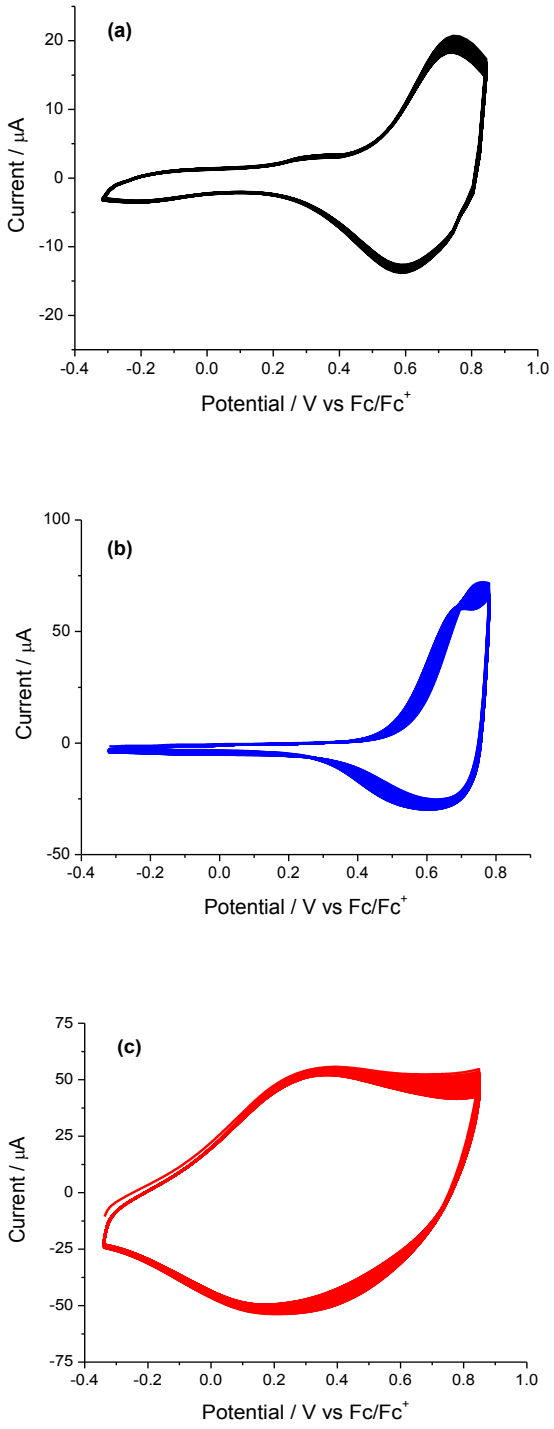

Figure2.50. Oxidation stability of polymers (**a**) poly**17**, (**b**) poly**18** and (**c**) poly**19** in monomer-free acetonitrile solution

A peak maximum shifts to higher values in figure 2.51 after each run in cyclic voltammograms of three polymers at different scan rates.

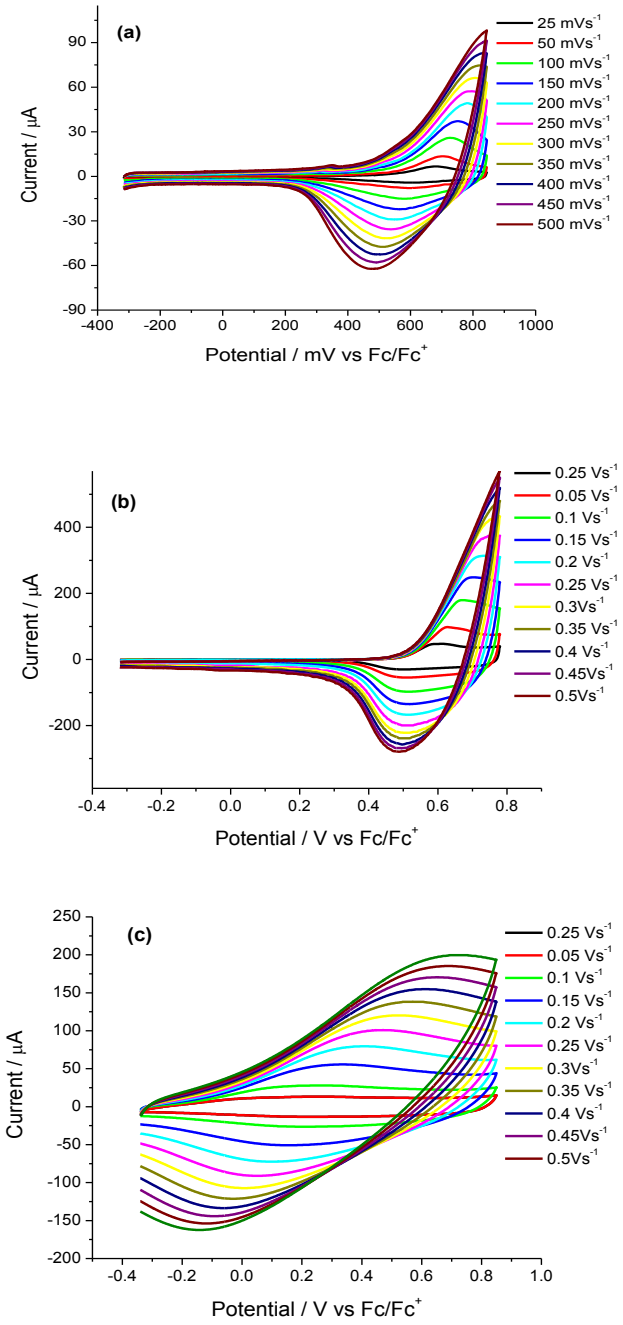

Figure2.51. Cyclic voltammograms of (**a**) poly**17**, (**b**) poly**18** and (**c**) poly**19** with varying scan rates

A linear relationship between scan rate and current peak maxima was observed for all three polymers (Figure 2.52), with correlation factor values of 0.9906, 0.9641 and 0.9984 for poly**17**, poly**18** and poly**19**, respectively. This behaviour proves that the charge transport process is not diffusion limited**.**

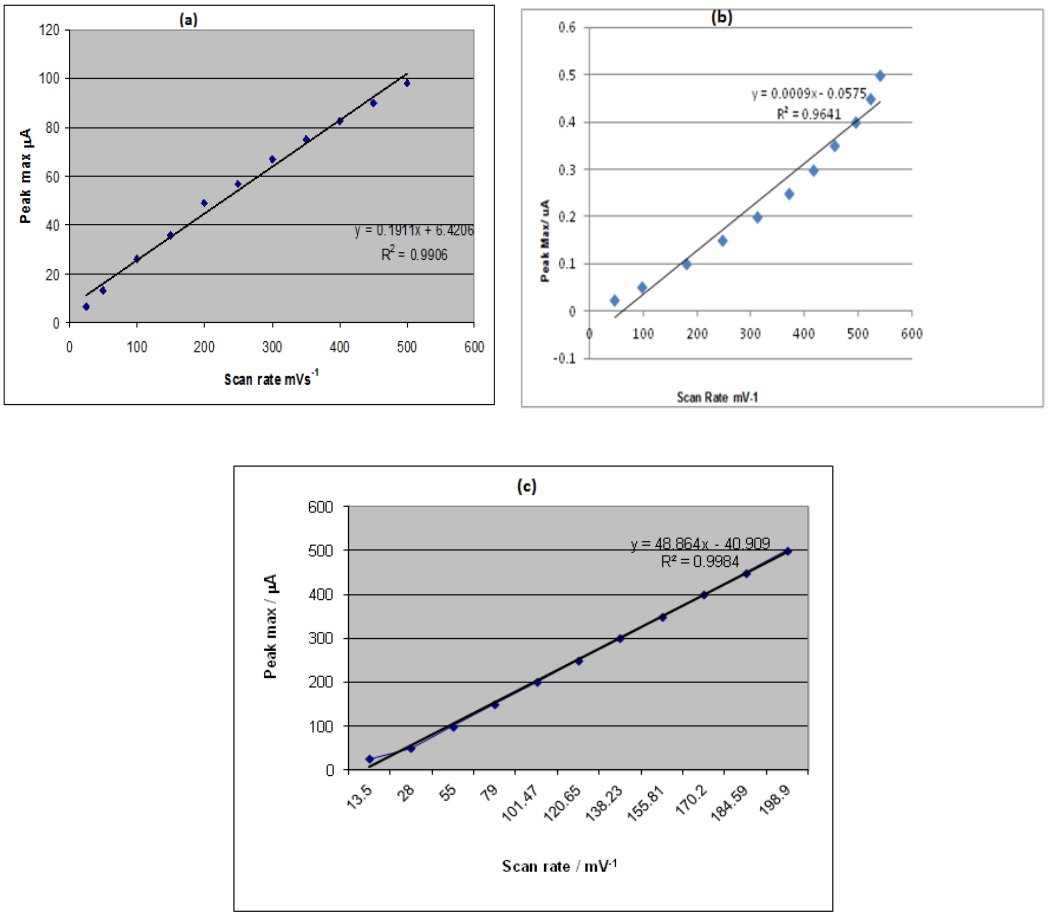

Figure 2. 52. Scan rate vs. peak current maxima of (**a**) poly**17**, (**b**) poly**18** and (**c**) poly**19**.

The three polymers were prepared from a monomer solution with acetonitrile as solvent. During this experiment, the polymers were grown by repetitive cycling and then de-doped between -0.4 to -0.2 V for poly**17** and poly**18** whilst between -0.7 and -0.5 V for poly**19**.

The spectra of the three polymers show a λ_{max} peak at 528, 627 and 743 nm for poly**17,** poly**18** and poly**19** respectively (Figure 2.53). The polymers display several colours in both doped and de-doped states. Poly**17** exhibits a dark red in the neutral state and brown in the oxidised state, whereas, poly**18** changes between light and dark violet in doped and de-doped states respectively. However, poly**19** appears light blue in the doped state and green in the de-doped state. The absorption peak (528 nm) in poly**17** shows **a** hypsochromic shift compared to poly**18** and poly**19**, owing to the effect of steric hindrance from (S···S contact) of the neighbouring unit in poly**17**. Therefore, this effect will decrease the degree of planarity throughout this polymer, whereas, distortion effect from (S···S contact) disappeared in poly**19**,[43] which is exhibited broad absorption at 743 nm.

The onsets of the longest wavelength absorption edge of three polymers exhibited optical band gaps of 1.76 eV for poly**17**, 1.57 eV for poly**18** and 1.26 eV for poly**19**. However there is a significant difference between these optical band gap values of the polymers and their electrochemical band gaps.

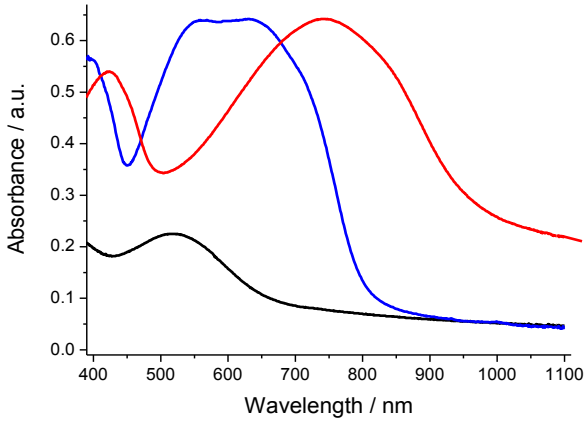

Figure 2.53. Electronic absorption spectra of poly**17**, poly**18** and poly**19**.The spectra were recorded as a thin film deposited on ITO-coated glass

2.2.6. UV-vis Spectroelectrochemistry

UV-vis spectroelectrochemical measurements were performed on films grown on ITO glass and then de-doped. The spectroelectrochemical plots for the oxidation of poly**17**, poly**18** and poly**19** are shown in Figure 2.54. UV-vis spectroelectrochemistry was carried out for the polymers under oxidative conditions, however all three polymers show similar doping processes. Increasing oxidation leads to a decrease in the intensity of the π-π* transition at 450, 550 and 740 nm for poly**17**, poly**18** and poly**19**, respectively. For poly**17**, new absorption waves were generated at longer wavelengths (between 500 and 1000 nm) beyond 950 mV. This behaviour is attributed to the formation of polarons in the conjugated chain. The signatures for polarons for poly**18** and poly**19** appeared as broad absorption peaks ranging from between 860 to 1000 nm. In poly**19**, following the polaron formation, there is a new peak at +0.3 V that possibly corresponds to a localised bipolaron which features as a

broad band in the near IR region. After +1.7 V there is a drop in absorbance in the three polymers that corresponds to the breakdown of the polymer into the solution.

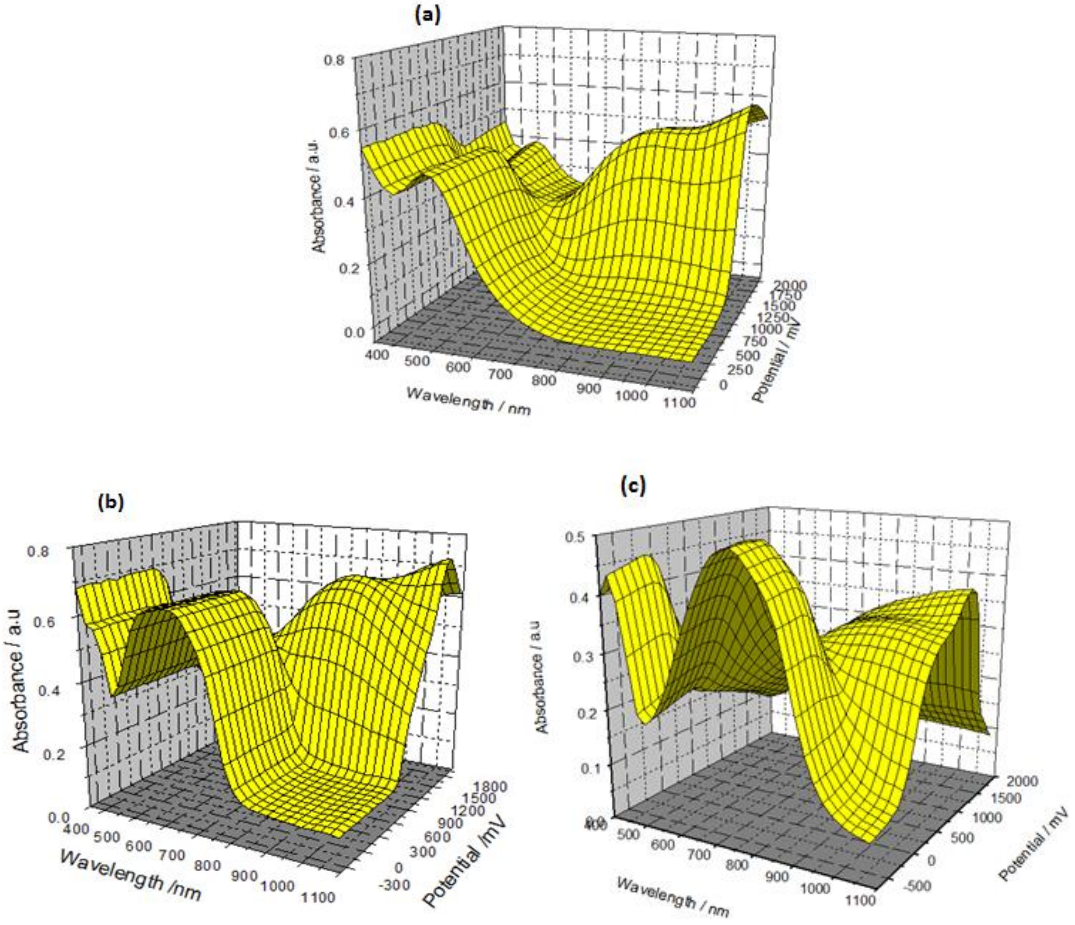

Figure 2.54. Absorption spectroelectrochemical plots of oxidation of (**a**) poly**17**, (**b**) poly**18**, (**c**) poly**19** Potentials are given vs. Ag wire reference electrode

Reduction spectroelectrochemistry measurements were performed for poly**17** and poly**19** **(**Figure 2.55). During n-doping, poly**17** does not show any significant change, whereas for poly**19** considerable change was clear, with high broadening of the absorbance between 600 and 900 nm, in the range between -0.1 to -2.0 V, with a

corresponding decrease in the π-π* transition at 521 nm. Therefore these effects can be ascribed to the n-doping of the BT units.

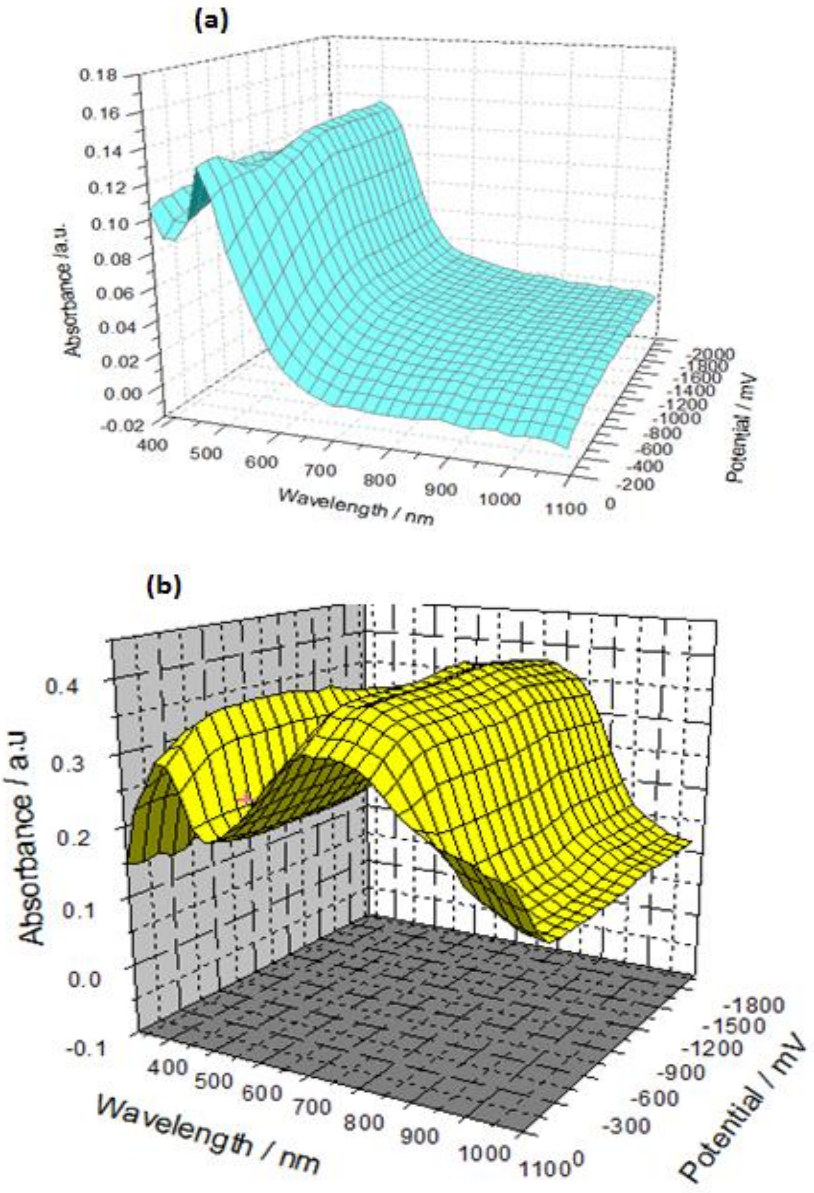

Figure 2.55. UV-vis spectroelectrochemical plot for the reduction of (**a**) poly**17** and (**b**) poly**19** deposited on ITO glass. Potentials are given *vs.* Ag wire reference electrode

2.2.7. Polymer Switching

The rate of the change in the transmittance is a reflection of the ability of the polymers to switch between two colour states.

This was investigated by monitoring the absorption between different potentials and at a specific wavelength, since the potentials will alter the polymer between the neutral and oxidised states. All three polymers were grown on ITO slides and then de-doped in monomer-free acetonitrile.

The polymers were investigated by testing the absorption at 847 nm for poly**17** and at 748 nm for poly**18** and poly**19**. The potentials were switched between -0.4 V and 1.3 V for poly**17** and poly**18** and between -0.7 V and 1.5 V for poly**19**. The switching time experiments were determined at 10, 5, 2.5, 1.25, 0.5, and 0.25 seconds. Figures 2.56, 2.57 and 2.58 illustrate the changes in absorbance of all three polymers.

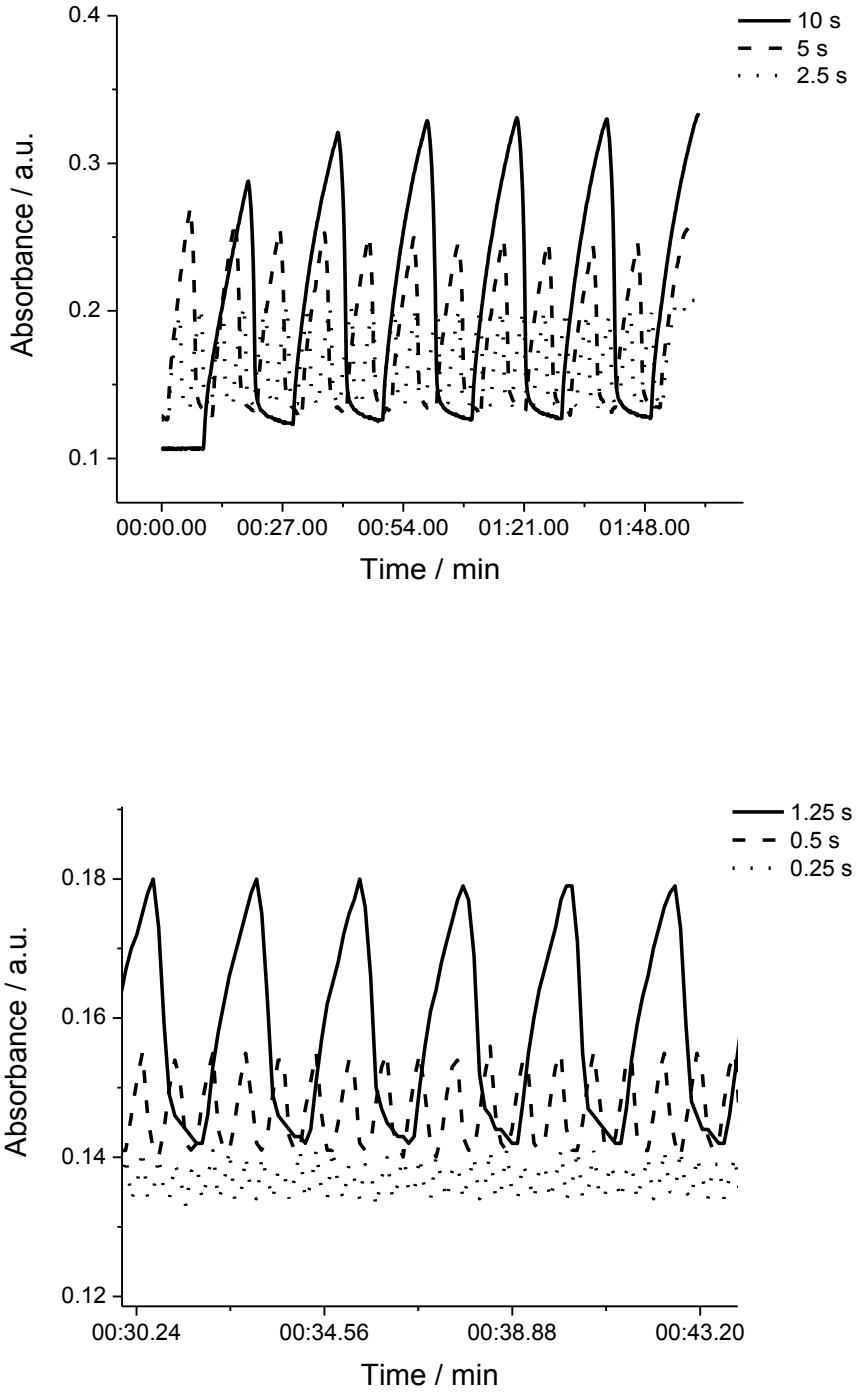

Figure 2. 56. Change in optical absorbance for poly**17**. On ITO glass as function of switching rate between -0.4 and 1.3 V and was monitored at 847 nm.

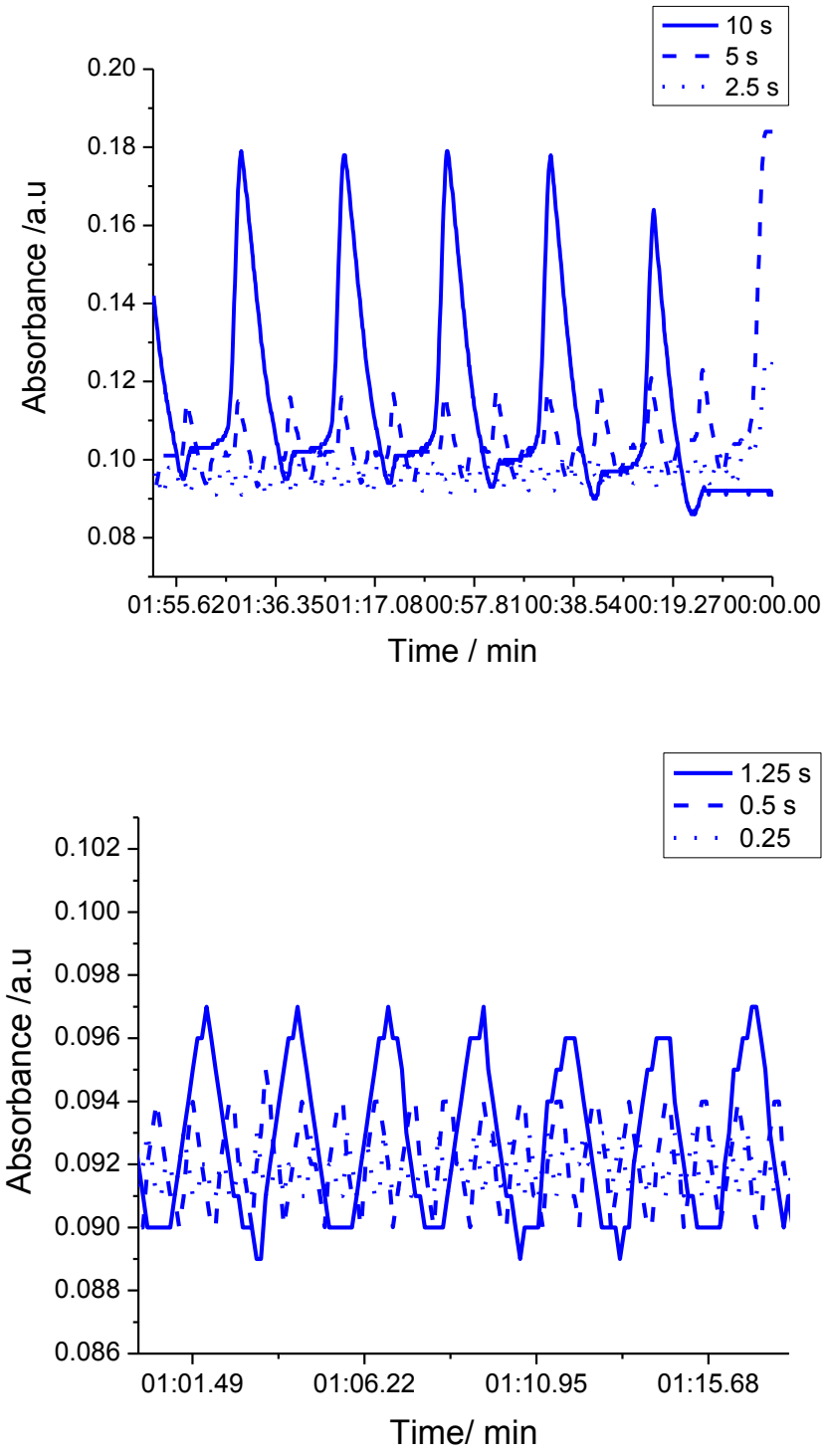

Figure 2. 57. Change in optical absorbance for poly**18**. On ITO glass as function of switching rate between -0.7 V and 1.5 V and was monitored at 748 nm.

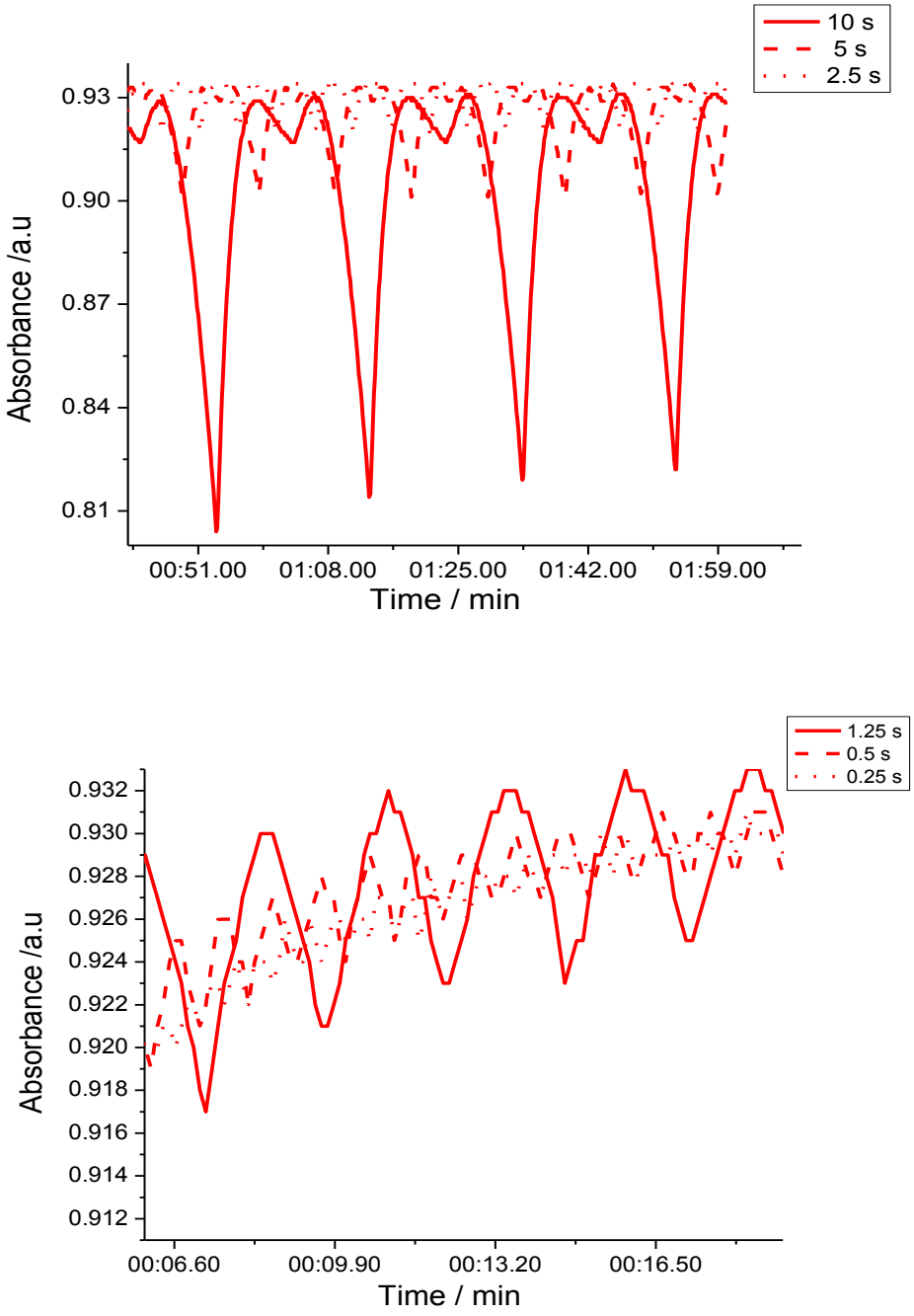

Figure 2. 58. Change in optical absorbance for poly**19**. On ITO glass as function of switching rate between -0.7 V and 1.5 V and was monitored at 748 nm.

Reasonable switching rates were observed for all three polymers; however a greater change was shown for poly**19** compared to the other two polymers (Table 2.7).

This is expected from PEDOT derivatives.[136] The percentage change in absorption in poly**19** was a 99.8 % change in absorbance, which is a slow change with high contrast. With a 0.25 second switching rate, the change in absorbance was 26.4 %. Poly**18** gives faster switching times than poly**17,** where the percentage change with a 10 second switch is 62.5% and 46.9% for poly**17** and poly**18** respectively and with 0.25 seconds is 4.2% for poly**17** and 3.22% for poly**18**.

Table 2.7. Switching times and % change in absorbance.

Switching time /s	% Change Poly**17**	% Change Poly**18**	% Change Poly**19**
10	62.5	46.9	99.8
5	48	20	95.5
2.5	31.6	9	93.4
1.25	22	8.24	91
0.5	6.6	5.31	62
0.25	4.2	3.22	26.4

2.2.8 Conclusions

The monomers and their subsequent polymers have been synthesised and characterised by cyclic voltammetry, UV-vis absorption spectroscopy, UV-vis spectroelectrochemistry, and switching times.

The three monomers contain a benzothiadiazole unit as an electron acceptor and EDTT, 3-hexylthiophene or EDOT units as donor components for monomers **17**, **18**

and **19**, respectively. All three monomers show differences in oxidation and reduction potentials. The monomers were polymerised under oxidative conditions, however, monomer **18** deposits slowly on the electrode under the conditions used because of its high solubility due its side groups. The band gap calculations show similar values between the optical and electrochemical band gaps in monomers **18** and **19**, with a slight difference in monomer **17**. These polymers show electrochromic behaviour with a visible colour change between the neutral and oxidation states. Poly**19** gives a lower optical and electrochemical band gap value when compared to poly**17**, owing to the neighbouring units in this polymer suffering from chalcogen---chalcogen steric interactions between the sulfur atoms (S···S contact). However, in poly**19**, the O···S interactions provide a degree of rigidification and therefore increase the effective conjugated length.[43] Poly**17** and poly**19** exhibited high stability toward repetitive oxidation cycles, whereas poly**18** was less stable on the electrode surface due to the presence of the solubilising hexyl chains. The polymers showed potential for use as electrochromic films.

2.3. Electropolymerisable Viologen Based Acceptors

2.3.1 Introduction

There is extensive interest in the conjugated polymer (PEDOT) and its derivatives for use in organic semiconductor electronic devices such as solar cell, light emitting diodes and electrochromic applications.[137,138] For example, PEDOT and its derivatives have traditionally been used in electrochromic applications due to their high electrochromic contrast, fast switching time, high stability, low band gap and ease of colour changing from dark blue to transparent blue between the neutral and doped states, respectively.[43] In recent years, PEDOT and its derivatives have been incorporated into electrochromic element (viologens) in the side chains of PEDOT to improving their properties such as enhancement of the electrochromic contrast.[137,139,140] Viologens have been investigated in electrochemistry and spectroelectrochemistry studies because they have their own distinguishing colours and reversible change in its three different oxidation states.[138] They have also been used as electron acceptors in charge-transfer complexes.[141] Therefore a cooperative electrochromic action has resulted through electrochemical studies on these materials from both PEDOT and viologen portions.[139,141] PEDOT-based small molecules such as viologen show both p-type (hole) and n-type (electron) conductivity and high absorbance in the visible region. This behaviour with suitable properties has promoted these materials as strong candidates for use in organic photovoltaics devices.[138]

In this section of this chapter, the properties of monomers (**20**-**24**) and their polymers were investigated using cyclic voltammetry and UV/Vis absorption spectroscopy. Spectroelectrochemical measurements revealed that the polymers showed electrochromic behaviour with switching time measurements. All five compounds contain a heterocyclic organic compound (phenanthroline) as the core unit that has been attached to two EDOT units in compounds **20** and **21**, or with a bithiophene unit attached to two EDOT units in compounds **22**, **23** and **24**. The structures of these compounds are shown in Figure 2.59, and scheme 2.4 depicts the synthesis of these compounds.

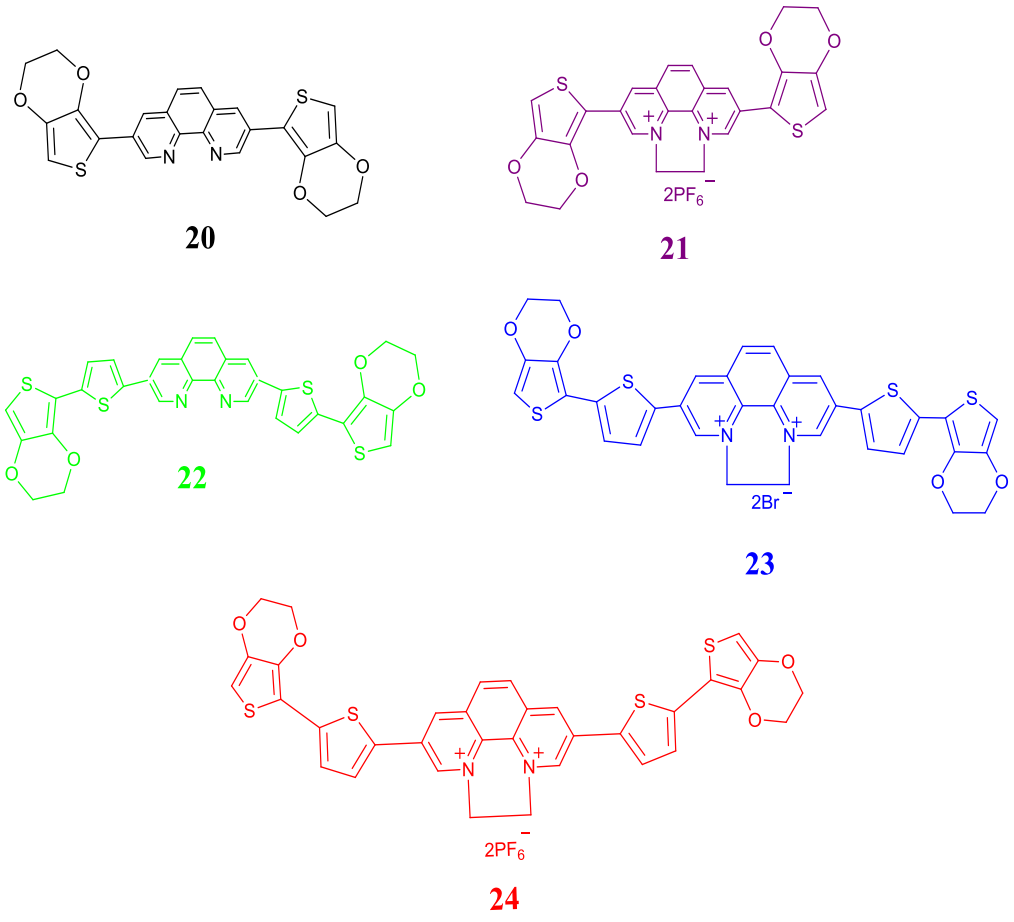

Figure 2. 59. Structures of monomer **20**, **21**, **22**, **23** and **24**

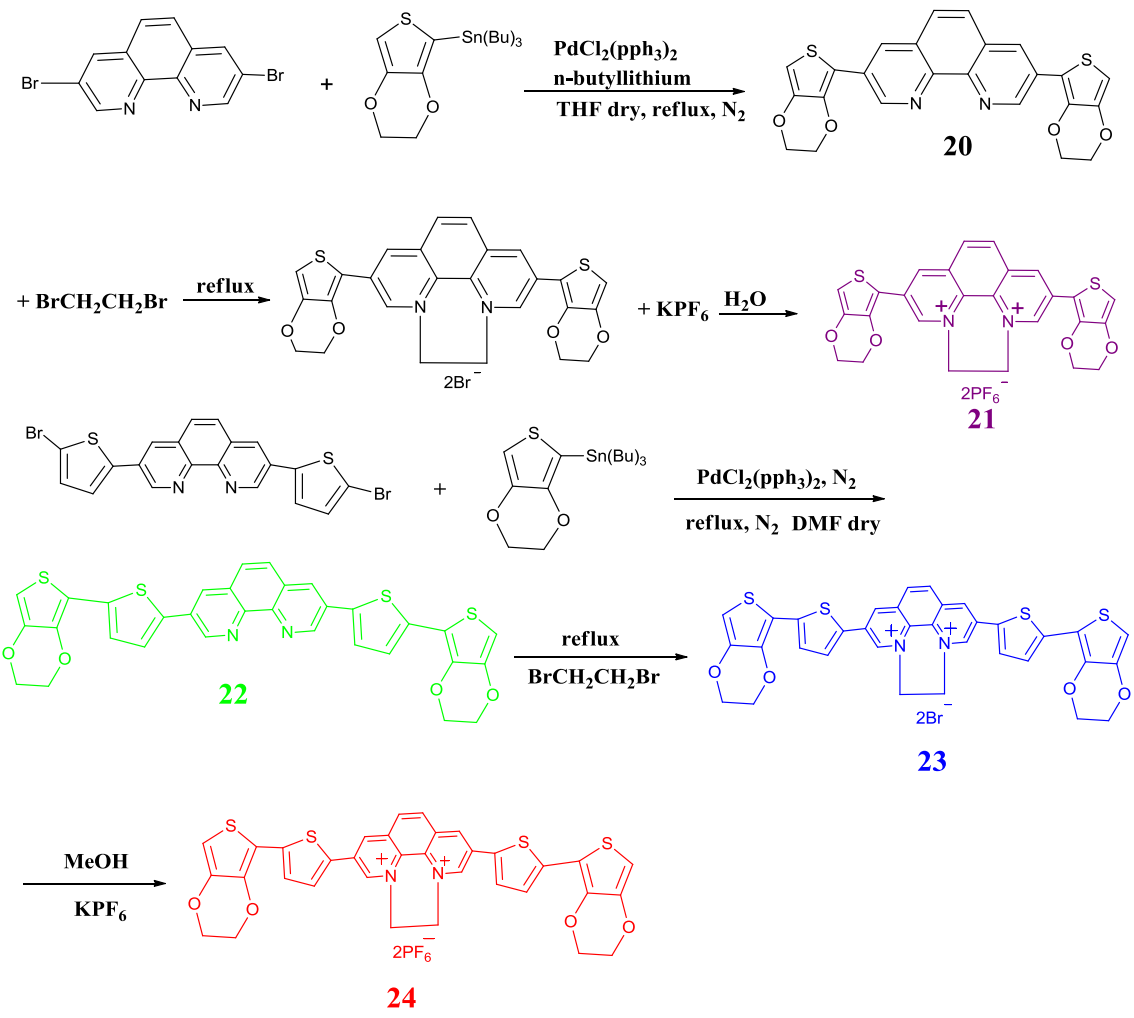

Scheme 2.4. Syntheses of compounds **(20-24)**

2.3.2. Experimental

The five monomers were synthesised by Abbas Lafta (Glasgow University) under the supervision of Graeme Cooke (Glasgow University) and Peter Skabara (University of Strathclyde).

Cyclic voltammetry measurements were performed on a CH Instruments 660A electrochemical workstation with *iR* compensation using dichloromethane and acetonitrile as the monomer and monomer free solutions. The electrodes in the electrochemical setup consisted of a platinum wire counter electrode and silver wire reference electrode. Two types of working electrode, glassy carbon or an indium tin oxide (ITO) glass slide, depending on the type of experiment were used. Before every measurement the reference electrode was calibrated against the $E_{1/2}$ of the ferrocene/ferrocenium redox couple.

All solutions were degassed (Ar) during a reduction experiment and contained monomer substrates at a concentration of *ca.* 10^{-4} M, together with *n*-Bu_4NPF_6 as the supporting electrolyte (0.1 M). Absorption spectra, spectroelectrochemical studies and switching procedures were recorded on a UNICAM UV 300 instrument.

2.3.3. Absorption and Cyclic Voltammetry of monomers

The electronic absorption spectra of compounds **20**, **21** and **22** in dichloromethane solution and compounds **23** and **24** in acetonitrile solution are shown in Figure 2.60. The absorption spectra of monomer **20** show peaks at 291, 362 and 381 nm, with the final peak at 381 nm being the π-π* transition from the conjugated portion of the compound. The peaks at (281, 341, and 566 nm) in monomer **21** have been shifted bathochromically compared to monomer **20** and **22** (at 263, 314, and 415 nm); the π-π* transition of monomer **21** exhibits a large red shift of 185 nm compared to monomer **20**, while such transitions have similar values in the rest of the compounds. The peaks for monomers **23** and **24**, at 416 and 424 nm respectively, are the absorption maxima corresponding to the π-π* transition from the conjugated component of the compounds. The small peaks for monomers **23** and **24**, which appear at 570 and 555 nm respectively, correspond to charge transfer absorption bands between the donor and acceptor units in these compounds.

Optical HOMO-LUMO gaps **20**, **21**, **22**, **23** and **24** were calculated from the onsets of the longest wavelength absorption peaks. The data for all the absorption maxima and the optical band gap values are summarised in Table 2.8. The optical HOMO-LUMO gaps of **20**, **21**, **22**, **23** and **24** are 3.06, 1.97, 2.66, 1.65 and 1.91 eV, respectively. Smaller optical band gap values are evident in monomers **23** and **24**, which are expected due to the increased conjugation length of these compounds.

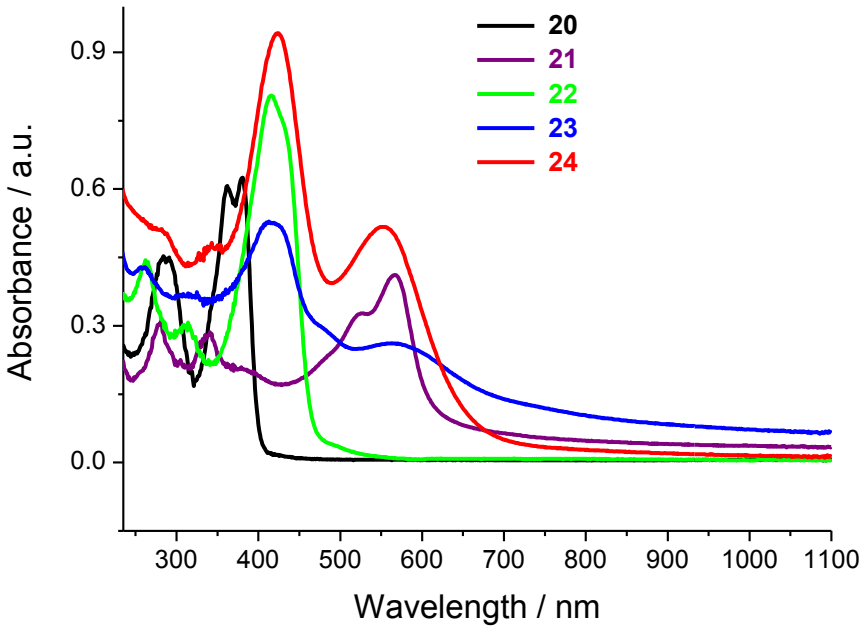

Figure 2.60. UV/vis spectroscopy of monomers **20**, **21** and **22** measured in dichloromethane and monomers **23** and **24** measured in acetonitrile solution.

Table 2.8. Absorption spectroscopy data for monomers **20**, **21**, **22**, **23** and **24**

Monomer	UV-vis peaks (nm)				
	1st	2nd	3rd	4th	Optical E_g / eV
20	291	262	381	-	3.06
21	281	341	525	566	1.97
22	263	314	415	-	2.66
23	260	320	416	570	1.65
24	280	340	424	555	1.91

The cyclic voltammogram experiments of monomers **20**, **21**, and **22** were performed in dichloromethane solution and for monomers **23** and **24** in acetonitrile. The monomer oxidation gives one irreversible wave for monomers **20** and **21**, at +1.02 and +0.6 V respectively, producing a radical cation species in each case. Two

irreversible peaks for monomer **22**, at +0.60 and +0.75 V, and a quasi reversible peak for **23** (at +0.60 V) are evident. Two reversible waves at +0.57/+0.53 V and +0.99/+0.91V are clear in monomer **24**, which are likely to be from the removal of two electrons from the EDOT units. All monomer oxidation processes are depicted in Figure 2.61. The reduction processes of **20**, **21**, **22**, **23** and **24** are shown in Figure 2.62. All five monomers reveal irreversible reduction peaks at -2.15, -1.84, -1.98, -1.62 and -1.87 V, which are likely to be from reduction of the central core unit.

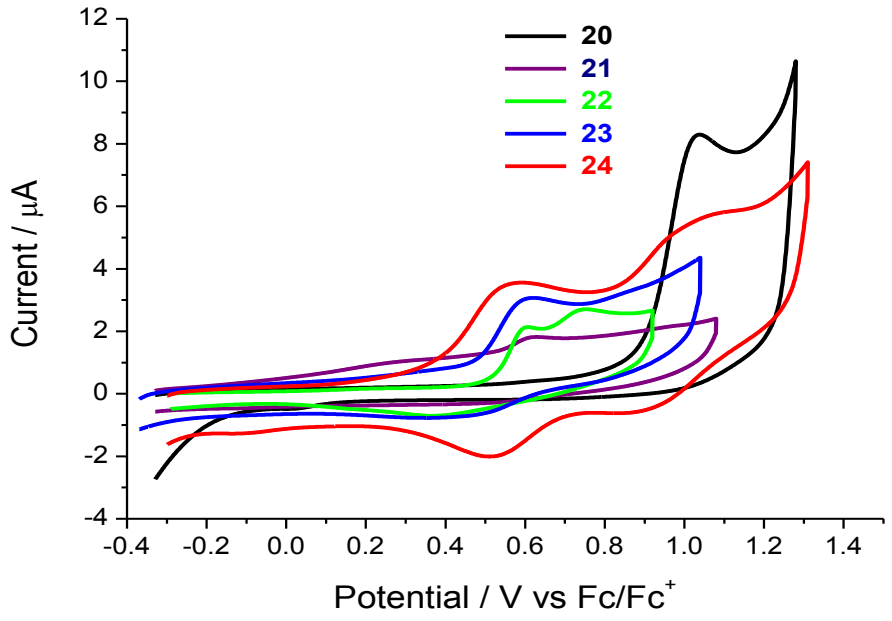

Figure 2.61. Cyclic voltammograms of oxidation of monomers **20**, **21** and **22** (with dichloromethane as solvent) and monomers **23** and **24** (with MeCN solution) on a glassy carbon working electrode

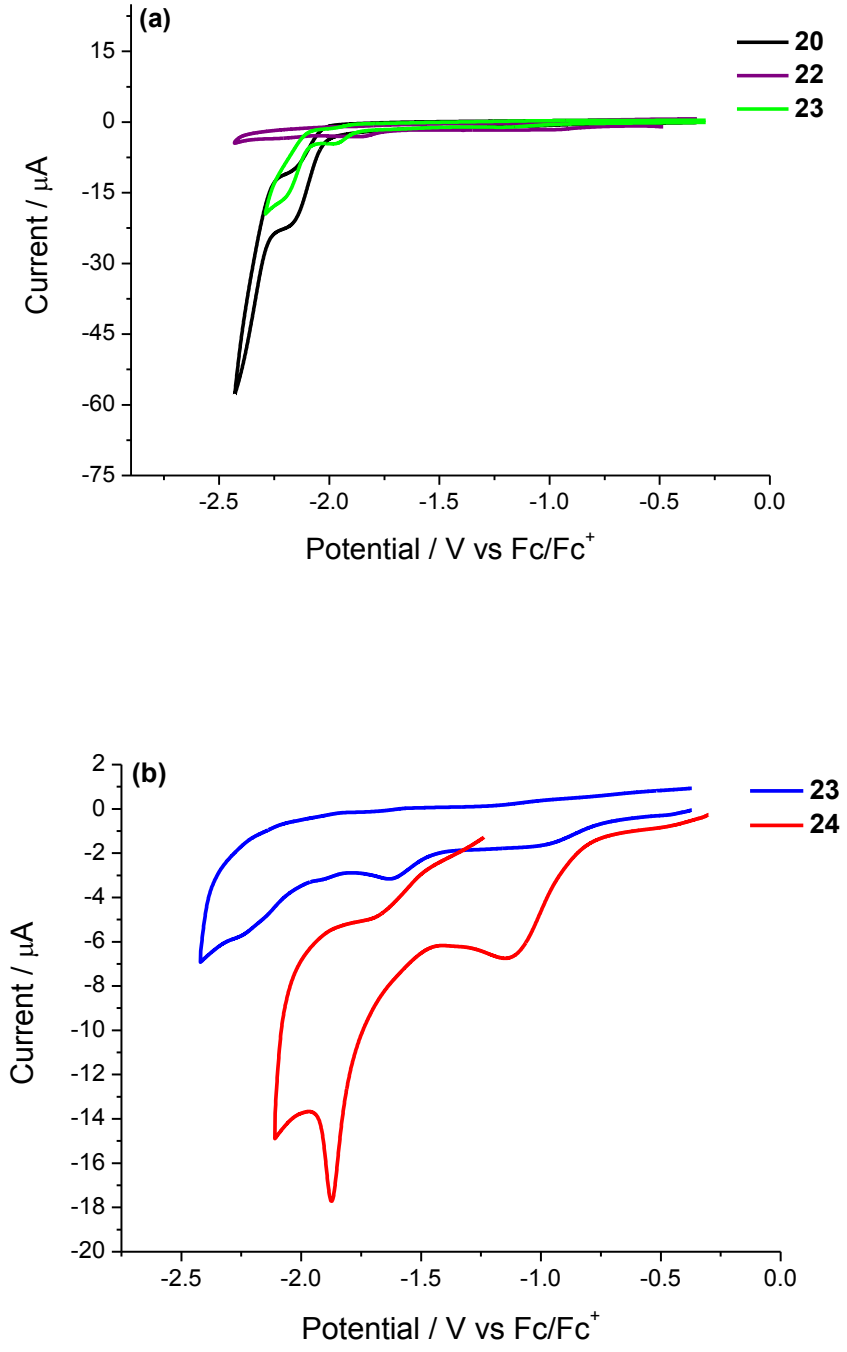

Figure 2.62. Cyclic voltammograms of reduction of monomers (**a**) **20**, **21**, **22**, and (**b**) **23** and **24**

The electrochemical HOMO-LUMO gap of the five monomers was determined from the difference in the onset of the first oxidation and reduction peaks (Figures 2.61 and 2.62). HOMO and LUMO levels are calculated by subtracting the onsets from the HOMO of ferrocene. All data are summarised in Table 2.9. By comparing the energy levels, the difference between the HOMO and LUMO values gave electrochemical HOMO-LUMO gaps for the monomers that are slightly different from the optical values although the overall trend across the series is maintained. The extended conjugation effect has been obvious in monomer **23** by giving lowest band gap value (1.92 eV).

Table 2.9. Electrochemical Data for Energy levels of monomers **20**, **21**, **22**, **23** and **24**

Monomer	HOMO / eV	LUMO / eV	E_g / eV
20	-5.70	-2.77	2.93
21	-5.32	-3.08	2.24
22	-5.33	-2.92	2.34
23	-5.28	-3.36	1.92
24	-5.19	-3.02	2.17

HOMO and LUMO values are calculated from the onset of the first peak of the corresponding redox wave and referenced to ferrocene, which has a HOMO of -4.8 eV. E_g is the HOMO-LUMO energy gap.

2.3.4. Cyclic Voltammetry and Absorption of Polymers

The five monomers were subjected to electropolymerisation by repetitive cycling over the first oxidation wave. The polymer of monomer **20** was grown using a high concentration solution (10^{-2} M), but was not stable on the electrode surface. Monomer **21** was subjected to many attempts to electropolymerise by using several solvents and also by changing the experimental conditions, including using different potentials, substrate concentrations and number of cycles, but no polymerisation was

observed. Monomers **22**, **23** and **24** were polymerised electrochemically, with the growth traces of the corresponding polymers shown in Figure 2.63 and 2.64.

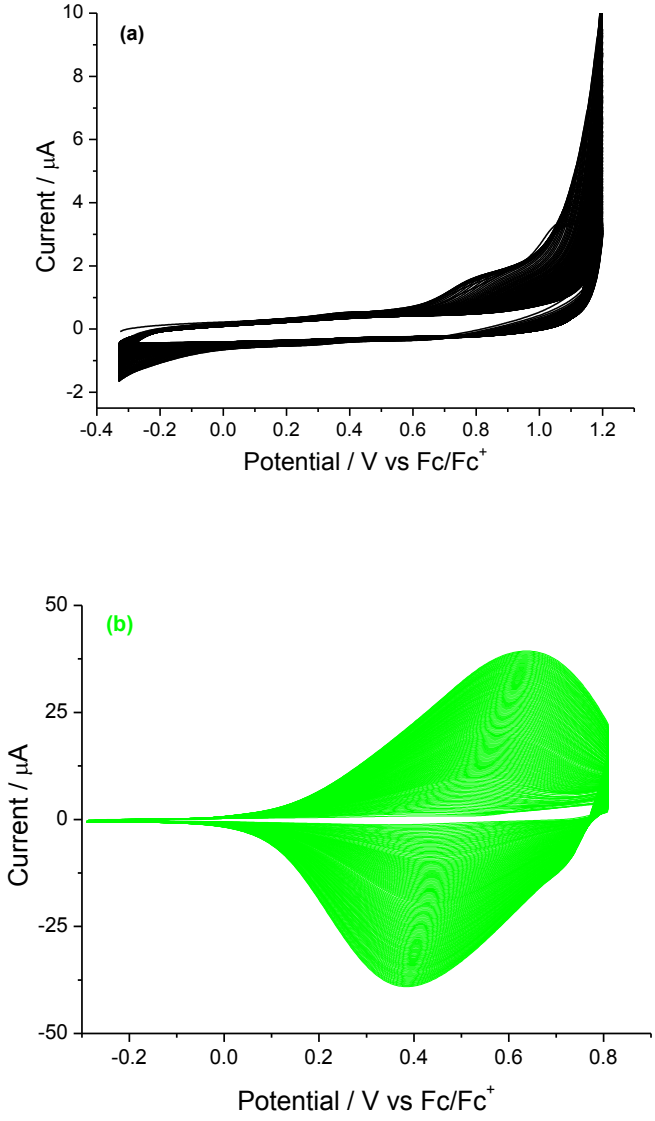

Figure 2.63. Electrochemical growth of (**a**) poly**20**, (**b**) poly**22** (both in dichloromethane), using a glassy carbon working electrode, Ag wire reference electrode and Pt counter electrode, concentration of ca. 10^{-4} M, (0.1 M $TBAPF_6$ as supporting electrolyte). The data is referenced to the Fc/Fc+ redox couple, at a scan rate of $100mVs^{-1}$, over 300 segments.

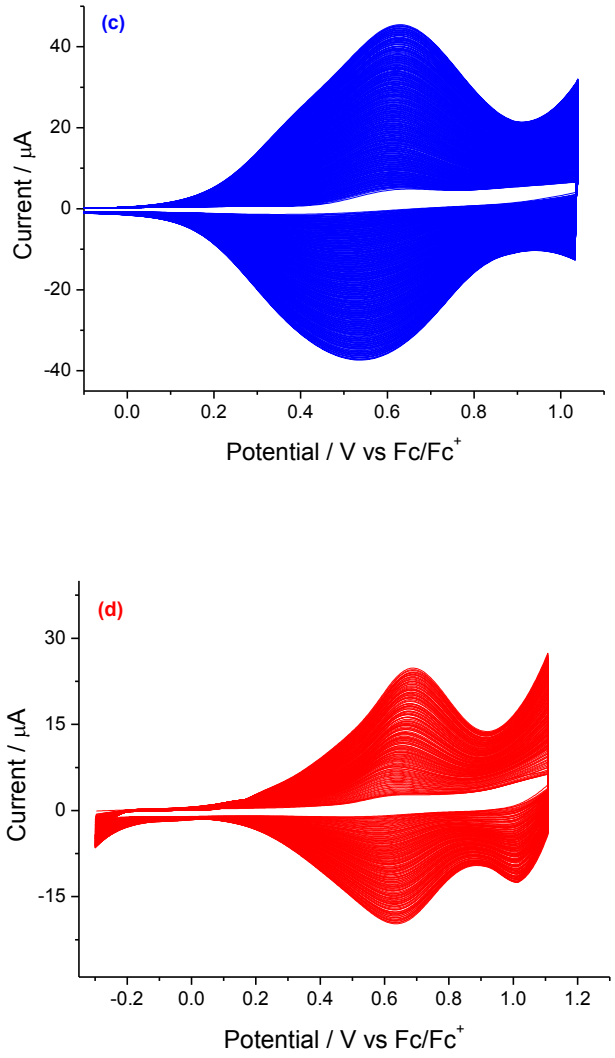

Figure 2.64. Electrochemical growth of (**c**) poly**23** and (**d**) poly**24** (in MeCN), using a glassy carbon working electrode, Ag wire reference electrode and Pt counter electrode, concentration of ca. 10^{-4} M, (0.1 M TBAPF$_6$ as supporting electrolyte). The data is referenced to the Fc/Fc+ redox couple, at a scan rate of 100mVs^{-1}, over 300 segments.

In the oxidation and reduction analysis of the polymers (Figure 2.65), all the polymers revealed varied peaks at different potential values. Poly**20** revealed an irreversible peak at +0.75 V due to the formation of a radical cation on the terminal

units. Poly**22** indicated a broad reversible peak at +0.64/+0.63V. Poly**23** and poly**24** exhibited broad reversible oxidation waves at lower potential, with values of +0.43/+0.33 V and +0.42/+0.39 V, respectively. The lower oxidation potential values and reversibility of poly**22**, poly**23** and poly**24** compared to poly**20** can be attributed to the extended conjugation of having thiophene units in the polymer chain. The reduction of poly**20** showed two irreversible peaks at -1.75 and -2.28 V. Poly**22** shows a quasi reversible and one irreversible reduction peak at -1.89/-1.78 and -2.13 V. Irreversible peaks appeared at -2.25 and -2.12V for poly**23** and poly**24** respectively. The irreversible reduction peaks in all polymers are from the formation of an anion radical species stabilised on the core unit.

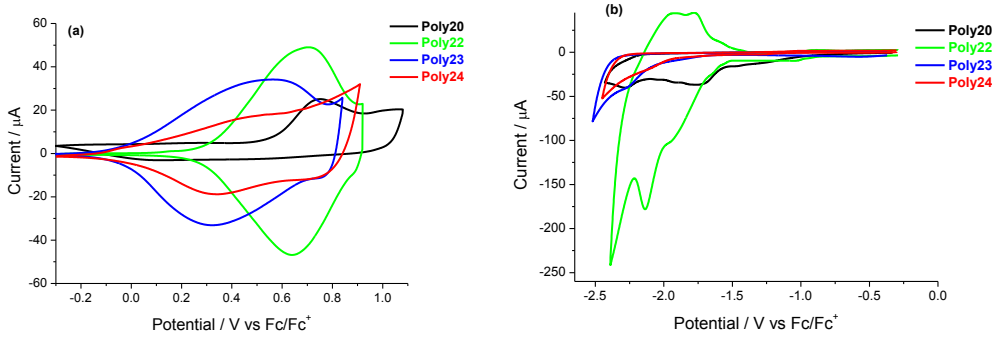

Figure 2.65. Cyclic voltammograms of (**a**) polymer oxidation and (**b**) polymer reduction of poly**20**, and poly**22** (in CH_2Cl_2 as solvent) and poly**23** and poly**24** (in acetonitrile solution) as a thin film on a glassy carbon working electrode, Ag wire reference electrode and Pt counter electrode (0.1 M $TBAPF_6$ as supporting electrolyte, at a scan rate of 100mVs^{-1}).

By the same procedure as before for energy level determination, the electrochemical HOMO-LUMO gap of the polymers was calculated from the difference in the onset of the first oxidation and reduction (Table 2.10). Thus, the difference between the HOMO and LUMO values gave electrochemical band gap values of 2.07, 1.94, 1.88

and 1.41 eV for poly**20**, poly**22**, poly**23** and poly**24** respectively. These values are lower than the calculated electrochemical HOMO-LUMO gap of their monomer, due to the extra conjugation length provided by the EDOT and thiophene units.

Table. 2.10. Electrochemical data of poly**20**, poly**22**, poly**23** and poly**24**

Polymer	Oxidation / V		Reduction / V		HOMO	LUMO	E_g
	1st	2nd	1st	2nd	/ eV	/ eV	/eV
Poly**20**	+0.75	-	-1.75	-2.28	-5.36	-2.29	2.07
Poly**22**	+0.64/+0.63	-	-1.89 / -1.78	-2.13	-5.10	-3.16	1.94
Poly**23**	+0.43/+0.33	-	-2.25	-	-4.68	-2.80	1.88
Poly**24**	+0.42/+0.39	-	-2.12	-	-4.93	-2.95	1.41

HOMO and LUMO values are calculated from the onset of the first peak of the corresponding redox wave and referenced to ferrocene, which has a HOMO of -4.8 eV. E_g is the HOMO-LUMO energy gap.

The stability of the polymers (Figure 2.66) to adhere to the glassy carbon electrode was evaluated by cycling over the redox-active peak for 100 segments, and measuring the percentage decrease in the current response. Poly**20** is unstable to anodic conditions, and poly**23** is relatively stable (50%), however poly**22** and poly**24** are highly stable to anodic conditions, with only a 7.8 and 5.3 % decrease in the current response over repetitive segments.

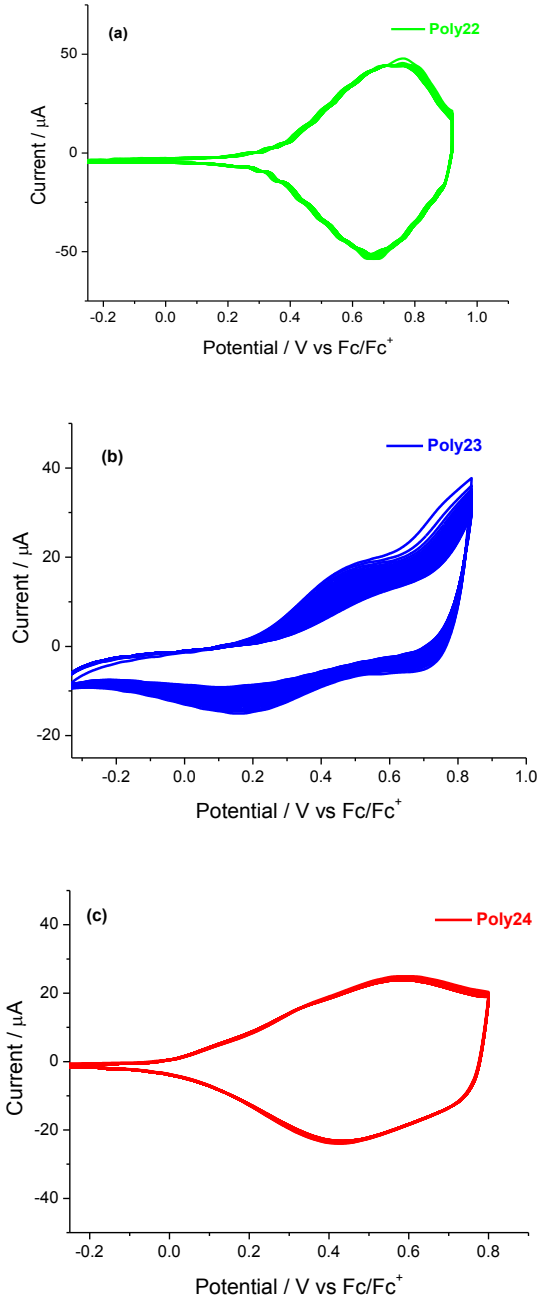

Figure 2.66. Oxidative stability test of (**a**) poly**22** in monomer-free acetonitrile and (**b**) poly**23** and (**c**) poly**24** in monomer free dichloromethane, at a scan rate 0.1 V^{-1}, over 100 segments, using glassy carbon working electrode, with 0.1 M $TBAPF_6$ as supporting electrolyte. The data is referenced to the Fc/Fc+ redox couple.

To further assess the stability and electrochemical behaviour of the polymers, oxidation cycles over the first peaks were measured at increasing scan rates from 25-500 mVs^{-1} as displayed in Figure. 2.67. The peak maximum of the anodic steps was then plotted against the scan rate and a line of best fit applied (Figure 2.68). In each case, a linear line with a high R^2 (0.9997, 0.992 and 0.9975 for poly**22**, poly**23** and poly**24**, respectively) was observed, showing that the redox processes of the polymers are not diffusion limited and stable on the working electrode surface.

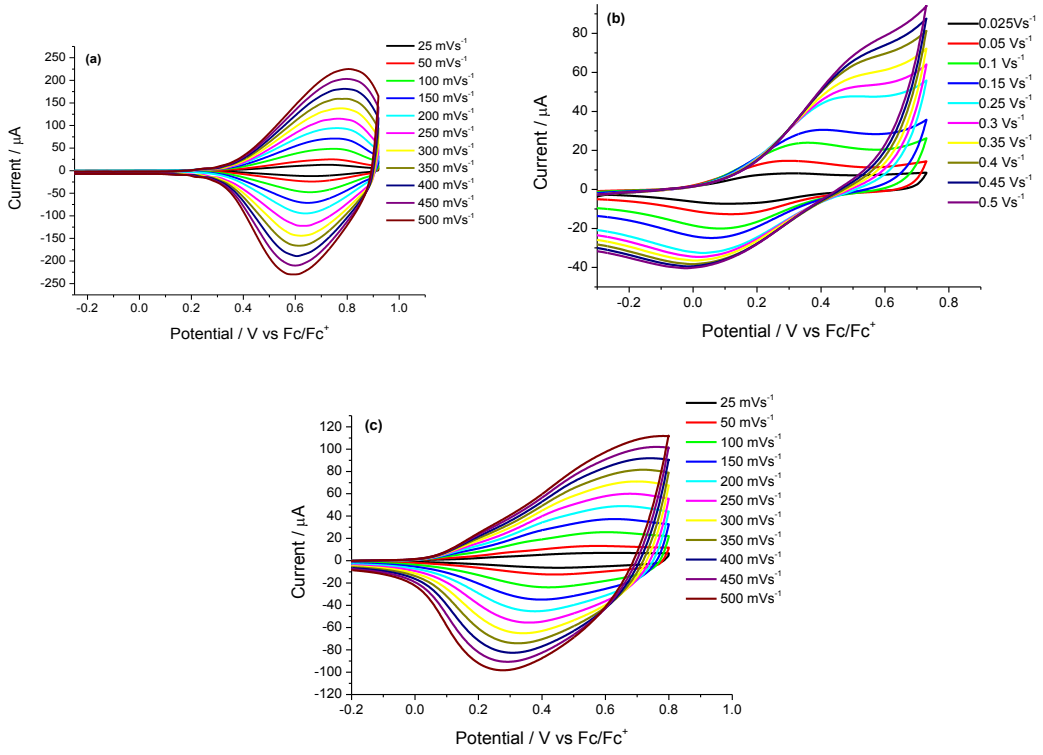

Figure 2.67. Scan rate experiments of (**a**) poly**22** in monomer free acetonitrile and (**b**) poly**23** and (**c**) poly**24** in monomer free dichloromethane at varying scan rates

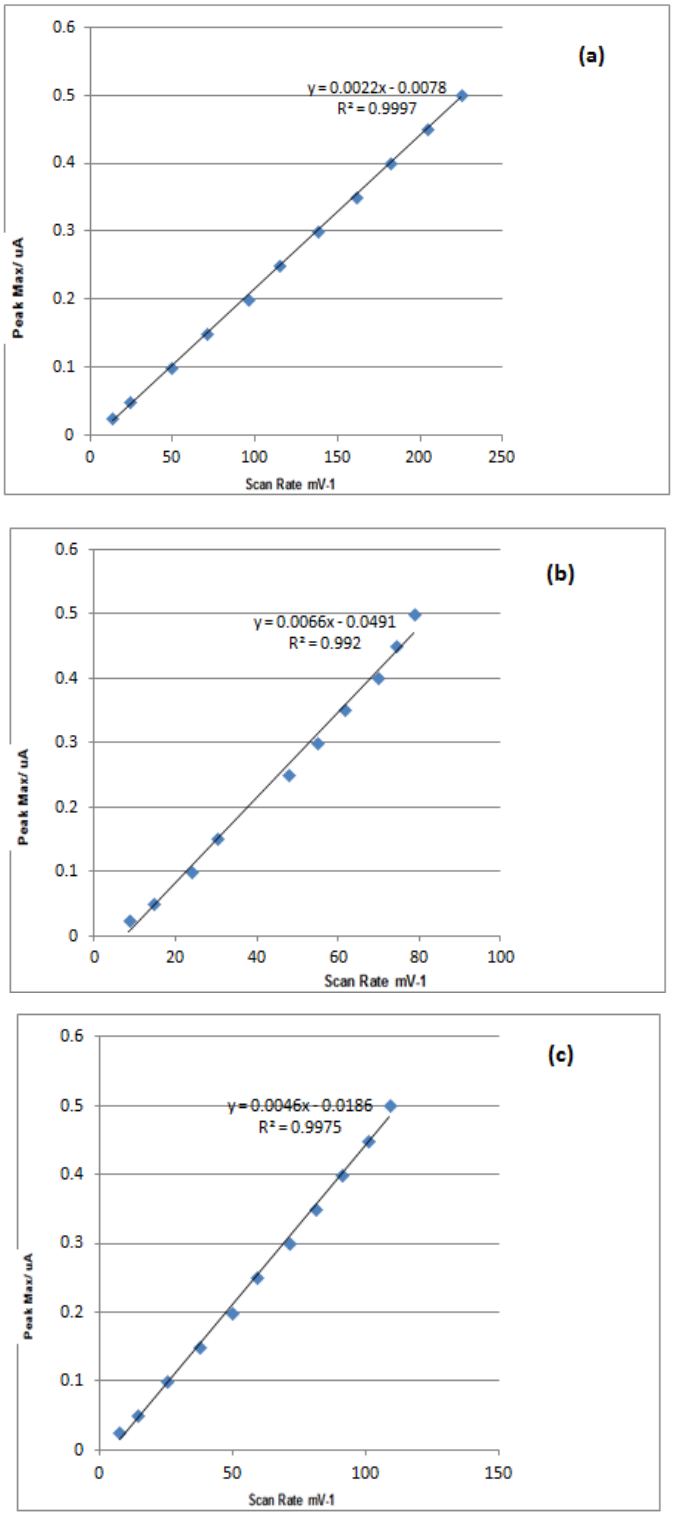

Figure 2.68. Scan rate vs. peak current maxima of (**a**) poly**22**, (**b**) poly**23** and (**c**) poly**24**.

The optical band gaps of the polymers were calculated by growing the polymer onto a piece of ITO coated glass slide. The polymers were grown by cycling between 0 and 1.3 V vs. Fc/Fc^+ as doped, and then each polymer was de-doped between -0.7 and -0.5 V for poly**20**, and between -0.5 and -0.3 V for the rest of the polymers (poly**22**, poly**23** and poly**24**), in monomer-free acetonitrile for poly**20** and **22** and dichloromethane for poly**23** and **24**. The absorption maxima and the optical band gaps were calculated from the onset of the longest wavelength absorption edge. The optical data for the four polymers are summarised in Table 2.11 and Figure 2.69. The spectrum of poly**20** shows a λ_{max} peak of 392 nm for the polymer, indicating that the π-π* transition has bathochromically shifted compared to its monomer by 11 nm. The peaks for poly**22**, poly**23** and poly**24** all exhibited a red shift compared to poly**20**, which can be attributed to the appearance of the extended conjugation of extra terminal units in their polymer chains. Poly**22** and poly**24** have optical band gaps that are slightly lower than poly**20**, with the values being 2.11, 1.85 and 1.41 eV for poly**20**, poly**22** and poly**24**, respectively. This also supports the assumption that poly**20** has inferior conjugation in the polymer chain compared to poly**22** and poly**24**. A reasonable agreement between optical band gaps with the electrochemically determined band gaps is obvious in these polymers. Poly**23** shows no clear absorbance edge therefore the optical band gap could not be calculated in this case.

Table. 2.11. Absorption spectroscopy data for poly**20**, poly**22**, poly**23** and poly**24**

Polymer	UV-vis λ_{max} / nm	Optical E_g / eV
Poly**20**	392	2.11
Poly**22**	533	1.85
Poly**23**	611	-
Poly**24**	430	1.41

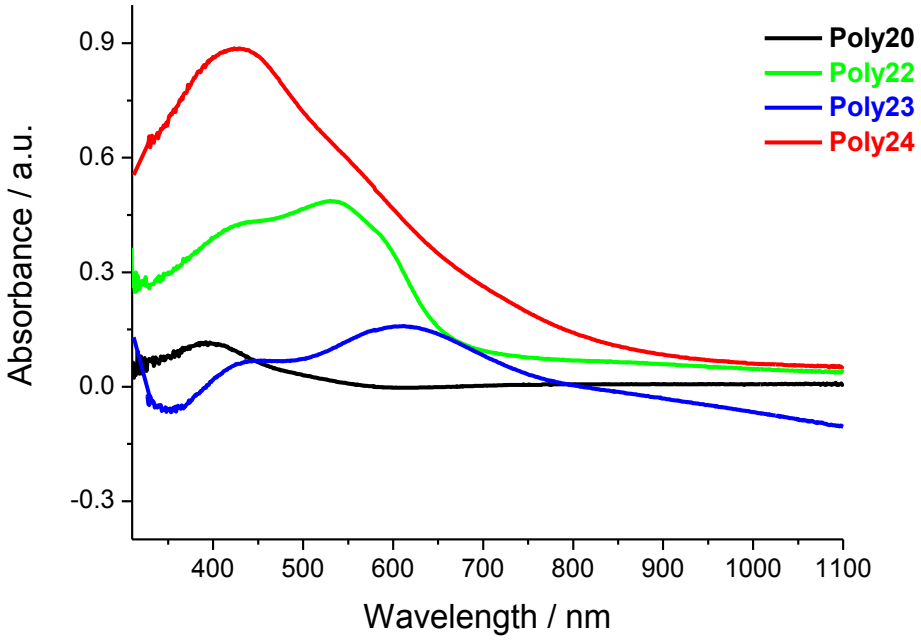

Figure 2.69. UV-vis spectra of poly**20** and poly**22** in monomer-free acetonitrile and poly**23** and poly**24** in monomer-free dichloromethane solution on ITO slides

2.3.5. Spectroelectrochemical Analysis of the Polymers

UV-vis spectroelectrochemistry experiments were performed on poly**22**, poly**23** and poly**24** to investigate the effect that p-doping has on the electronic spectra of the polymer. P-doping of poly**22**, poly**23** and poly**24** is shown in Figures 2.70, 2.71 and 2.72. All three polymers show a loss of intensity of the π-π* band at 550, 470 and

450 nm for poly22, poly23 and poly24, respectively. Each polymer has started to form polarons in the polymer chain, and this behaviour can be seen from the development of new absorption bands between 600 and 800 nm that result at potentials between 1100 to 1250 mV. The spectroelectrochemical plots of the polymers also show the generation of new absorption waves forming at 1500 to 1700 mV that correspond to the bipolaron bands. These can be seen to form with the appearance of a new absorption band at 900 to 1000 nm. Poly23 exhibits a surprise drop in absorbance between 750 and 1000 nm. This drop possibly corresponds to the breakdown of the polymer into soluble materials.

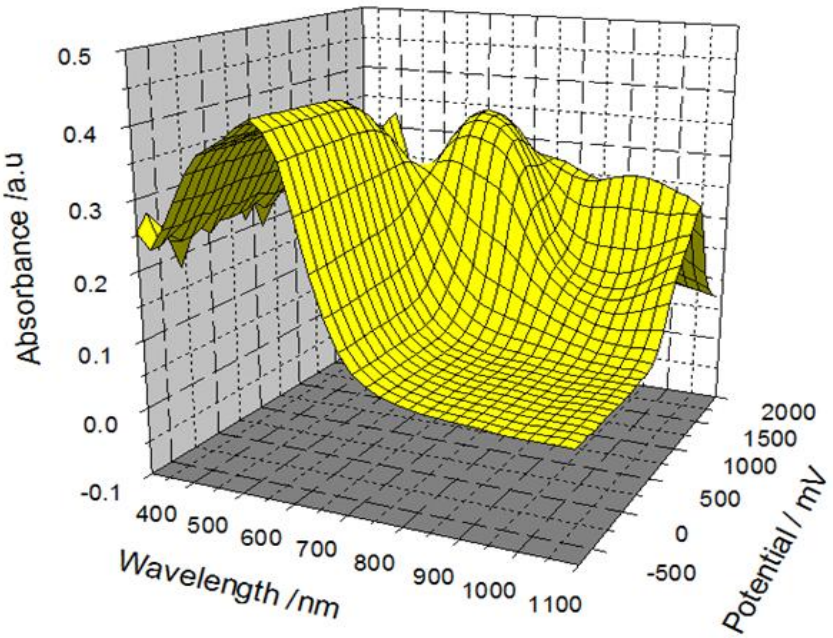

Figure 2.70. UV-vis spectroelectrochemistry of poly22 upon p-doping

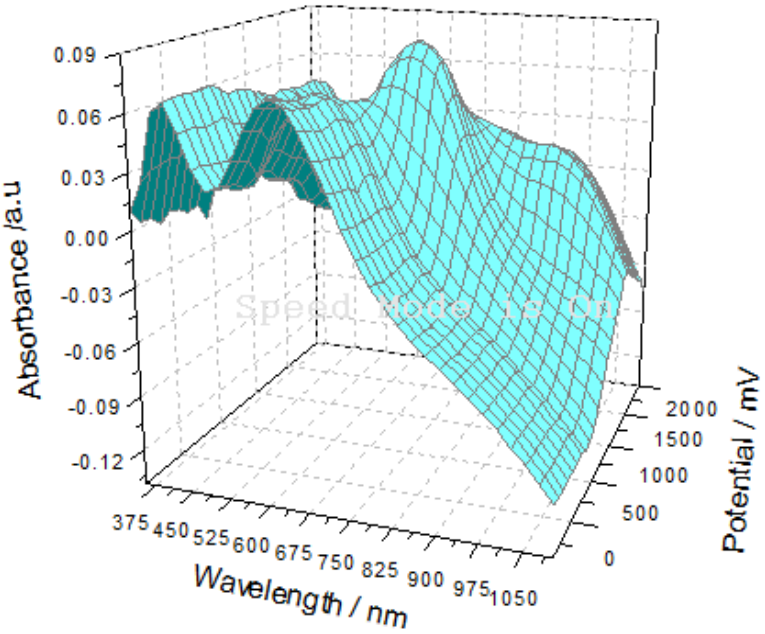

Figure 2.71. UV-vis spectroelectrochemistry of poly**23** upon p-doping

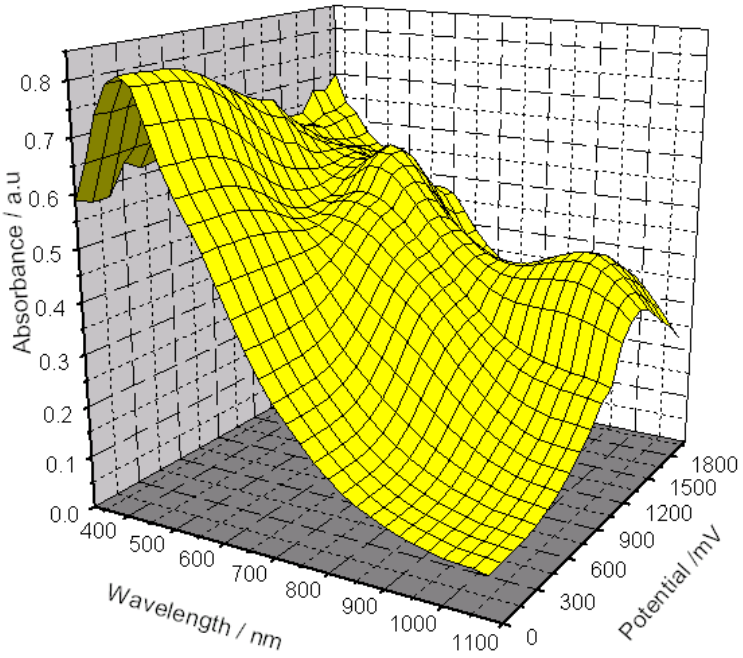

Figure 2.72. . UV-vis spectroelectrochemistry of poly**24** upon p-doping

2.3.6. Polymer Switching

For the switching time measurements, fresh polymers were grown on ITO glass and de-doped. The ability of the poly**22** and poly**24** to switch between colour states was investigated by measuring the absorbance at 750 nm for both polymers and switching the potential between -0.7 and +1.35 V for poly**22** and between 0 and +1.35 V for poly**24** at different rates, as shown in Figures 2.73 and 2.74.

The switching times used for these measurements were 10, 5, 2.5, 1.25, 0.5, and 0.25 seconds. The % change in absorbance for each experiment against the corresponding time is shown in Table 2.12.

Table. 2.12. Switching times and percentage change in absorbance of poly**22** and poly**24**

Switching Time / s	% change poly**22**	% change poly**24**
10	59.28	29.26
5	55.94	21.95
2.5	45.35	12.5
1.25	31.81	5.12
0.5	12.75	2.63
0.25	5.92	0.26

Comparison of the results shows that poly**22** gives the best switching rates compared to poly**24**, since with a 10 second switching time the absorbance of poly**22** was 59.28%, while the corresponding value was 29.26% for poly**24**. However, with a

0.25 second switching rate, the change in absorbance was much lower at 5.92% and 0.26% for poly**22** and poly**24**, respectively.

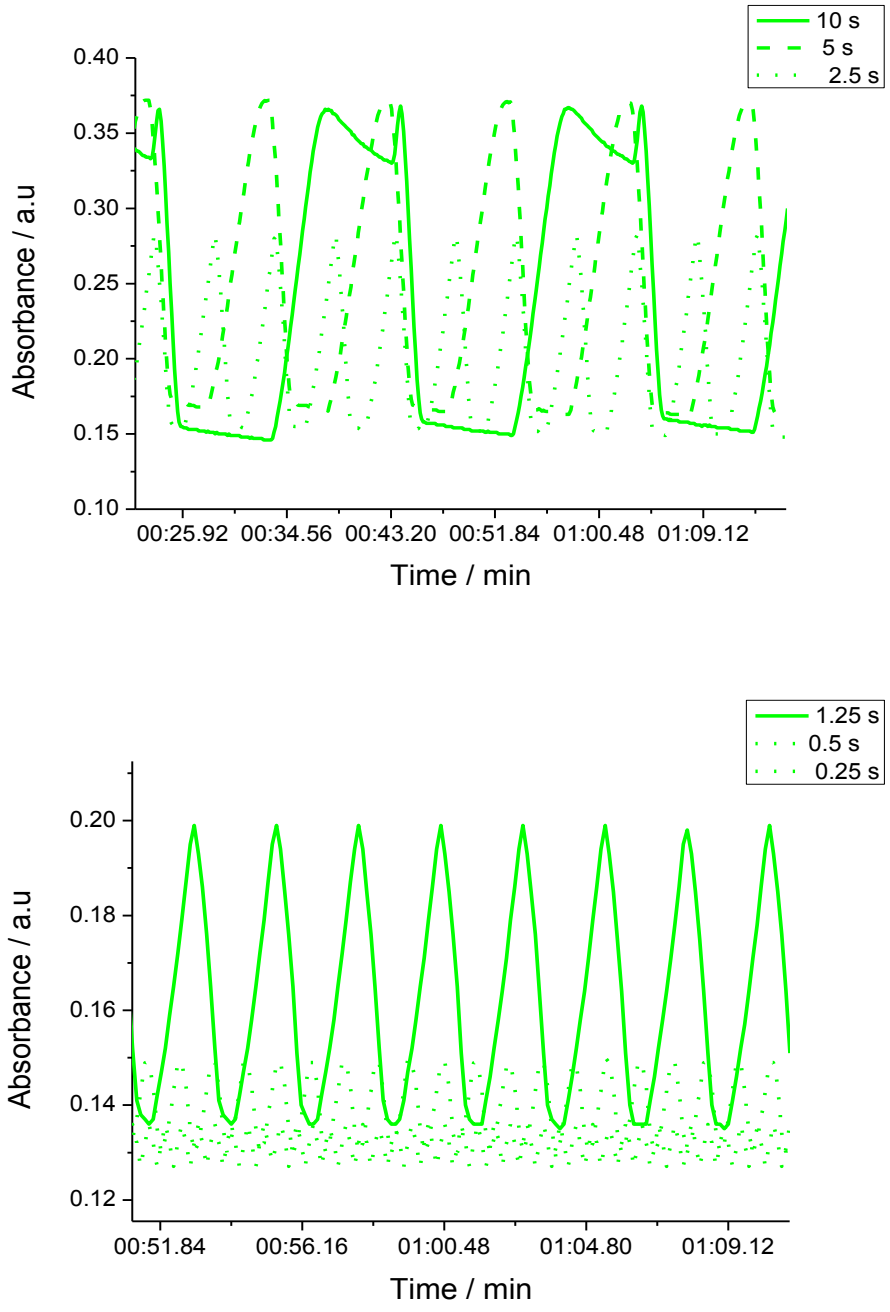

Figure 2.73. Switching times of poly**22** at 750 nm on ITO glass at varying times: 10, 5, 2.5 1.25, 0.5 and 0.25 seconds

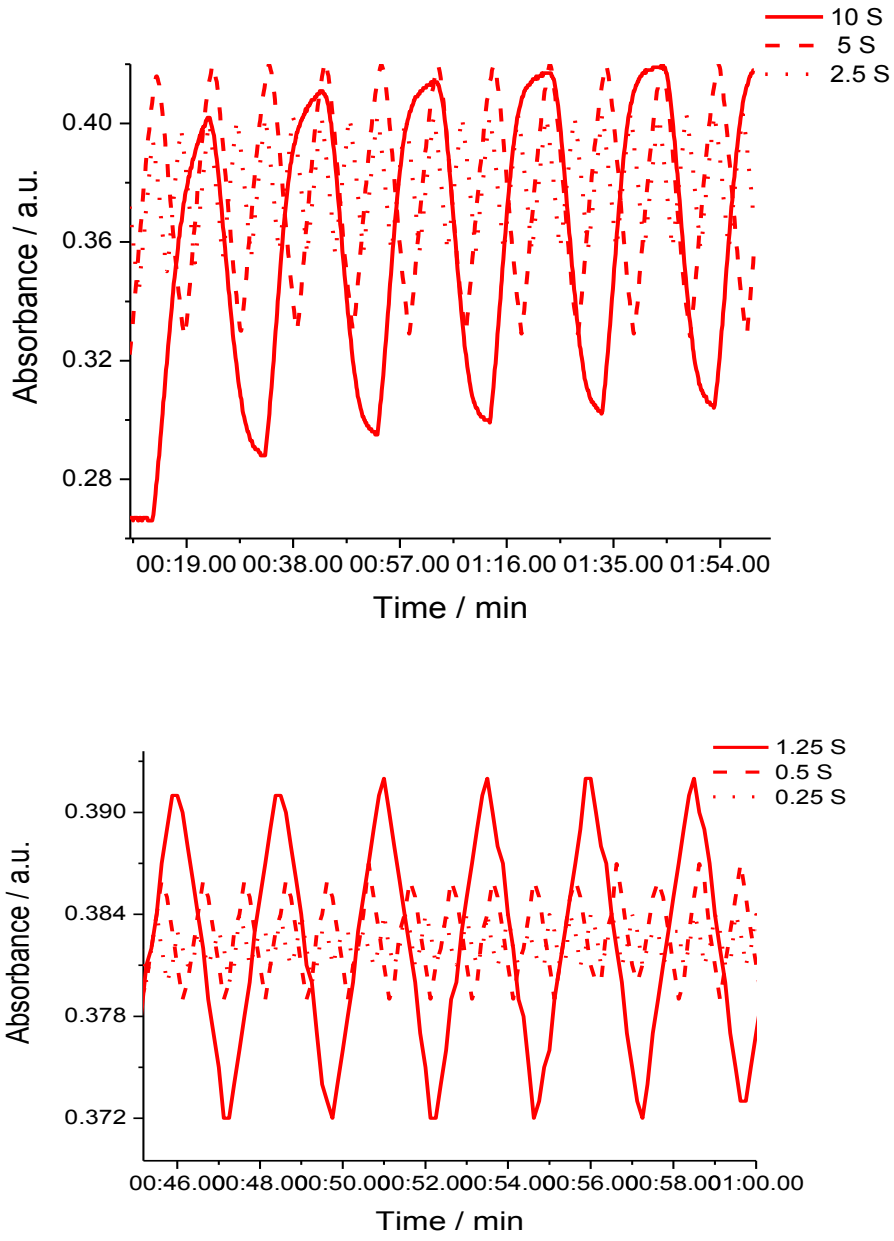

Figure 2.74. Switching times of poly**24** at 750 nm on ITO glass at varying times: 10, 5, 2.5 1.25, 0.5 and 0.25 seconds

2.3.5. Conclusion

The electropolymerisation of five new monomers has been reported, where four new polymers have been characterised by a variety of techniques (absorption spectroscopy, CV, UV-vis spectroelectrochemistry, and switching times). Although monomer **21** does not electropolymerise, the remaining monomers (**20,** **22**-**24**) form thin-films under anodic polymerisation conditions. The electrochemical band gaps of the polymers have lower values than their monomers, due to the extension of conjugated chain length in the polymer. Poly**20** has displayed a higher band gap possibly due to the accepting units directly bonded to the EDOT units compared to the other polymers. A plot of scan rate versus peak current provides a straight-line graph with high R^2 values in poly**22**, poly**23** and poly**24**, indicating that the polymers are not diffusion limited. These films were studied for their stability, redox and optical properties, as well as their potential suitability for electrochromic switches.

2.4. Electropolymerisation of Thiophene derivatives based on Viologen with Ruthenium Complex

2.4.1 Introduction

This section discusses similar compounds as disclosed in the previous section, but here the central core appears coordinated to ruthenium forming complexes. Two novel complexes containing either bisEDOT or bis[EDOT-thiophene] units (compounds **25** and **26** respectively) attached to the 1,10-phenanthroline central core unit are revealed. Therefore, electrochemical and spectroscopic experiments have been applied on (terthiophenyl-phenanthroline with [$Ru(bpy)_2$]) materials producing stable molecular devices with small band gap.[142] The chemical structures and synthesis of compound **25** and **26** are illustrated in Figure 2.75 and Scheme 2.5.

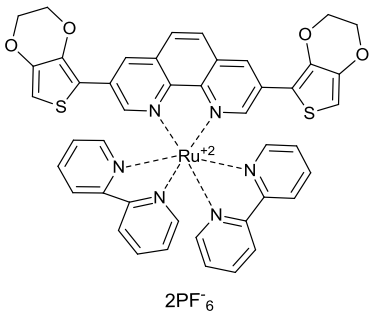

25

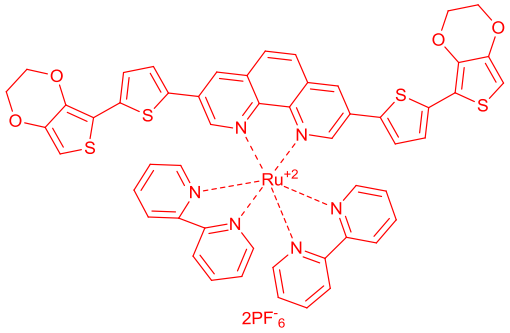

26

Figure 2.75. Structures of monomer **25** and **26**

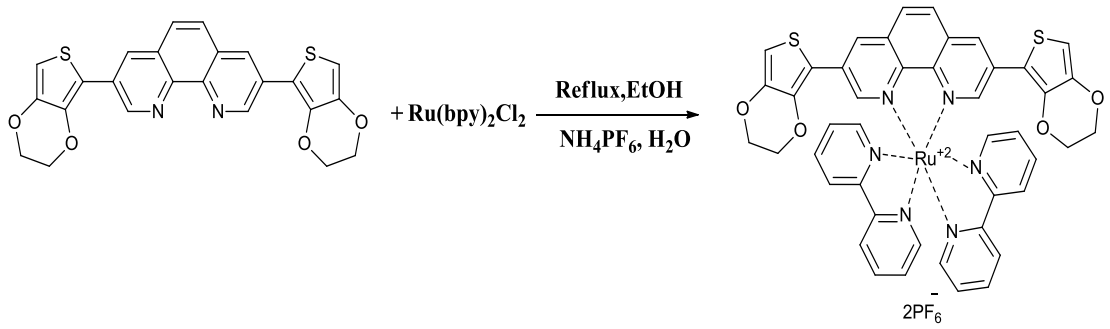

25

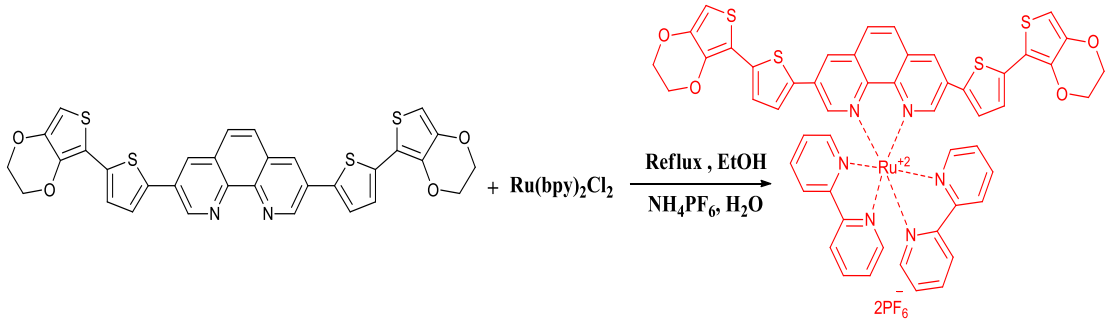

26

Scheme 2.5. Synthesis of compounds **25** and **26**

2.4.2. Experimental

The synthesis of monomers **25** and **26** was performed by Abbas Lafta from Professor Graeme Cooke's group at the University of Glasgow.

Electrochemical and spectroscopic techniques were carried out using a CH Instruments 660A electrochemical workstation with *iR* compensation and UV/Vis absorption spectroscopy on a UNICAM UV 300 instrument respectively. Acetonitrile was used as the monomer solvent. The electrodes were glassy carbon, platinum wire, and silver wire as the working, counter, and reference electrodes, respectively, and contained monomer substrates in a concentration of *ca.* 10^{-4} M, together with *n*-Bu_4NPF_6 as the supporting electrolyte (0.1 M).

All measurements are referenced against the $E_{1/2}$ of the Fc/Fc^+ redox couple. Spectroelectrochemical experiments were achieved on indium tin oxide (ITO) coated glass.

2.4.3. UV-vis Absorption Spectroscopy and Cyclic Voltammetry of The Monomers

The electronic absorption specta of monomers **25** and **26** were recorded in acetonitrile solution and are shown in Figure 2.76. The absorption spectra exhibited obvious differences between the two structures. Hence, the spectrum of monomer **25** gives three main peaks at 287, 390 and 414 nm, as well as a shoulder at 468 nm. Monomer **26** exhibits two peaks at 286 and 450 nm. The first two peaks in both monomers are attributed to a π -π* transition of bipyridine and ruthenium in the core unit,[142] while the peaks at 414 and 450 nm in monomers **25** and **26** respectively are assigned to the π-π* transition of their conjugated system. The onsets of the absorption edge give the optical band gap for both monomers. Consequently, the calculated band gap of monomer **26** is 2.32 eV; this is slightly lower than that of monomer **25** (2.36 eV), which is expected to be due to the addition of the additional conjugated units in monomer **26**.

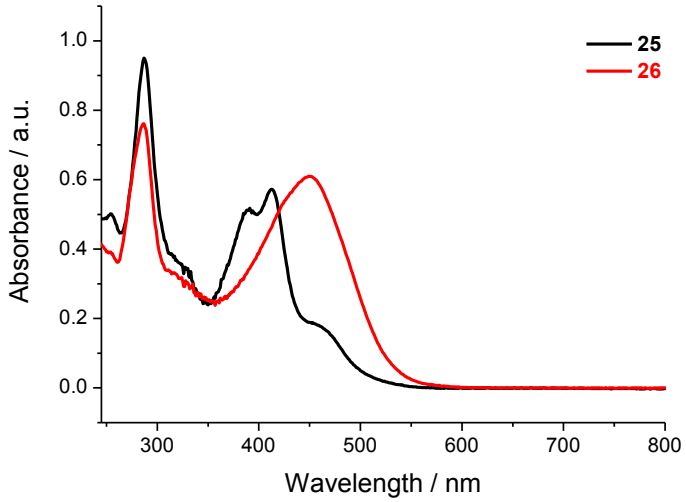

Figure 2.76. UV-vis spectroscopy of monomer **25** and **26** in MeCN

The electrochemical behaviour of monomers **25** and **26** was analysed by cyclic voltammetry.

The oxidation and reduction of both monomers is illustrated in Figure 2.77. Monomer **25** shows reversible and quasi reversible oxidation peaks at +0.24/+0.20V and +0.54V respectively. Two reversible oxidation peaks at +0.80/+0.70 and +1.1/+1.0 V have appeared by monomer **26**. The first oxidation will be the removal of an electron from EDOT group to forming a radical cation. The second oxidation could be one of two possibilities, either the removal of a second electron to give the dication (further oxidation of the EDOT unit) or possibly from the oxidation of the Ru^{II}/Ru^{III} process.

The trace of the reduction processes of the two monomers is more complicated. Monomer **25** gives three reversible peaks at -1.47/-1.42V, -1.72/-1.65V and -1.95/-1.88V, and a quasi-reversible peak at -2.2V. For monomer **26**, the peaks occurred at -1.38/-1.32 V, -1.70/-1.64 V, -1.92/-1.83 V and -2.12/-2.00 V. All the reduction processes were attributed to the reduction of each of the bipyridine ligands.

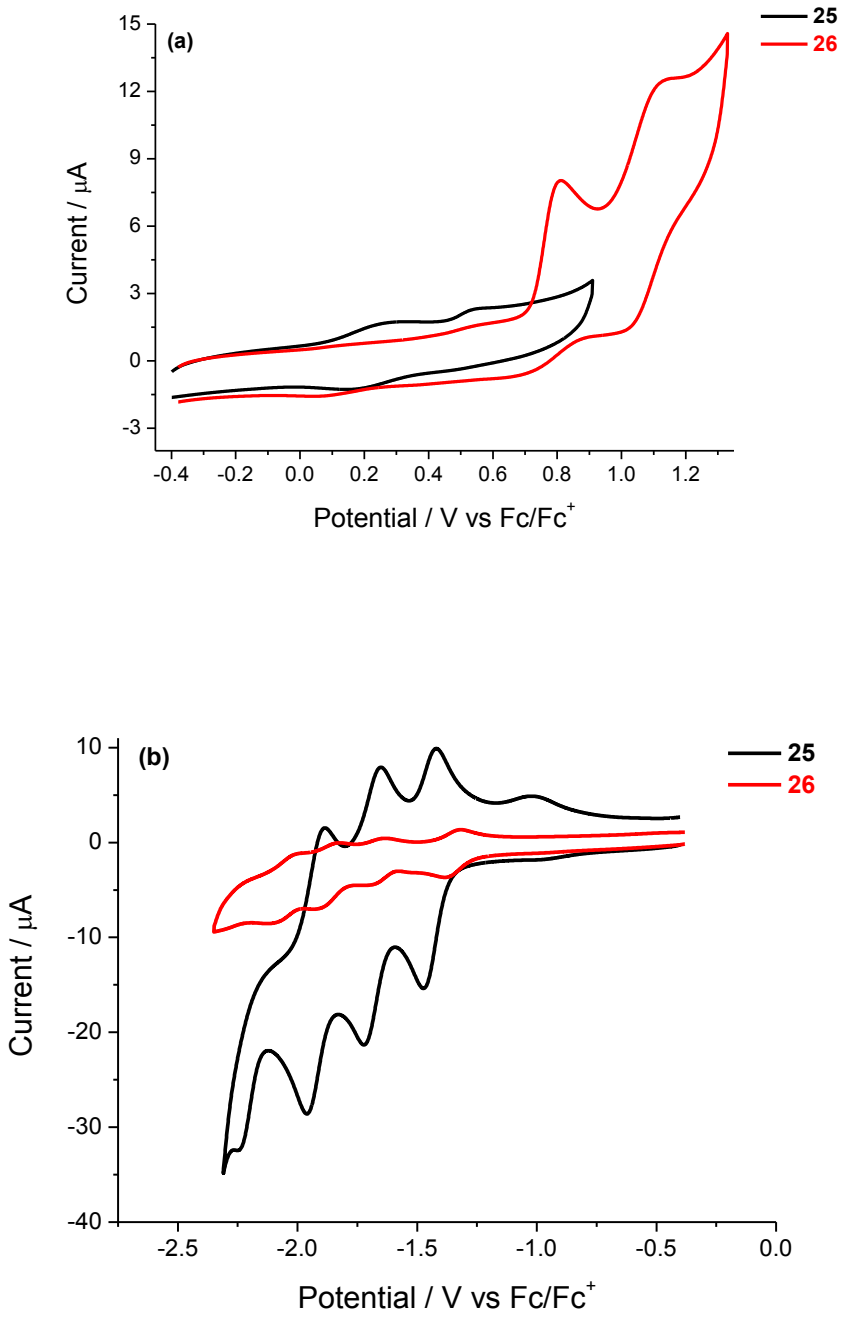

Figure 2.77. Cyclic voltammograms of (**a**) oxidation and (**b**) reduction of monomer **25** and **26** on a glassy carbon working electrode, , Ag wire reference electrode and Pt counter electrode in MeCN, monomer concentration ca. 10^{-4} M at a scan rate of 100mVs^{-1}

The electrochemical HOMO-LUMO gaps of monomers **25** and **26** were estimated from the difference between the onsets of both oxidations and reductions to find the HOMO and LUMO energy levels, respectively.

Table 2.13 shows the electrochemical data of both monomers. The difference between the HOMO and LUMO values of monomer **25** gave an electrochemical HOMO-LUMO gap of 1.42 eV, which is lower than the calculated optical HOMO-LUMO gap (2.36 eV). Monomer **26** has given an electrochemical HOMO-LUMO gap of 2.09 eV, which is also lower than the calculated optical HOMO-LUMO gap (2.32 eV). Therefore, there is a significant difference between the electrochemical and optical HOMO-LUMO gaps in both monomers. This possibly can be attributed to the effect of the distance between the centre unit and the terminal units in both monomers.

Table 2.13. Electrochemical Data for Energy levels of monomers **25** and **26**

Monomer	Onset of oxidation /V	Onset of reduction /V	HOMO / eV	LUMO / eV	E_g / eV
25	+0.079	-1.35	-4.879	-3.45	1.42
26	+0.71	-1.34	-5.51	-3.46	2.05

2.4.3. Electropolymerisation

Many attempts were made for the electropolymerisation of monomer **25** by varying the experimental conditions**,** including using different potentials, substrate concentrations and number of cycles. However, the polymer does not grow, possibly due to the distance between the donor and core units being too short compared to in

monomer **26.** This could lead to the cation radical being unstable. Additionally, it is possible that the Ru^{II}/Ru^{III} oxidation process occurs rather than oxidation of the EDOT units. Monomer **26** does polymerise, and the growth traces for the corresponding polymer is shown in Figure 2.78. All conditions are shown in the graph below. The polymer was grown by cycling between 0 and +1.1 V.

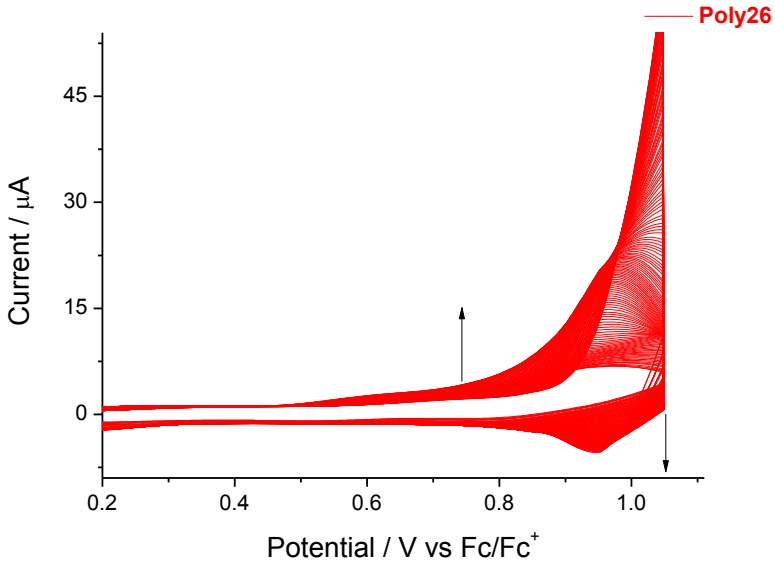

Figure 2.78. Electrochemical growth of poly**26** using a glassy carbon working electrode, Ag wire reference electrode and Pt counter electrode in MeCN as solvent (0.1 M $TBAPF_6$ as supporting electrolyte). The data is referenced to the Fc/Fc^+ redox couple, at a scan rate of $100mVs^{-1}$, over 300 segments.

The oxidation and reduction processes of poly**26** were investigated in monomer-free dichloromethane, on a glassy carbon working electrode as a thin film with the same concentration of supporting electrolyte as before (0.1 M $TBAPF_6$). The cyclic voltammograms of poly**26** are shown in Figure 2.79. The oxidation of the poly**26** shows two reversible peaks at +0.40/+0.37V and +0.74/+0.73V. The first reversible

peak is from the oxidation of EDOT units and the second one is likely to be from Ru^{II}/Ru^{III} oxidation. The reversible reduction peak at -1.91/-1.81 V will be the formation of a radical anion, which will be stabilised on the bipyridine units.

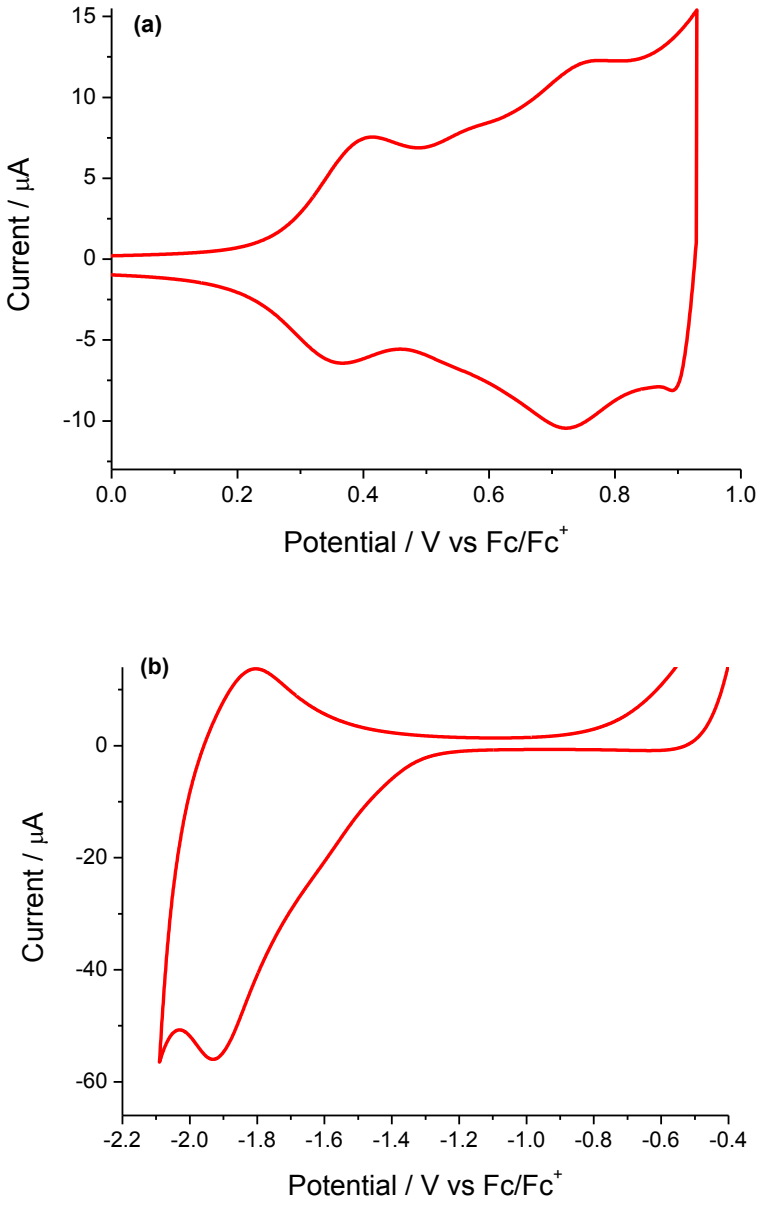

Figure 2.79. (a) Oxidation and (b) reduction of poly**26** as a thin film on a glassy carbon working electrode, Ag wire reference electrode and Pt counter electrode, in monomer-free dichloromethane (0.1 M $TBAPF_6$ as supporting electrolyte). The data is referenced to the Fc/Fc^+ redox couple, at a scan rate of 100 mVs^{-1}.

Poly**26** gives an electrochemical band gap with a lower value (1.78 eV) compared to its monomer case (2.05 eV) as depicted in Table 2.14.

Table 2.14. Electrochemical Data for Energy levels of monomer **26**

Polymer	Onset of oxidation /V	Onset of reduction /V	HOMO / eV	LUMO / eV	E_g / eV
26	+0.26	-1.52	-5.06	-3.28	1.78

HOMO and LUMO values are calculated from the difference onsets oxidation and reduction and subtracted from a HOMO of ferrocene, which has a HOMO of -4.8 eV.

Cyclic voltammograms of poly**26** at different scan rates (Figure 2.80) showed that the potential at peak maximum shifts to higher values after each run. Figure 2.81 displays a linear relationship between scan rate and current peak maxima, with a good correlation factor. This behaviour shows that the redox process of poly**26** is not diffusion limited.

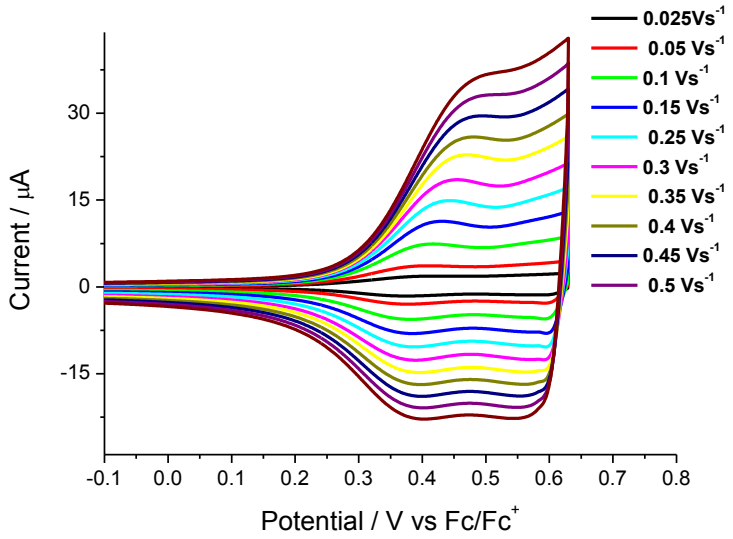

Figure 2.80. Cyclic voltammograms of poly**26** in monomer free dichloromethane with varying scan rate

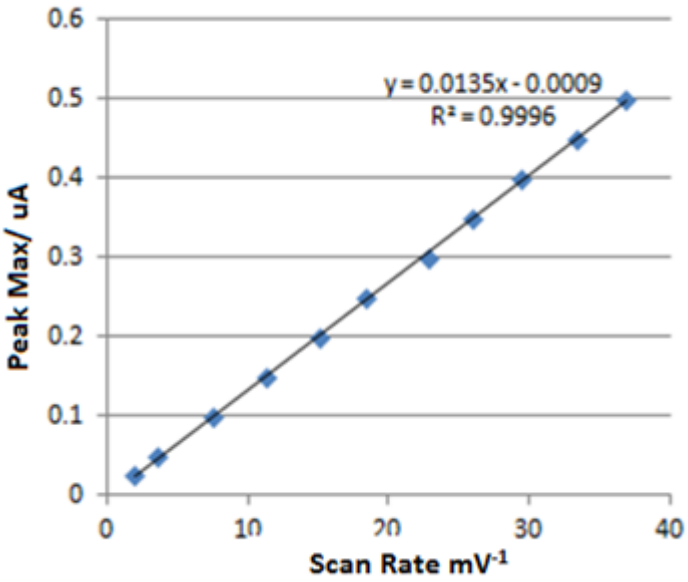

Figure 2.81. Current max *vs.* scan rate of poly**26**

2.4.4. Stability of Polymer 26

Stability studies of the polymer **26** were performed on a glassy carbon electrode in monomer-free dichloromethane to monitor the change in the current response. Accordingly, the polymer is highly stable to anodic conditions with only a 3.12 % decrease in the current reply over 100 segments. The oxidative stability of polymer **26** is shown in Figure 2.82.

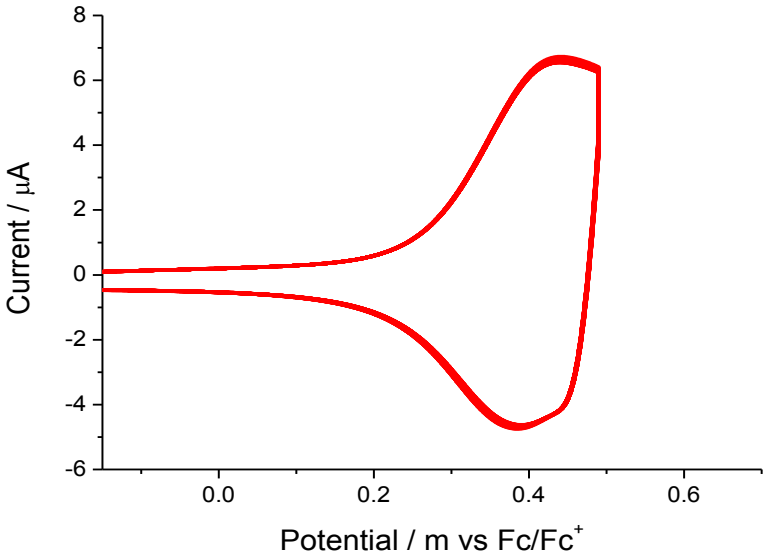

Figure 2.82. Oxidative stability of poly**26** in monomer free dichloromethane, at a scan rate of 100mVs^{-1}, over 100 segments, using a glassy carbon working electrode

2.4.5. Optical and Spectroelectrochemical properties of Poly26

A thin film of poly**26** was grown onto an ITO coated glass and then de-doped to reduce the polymer back to its neutral state. The polymer was studied in both doped and neutral form. Two peaks have appeared in the doped state at 439 and 578 nm from a π-π* transition and an ICT process respectively between donor-acceptor units, which has a bathochromic shift compared to the monomer case. The spectrum in the de-doped state gives an absorption peak maximum at 434 nm. The colour has changed from brown in de-doped state to dark yellow in the doped state. The optical band gap was calculated from the edge of the absorption band of the polymer. The calculated optical band gap of poly**26** is 1.90 eV, which is slightly higher than the

electrochemical band gap determined in this (1.78 eV). The solid state spectrum of the polymer is shown in Figure 2.83.

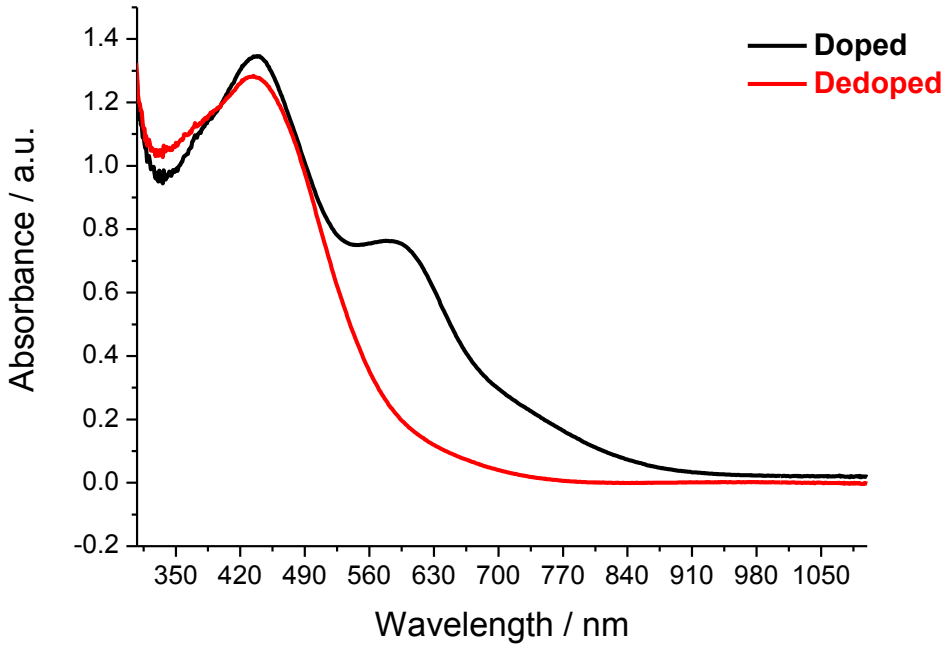

Figure 2.83. Solid state electronic absorption spectrum of poly**26** de-doped and doped, recorded as a thin film deposited on ITO glass, in (Dichloromethane as monomer-free).

The p-doping effect of poly**26** was studied by spectroelectrochemical measurements on an ITO slide and the data is presented as a three dimensional plot in Figure 2.84. A new absorption wave was generated between 500 and 900 nm corresponding to a higher potential from 1.2 to 1.3 V. This trace can be attributed to the formation of positive polarons and bipolaron signatures within the polymer chain. The polymer chain has shown reduce in π-transition at 450 nm.

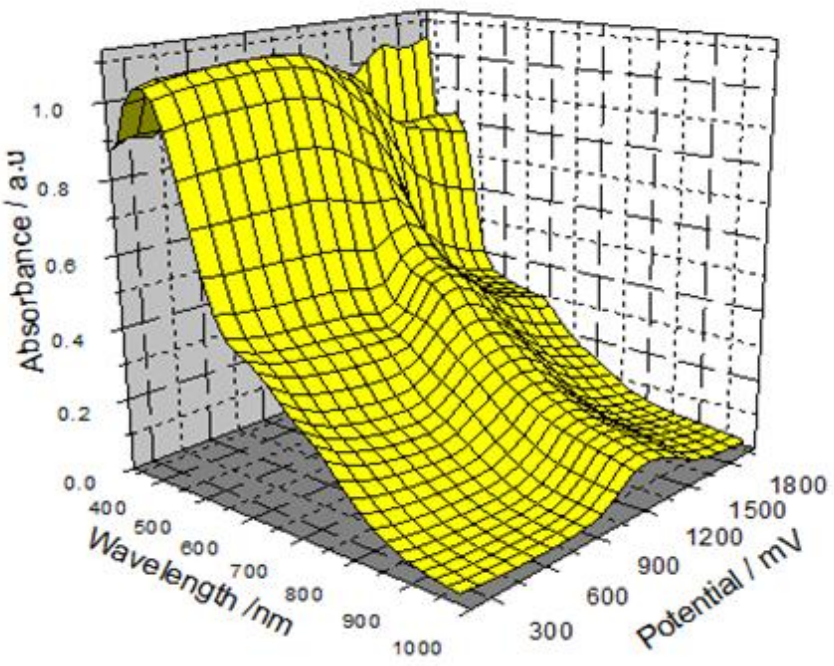

Figure 2.84. UV-vis spectroelectroelectrochemical plot of upon p-doping poly**26** deposited on ITO glass. Experiments were performed in monomer-free dichloromethane solution and in the presence of $TBAPF_6$ (0.1 M).

2.4.6. Conclusion

Two new monomers have been synthesised and analysed by spectroscopy, electrochemical and spectroelectrochemical tests. Monomers **25** and **26** exhibited some differences between their optical and electrochemical band gap values. That was ascribed to the reductive electroactivity of the core unit independent from the thiophene derivatives chain. Electrochemical polymerisation of monomer **25** was unsuccessful despite repetitive cycling over the oxidation peaks, which is likely to be due to the highly dominating Ru^{II}/Ru^{III} oxidation process. However, monomer **26**

was grown successfully on the electrode surface throughout repetitive cycling. Poly**26** exhibited a lower electrochemical band gap value compared to its monomer with high oxidative stability under anodic conditions. Poly**26** shows agreement between the optical and electrochemical band gaps, which were 1.78 to 1.90 eV, respectively. The polymer showed a change in colour between its neutral and doped states.

2.5. Electrochemical characterisation of new organic molecules based on Bis-EDOT Pyridine.

2.5.1. Introduction

The small energy gap present in donor-acceptor systems through the oxidation and reduction processes created through the relationship between the strong donor group and acceptor group. This increases the HOMO level and decreases the LUMO level.[143,144,53] The electropolymerisation of a donor-acceptor system based on EDOT-Pyridine heteroaromatic rings containing vinylene-spacer groups[143] between the units has been shown to form efficient polymers with attractive properties such as low energy band gap, that can be used in photovoltaics devices.[143,144]

In this section, two heteroarylene molecules **27** and **28** containing the bis-EDOT unit have been appended directly to a pyridine unit as shown in Figure 2.85 and their synthesis is depicted in scheme 2.6.

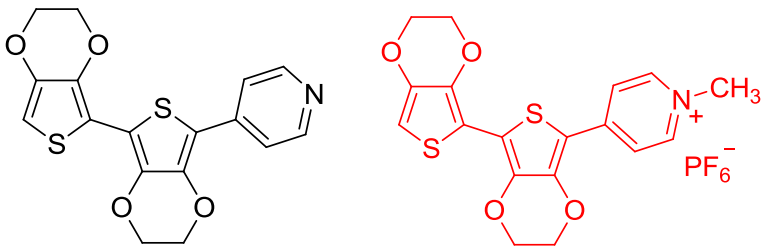

27 **28**

Figure 2.85. Structures of monomers **27** and **28**

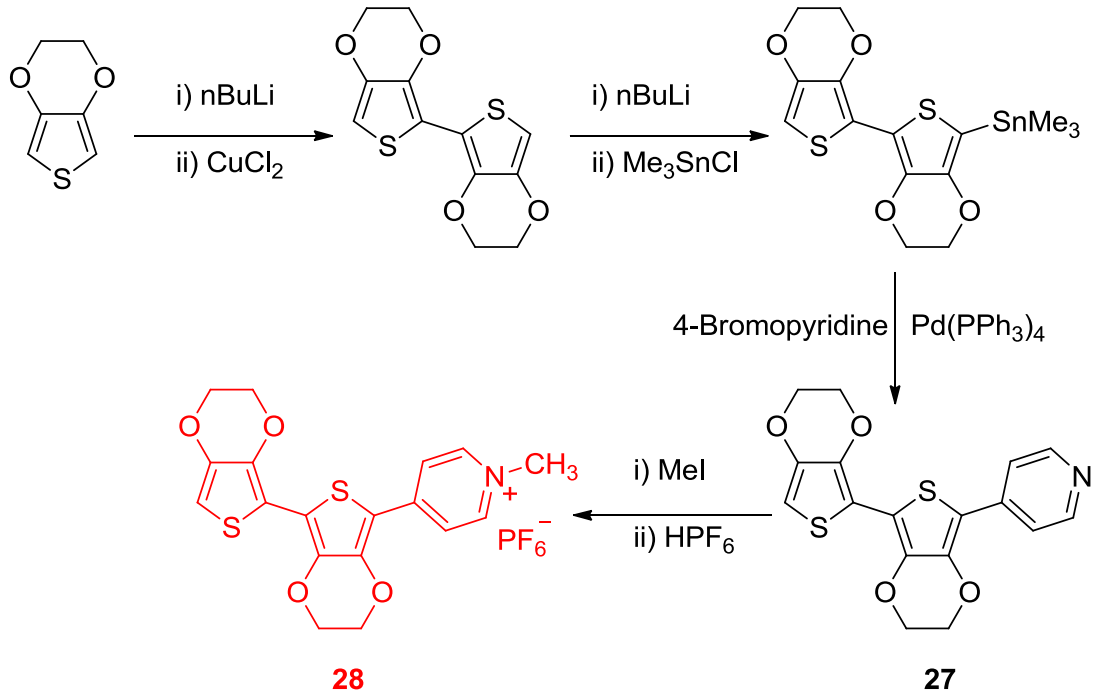

Scheme2.6. Synthesis of monomers **27** and **28**

2.5.2. Experimental

The synthesis of compounds **27** and **28** was achieved by Filipe Vilela and Neil Findlay (University of Strathclyde).

Cyclic voltammetry measurements were performed on a CH Instruments 660A electrochemical workstation with *iR* compensation using dichloromethane as the monomer solvent and acetonitrile for the monomer-free solvent. The electrodes were glassy carbon, platinum wire, and silver wire as the working, counter, and reference electrodes, respectively. All solutions were degassed (Ar) and contained monomer substrates at a concentration of *ca.* 10^{-4} M, together with tetrabutylammonium hexafluorophosphate (0.1 M) as the supporting electrolyte, All measurements are referenced against the $E_{1/2}$ of the Fc/Fc^{+} redox couple.

All electronic absorption spectra experiments were recorded at room temperature on a UNICAM UV 300 spectrophotometer, which was operating between 190 and 1100 nm for solution spectra, a $1cm^3$ path length quartz cell was used and the baselines were measured before analysis. Films were grown on indium tin oxide (ITO) glass slides, and then de-doped in monomer-free solution for one hour by cycling over a small potential, where no electroactivity takes place. The deposited film measurements were measured in the range between 300 and 1100 nm.

2.5.3. UV-vis absorption studies of monomers 27 and 28

The electronic absorption spectra for monomers **27** and **28** were recorded in dichloromethane solution (Figure 2.86). Monomer **27** gives four peaks at 270,292, 374 and 391 nm and the peaks for monomer **28** emerged at 257, 287, 363 and 459 nm. From the Figure 2.86, it is clear that there is an increase in the absorption spectra peak for monomer **28** (459 nm) compared to monomer **27** (391 nm). This suggests the effect of CH_3 group, which increases the acceptor property of the pyridine unit. Therefore this can be ascribed to an intramolecular charge transfer (ICT) process between the donor and acceptor units. The ICT interaction is illustrated in Figure 2.87. The onset of the absorption edge gives the optical HOMO-LUMO gap for the monomers. The values were calculated as 2.95 eV for monomer **27** and 2.44 eV for monomer **28** representing that the alkylation effect and ionic effect in the structure of monomer **28**.

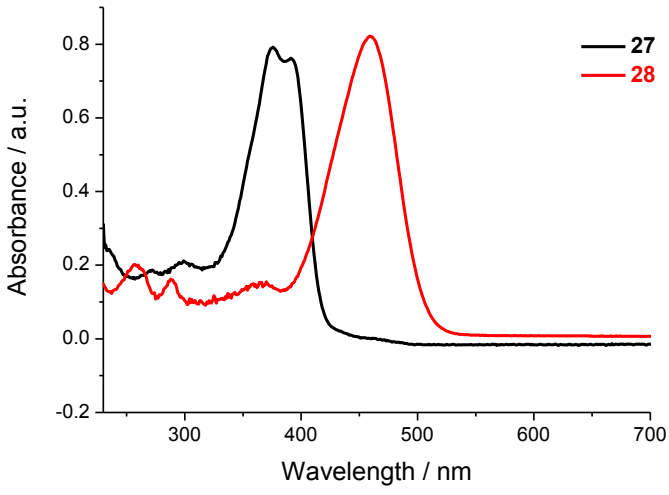

Figure2.86. Absorption spectra of monomers **27** and **28** measured in dichloromethane solution

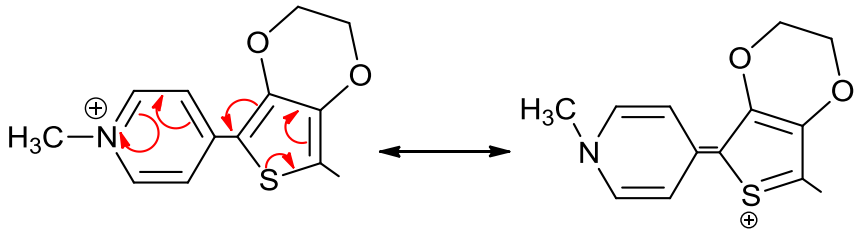

Figure2.87. ICT process of monomer **28**

2.5.4. Cyclic Voltammetry experiments of monomers 27 and 28

The cyclic voltammograms of monomers **27** and **28** were performed in dichloromethane solution with a glassy carbon working electrode and silver reference electrode. Oxidation of monomer **27** (Figure 2.88a) offers two irreversible peaks at +0.49 and +0.59V, while oxidation of monomer **28** revealed irreversible peak at +0.53 V and reversible peak at +0.86/+0.80 V. The oxidation peaks in both monomers are likely to be a two-electron oxidation, generating radical cations and dication respectively from the EDOT units.

The reduction processes of monomers **27** and **28** are shown in Figure 2.88b. Irreversible reduction of monomer **27** occurs at -2.0 V; however, monomer **28** shows a reversible reduction peak at -1.44/-1.37V that corresponds to the reduction of the pyridinium unit in two monomers.

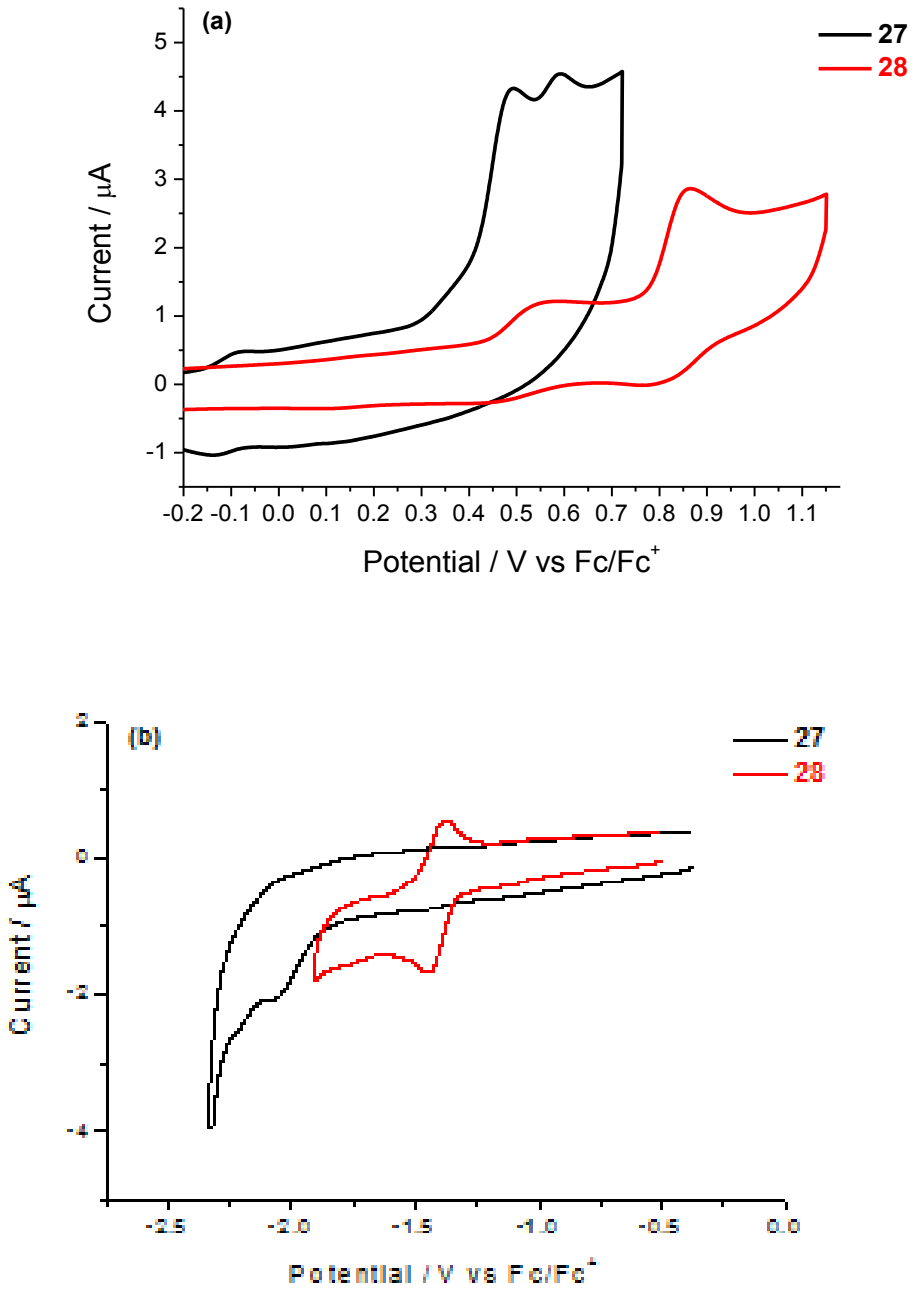

Figure 2.88. Cyclic voltammograms of (**a**) oxidation and (**b**) reduction of monomers **27** and **28**, on a glassy carbon working electrode, Ag wire reference electrode and Pt counter electrode, in dichloromethane solution and the monomer concentration is ca. 10^{-4} M, at a scan rate of $0.1 Vs^{-1}$. The data is referenced to the Fc/Fc^{+} redox couple

The onset of the first oxidation and reduction values have subtracted from the HOMO of ferrocene (-4.8 eV) as before to find the electrochemical band gap (Table 2.15). By comparing the energy levels of two monomers, monomer **28** has lower LUMO (-3.46 eV) compared to that of monomer **27**. There is no significant difference in the HOMO level values in two monomers, as such monomer **28** gives a lower electrochemical band gap value (1.76 eV) than that of monomer **27** (2.26 eV). This is likely to be the influence of the intramolecular charge transfer effect in monomer **28**.

Table 2.15. Electrochemical Data for Energy levels of monomers **27** and **28**

Monomer	Onset of oxidation /V	Onset of reduction /V	HOMO / eV	LUMO / eV	E_g / eV
27	+0.38	-1.88	-5.18	-2.92	2.26
28	+0.42	-1.34	-5.22	-3.46	1.76

HOMO and LUMO values are calculated from the difference onsets oxidation and reduction and subtracted from a HOMO of ferrocene, which has a HOMO of -4.8 eV.

2.5.5. Electrochemical and Spectroscopic Studies of Monomers 27 and 28

Both monomers were subjected to deposition by repetitive cycling over their redox-active peaks. Both monomers showed good growth on the electrode surface, with the growth traces (dimers) shown in Figure 2.89.

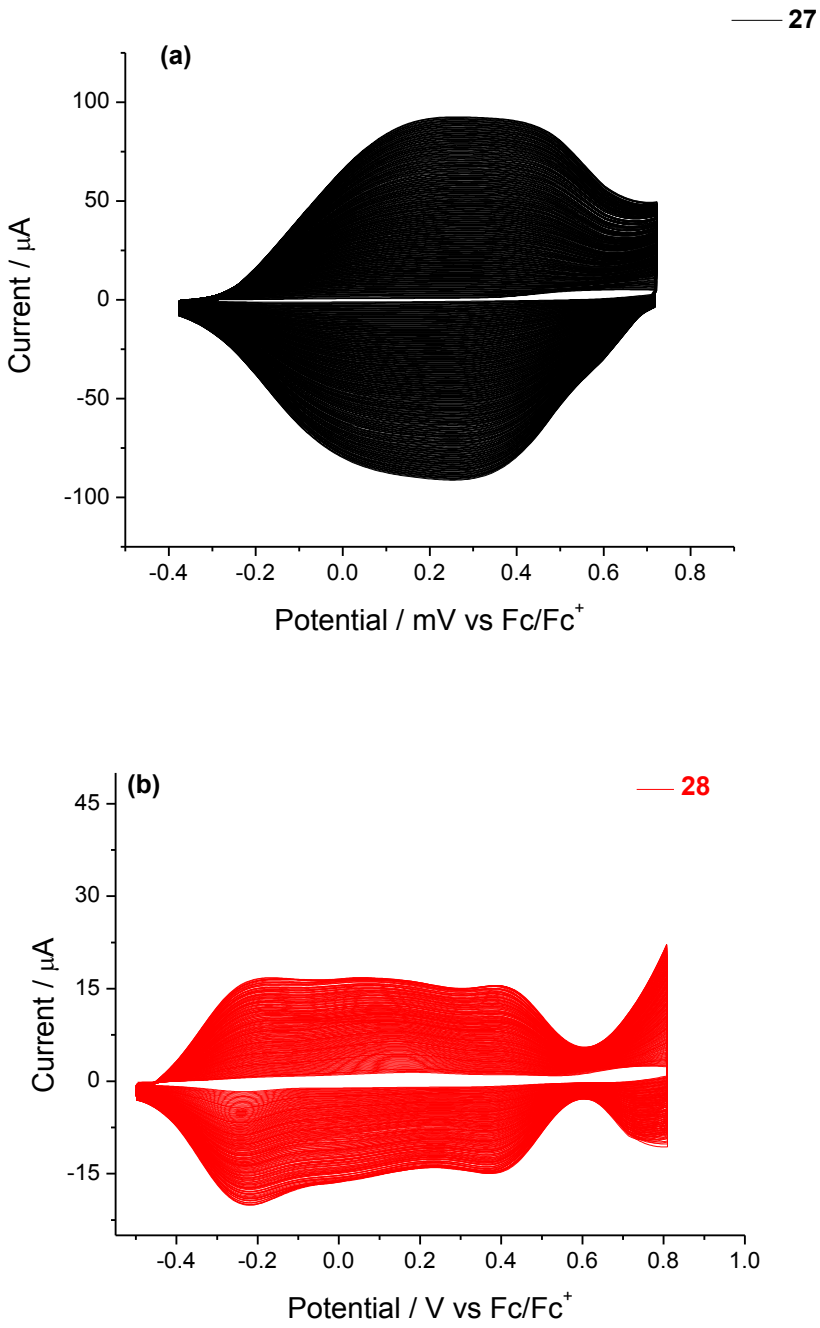

Figure2.89. Electrochemical growth of compounds (**a**) **27** and (**b**) **28**, in dichloromethane, using glassy carbon as working electrode Ag wire reference electrode and Pt counter electrode, concentration ca. 10^{-4} M , (0.1 M TBAPF6 as supporting electrolyte). The data is referenced to the Fc/Fc+ redox couple, at a scan rate of $0.1Vs^{-1}$, over 300 segments.

The electrochemical oxidation and reduction processes of the two grown compounds were studied in monomer-free acetonitrile solution with the same concentration of supporting electrolyte as earlier; the cyclic voltammograms of both compounds are illustrated in Figure 2.90.

The oxidation process (Figure 2. 90a) of both compounds features broad reversible peaks with a slight difference in the oxidation potential values. This indicates the oxidation of EDOT units in both compounds.

The reduction process of deposited films **27** and **28** is shown in Figure 2.90b, where the dimer **27** exhibits an irreversible peak at -2.0 V, which is almost the same value compared to its monomer case. Dimer **28** gives two irreversible reduction peaks at -2.0 and -2.34 V.

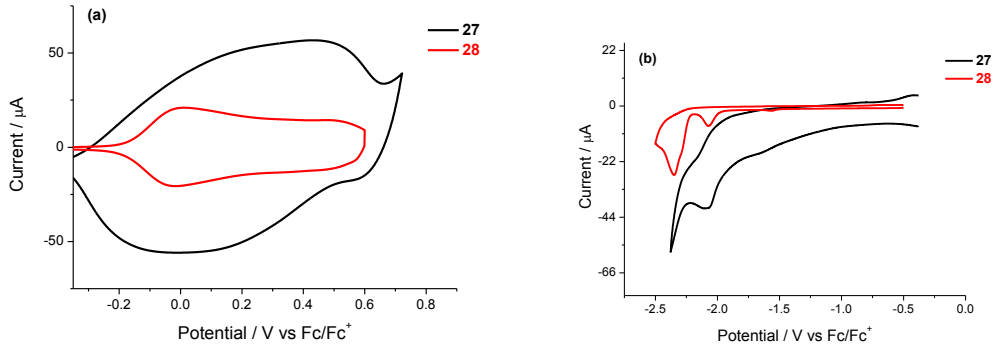

Figure 2.90. Cyclic voltammograms for (**a**) oxidation and (**b**) reduction of dimers **27** and **28** in monomer- free MeCN solution.

The HOMO-LUMO gap of dimer**27** and dimer**28** was calculated by determining the onsets of both the oxidation and reduction for each to give the HOMO and LUMO energy levels, respectively, when subtracted from the known HOMO of ferrocene (-4.8 eV). All data are summarised in Table 2.16. No significant difference between

the HOMO-LUMO gaps of both compounds (dimers) after electrodeposition was observed. However there is significant difference in the HOMO-LUMO gap of dimer**27** when compared to its monomer in solution (2.26 eV). This could be due to its increase of the conjugation chain.

Table 2.16. Electrochemical Data for Energy levels of compounds **27** and **28**

Dimer	Onset of oxidation /V	Onset of reduction /V	HOMO / eV	LUMO / eV	E_g / eV
27	-0.30	-1.90	-4.50	-2.90	1.60
28	-0.19	-1.98	-4.61	-2.82	1.79

HOMO and LUMO values are calculated from the difference onsets oxidation and reduction and subtracted from a HOMO of ferrocene, which has a HOMO of -4.8 eV.

To investigate the electronic properties of the dimer**27** and dimer**28**, each was grown on an ITO-coated glass slide by repetitive cycling, and then de-doped in the range between -0.7 and -0.5 V for one hour in monomer-free acetonitrile. UV-vis analysis shows the spectra in Figure 2.91.

Three peaks occur at 470, 509 and 557 nm for dimer**27** and one peak at 587 nm for dimer**28**. The longest wavelength absorption peak at 557 nm in dimer**27** exhibits a hypsochromic shift compared to the absorption maximum peak in dimer**28** that supports the presence of the ICT process between the donor and acceptor units in dimer**28**. Dimer**27** and dimer**28** exhibit bathochromic shifts in comparison to their monomers (166 and 128 nm for **27** and **28** respectively), which indicated that dimerisation (or polymerisation has occurred). The onset of the longest wavelength absorption edges were used to calculate the optical HOMO-LUMO gap for both,

which corresponds to values of 1.63 and 1.33 eV for dimer**27** and dimer**28** respectively.

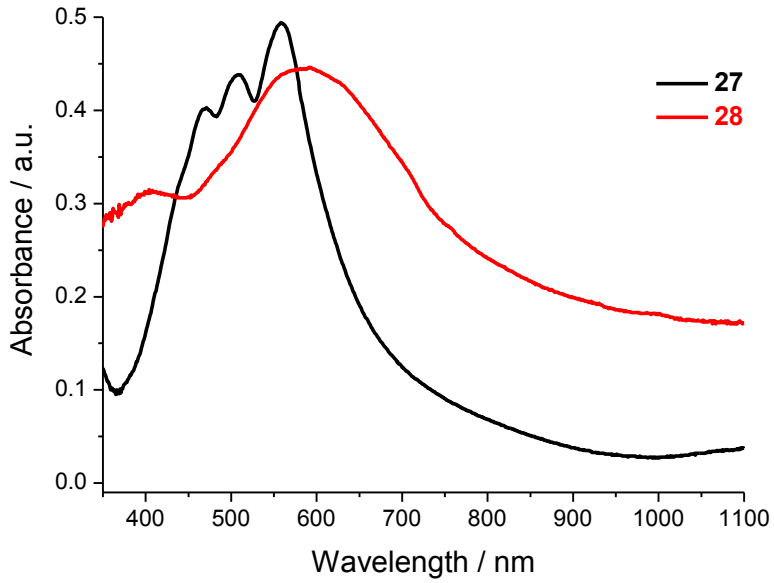

Figure 2.91. UV-vis spectrum after electropolymerisation of compounds **27** and **28**

2.5.6. Stability and Scan Rates of Dimer27 and Dimer28

The stability of dimer**27** and dimer**28** (Figure 2.92) on the glassy carbon electrode was observed through freshly grown films by cycling over the appropriate redox active peaks 150 times.

The two dimers exhibited high stability under anodic conditions with just 2% and 7% loss for dimer**27** and dimer**28**, respectively.

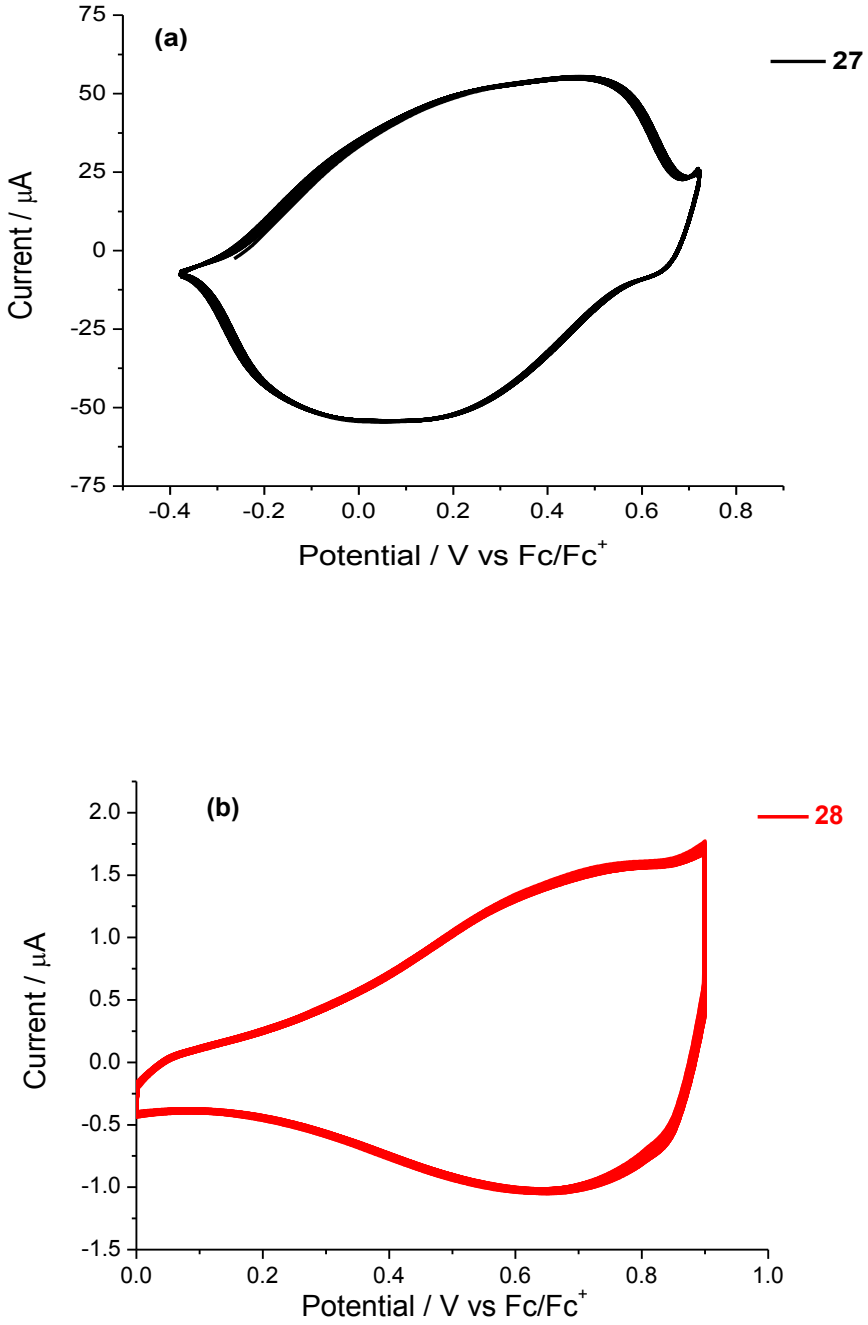

Figure 2. 92. Oxidative stability test of (**a**) dimer**27** and (**b**) dimer**28**

To test the electrochemical behaviour and the stability of both compounds, the oxidative stability was determined at increasing scan rate values over the first oxidation peaks as depicted in Figure 2.93.

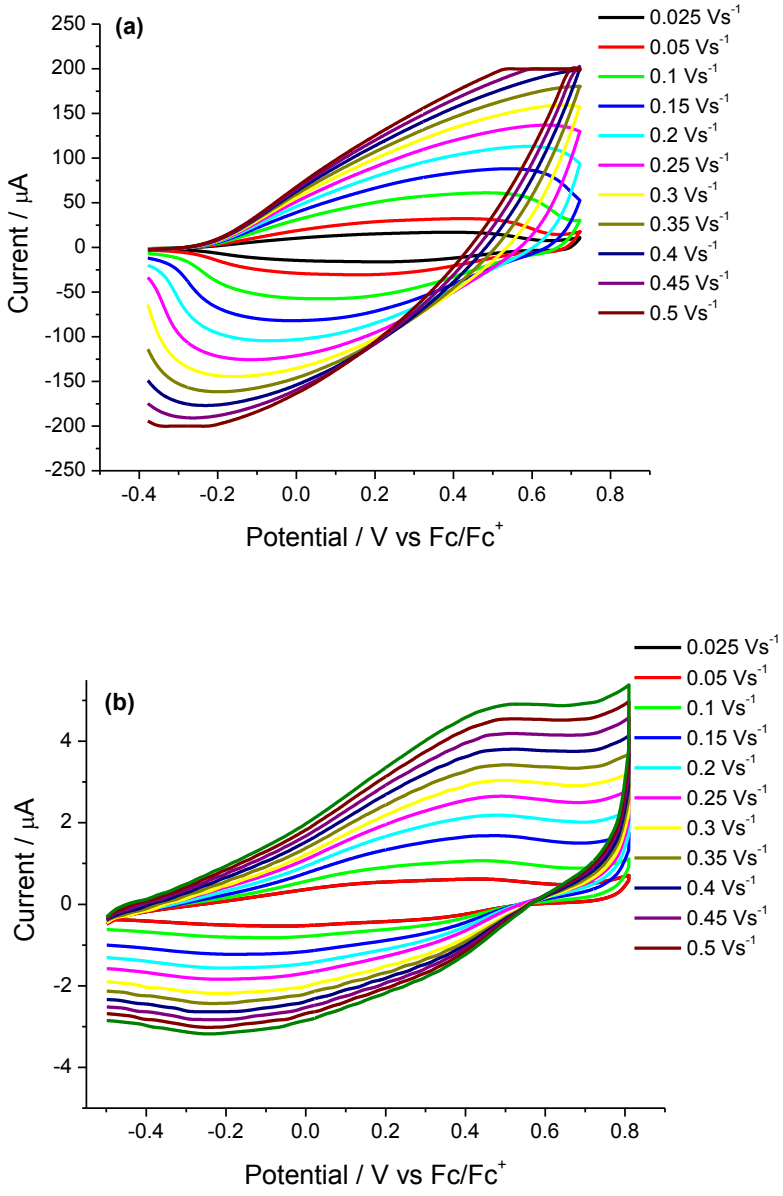

Figure 2.93. Cyclic voltammograms of (**a**) dimer**27** and **(b)** dimer**28** with varying scan rates scan rates

The relationship between the scan rate and the current peaks maxima (Figure 2.94) gives a linear fit with high R^2 values for each compound, which were 0.9615 for dimer**27** and 0.9865 for dimer**28**. This confirms that charge transport through the films is limited by diffusion, but controlled by the electrode surface.

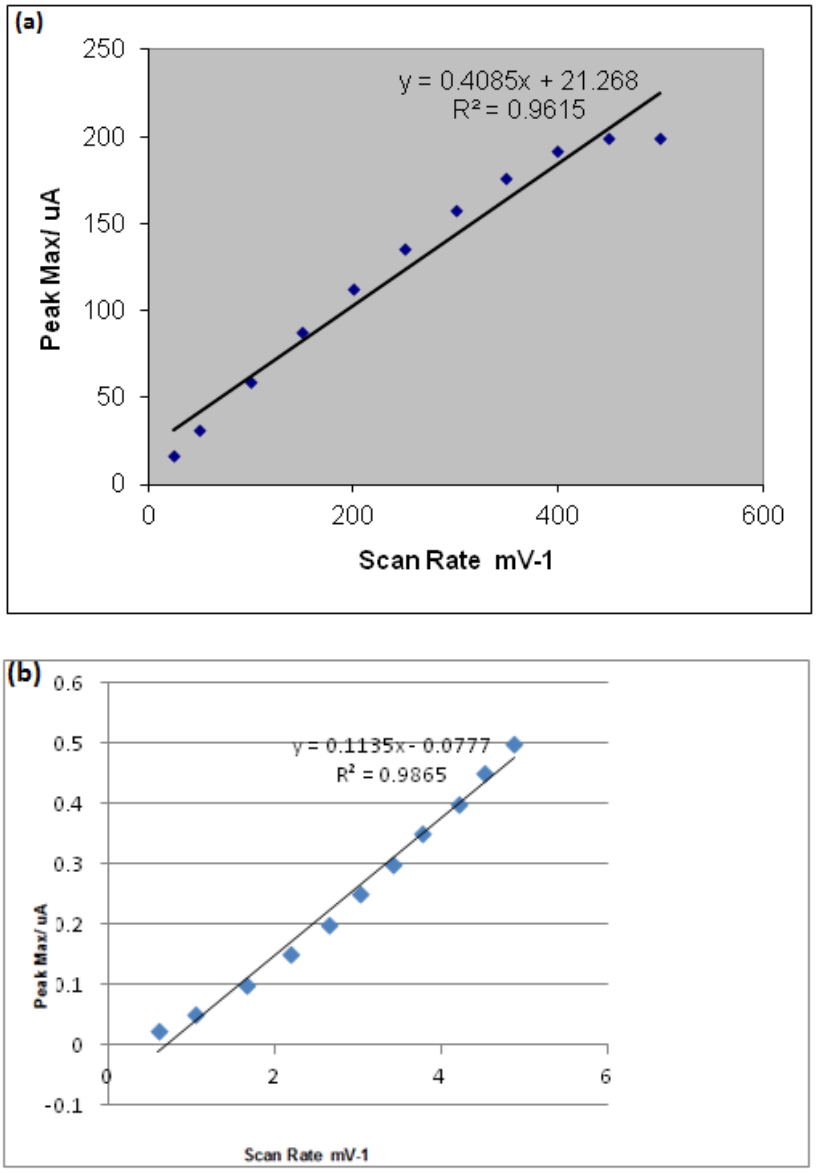

Figure 2.94. Plot of current versus scan rate for **(a)** dimer**27** and **(b)** dimer**28**

2.5.7. Conclusions

Two new monomers and their respective dimers have been characterised by UV-vis absorption spectroscopy and cyclic voltammetry. The compounds **27** and **28** have a bisEDOT unit attached to a pyridine unit, with an additional methyl group in compound **28**. Compound **28** has shown clear evidence of an ICT process in the monomer case compared to monomer **27**. After electrodeposition both compounds give excellent growth with a blue colour that is indicative of the dimer, which is deposited on the electrode surface. The electronic absorption spectra confirm the dimer formation by showing significant extension of the conjugation length through dimer**27** and dimer**28** compared to their monomers.

2.6. New Redox Bodipy Based on Conjugated Materials

2.6.1 Introduction

The well known compound 4,4-difluoro-4-borata-3a-azonia-4a-aza-s-indacene (BODIPY) is an efficient fluorescent dye. BODIPY has been coupled with EDOT to produce conjugated materials with unique properties such as low band gap, high efficient absorption and tunable colour characteristics, therefore these materials were potential candidates to be used as components in several applications such as electrochromic devices and organic solar cells.[145,124]

The main focus of this section is three compounds containing BODIPY as the central core and attached to either EDOT, thiophene or EDTT as terminal units in compounds **29**, **30** and **31** respectively. The synthesis of all three compounds is illustrated in scheme 2.7 and The structures of these compounds are shown in Figure 2.95.

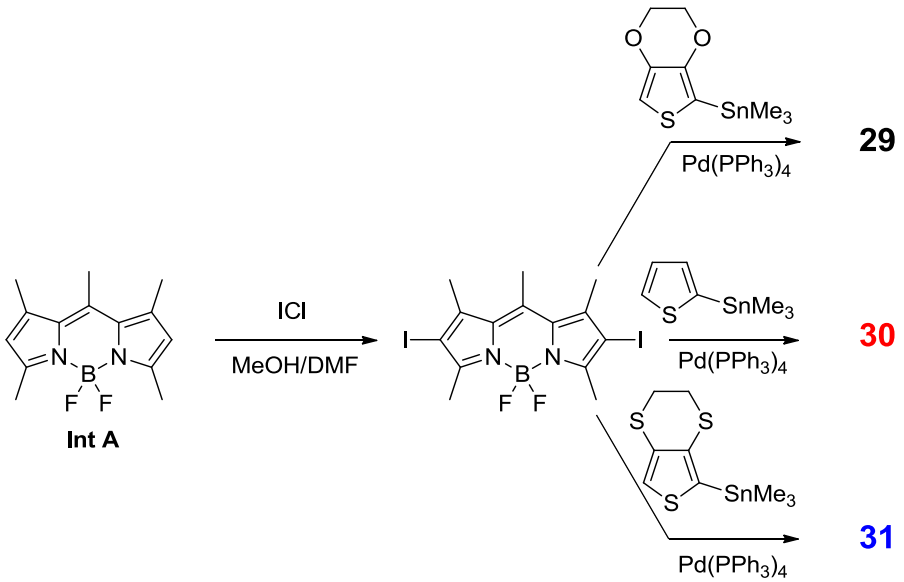

Scheme 2.7. Synthesis of compounds **29** and **30** and **31**

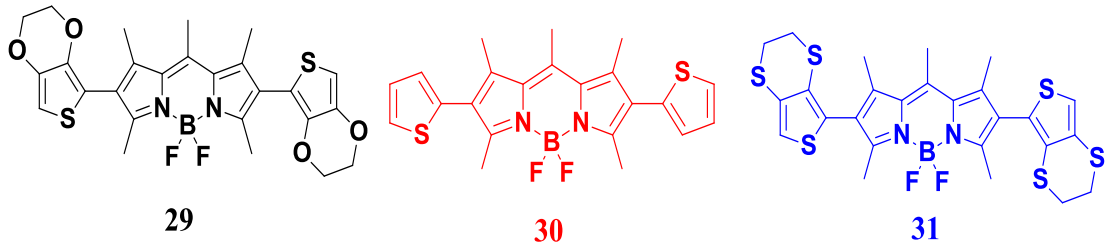

Figure2.95. Structures of compounds **29**, **30** and **31**

2.6.2 Experimental

The synthesis of compounds **29**, **30** and **31** was completed by Jordon Wragg (University of Strathclyde).

Cyclic voltammetry measurements were performed on a CH Instruments 660A electrochemical workstation with *iR* compensation using dichloromethane as the monomer solvent and acetonitrile for the monomer-free solvent. The electrodes were glassy carbon, platinum wire and silver wire as the working, counter, and reference electrodes, respectively. Bu_4NPF_6 (0.1 M) was used as the supporting electrolyte and the monomer substrates were analysed at a concentration of *ca.* 10^{-5} M. All solutions were degassed by (Ar) during the reduction stage. All measurements were referenced against the $E_{1/2}$ of the Fc/Fc^+ redox couple. Absorption spectra were recorded on a UNICAM UV 300 instrument.

2.6.3 Electrochemical and optical properties of monomers

The electronic absorption spectrum of all three monomers **29**, **30** and **31** was recorded in dichloromethane solution and is exhibited in Figure 2.96.

The spectra show similarities in all three monomers, however monomer **29** exhibits a bathochromic shift compared to monomers **30** and **31** with a main peak at 528 nm for monomer **29**, whereas the coresponding peaks occur at 521 and 518 nm for monomers **30** and **31** respectively. Consequently, the absorption maxima for the three molecules containing either EDOT, thiophene or EDTT units (528, 521, and 518 nm, respectively) represent substituent effects of the different chalcogen atoms at the 3,4-positions on the thiophene. Therefore, the absorption spectra signature shows the higher conjugated length of the EDOT units in monomer **29**, compared to the other molecules. The data for all the absorption peaks and optical band gap are summarised in Table 2.17 for easeir comparison.

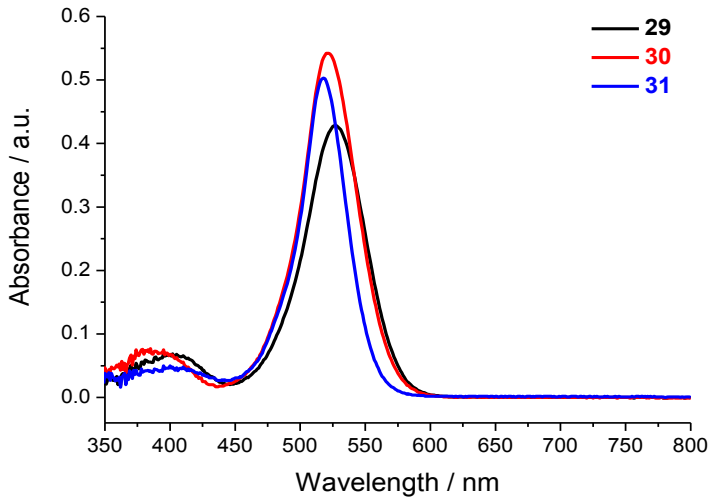

Figure2.96. UV-Vis spectra of monomer **29**, **30** and **31** measured in dichloromethane

Table 2.17. Optical absorption data for monomers **29** and **30** and **31**

Monomer	Main absorption peak / nm	Optical band gap / eV
29	528	2.14
30	521	2.16
31	519	2.19

From Table 2.17, the optical band gap of monomer **29** is slightly lower than other monomers. This is not surprising considering that this compound contains two EDOT units that are stronger electron donors than the other terminal units (thiophene and EDTT units respectively) in monomers **30** and **31**. The electrochemical properties of the monomers were determined by cyclic voltammetry in dichloromethane solution on a glassy carbon working electrode with silver wire as reference (Figure 2.97). Two reversible oxidation peaks (Figure 2.97a) were revealed in all three monomers, with the peaks in monomer **31** appearing at a higher oxidation potential compared to monomer **29** and **30**. The first peaks at +0.34/+0.30 V, +0.34/+0.31 V and +0.54/+0.53 V for monomers **29**, **30** and **31** respectively, produce a radical cation species in each case. The second oxidation waves of the three compounds occur at +0.67/+0.53 V and +0.55/+0.52 V for monomers **29** and **30**, respectively, and again at a higher oxidation potential (+0.74/+0.68 V) for monomer **31**. The reduction scans for monomers **29**, **30** and **31** are shown in Figure 2.97b. All three monomers show similar reduction peaks, where monomer **29** gives a reversible wave at -1.64/-1.58 V and an irreversible peak at -2.05 V. Monomer **30** shows reversible peak at -1.55/-1.49 V and quasi-reversible peak at -2.02 V, while there are two irreversible peaks at -1.46 V and at -2.02 V for monomer **31**. Therefore the reduction peaks are pointed to the reduction of BODIPY units.

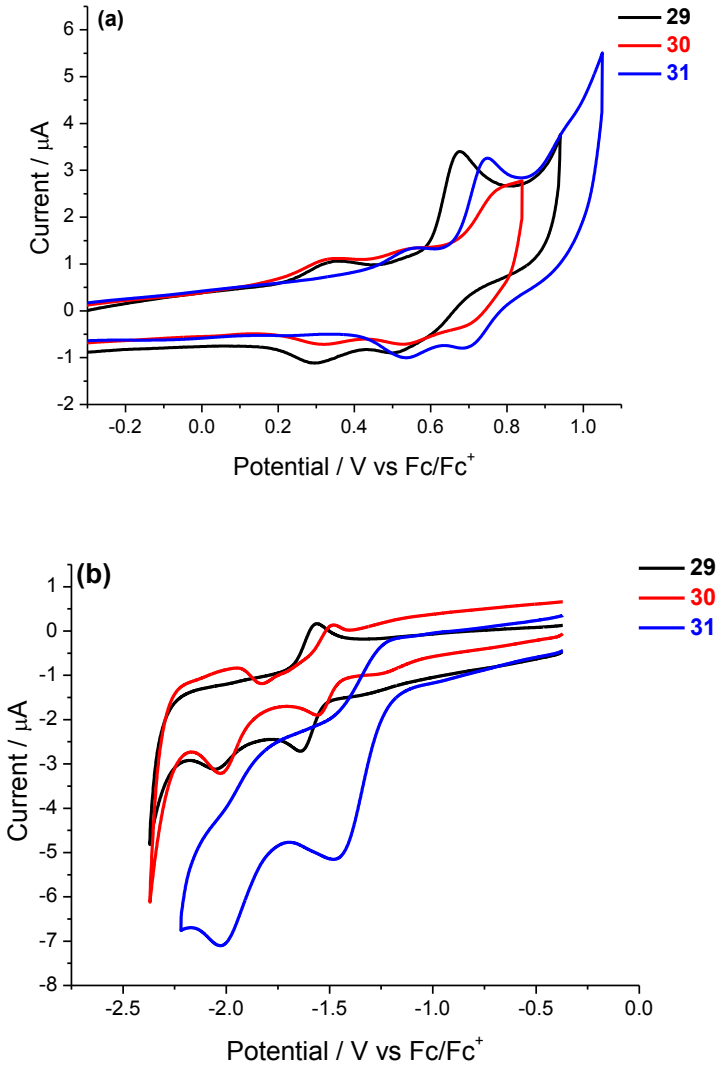

Figure 2.97. (**a**) oxidation and (**b**) reduction of three monomers in dichloromethane solution with 0.1 M $TBAPF_6$ as supporting electrolyte, on a glassy carbon working electrode. at a scan rate of $0.1Vs^{-1}$.

To determine the HOMO and LUMO energy levels and then the electrochemical HOMO-LUMO gap, CVs of three monomers were calculated by subtracting the onset of the first oxidation and reduction waves from the HOMO of ferrocene (-4.8 eV) (Table 2.18). There is no considerable differences between all the HOMO and

LUMO level values of all three monomers. Therefore, they have almost similar electrochemical band gap values.

Table 2.18. Electrochemical Data for Energy levels of monomers **29, 30** and **31**

Compound	Onset of oxidation /V	Onset of reduction /V	HOMO / eV	LUMO / eV	E_g / eV
29	+0.21	-1.54	-5.01	-3.26	1.75
30	+0.15	-1.45	-4.95	-3.35	1.60
31	+0.40	-1.23	-5.20	-3.57	1.63

HOMO and LUMO values are calculated from the difference onsets oxidation and reduction and subtracted from a HOMO of ferrocene, which has a HOMO of -4.8 eV.

2.6.4. Electropolymerisation

The polymer growth process of the three monomers was achieved by repetitive cycling over the first oxidation peak on a glassy carbon electrode as shown in Figure 2.98. The development of the growth traces of the three polymers can be seen with the increase in current and creation of low polymer growths on glassy carbon electrode surface were observed. The polymers were subjected to oxidation and reduction tests but unfortunately no clear peaks were apparent and the results were not reproducible. The experiments were repeated using an ITO coated glass slide as the working electrode, but pale colours appeared and this was not observed in the UV-vis spectroscopic experiment. Many other attempts were also made to study the oxidation and reduction of the polymer using different solvents, potentials, and number of cycles, but there was no evidence of polymer oxidation and reduction trace suggesting that the polymers were unstable on the electrode surface.

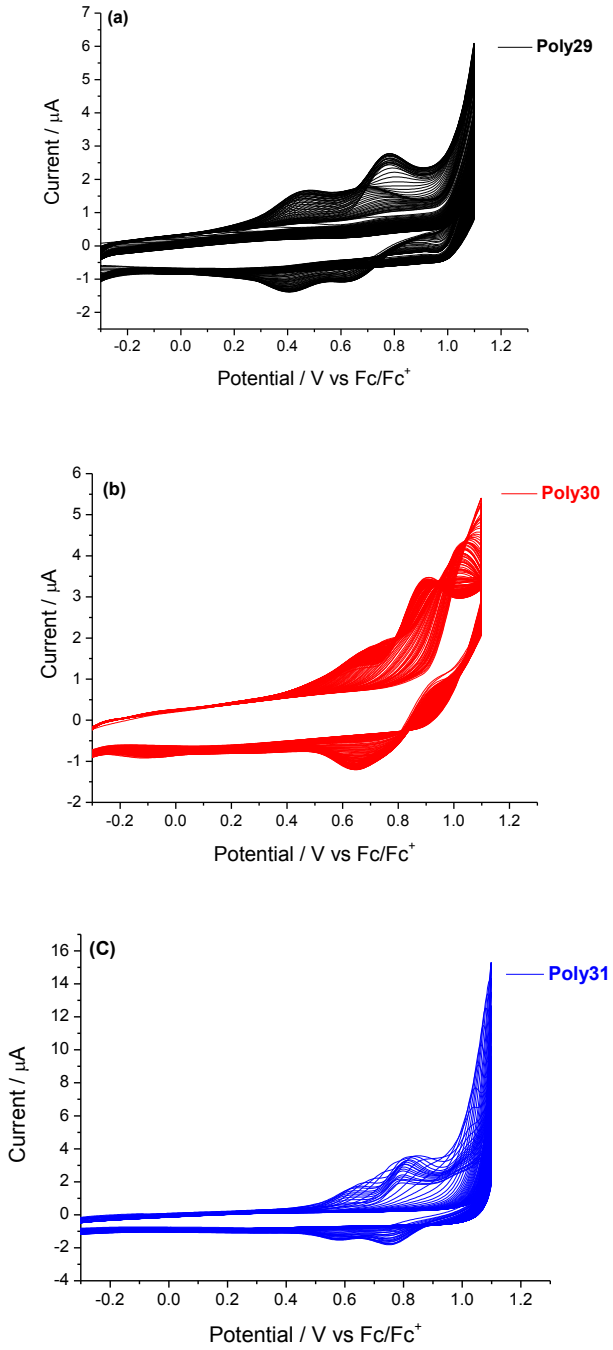

Figure 2.98. Electrochemical growth of (**a**) poly**29**, (**b**) poly**30** and (**c**) poly**31** in dichloromethane solution on a glassy carbon electrode as the working electrode, Ag wire reference electrode and Pt counter electrode. The concentration was *ca.* 10^{-4} M (0.1 M $TBAPF_6$ as supporting electrolyte),at a scan rate of 0.1 Vs^{-1}, over 300 segments.

2.6.5. Conclusion

Three new compounds incorporating a BODIPY core with either two EDOT, thiophene or EDTT units have been characterised by UV-vis absorption spectroscopy and cyclic voltammetry. The EDOT units in compound **29** has a pronounced influence on the absorption maximum, which gives a bathochromic shift compared to the rest of the monomers. This feature can be attributed to the stronger electron donor effect of the EDOT unit than the other two heterocycles. The cyclic voltammetry analysis follow the same trend as the spectroscopic analysis, where all three monomers have shown similar peaks with slightly greater oxidation potential in the monomer **31** than monomer **29** and **30**. This was ascribed to the increased number of sulfur atoms in the chain of compound **31**.[39] After electropolymerisation, all three polymers exhibited weak growths on the electrode surface, therefore the cyclic voltammetry and optical experiments did not produce a good set of data points. As such, a full electropolymerisation investigation was not possible with these compounds, due to their instability on the electrode surface.

Chapter 3

Electrochemical and Optical Properties of Truxene-BT-Oligofluorene and Oligofluorene-DPP Monodisperse Macromolecular Systems.

3.1. Well-Defined and Monodisperse Linear and Star-Shaped Quaterfluorene-DPP Molecules: the Significance of Conjugation and Dimensionality

3.1.1. Introduction

Linearly extended monodisperse π -conjugated oligomers are important class of organic molecules and can be used as models for high molecular weight polymers. In addition, the synthesis of the molecules is 100% reproducible, providing high purity of well-defined structures with controllable solubility in organic solvents. Increasing the dimensionality of oligomers into two or three dimensions through a central core produces materials with physical properties that can be noticeably different from their simple, linearly conjugated analogues. Such conjugated systems are called star-shaped oligomers that have been the subject of intense research in recent years.[146] An attractive interaction between the central aromatic unit and the conjugated arms leading to antennae-type light harvesting by the arms followed by energy transfer to the core is shown.[146] The compound 1,4-diketo-2,3,5,6-tetraphenylpyrrolo[3,4-c]pyrrole (DPP)[147]represents an ideal structure for application as a central core unit in star –shaped conjugated systems. The conjugated materials based on DPP unit has been incorporated and use as components in solar cell applications[148,149,150,151,152,153,154,155,156,157,158,159,160] and as efficient light emitters.[147,161, 162,163,164,165,166,167]. However, despite of these recent attention to DPP derivatives, there are only a limited examples of structures tetrasubstituted with conjugated chains[168] and certainly no examples of macromolecular single molecules. The first section of this chapter reports on the properties of three oligofluorene

substituted DPP macromolecules. The largest molecule in the series is defined as **32** in which the DPP core has four quaterfluorene arms. Twofold substitution of the core with quaterfluorenes is represented by **33** and **34** (Scheme 3.1). The terminology here refers to the conjugated pathway, which propagates throughout the molecule in the former and is restricted to quaterfluorenylphenylenes in the linear-c and linear-nc. The study in this section is focused on the comparative properties of the compounds possessing these different features (Scheme **3.1**), which offers perfect description of the significance and dimensionality of dissimilar architectures in closely related conjugated structures.

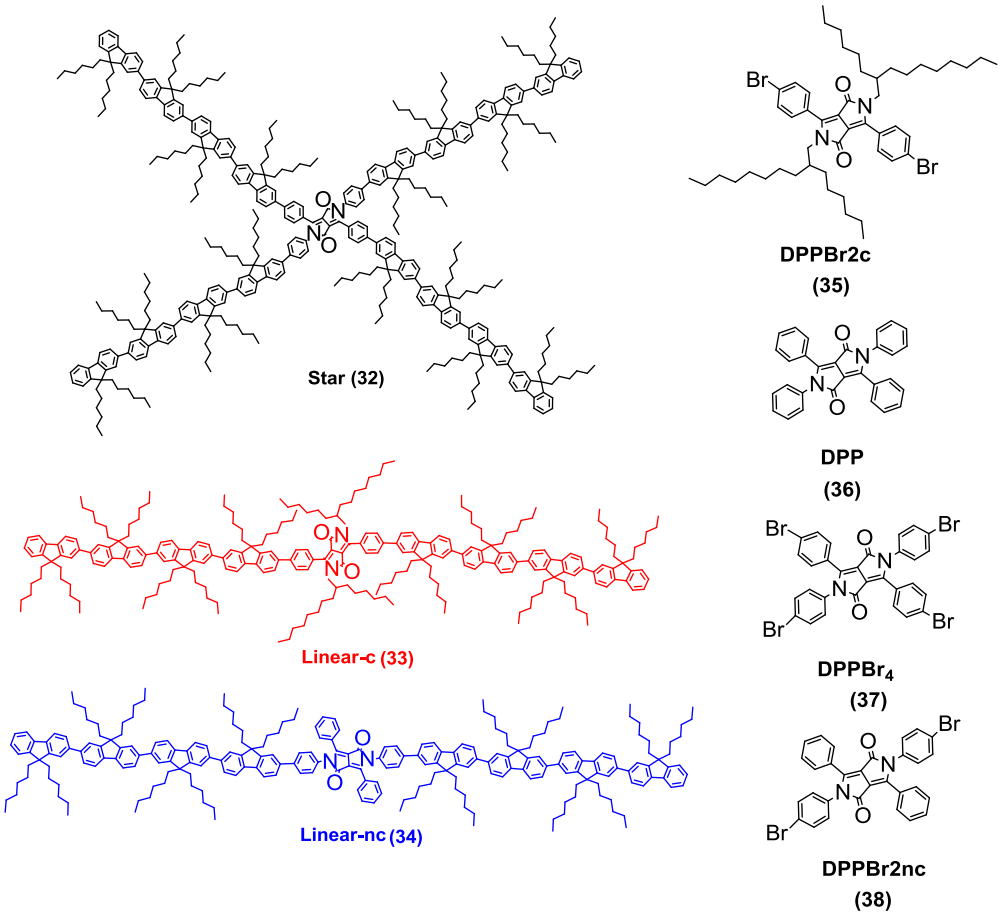

Scheme 3.1. Structures of Oligofluorene DPP systems alongside the corresponding DPP cores

The full synthetic procedure of the aforementioned compounds is summarised in Scheme **3.2.**

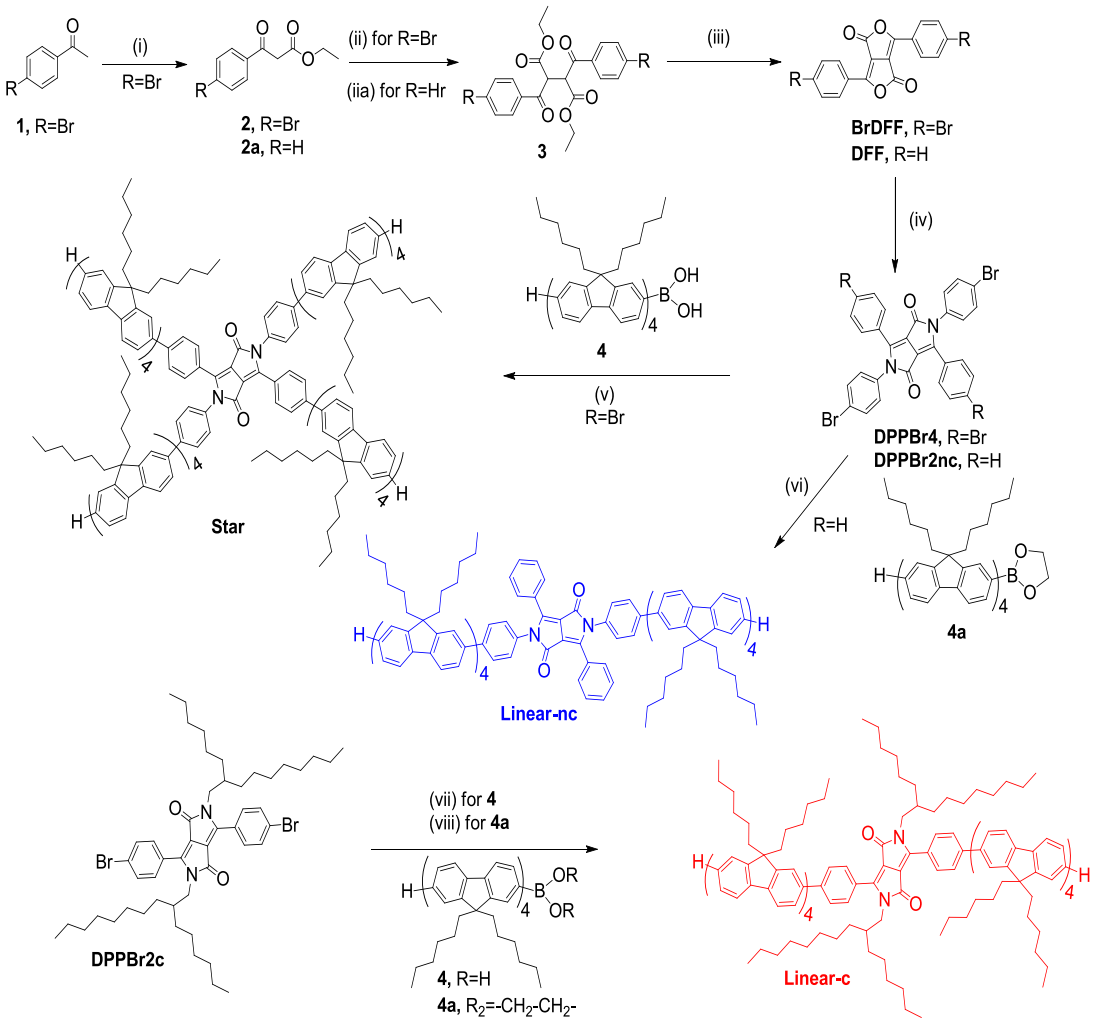

Scheme 3.2. Syntheses of **Star (32)**, **Linear-c (33)** and **Linear-nc (34)**

Scheme SI1 - Reagents and Conditions: (i) diethyl carbonate, NaH, toluene, reflux. (ii) (a) Br_2, CH_2Cl_2; (b) NaH, CH_2Cl_2, reflux. (iia) 1 equiv. of Na in ether, then ½ equiv. of I_2 in ether 2h, r.t. (iii) 250°C, 20 min. (iv) p-bromoaniline, N,N-dicyclohexylcarbodiimide, CF_3COOH, $CHCl_3$, 3d. (v) $Pd(PPh_3)_4$, K_2CO_3, toluene/H2O, 100°C, overnight. (vi) $Pd(PPh_3)_4$, K_3PO_4, DMF, 100°C, 16 h. (vii) $Pd(PPh_3)_4$, $Ba(OH)_2$, DME/H_2O, 80°C, 8 h. (viii) $Pd(PPh_3)_4$, K_3PO_4, DMF, 80°C, 45 h.

3.1.2. Experimental

The DPP materials were analysed by thermogravimetric analysis (TGA), differential scanning calorimetry (DSC), cyclic voltammetry, and absorption and emission spectroscopy.

The oligomers were synthesised by Alexander Kanibolotsky (University of Strathclyde) and Kai Zhang (Department of Chemistry University of Cologne, Germany). Thermogravimetric analysis (TGA) and differential scanning calorimetry (DSC) measurements were achieved by Filipe Vilela (University of Strathclyde). Electrochemistry measurements were performed on a CH Instruments 660A electrochemical workstation with *iR* compensation using anhydrous dichloromethane as the solvent. The electrodes were glassy carbon, platinum wire, and silver wire as the working, counter, and reference electrodes, respectively. All solutions were degassed (Ar) and contained monomer substrates in concentrations ca. 10^{-4} M, together with *n*-Bu_4NPF_6 (0.1 M) as the supporting electrolyte. All measurements are referenced against the $E^{1/2}$ of the Fc/Fc^+ redox couple. Absorption and emission measurements were taken using on a UNICAM UV 300 instrument and Perkin Elmer LS 45 Luminescence spectrometer respectively.

3.1.3. Optical properties of Oligofluorene DPP systems

The absorption spectra of fluorene derivatives was measured in dichloromethane solution, all molecules showed two peaks, the first one at 368-370 nm is attributed to $\pi - \pi^*$ transition of quaterfluorene arms.[169] A second weaker band was exhibited at longer wavelengths and the peak maximum was at 515, 491 and 486 for molecules **32**, **33** and **34** respectively, with the optical band gaps being 2.2 eV for **32** and **33** and 2.4 eV for **34**. Compounds DPPBr2c **(35)**, DPPBr4 **(37)** and DPPBr2nc **(38)** showed the longest wavelength absorption maxima in the range 475–491 nm. This fact provides the evidence that the absorption peaks at lower energy in the spectra of fluorene derivatives were related to the presence of DPP core in these molecules. Compound **34** showed emission and the longest wavelength absorption spectra similar to those in compound **37** and almost identical to the corresponding absorption and emission bands of **DPP (36)** (λ_{abs} = 484 nm, λ_{PL} = 520 nm in Chloroform solution)[170] and compound **38**, confirming that the absorption and emission bands related to the presence of DPP unit are not affected by oligofluorene substituents from the sides of 2- and 5-positions. On the contrary, similar absorption and emission bands in the spectra of **32** exhibited bathochromic shift of $\Delta\lambda$ = 33 and 48 nm respectively compared to compound **36**. The large influence of substituent effects at the 3- and 6-positions on the absorption spectra of the core unit is the evidence of intramolecular charge transfer (ICT), assuming that the ICT is a dominant feature in the fluorene-DPP compounds, occurring from a push of electrons from substituents at the 3,6-positions to the 1,4-carbonyls. The wavelength for ICT peak is known to increase with greater conjugation length and this would explain the large difference

between the compound **32** and compound **34**. All absorption and emission spectra of six compounds are shown in Figure3.99 and Table.3.1.

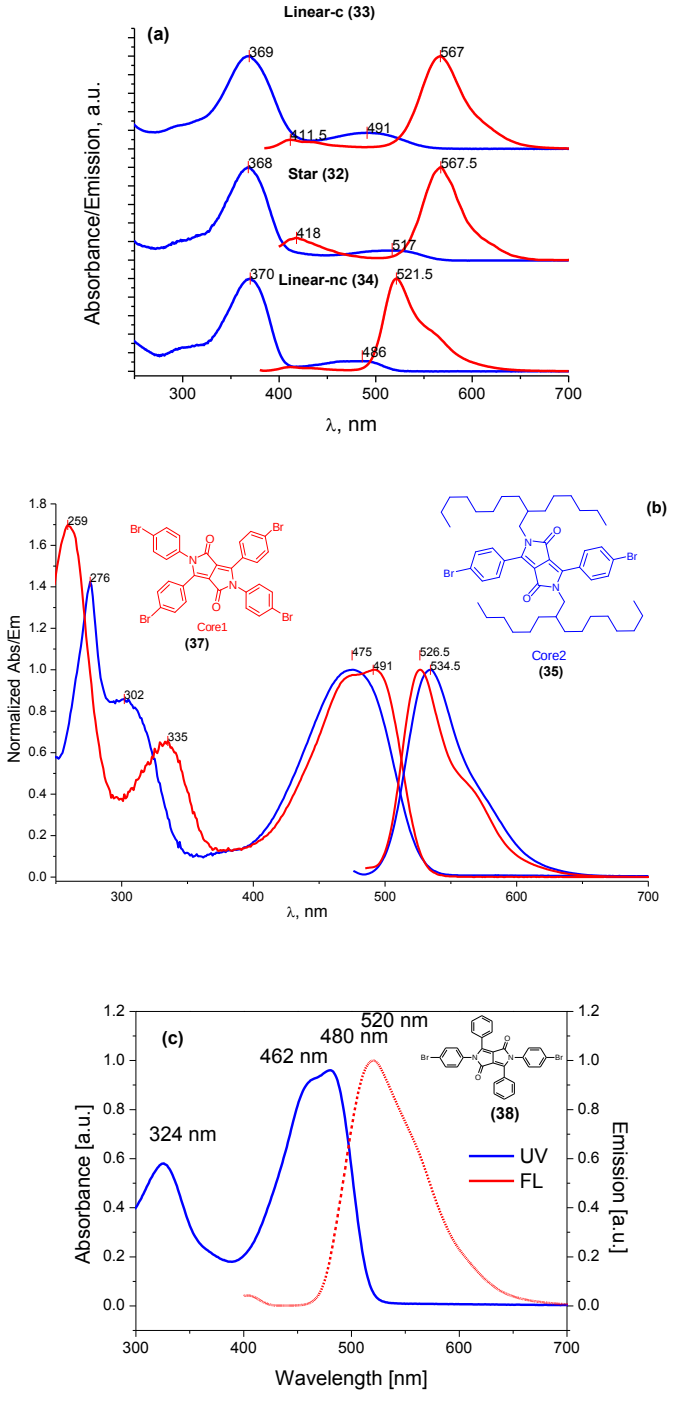

Figure 3.99. Absorbance and emission of oligofluorene DPP (**a**) **32**, **33** and **34** (**b**) **35** and **37** (**c**) **38** in dichloromethane solution

Table. 3.1. Absorption and emission spectra of **32**, **33**, **34**, **35**, **37** and **38** in dichloromethane solution

Compound	Absorption spectra (nm)		Emission spectra (nm)
	$\pi \rightarrow \pi^*$	ICT	
32	368	517	568
33	368	491	567
34	369	486	522
35	-	475	535
37	-	491	527
38	-	480	520

Compound **33** shows the evidence of ICT behaviour similar to that of compound **32**, but with reduction of the electron-withdrawing effect of the carbonyls due to the presence of a more electron-donating N-alkyl groups in this molecule instead of aromatic substituents in compound **32**. In push-pull systems, hypsochromic shift of ICT band is observed due to the decreasing of the donor/acceptor strength in these systems, consequently this explains the decreasing of the longest wavelength maxima in compound **33** compared to compound **32**. In addition, in compound **33** the intramolecular charge transfer (ICT) behaviour can be reduced due to more twisted ground state conformation of the 3-Ph-DPP-6-Ph fragment where Ph is a phenylene group. Interestingly, compounds **32** and **34**, which share a general core substitution pattern (i.e., tetra phenyl DPP) show a non-symmetrical longest wavelength absorption band with obvious shoulders at the lower wavelength side of the peak.

The concentration dependence of absorption spectra of all three DPP-oligofluorene in hexane was studied and shown in Figure 3.100. Both compounds **33** and **34** exhibited the spectra that follow the Lambert-Beer law, while the shape of the long wavelength absorption peak of compound **32** was highly dependent on the concentration. In more concentrated solutions the absorption shows the shorter

wavelength feature at 449 nm as a dominant peak, while the longer wavelength feature is emerged as shoulder at 522 nm. This behaviour can be described by the aggregation of the **32** molecules in high concentration solutions accompanied by a change in the conformation of the central tetra phenyl DPP unit. The planar 3-Ph-DPP-6-Ph fragment in the non-aggregated state changing to propeller-like shape in the aggregate with the identical twisting for all four phenyl fragments. The π – π stacking of an oligophenylenevinylene star-shaped system is known to cause the aggregation of star-shaped molecule in low polarity solvent.[171,172] In star shaped oligofluorenes this type of aggregation is usually hindered by alkyl chains at the 9,9-positions of a fluorene unit. However due to the exceptional arrangement of the oligofluorene arms and the DPP core, hydrophobic interactions between alkyl chains cause aggregation in hexane solution.

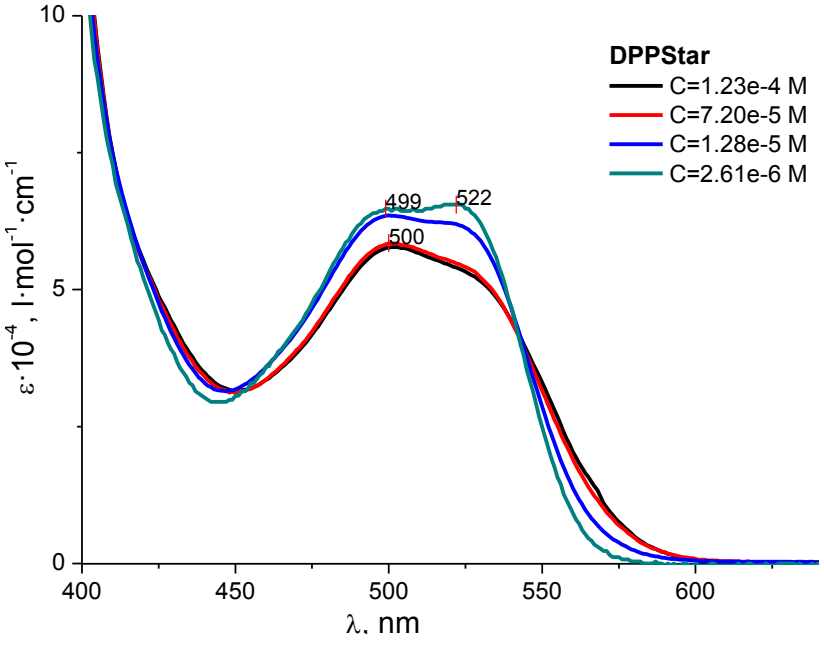

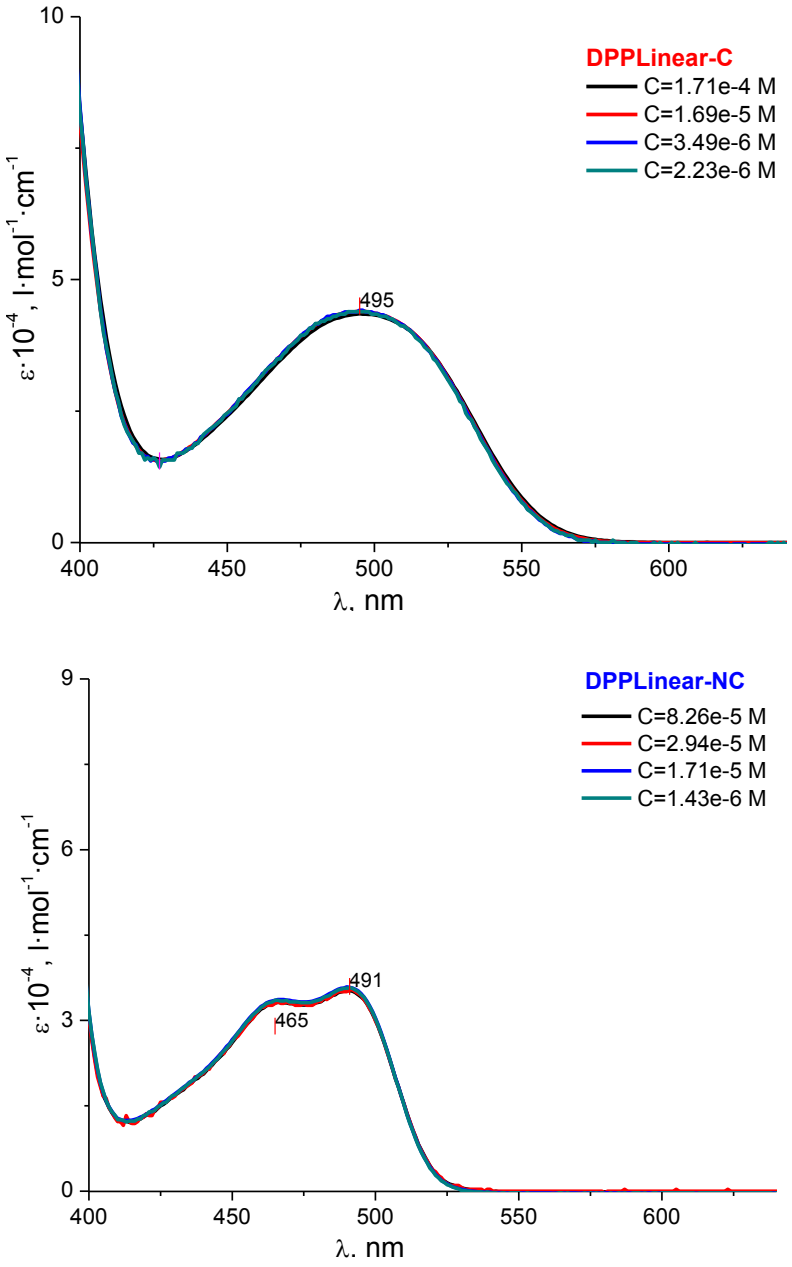

Figure 3.100. Molar absorptivity spectra for the longest wavelength bands of oligofluorene-DPP compounds in hexane at various concentrations

For comparison, Figure 3.101 shows the longest wavelength absorption band in normalised spectra of DPP-oligofluorene systems of compounds **32**, **33**, **34** and core precursors **35**, **37**, **38** in solution states. In the spectrum of compound **32** the longest

wavelength absorption bands exhibit vibronic structure in the form of two maxima at 499 and 522 nm with red shift (31 nm) compared to compound **37**. On the other hand, the corresponding band of compound **33** is symmetrical and featureless in both dichloromethane and hexane solutions, similar to the featureless absorption of its core precursor compound **35**.

For related compound 2,5-dimethyl-3,6-diphenylpyrrolo[3,4-c] pyrrole-l,4-dione(**39**), a loss of vibrational structure was rationalised on the basis of poor Frank–Condon overlap between the ground and first excited states due to non-planarity of the molecules in the ground state.[173] The normalised long waves absorption bands for all aforementioned compounds are shown in the Figure 3.101.

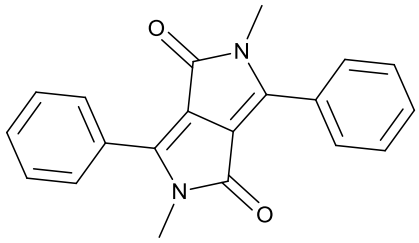

39

Different equilibrium conformations in ground and excited states of compound **35** also lead to a more pronounced Stokes shift compared to that of compound **37** as displayed in Table 3.2.

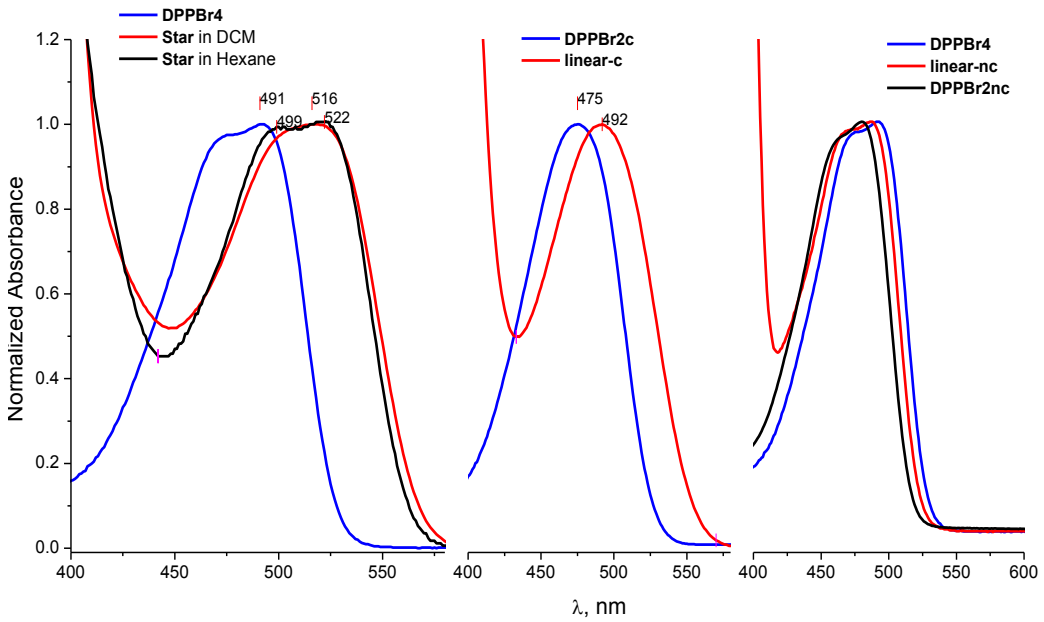

Figure 3.101. The longest wavelength absorption band in normalised spectra of DPP-oligofluorene systems (compounds **32**, **33**, **34**) and core precursors (compounds **35**, **37**,**38**)

Table 3.2. The Stokes shift calculated for the DPP emitter in **32**, **33**, **34**, **35, 37** and **38** molecules.

Compound	Stokes Shift (nm)
32	51
33	**76**
34	36
35	**60**
37	**36**
38	40

The spectra of DPP-oligofluorenes are also studied in toluene solution and the results are consistent with the dominant effect of ICT on electronic properties of these compounds. For compounds **33** and **32** identical emission peaks were observed at 567 and 568 nm respectively. Due to more planar arrangement of 3-Ph-DPP-6-Ph

unit of compound **33**, in exited state compared to that of its ground state the increase in the Stokes shift for this compound was observed.

In the solid state, all three oligomers show similar absorption spectra, where the peaks at 365-366 nm are attributed to quaterfluorenes absorption spectra and the DPP units causes the appearance of broad peak at lower energy absorption. The long wave absorption of the compound **32** reveals the signature of the aggregation of the tetraphenyl DPP unit (the dominance of the short wavelength feature as a maximum and the appearance of a long wavelength feature as a shoulder). Compound **33** shows the non-symmetrical absorption peak, the shorter wavelength feature being followed by the shoulder at longer wavelength. The absorption band of the **34** film exhibits vibronic splitting with two features at 473 and 491 nm. In addition, for the compound **34** in comparison to the other two compounds a blue shift of the longest wavelength absorption band is observed due to weaker ICT. Large Stokes shifts of the fluorene-DPPs absorption-emission spectra similar to that observed for polymeric DPPs[163,174] makes these compounds promising for high-gain materials in lasing applications.[6] In the solid state the emission spectra of three molecules exhibit similar bands, at 634 and 633 for compounds **32** and **33** respectively, while the emission of compound **34** is blue shifted with peak at 575 nm. The absorption and emission maximum spectra in solid state are illustrated in Figure 3.102 and Table 3.3. The solid-state PL exhibits a considerable red-shift when compared to the emission in solution state. The emission in solution state and the film photoluminescence can only be observed from the DPP core and indicates complete energy transfer from the quaterfluorene arms.

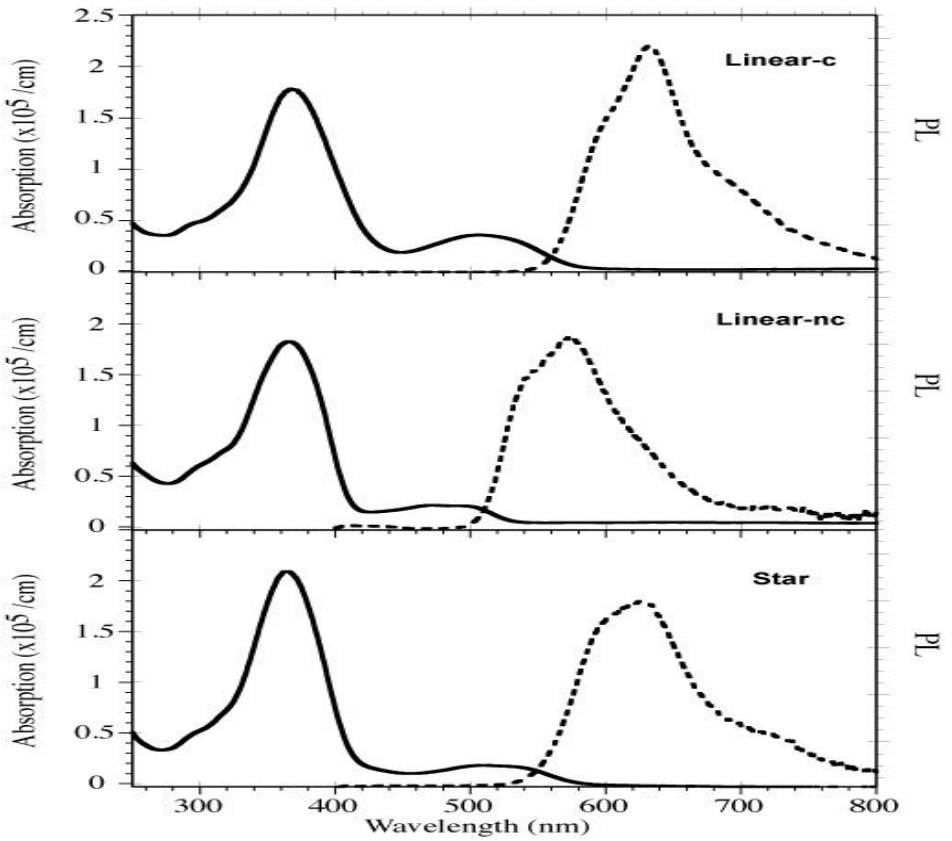

Figure 3.102 Absorption coefficient spectra (solid lines) from spin-coated f lms of Linear-c(**33**) (upper panel), Linear-nc(**34**) (middle panel), and Star(**32**) (lower panel) DPP films. Corresponding PL spectra (dotted lines) excited at 365 nm. The PL data have been normalized so that the area beneath each curve is equal.

Table 3.3. The absorption and emission maximum spectra in solid state of **32**, **33** and **34** molecules

Molecule	Absorption max Spectra (nm)		Emission Spectra (nm)
	Oliogofluorene	DPP unit	
32	365	506	634
33	366	506	633
34	366	473	575

3.1.4. Electrochemical properties of molecules

The highest occupied molecular orbital (HOMO) and the lowest unoccupied molecular orbital (LUMO) energies of these molecules were determined by cyclic voltammetry; the redox behaviour and the data are summarised in Figure 3.103 and Table 3.4. Two reversible oxidation waves were observed for each compound. Compounds **32** and **33** show similar oxidation peaks at $E_{1ox}^{1/2}$ = +0.82 and $E_{1ox}^{1/2}$ = +0.96 V respectively, while compound **34** exhibits slightly lower two oxidation waves than compounds **32** and **33** at $E_{1ox}^{1/2}$ = +0.80 V and $E_{1ox}^{1/2}$ = +0.93 V for first and second oxidation peaks respectively.

Compound **34** was also the only material to feature a reversible reduction process, which was observed at a significantly lower potential than for **32** and **33** compounds.

The HOMO and LUMO energies were found from the onsets of the first oxidation and reduction waves, respectively, and the calculated electrochemical band gaps were in good agreement with the optical HOMO-LUMO gaps. Compound **33** exhibits a higher value of LUMO level compared to those of **32** and **34** compounds, which is consistent with the different effects of the hexyldecyl and phenyl groups (Table 3.4).

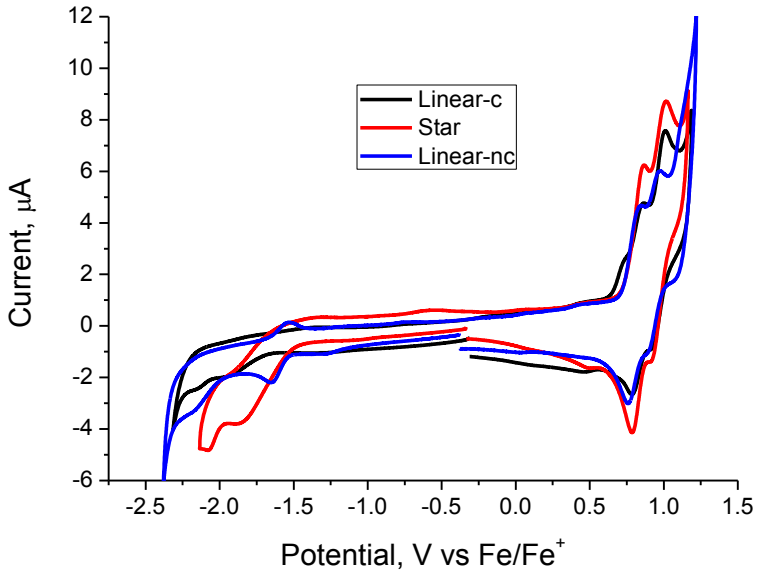

Figure 3.103 Cyclic voltammetry of oligofluorene-DPP on glassy carbon electrode in 0.1M Bu_4NPF_6 at 0.1 $V \cdot s^{-1}$ scan rate

Table 3.4. Electrochemical Data for Energy levels of molecules **32, 33** and **34**

Molecule	First oxidation potential $E_{1ox}^{1/2}$ /V	Second oxidation potential $E_{2ox}^{1/2}$ /V	Reduction potential $E_{red}^{1/2}$ /V	HOMO / eV	LUMO / eV	E_g / eV
32	+0.82	+0.96	-1.85^{irrev}	-5.5	-3.3	2.2
33	+0.82	+0.96	-1.90^{irrev}	-5.4	-3.1	2.3
34	+0.80	+0.93	-1.59	-5.5	-3.3	2.2

HOMO and LUMO values were determined by cyclic voltammetry from the onsets of the first oxidation and reduction waves; the data are referenced against the half-wave potential, $E_{1/2}$, of the Fc/Fc + redox couple, which has a HOMO energy level of −4.8 eV.

3.1.5. Thermal Analysis of the compounds

Differential scanning calorometry measurements of the three compounds exhibits the glass transition temperature (T_g = 74 ° C) for compound **32**, which is significantly lower than that of compound **34** (**T_g** = 101 ° C) due to the increased free volume of compound **32**.

In DSC trace of compound **33** a glass transition does not appear, but the presence of well-defined melting point (T_m = 168 ° C) and crystallisation point, (Tc = 101 ° C and 127 ° C) is revealed, which is the evidence of a certain degree of crystallinity for compound **33**.

All three compounds exhibit a good thermal stability with decomposition temperature in the range between (T_d = 420 to 440 ° C). All the thermal analysis results are depicted in Figures 3.104 and 3.105.

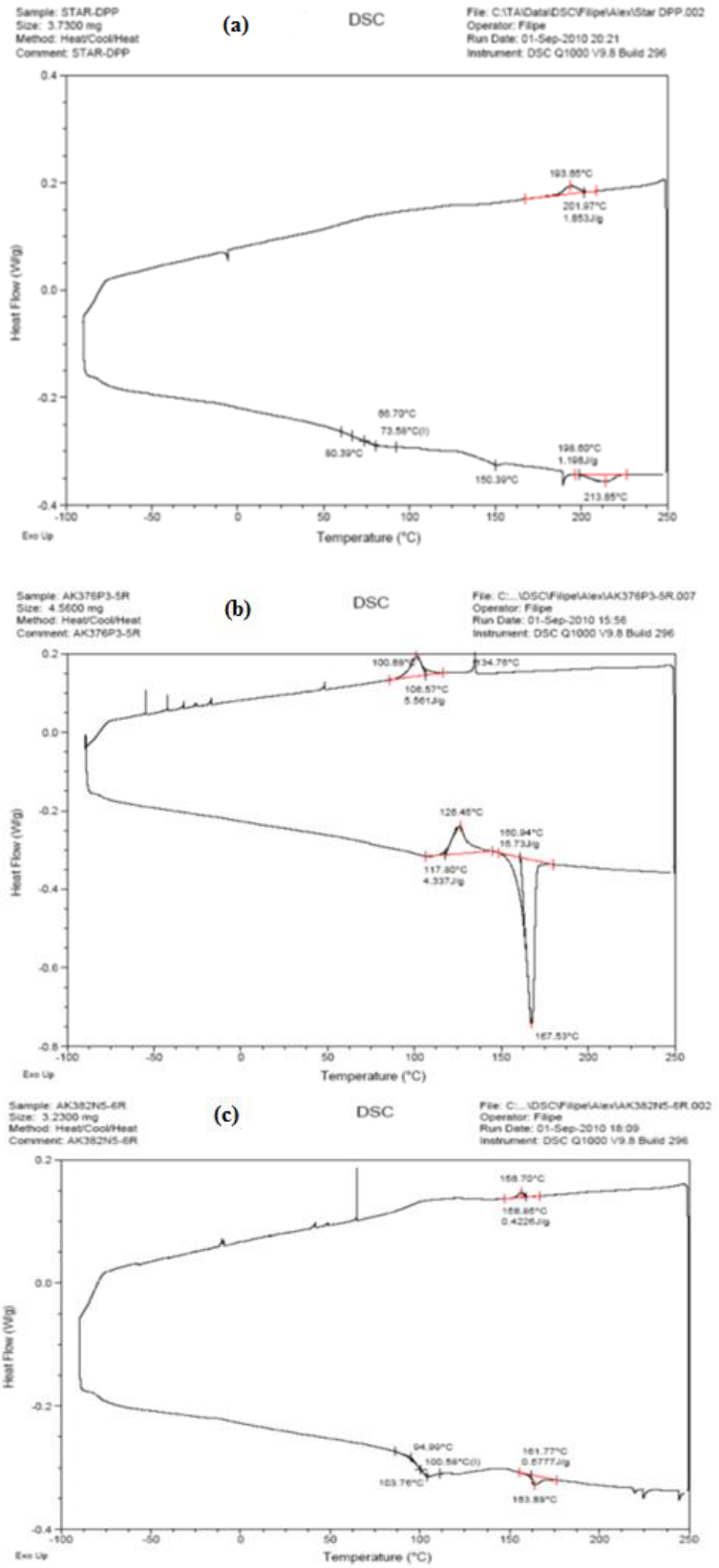

Figure3. 104. DSC heating and cooling cycles for **(a) 32**, **(b) 33** and **(c) 34**

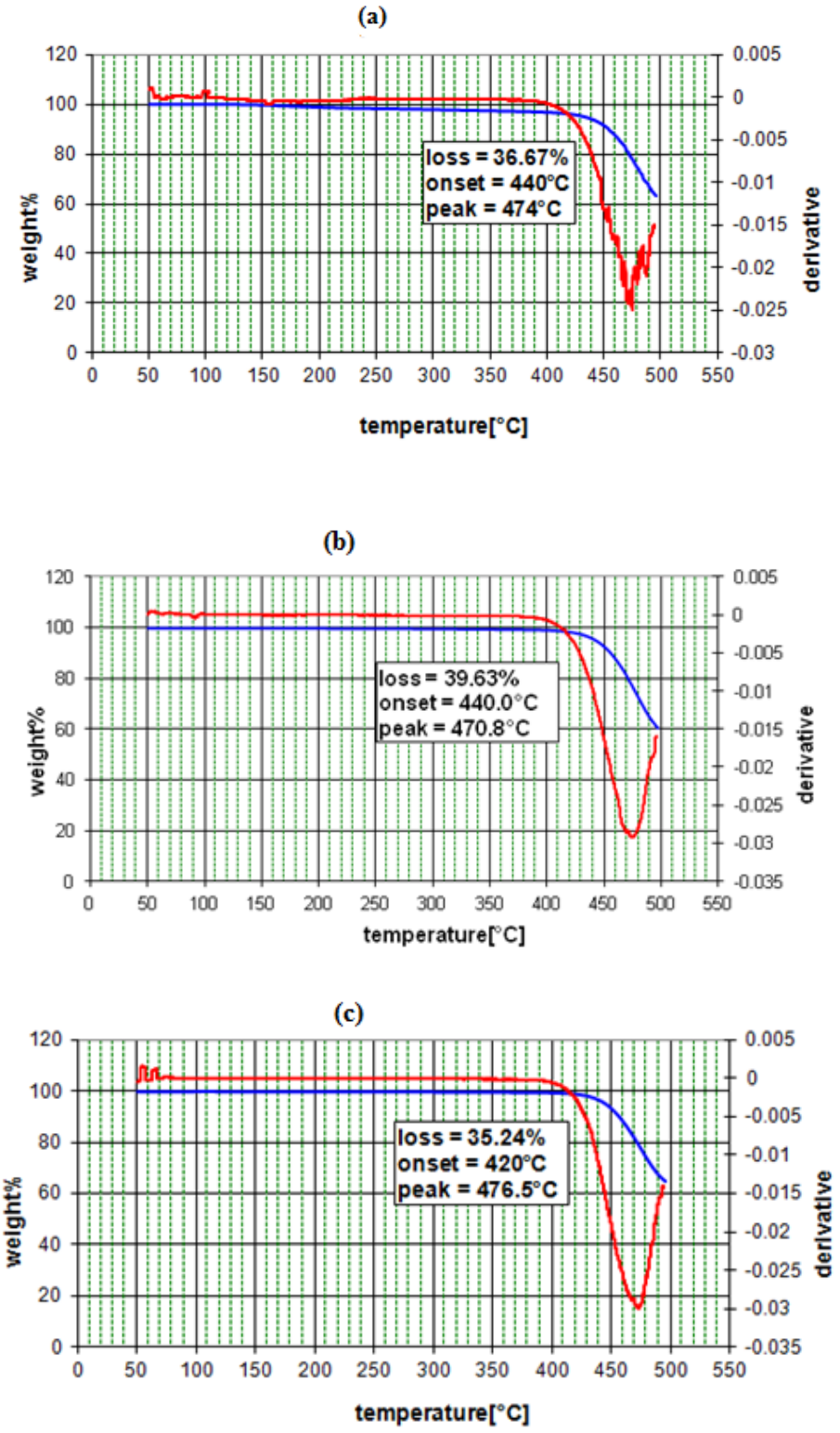

Figure 3.105. Thermogravimetric analysis trace for (a) **32**, (b) 33 and (c) 34

As shown above, the Differential Scanning Calorimetry (DSC) measurements of Linear-c**(33)** indicated that in the condensed state this compound formed a crystalline phase. The higher crystallinity degree of Linear-c**(33)** compared to Linear-nc**(34)** and Star**(32)** oligomers suggests the cooperative effect of quadrupole–quadrupole interactions in the condensed phase, which make the aggregation favourable and leads to a red shift of the longest wavelength absorption spectra. The type of aggregation in this case has essentially one dimensional character with all quadrupole ellipsoids aligned in one direction, as shown in Figure 3.106a. On the contrary, the aggregation of the Star(**32**) macromolecules involves tow dimensional interactions between more electron-rich 2,5-phenylene rings (blue colour in Figure 3.106b) and electron deficient 3,6-phenylene spacers (red colour). The overall effect of such interactions will cause decreasing the degree of intramolecular charge transfer.

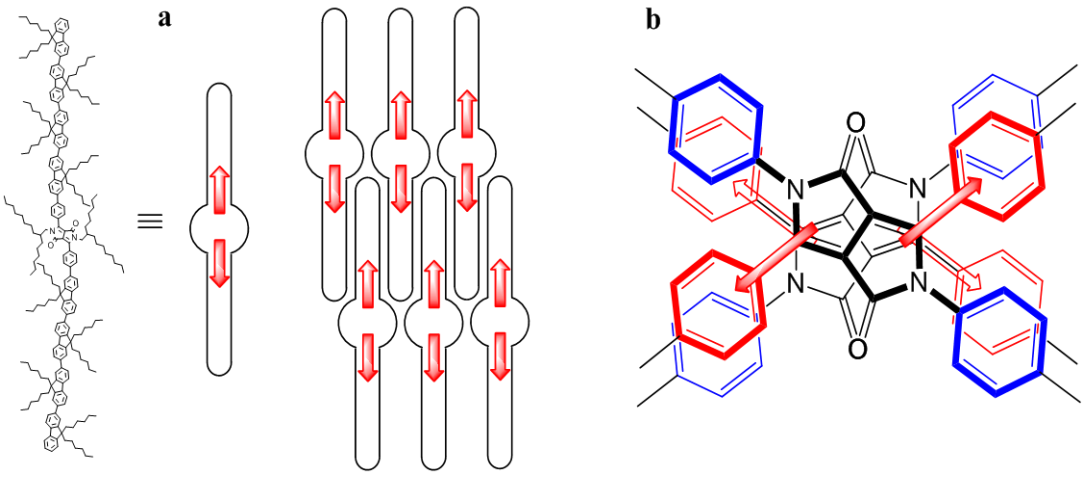

Figure3. 106. Schematic representation of 1D (**a**) and 2D (**b**) interactions between molecules in aggregates. Quadrupoles are represented by two dipoles originating from ICT and directed in opposite directions

3.1.6. Conclusion

New oligofluorene-substituted DPP macromolecules have been studied and analysed by absorption and emission spectroscopy, cyclic voltammetry, thermogravimetric analysis (TGA), differential scanning calorimetry (DSC). The comparison of optical characteristics of compound **32** and compound **33** in solution and in the solid film demonstrates the influence of the molecular dimensionality and substituent effect on the property of the material in the bulk. In the solid state the compounds **32**, **33** and **34** exhibit similar response in absorbance at short wave region. The linear shape of the linear-c (**33**) system and the conjugation between the arms and the DPP core lead to the increase in ICT in the solid state due to aggregation, and the opposite effect of aggregation on ICT is observed for compound **32** and to a lesser degree for compound **34**. Compound **34** gives slightly lower oxidation and reduction potential compared to the compounds **32** and **33**, and there is slight difference between the electrochemical and optical HOMO-LUMO gap. Compound **33** exhibit higher value of the LUMO level than those of compounds **32** and **34**, which indicates the different effects of the hexyldecyl and phenyl groups. The two dimensional character of the Star system and the alternating positions of phenylene spacers between the core and the arms generate very strong aggregating propensity in the solid state and also in hexane solutions. The different types of aggregation in the solid phase provided by ICT, the substitution pattern, and the dimensionality of the molecular system must be taken into account during the design of new materials. The DPP unit is clearly an interesting and exciting unit for use as a core in star-shaped conjugated architectures.

3.2. Strategic positioning of 2, 1, 3 benzothiadiazole units within oligofluorene-truxene star shaped structures for tuning photophysical properties

3.2.1. Introduction

A number of heterocyclic units can be incorporated into a conjugated system to alter its optical and electrochemical properties. An example of these units is the fused bicyclic 2,1,3- benzothiadizole moiety (BT),[50]which is an electron- deficient system. This has been incorporated within electron-donor oligofluorene and oligothiophene derivatives to produce donor-acceptor conjugated materials. Oligofluorene–BT conjugates can be used for applications in organic light emitting devices,[175,176] whereas corresponding thiophene derivatives are found to be effective donor compounds for organic photovoltaic cells.[177,178,179,180,181,182,183]

BT unit has been used in a number of conjugated polymers and molecular based materials.[184,185,186,187,188,189] However little is understood about the intricate association and electronic interplay between the donor and acceptor components of these materials, this understanding would be extremely useful to the organic electronics community. In recent years the organic lasers have attracted attention due to flexibility and tunability of organic gain materials.[6] Poly (*p*-phenylenevinylene) and poly(fluorene) derivatives have been investigated for lasing with potential applications in explosive sensing.[190,191,192]

In our group, the work in this area is focused on creating monodisperse conjugated macromolecular systems with well-defined structures. The most illustrative example

of these systems are the series of trigonal star-shaped structures featuring oligofluorene arms attached to a truxene core.[64]

Poly(fluorene) containing BT comonomer units F8BT (**40**) (Figure 3.107) has attracted vast attention due to its potential use as a charge transport material[193] and an application in organic light emitting transistors.[194,195] Bathochromic shift of the emission from blue to green as result of the introduction of BT unit in the polymer backbone of polyfluorene (PF8) and increased Stokes shift are favourable optical properties for lasing applications. Whereas the cooperative benzothiadiazole dipole-dipole interactions within one-dimensional architecture of F8BT(**40**) may lead to different types of aggregates.[196]

In order to combine the advantage of isotropic morphology of a film originated from the two dimensional well defined star shaped architecture and aforementioned optical properties of F8BT system a series of structural isomers on the basis of trigonal quaterfluorene-truxenes **42**, **43**, **44**, **45** and **46** with BT unit incorporated in every possible positions have been synthesised.

The structures of these compounds are shown in the Figure 3.107 the compound **41** contains a benzothiadiazole (BT) units attached to a central truxene core and has been studied for comparison.

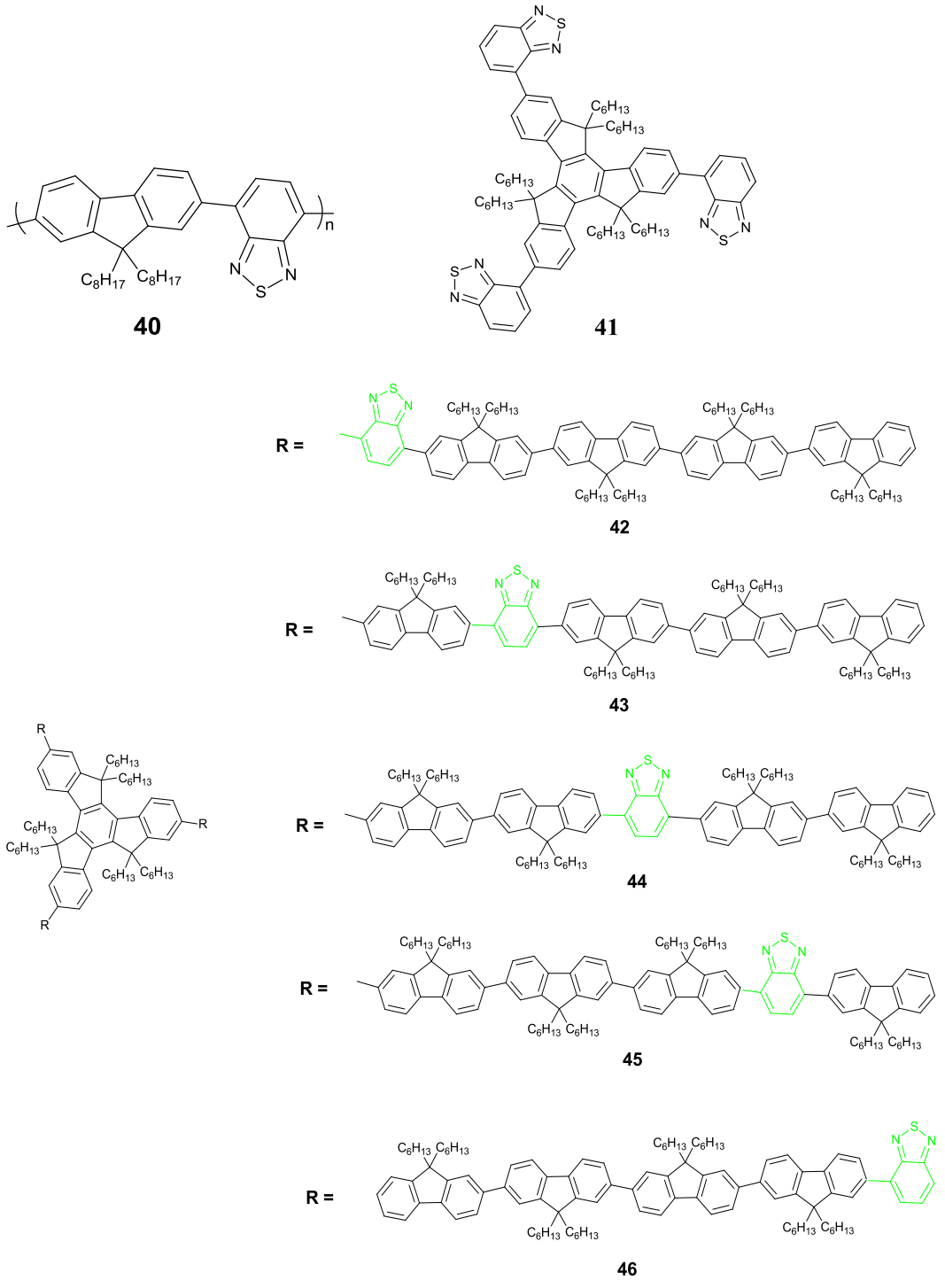

Figure3. 107. Structures of F8BT (**40**), T0BT (**41**) and T4BT series (**42** to **46**)

The retrosynthetic scheme of T4BT series compounds is shown in Scheme 3.3.

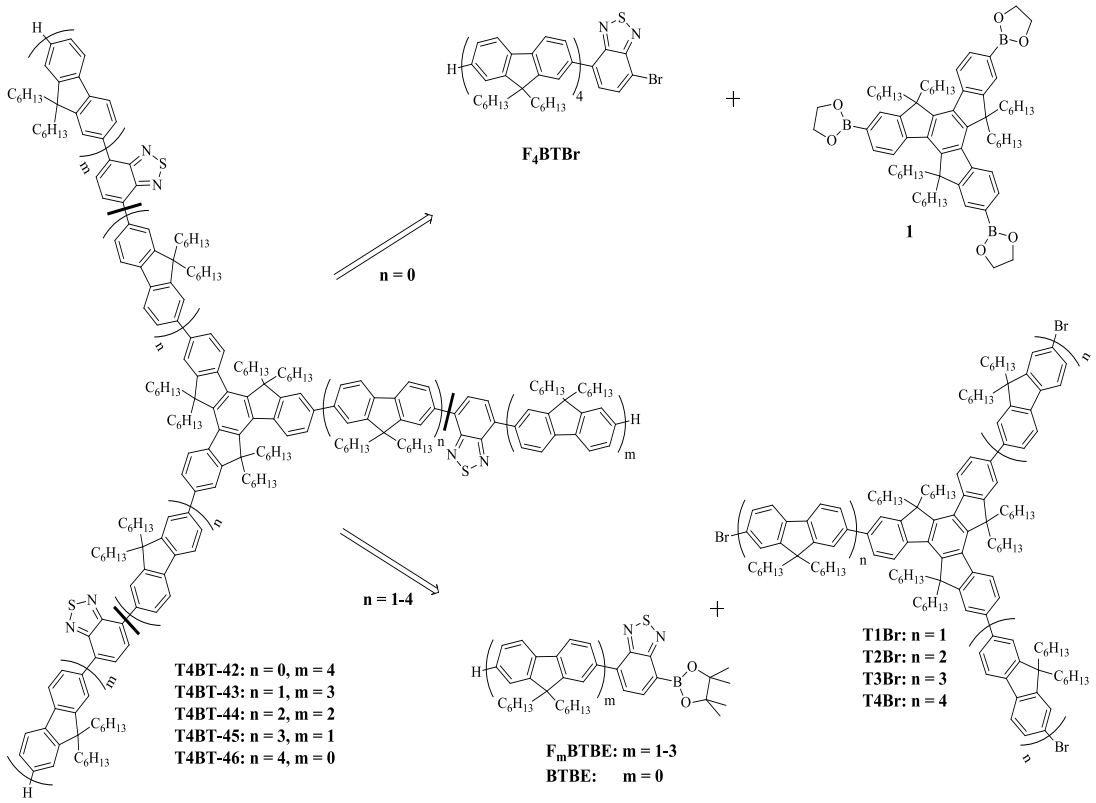

Scheme 3.3. Retrosynthetic scheme of the members of the T4BT series

3.2.2. Experimental

All the six compounds were synthesised by Alexander Kanibolotsky (University of Strathclyde). The absorption and emission spectra were determined in both in dichloromethane solution and in solid state. Thin films were prepared on a quartz slide by spin coating. Absorption spectrum was recorded on a UNICAM UV 300 instrument and emission spectrum was measured by Perkin Elmer LS 45 Luminescence spectrometer.

Cyclic voltammetry measurements were performed on a CH Instruments 660A electrochemical workstation with *iR* compensation using dichloromethane as the solvent. The electrodes were: glassy carbon as a working electrode, silver wire as a quasi reference and platinum wire as a reference electrode. All solutions were degassed and contained an analysed compound in concentration of ca. 10^{-4} M, as well as *n*-Bu_4NPF_6 as a supporting electrolyte in concentration of ca. 10^{-1} M. All measurements are referenced against the $E_{1/2}$ of the Fc/Fc^+ redox couple.

3.2.3. Absorption and Emission Studies in solution and solid state

The optical properties of the parent poly[2,7-(9,9-di-*n*-octylfluorene)$_{(1-x)}$-co-4 ,7-(2,1,3-benzothiadiazole)$_{(x)}$] copolymers ($0<x\leq0.5$) **40** (F8BT) were studied previously.[197]

The UV-Vis absorption spectra of these polymers were found to comprise the two main bands in the regions of ~300-370 nm (high energy transition) and ~ 420-450 nm (lowest energy transition). Using semi-empirical Hartree-Fock methods these bands were assigned as the delocalised HOMO – delocalised LUMO (π-π*) and delocalised HOMO – localised LUMO (ICT) transitions respectively[197,198] It was found that with decrease of the BT ratio (x) both the π-π* and ICT bands subjected to the shift into red and blue regions respectively with decreasing intensity of ICT transition. The UV-Vis absorption of T4BT compounds with BT units located in positions of the arms close to the core (**42**, **43** and **44**) contains well resolved ICT feature and is very similar to the calculated spectrum of the polymer with the BT contents of 16.7 molar percent (1 BT to 5 fluorene units),[197] which is the real molar content for BT units in the T4BT series isomers, if one considers the truxene moiety as another fluorene unit for each arm. The isomer **45** exhibits a poor separation between π-π* transition and ICT, the letter appearing in the spectrum as a shoulder. The isomer **46** with BT unit at terminal position does not show any separate charge transfer band due to poor overlap between local HOMO of quaterfluorene-truxene conjugated backbone and localised on BT LUMO, which make this transition not so intense. The red-shifted intense π-π* band (379 nm) in this case also makes resolving ICT band impossible. The absorption spectrum of compound **41** on the other hand

does reveal resolved ICT feature due to blue shifted and not intense π-π* transition (303 nm). Due to poor overlap between delocalised HOMO and localised on BT LUMO the band gap of compounds **41** and **46** is wider than that of compounds **42 - 45**. The photoluminescence spectra of compounds **42 - 45** exhibit very similar emission band with some small shifts in the peak value and negligible changes in emission profile. On the other hand the emission spectra of compounds **41** and **46** are blue shifted and exhibit more sharp peak profile.

All the data from absorption spectra and the optical band gap values of all compounds are summarised in Table 3.5. and Figure 3.108.

Table 3.5. Absorption spectra and optical band gap of compounds **41- 46** in solution state.

Molecule	π-π* transition (nm)	ICT (nm)	Optical HOMO-LUMO gap	Emission Spectra max
41	303	392	2.74	511
42	366	429	2.53	543.5
43	358	425	2.53	545.5
44	355	412	2.55	544
45	375	430	2.59	536.5
46	379	-	2.96	511

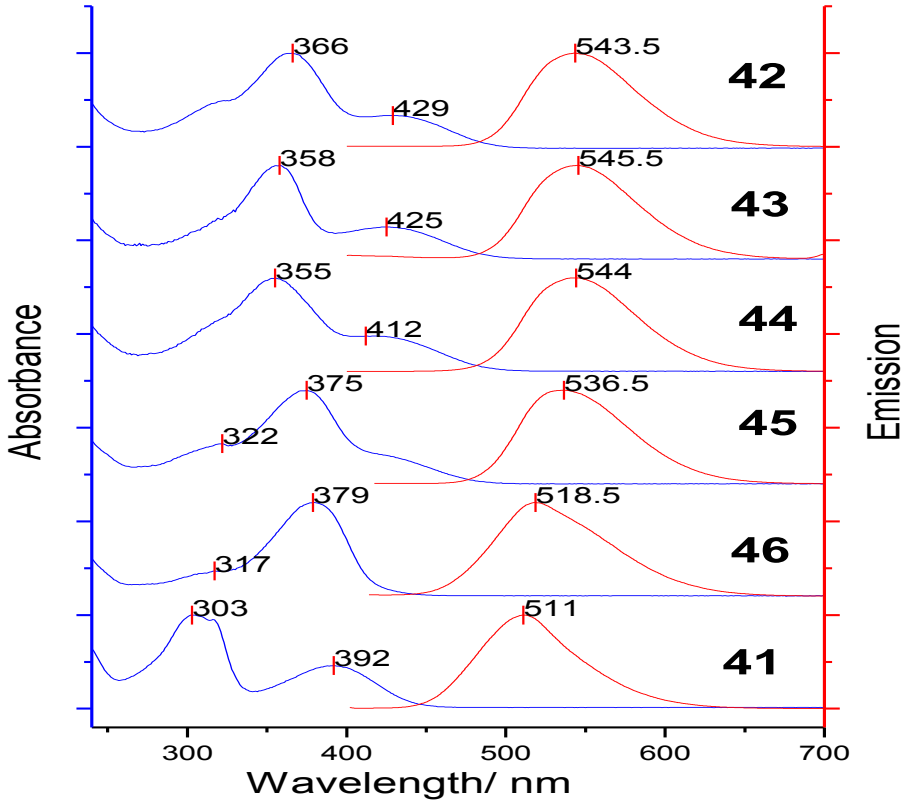

Figure3. 108. Absorption and photoluminescence spectra in of **41** (**T0BT**) and **T4BT** series (**42-46**) in dichloromethane solution.

In the solid state the UV absorption spectra of **T4BT** series (**42-46**) remain similar to that in dichloromethane solution with the same position of π-π* transition peak and slightly red-shifted ICT band (Figure 3.109).

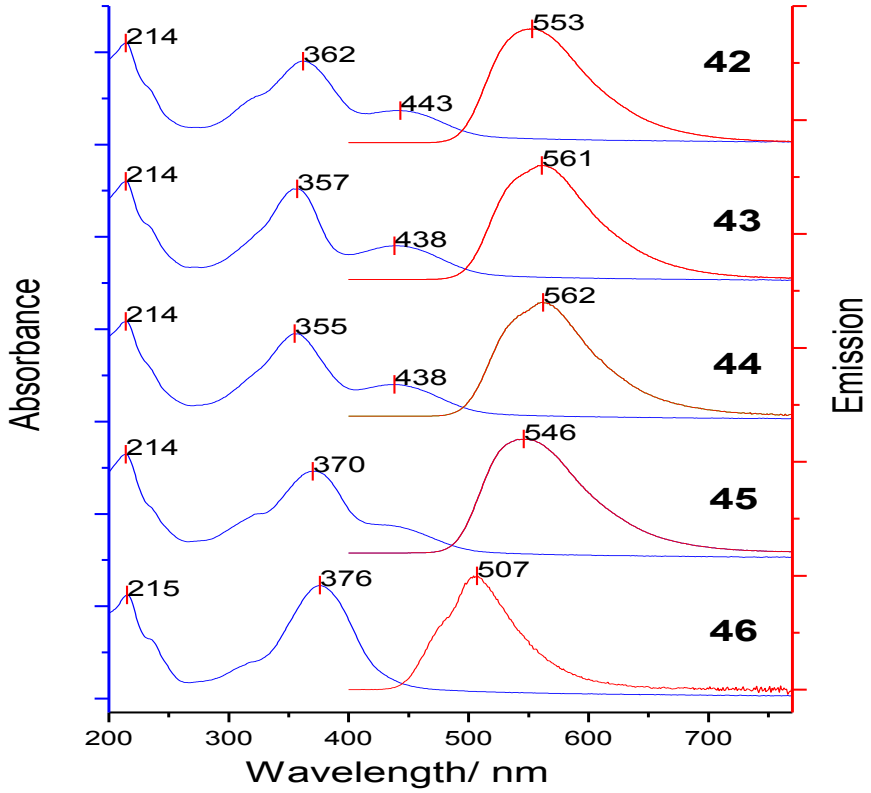

Figure3.109. Absorption-emission spectra of **T4BT** series compounds **42** - **46** in solid state.

Similar to the absorption in the solution, the solid state spectra reveal dependence of the π-π* transition peak wavelength on the BT unit position within oligofluorene arm (Figure 3.110). This dependence is a consequence of the different maximum conjugation length of oligofluorene units attached to BT moiety.

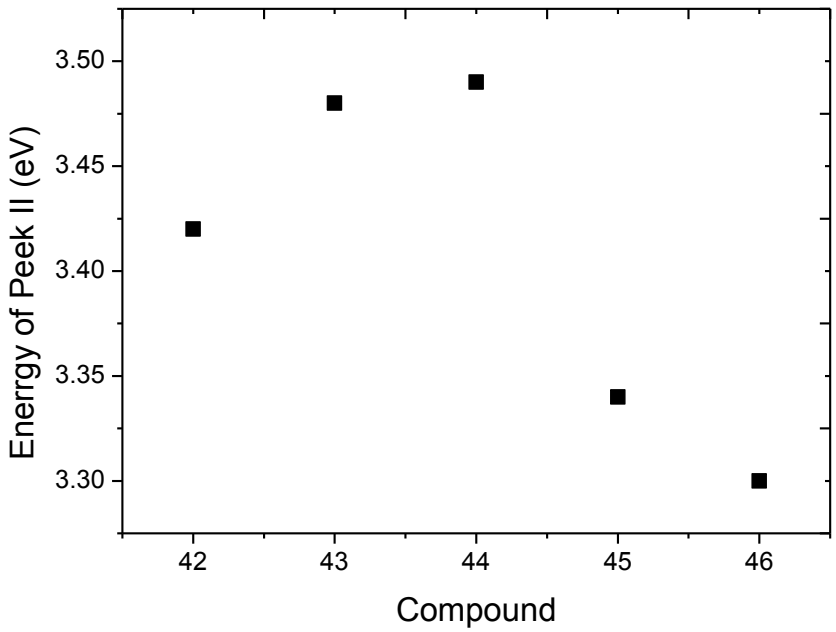

Figure 3.110. Variation the photophysical properties of the energy of the absorption band **II** as a function of the **BT** unit position for compounds (**42** to **46**).

The emission spectra of **T4BT** series compounds in the solid state a slightly red shifted for **42-45** and blue shifted for **46** compared to those in the solution. The peak positions (Figure 3.111) and the band profiles of BT series exhibit the pair-wise correspondence of **43** with **44** (the most red shifted emission and the hint of vibronic splitting) and **42** with **45**, the isomer **46** being the unique member of the series. This correspondence originates from the substitution pattern of BT unit. The reduction in the fluorescence quantum efficiency is found when moving on from compounds **42** to **46** as shown in Figure 3.111.

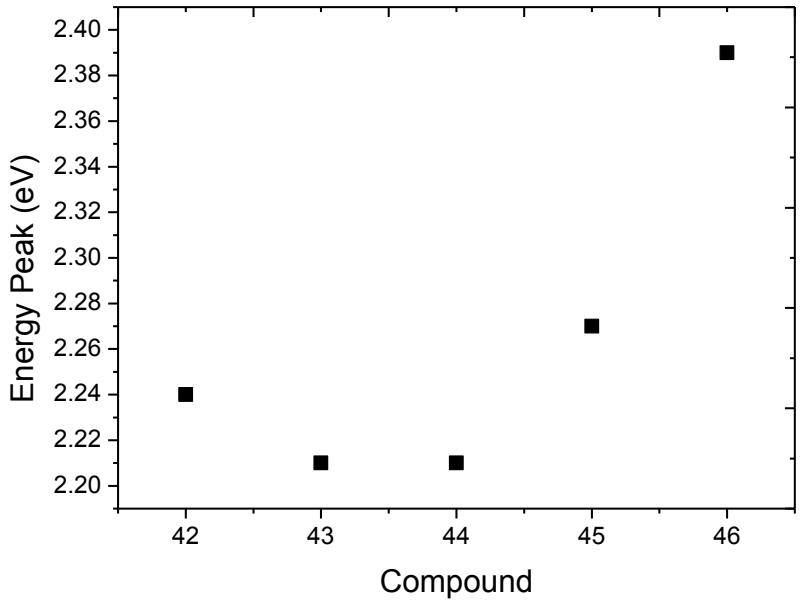

Figure3.111. Variation the photophysical properties of the energy of the peak emission energy as a function of the BT unit position for compounds (**42** to **46**).

3.2.4. Electrochemical Studies

The cyclic voltammetry experiments of compounds (**41** to **46**) were performed in dichloromethane solution with glassy carbon as a working electrode. Oxidation and reduction processes of six compounds are depicted in the Figures 3.112. The highest first oxidation potential among truxene – BT series is shown by T0BT (**41**) and T4BTC (**44**) with a reversible peak at +1.00 / +0.94V, and +1.01 /+0.90V due to the lest possibility for stabilising the cation radical in these conjugated systems.[199, 200] Compound **43** exhibits three reversible oxidation waves at +0.88/+0.80, +0.99/+0.92 and +1.14 /+1.04V, and the other isomers of T4BT series shows two reversible oxidation peaks at +0.86/+0.78 V and +1.0/+0.90 V for compound **42** and at +0.77 /+0.70 V and +0.91 /+0.84V and +0.75 /+0.68 V and +0.86 /+0.79 V for

compounds **45** and **46** respectively. All the six compounds exhibit reversible reduction peak that corresponds to the reduction of the benzothidiazole units. The oxidation and reduction peaks values are represented in Table 3.6.

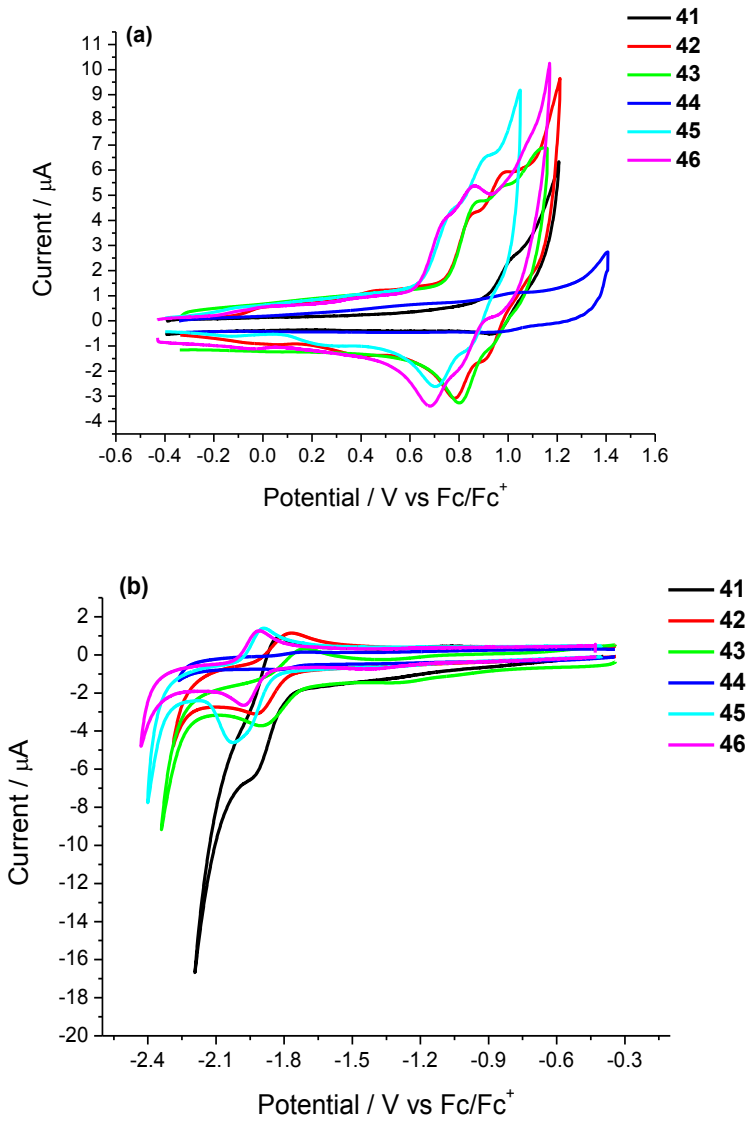

Figure 3.112. (**a**) Oxidation and (**b**) reduction of six compounds in dichloromethane solution with 0.1 M $TBAPF_6$ as supporting electrolyte, on a glassy carbon working electrode

Table 3.6. Oxidation and reduction processes of compounds **41** to **46** in solution state

Compound	Oxidation (V)	Reduction (V)
41	+1.00 / +0.94	-1.92 / -1.82
42	0.86/0.78 and 1.0/0.90	-1.93/-1.77
43	0.88/0.80, 0.99/0.92 and 1.14/1.04	-1.90/-1.71
44	1.01/0.90	-1.83/-1.73
45	0.77/0.70 and 0.91/0.84	-1.96/-1.89
46	0.75/0.68 and 0.86/079	-1.98/-1.91

The HOMO-, LUMO-levels and the gap are calculated (Figure 3.113 and Table 3.7). The HOMO-levels of six compounds are found to be within the range of 5.4-5.6 eV. The highest HOMO-levels are observed for the compounds **46** and **45** that contain the most extended T4 and T3 conjugated cores. The deepest HOMO-levels of compounds **44** and **41** are consistent with their highest oxidation potentials.

There is a good agreement between the electrochemical and optical HOMO-LUMO gap for all the compounds of truxene BT series except the T4BT-E isomer **46**.

The significant difference between electrochemical and optical HOMO-LUMO gaps in this case (about 0.48 eV) is an additional confirmation of a poor overlap between delocalised HOMO and localised on BT LUMO in conjugated system of **T4BT-E** compound.

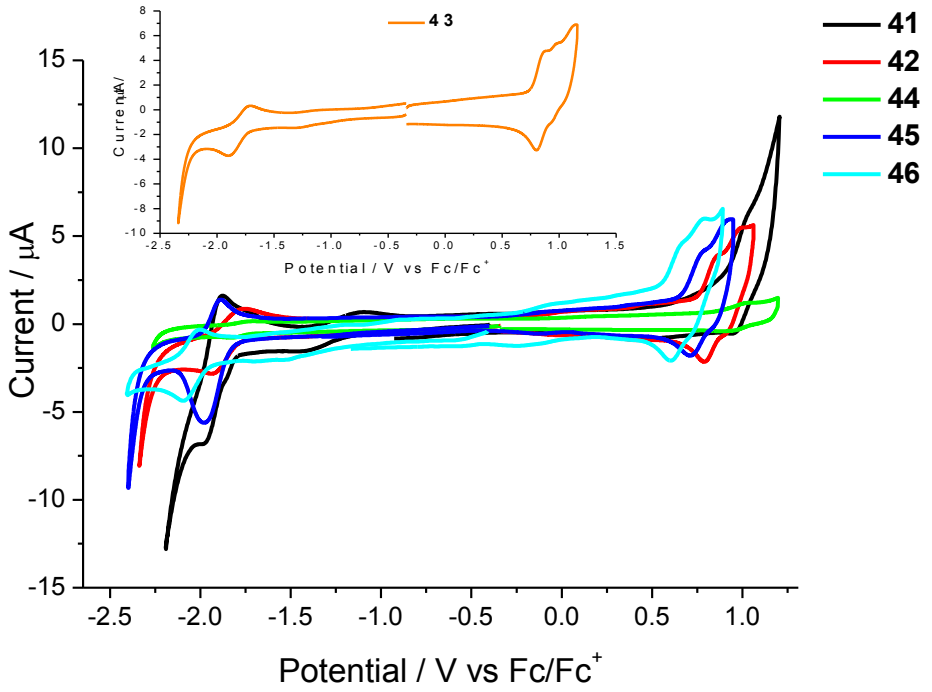

Figure 3.113. Cyclic voltammogram of compound **41**, **42**, **43**, **44**, **45** and **46** on glassy carbon electrode, in 0.1M Bu_4NPF_6 at 0.1 $V \cdot s^{-1}$ scan rate

Table 3.7. Oxidation and reduction processes of compounds **41** to **46** in solution state

Compound	Onset of oxidation (V)	HOMO (eV)	Onset of Reduction (V)	LUMO (eV)	HOMO-LUMO gap (eV)
41	+85	-5.65	-1.85	-2.95	2.70
42	+0.76	-5.56	-1.78	-3.02	2.54
43	+0.76	-5.56	-1.73	-3.07	2.49
44	+0.82	-5.62	-1.72	-3.08	2.54
45	+0.65	-5.45	-1.85	-2.95	2.50
46	+0.63	-5.43	-1.85	-2.95	2.48

3.2.5. Conclusion

New series of structural isomers of trigonal star-shaped molecules have been synthesised and characterised by cyclic voltammetry, UV-vis and emission spectroscopy. Using these techniques, the electrochemical and optical properties of the compounds were determined. The optical properties were found to be affected by the variations of the donor environment around the BT unit. The absorption spectra of compounds **41** - **45** showed an ICT absorption band, which was blue shifted in the case of compound **41** compared to those of the rest of the truxene – BT conjugated systems (compounds **42** to **45**). The ICT band was not resolved in the case of compound **46** due to the decrease in the overlap between delocalised HOMO and localised on BT LUMO. The materials were found to be efficient green and yellow emitters with excellent solubility. The photoluminescence spectra exhibited blue shift in the emission of compounds **41** and **46** compared to the other members of the series. Regarding electrochemical behaviour, the compounds **41 - 44** exhibited a good agreement between electrochemical and optical HOMO-LUMO gap**.** Whereas the significant difference between electrochemical and optical HOMO-LUMO gaps of compound **46** was assumed to be the additional confirmation of the poor HOMO-LUMO overlap in this conjugated system.

Chapter 4

Multi-layer fabrication of organic devices via electrochemical polymerisation

4.1. Introduction

Polythiophene derivatives have become attractive materials for use in device applications, because they possessed tunable band gaps, good redox stable properties and high conductivity in doped state.[43,44] Ethylene3,4-dioxythiophene(EDOT) and ethylene 3,4-dithiathiophene (EDTT) are important thiophene derivatives with increased propensity to electropolymerisation and wide range possibility of chalcogen-chalcogen non-covalent interaction in electrodeposited polymers. The later provide a significant difference between the electrochemical and optical properties of PEDOT and PEDTT. For example, in the electrochemical experiments PEDTT exhibit higher oxidation potential and larger band gap than PEDOT, due to increasing the number of the sulfur atoms in PEDTT chain, where the adjacent units will suffer from steric hindrance by S···S intrachain interactions.[44,39,43]

In the past 20 years, the fabrication of multi-layer organic electronic devices has been extensively researched, resulting in several processes and techniques.[201] Recent advances include ink-jet printing[202] and direct stamping of the active layer to the substrate.[203] However, the usage of solvents in such processes is one of important issues, which can produce blended layers through dissolution of the initial layers.[204] While the use of water or fluorinated solvents can avoid such issues,[205,206] materials suitable for use in such solvents are to be specifically designed, meaning such processes are less suitable for general use.[204] Both EDOT and EDTT were chosen due to their ease of electropolymerisation and because of their likely compatibility with each other (due to similar morphologies).[43]

This chapter describes new process for fabrication of multi-layer organic electronic devices by using electopolymerisation technique of **EDOT** and **EDTT** monomers in a step-wise approach to produce **PEDOT/PEDTT** bi-layer as revealed Figure 4.114

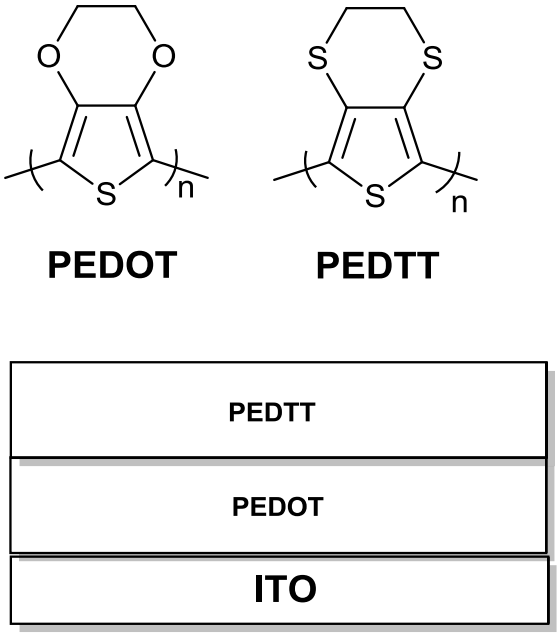

Figure 4.114. The structures of **PEDOT** and **PEDTT**, and the design of the electropolymerised **bi-layer**

Crucially, by this approach an insoluble conductive **PEDOT** layer is produced by initial deposition and then **PEDTT** as doped second layer is deposited on the top and subsequently de-doped, without compromising the initial PEDOT layer. Estrany *et al* has been demonstrated this technique through the manufacturing of multi-layer films,[207,208] alternating PEDOT and poly(*N*-methylpyrrole) to develop symmetric electric double-layer capacitor (supercapacitors).[209]

4.2. Experimental

3,4-Ethylenedioxythiophene (EDOT) was purchased commercially, and 3,4-ethylenedithiothiophene (EDTT) was prepared according to the literature procedures[210] by Neil Findlay (University of Strathclyde). Raman spectra measurements were performed and analysed by Luca Guerrini (University of Strathclyde). Raman spectra were recorded on Renishaw System *2000* Raman spectrometer equipped with a 785 nm excitation line and x50/0.75 Leica objective, (A ~8 mm x 20 mm) deposited polymer layer on indium tin oxide (ITO) slide. A simple, multilayer diode was performed by A.R. Inigo and Sasikumar Arumugam (University of Strathclyde).

Cyclic voltammetry (CV) measurements and electropolymerisations were performed on a CH Instruments 660A electrochemical workstation with *iR* compensation using anhydrous dichloromethane or acetonitrile (MeCN) as the solvent. The electrodes were glassy carbon or ITO glass slide, platinum wire or gauze and silver wire as the working, counter and reference electrodes, respectively. All solutions through the reduction process were degassed (Ar) and contained monomer substrates in concentrations of *ca.* 10^{-4} M, together with *n*-Bu_4NPF_6 (0.1 M) as the supporting electrolyte. All measurements are referenced against the $E_{1/2}$ of the Fc/Fc^+ redox couple. The absorption spectra measurements were recorded on a UNICAM UV 300 instrument, by using the grown film on ITO slide and operating between 300 and 1100 nm

4.3. Electrochemistry of Monomers and Polymers

EDOT and **EDTT** molecules were studied by cyclic voltammetry in dichloromethane solution. The thiophene derivatives display two irreversible oxidation peaks at +1.12 and +1.49V for **EDOT** and at +0.99 and +1.59V for **EDTT**. The cyclic voltammograms of these compounds are shown in Figure 4.115.

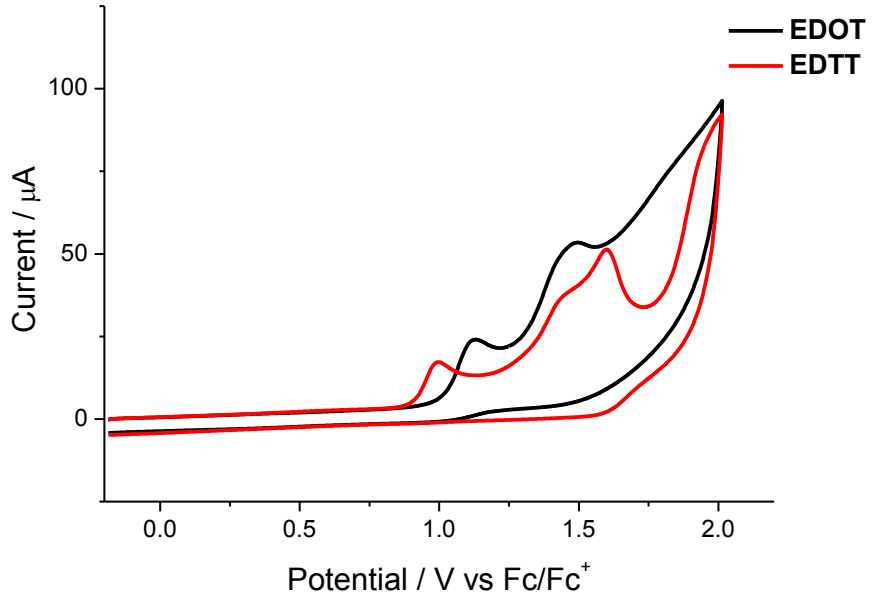

Figure 4.115. Cyclic voltammograms of **EDOT** and **EDTT** in dichloromethane solution, using a glassy carbon working electrode, Ag/AgCl reference electrode, platinum counter electrode, substrate concentration 10^{-4} M, tetrabutylammonium hexafluorophosphate as supporting electrolyte (0.1 M) and a scan rate of 0.1V s^{-1}.

Both **EDOT** and **EDTT** monomers were electropolymerised by repetitive cycling (300 segments) over the redox active peaks employing the same conditions and the same solvent, which were used for cyclic voltammetry. A good thin film of **PEDOT**

and **PEDTT** were obtained on the working electrode surface. The growth traces for the poly **EDOT** and poly **EDTT** are presented in Figure 4.116.

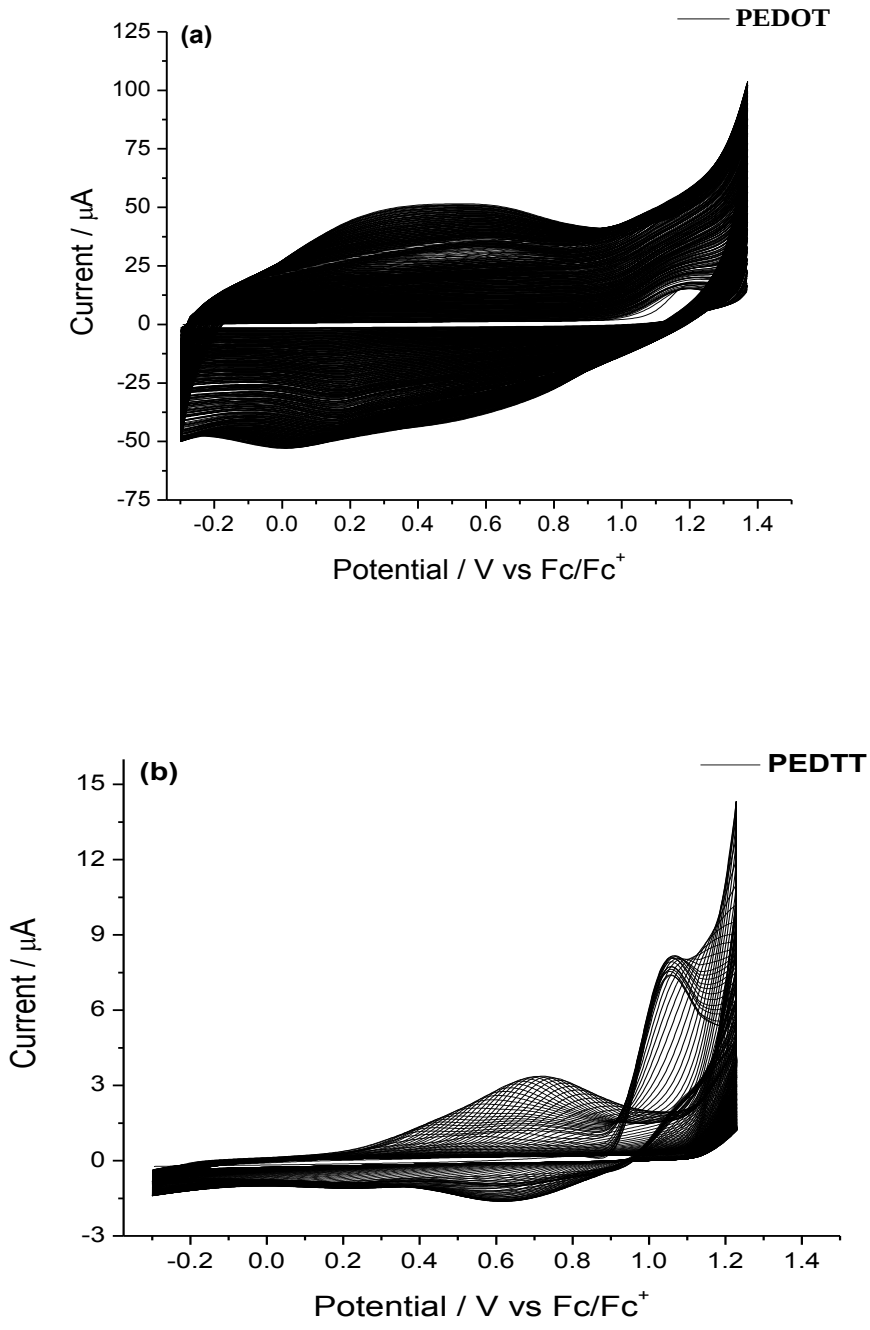

Figure 4.116. Electrochemical growth of (**a**) **PEDOT** and (**b**) **PEDTT**

The cyclic voltammetry of two polymers as films on ITO glass as working electrode was investigated with silver and platinum wires as reference and counter electrodes respectively in a monomer-free acetonitrile solution. The band gaps of **PEDOT** and **PEDTT** are in partial agreement with the previous literature values, which were 1.30 and 2.15 eV for **PEDOT** and **PEDTT** respectively. These have been reported by P. J. Skabara and co-workers as summarised in Figure 4.117 and Table 4.1.[43]

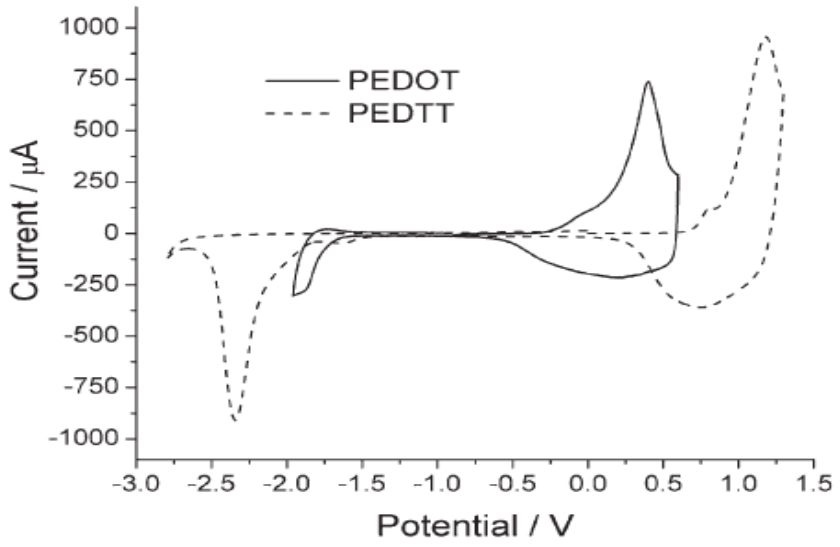

Figure 4.117. Cyclic voltammograms of **PEDOT** and **PEDTT** as films on ITO glass slide. In monomer-free acetonitrile solution at scan rate of 0.1V s^{-1}.[43]

Table 4.1. Electrochemical data for PEDOT and PEDTT.[43]

Polymer	E_{1ox} (V)	HOMO (eV)	E_{1red} (V)	LUMO (eV)	HOMO-LUMO gap (eV)
PEDOT	+40	-4.0	-1.89	-2.70	1.30
PEDTT	+1.18	-4.90	-2.34	-2.75	2.15

HOMO and LUMO values are calculated from the onset of the corresponding redox wave and referenced to ferrocene (E1/2 5 +0.54 V), which has a HOMO of 24.8 eV.

For the formation of the **PEDOT/PEDTT** bi-layer, firstly, PEDOT was deposited on indium tin oxide (ITO) glass slide as working electrode by electropolymerisation from a 10^{-4} M solution of EDOT in 0.1 M tetrabutylammonium hexafluorophosphate as supporting electrolyte (Bu_4) NPF_6/CH_3CN, using a Pt gauze counter electrode and a Ag wire reference electrode, with cycling between 0V and +1.1V over 150 cycles. This was sufficient to achieve good polymer growth. Under similar conditions, the **PEDOT/PEDTT** bi-layer was fabricated using a 10^{-4} M solution of EDTT in 0.1M $(Bu_4)NPF_6/CH_3CN$ and cycling over the range +0.3V to +1.78V over 300 segments as illustrated in Figure 4.118. The newly formed **PEDOT/PEDTT** bi-layer was de-doped by cycling between -0.5V and -0.3V over 300 segments in acetonitrile solution (CH_3CN).

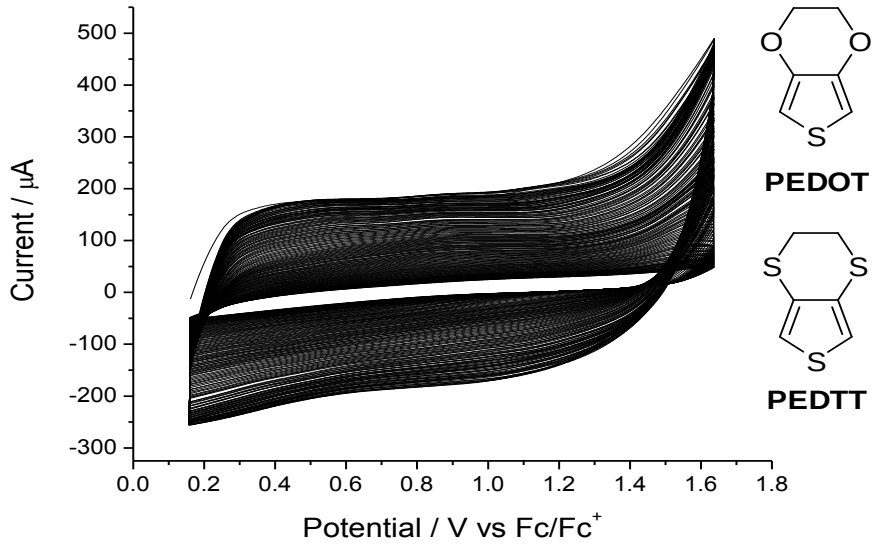

Figure 4.118. Polymer growth of **PEDOT/PEDTT** bi-layer on a glassy carbon working electrode, Ag wire reference electrode and Pt counter electrode in acetonitrile. A concentration of 10^{-4} M for both **PEDOT** and **PEDTT** was used, 0.1 M $(Bu_4N)PF_6$ as the supporting electrolyte, at a scan rate of $100mVs^{-1}$ over 300 segments.

Many attempts of the oxidation and reduction cyclic votltametry experiment in various experimental conditions were made to confirm the formation of the **PEDOT/PEDTT** bi-layer; however the redox behaviour did not provide any clear evidence of the presence of **PEDTT** on the top of **PEDOT** layer. One example of the oxidation and reduction CV experiments of bi-layer is given in Figure 4. 119.

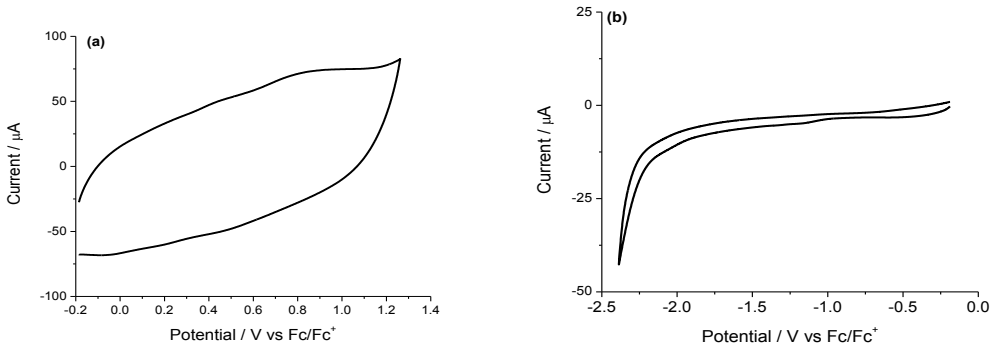

Figure 4.119. Oxidation profile (**a**) and reduction profile (**b**) of **PEDOT/PEDTT** bi-layer using glassy carbon working electrode, Ag wire reference electrode and Pt counter electrode in acetonitrile, at a scan rate of 100mVs^{-1}

The **PEDOT/PEDTT** bi-layer was tested by oxidation stability test, consequently it was found to be reasonably stable towards oxidation; under anodic conditions only a 16.33% decrease in the current response over 50 cycles was observed (Figure 4.120).

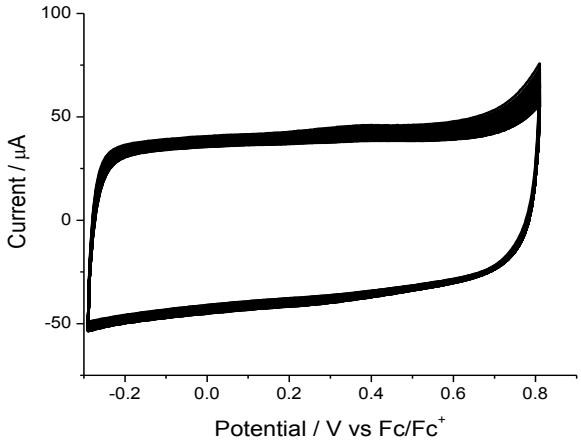

Figure 4.120. Oxidative stability of poly (**PEDOT/PEDTT**) bi-layer in monomer free acetonitrile, at a scan rate of 100 mVs^{-1}, over 50 cycles, using a glassy carbon working electrode

4.4.UV-vis Electronic Absorption Spectra of PEDOT, PEDTT and PEDOT/PEDTT

The absorption maxima are revealed at 579 nm for **PEDOT** and at 445 nm for **PEDTT**, which are in good agreement with the absorption maximum values reported in the literature (578 and 441 nm for **PEDOT** and **PEDTT** respectively)[43]. However, fabrication of a thicker bi-layer from more concentrated **EDOT** and **EDTT** solutions (10^{-2} M) leads to appearance of two absorption peaks. The first peak is observed at 445 nm, which corresponds to the PEDTT absorption, and the second one appeared as a broad absorption centred at 863 nm, suggesting assigned to the residual doping of PEDOT layer. The optical band gap of the thick bi-layer is calculated from the onset of the absorption, giving a value of 1.19 eV. All the electronic absorption spectra in acetonitrile solution for three polymeric species are shown in Figure 4.121.

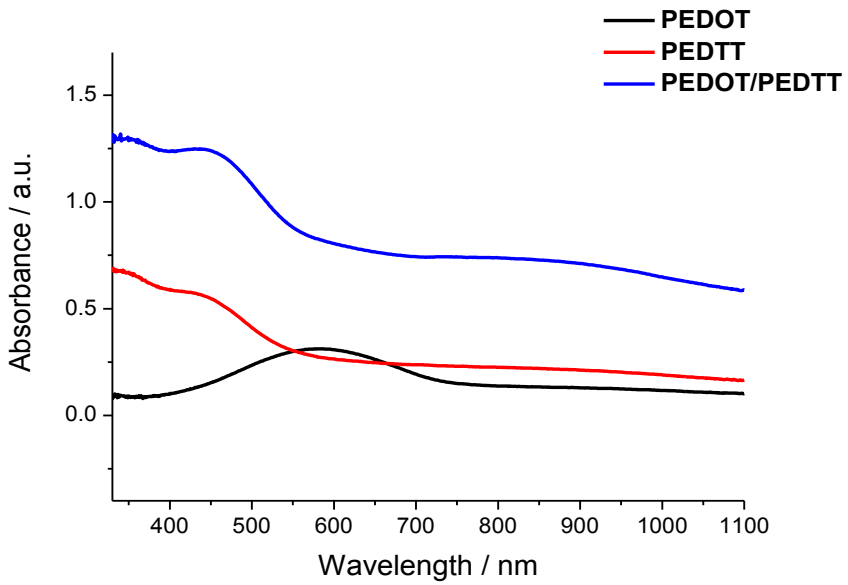

Figure 4.121. Absorption spectrum of **PEDOT**, **PEDTT** and **PEDOT/PEDTT** (bi-layer) as a thin film on ITO-coated glass prepared from monomer solution in acetonitrile, A concentration of **EDOT** and **EDTT** is 10^{-2} M for preparation of bi-Layer, and 10^{-4} M for that of both **PEDOT** and **PEDTT**

4.5. Raman spectroscopy of PEDOT, PEDTT and PEDOT/PEDTT

In order to confirm the formation of a **PEDOT/PEDTT** bi-layer by this technique, freshly fabricated bi-layers (using 10^{-4} M solutions of monomers) were analysed by Raman spectroscopy alongside with mono-layers of **PEDOT** and **PEDTT** for comparison. Figure.4.122 shows the Raman spectra of pure **PEDOT** and **PEDTT** polymers both in the doped and neutral states (Figure. 4.122a and b, Figure. 4.122c and d, respectively). There are two main spectral regions in the Raman spectra of these conjugated polymers. Below approximately 1150 cm^{-1}, the Raman spectrum is dominated by medium-weak bands mostly assigned to out-of-plan deformations[211] poorly sensitive to modifications in the electronic properties of the polymers.[212] By comparing **PEDOT** and **PEDTT**, contributions related to the dioxine ring of

PEDOT, such as the bands at 576 cm^{-1} and 991 cm^{-1}, assigned to oxyethylene ring deformations, and at 1099 cm^{-1}, assigned to C-O-C deformation, which are absent in **PEDTT** (Figure. 4.122c and d).[210,213] On the contrary, the Raman features appearing in the spectral region above 1150 cm^{-1} strongly depend on the π-electron delocalization within the polymer and, therefore, present dramatic changes both in frequency and intensity as a result of the different electronic structure of each polymer (Figure 4.122). In particular, in the doped **PEDOT** spectrum (Figure. 4.122a), the Raman feature corresponding to the thiophene ring at 1534 cm^{-1}, attributed to the C=C asymmetric stretching vibration, the one at 1413 cm^{-1} assigned to the symmetric $C_\alpha=C_\beta$ stretching mode, that at 1371 cm^{-1} is due to the $C_\beta=C_\beta$ stretching vibration, and the feature at 1255 cm^{-1}, ascribed to inter-ring $C_\alpha=C_{\alpha'}$ stretching.[212] However, when **PEDOT** is subjected to a de-doping process as depicted in Figure 4.122b, yielding the neutral polymer, the weak band at 1534 cm^{-1} shifts to 1521 cm^{-1} and increases its intensity, while the ν_{sym}(C=C) band shifts from 1413 cm^{-1} in doped state to 1426 cm^{-1} in de-doped. Additionally, the broad band at 1255 cm^{-1} splits into two (at 1227 and 1271 cm^{-1}).[214] The drastic enhancement and sharpening of the Raman band at 1370 and 1415 cm^{-1} after the de-doping process can be ascribed to the resonance effect.[211] By analogy with the band assignment for **PEDOT**, the Raman features in the **PEDTT** spectrum (Figure. 4.122c) at 1396 cm^{-1} and 1321 cm^{-1}, can be ascribed to $\nu_s(C_\alpha=C_\beta)$ and $\nu_s(C_\beta=C_\beta)$ symmetric stretching vibrations, respectively. Once more, the out-of-plane bands appearing in the less-than1150 cm^{-1} spectral region are less sensitive to the de-doping process, the group of C=C bands shows important changes, such as the marked downshift of the $C_\beta=C_\beta$ band from 1321 cm^{-1} to 1312 cm^{-1}, and the increase in intensity of the $C_\alpha=C_\beta$ band at

~1396 cm^{-1}. In particular, Kocharova *et al.*[215] Associated the intensity increase of the $C_\alpha=C_\beta$ band in polythiophene structures with higher localized charge at the $C_\alpha=C_\beta$ linkage as a consequence of the positively charged material upon doping and subsequent rearranging the electron density. Figures 4.122e and f illustrate the Raman spectra of the **PEDOT/PEDTT** bi-layer in the doped state and after de-doping of the **PEDTT** layer, respectively. It is clear that the doped bi-layer structure shows the characteristic Raman profile of the **PEDTT** doped system, proving the effective and successful coating of the underlying **PEDOT** layer (Fig. 4.122e). Accordingly, this is considered as evidence for formation of the bi-layer. Once the bi-layer is subjected to the de-doping process where, the Raman spectrum, shown in Figure 4.120f, retains the spectral features of the **PEDTT** neutral polymer (Figure 4.122d).

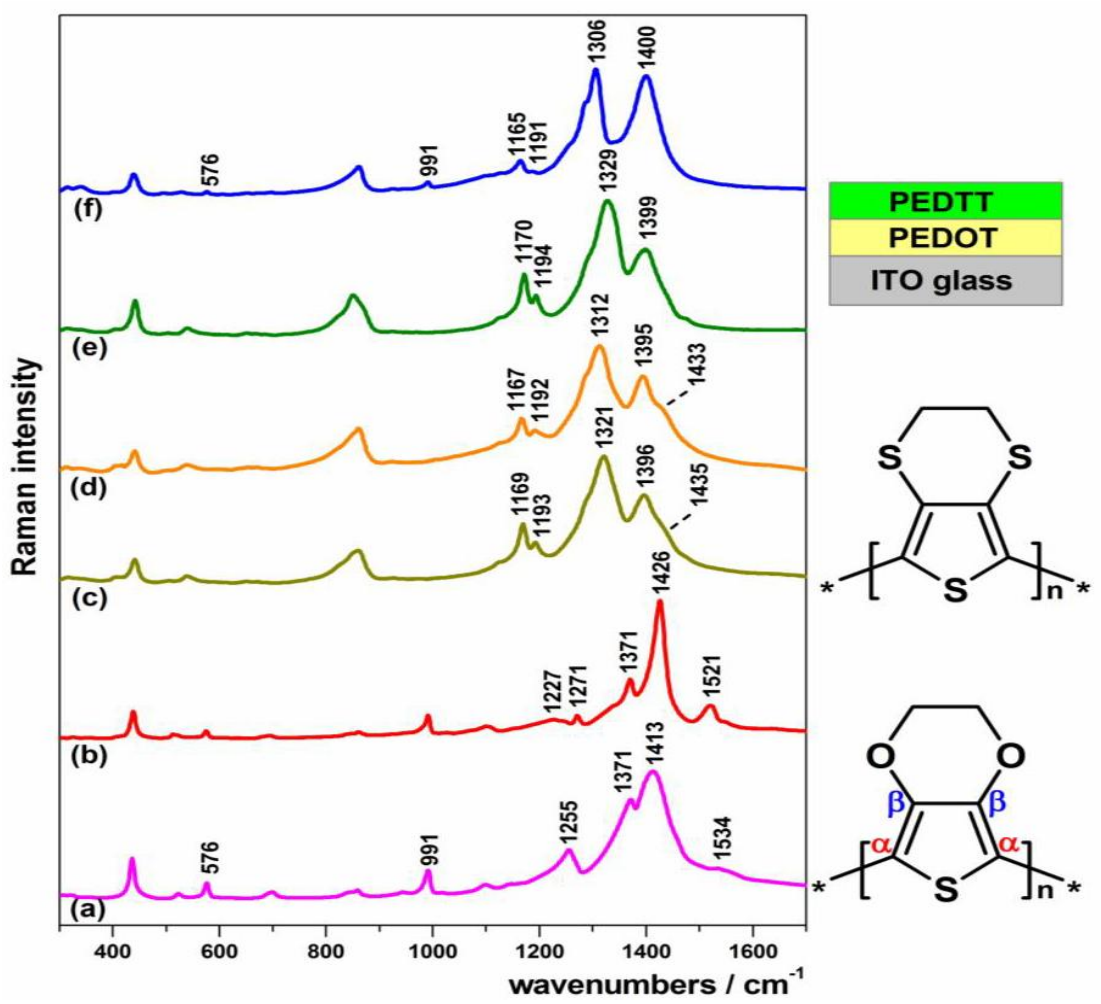

Figure 4.122. Normalised Raman spectra of (**a**) doped **PEDOT** monolayer; (**b**) neutral **PEDOT** monolayer; (**c**) doped **PEDTT** monolayer; (**d**) neutral **PEDTT** monolayer; (**e**) doped **PEDOT/PEDTT** bi-layer; (**f**) neutral **PEDOT/PEDTT** bi-layer

Very weak bands were attributed to the **PEDOT** system, such as bands at 576 and 991 cm^{-1}, can be recognized in the bi-layer spectrum. The appearance of this signals arising from the underlying **PEDOT** layer, although distant from the focal point of the laser, can be attributed to the much higher Raman scattering efficiency[216] of **PEDOT** in the neutral state with respect to **PEDTT** as depicted in Figure 4.123.

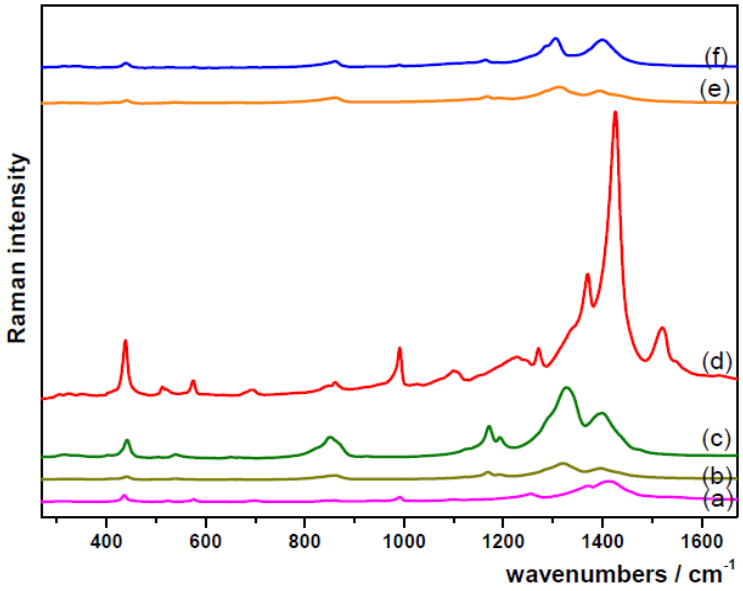

Figure 4.123. Original Raman spectra of (**a**) **PEDOT** doped, (**b**) **PEDTT** doped, (**c**) **Bi-layer** doped, (**d**) **PEDOT** neutral, (**e**) **PEDTT** neutral and (**f**) **Bi-layer** neutral.

4.6. Processing Methods

A stringent examination of this novel process was completed through the fabrication of a simple diode. As before, a **PEDOT/PEDTT** bi-layer was deposited electrochemically from the monomer solutions under the same, previously described conditions. This bi-layer has been assessed in a diode configuration to act as a potential candidate as hole injector/transporter in applications such as organic light emitting diodes (OLEDs), photodiodes or OPVs. An oligofluorene-DPP derivative, linear-c (**33**)[217] (Figure 4.124), has been chosen as an active material, which is an acceptor (electron transport material).[217] A layer of linear-c was spin coated onto the top of **PEDOT/PEDTT** bi-layer followed by thermal evaporation of Ca (40 nm) and Al (40 nm) by using a shadow mask.

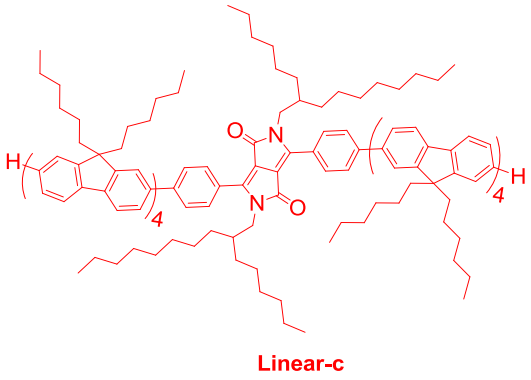

Figure 4.124. Structure of **Linear-c** (**33**)

The active area (6 mm^2) of the device is defined by the dimensions of shadow mask. The completed device (Figure.4.125) has the architecture of ITO/**PEDOT/PEDTT**/linear-c/Ca/Al, which is capable of transporting both electrons and holes. These were tested under dark and illumination in a glove box attached to a solar simulator. While, it does not show any distinct photo response, these devices still exhibited photovoltaic characteristics with an open circuit voltage of 80 mV in dark and 130 mV in light. This indicates that there is no efficient charge separation at the EDTT- linear-c interface. The relative barrier height of 0.4 eV for an electron and hole transport at the interface of EDTT (donor) and linear-c (acceptor) is not enough for effective charge separation of photogenerated electron hole-pairs at the interface and hence there is no distinct OPV performance.

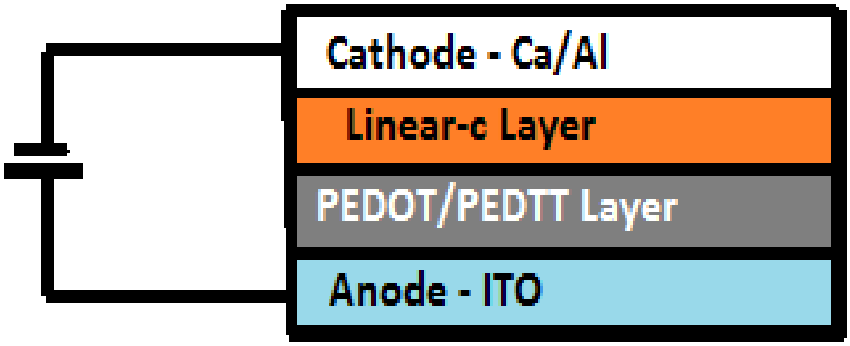

Figure4.125. The architecture of the device

4.7. Conclusion

Novel processing methodology for the fabrication of multi-layer organic electronic devices utilises electrochemical polymerisation to form the first two layers. Such a technique has advantages over traditional processing methods including the deposition of an insoluble, conductive PEDOT base layer that is not compromised through contact with solvents. Successful PEDOT/PEDTT bi-layer formation has been confirmed through the use of comparative Raman spectroscopy. Furthermore, a multi-layer organic diode has been engineered by combining the methodology developed here with conventional spin-coating. The current voltage characteristics under dark and illumination followed bulk limited space charge conduction.

5. Conclusions

In the first section in chapter two, a series of monomers are containing heteropentalene mesomeric betaine including compounds **9**, **11**, **15** and **16** have synthesized and characterized based on the incorporation of substituted groups for instance 3,4-ethylenedioxythiophene (EDOT) in compound **9**. UV spectroscopy and cyclic voltammetry techniques of monomers **15** and **16** have revealed slightly different properties when compared to compound **11**. A smaller optical and electrochemical HOMO-LUMO gap has exhibited in monomer **9** compared to the rest of the monomers, which is attributed to the stronger electron-donating group in monomer **9**. Compound **9** has been prepared and successfully electropolymerised by coated onto an indium tin oxide (ITO) covered glass slide, the optical band-gap of the polymer was determined as 1.75 eV, and the CV experiments of poly**9** have shown an electrochemical band-gap of 1.93 eV. The polymer of compound **9** is reasonably stable against the anodic conditions and the scan rate test gives straight-line graph with higher correlation factor value that indicating to the polymer is not diffusion limited. Spectroelectrochemical and switching times measurements of poly**9** have been reported, where, the changes in absorbance between various colour states displayed fast switching rate between doped and de-doped states, when a 10 second switch is applied there is an 80.8% change, but a 0.25 second switching rate afforded only a 4.0% change.

The second section of chapter two has shown the synthesis and characterisation of three monomers and their subsequent polymers. The monomers **17**, **18** and **19** contain EDTT, 3-hexylthiophene and EDOT units respectively, which have incorporated to benzothiadiazole unit as donor–acceptor units. A good agreement of the optical and electrochemical HOMO-LUMO gaps show in monomers **18** and **19**,

whereas monomer **17** exhibits a little difference. The monomers can be polymerised to produce conjugated polymer, however poly**18** deposits slowly on the electrode surface since its high solubility from an effect of hexyl chain. Poly**17** gives higher optical band gap compared to poly**19** attributed to steric hindrance from S···S contact between the sulfur atoms in poly**17**, while the O···S interactions in poly**19** increases the planarity degree thus; enhance the effective conjugated length. Poly**17** and poly**19** show higher oxidative stability, whereas poly**18** was less stable on the electrode surface due to the presence of the solubilising hexyl chains. The polymers showed potential for use as electrochromic films

The section three of chapter two, is produced five monomers are included phenanthroline as core unit, which is appended to two EDOT in compounds **20** and **21** and with bithiophene-bi-EDOT in compounds **22**, **23** and **24**. Compound **21** does not polymerise while, the remaining monomers have produced polymer state. The polymers exhibit lower electrochemical band gap compared to their monomers due to an extended conjugated chain of their polymers. Poly**20** gives slight higher electrochemical and optical band gap compared to other polymers suggesting that owing to reducing the conjugated length in this polymer. The spectroelectrochemical and switching times of the polymers were studied, where poly**22** shows the best switching rates compared to poly**24**.

Section four of chapter two is aimed at the analysed of new two monomers by electrochemical and spectroelectrochemical tests. The monomers are consisted from bis-EDOT and bis [EDOT-thiophene] units in compounds **25** and **26** respectively, are attached with 1,10-phenanthroline as core unit. Monomer **26** does polymerise with successful growth and with high oxidative stability to anodic conditions, which

attributed to the attendance of extended conjugated chain in poly**26**, however; monomer **25** does not polymerise, suggesting to the strong dominating of the Ru^{III}/Ru^{II} oxidation process in poly**25**. Poly**26** has switched between colour states and exhibits agreement between the optical and electrochemical band gaps, which were 1.78 to 1.90 eV, respectively.

In the fifth section, two new bis EDOT units attached with pyridine unit based monomers **27** and **28** with addition methyl group in monomer **28** were synthesised and investigated by electrochemical and spectroscopic techniques. Monomer **28** displayed significant effect of the intramolecular charge transfer (ICT) process and lower electrochemical band gap. Both monomers show successful growth as blue thin films on the working electrode surface with high oxidation stability. The spectroscopic properties of two dimers introduce dimer traces have lower optical band gaps compared to their monomers.

Three new compounds **29**, **30** and **31** in the sixth section of chapter two have incorporating BODIPY core with two EDOT, thiophene and EDTT units respectively. The spectroscopic analysis of three monomers introduced red shift in the absorption spectra of monomer **29** compared to the rest of the monomers, which ascribed to stronger electron donating effect of EDOT unit in this compound. CV analysis of the three monomers shows slight greater oxidation potential in monomer **31** compared to other monomers that is attributed to the raise the number of sulfur atoms in compound **31**. Weak polymer growths with instability have given by these compounds, which prevented the electropolymerisation investigations of these polymers, due to their instability on the electrode surface.

The first section of chapter three is reported on three oligofluorene substituted DPP macromolecules **32**, **33** and **34** and the core precursors (**35**, **36**, **37** and **38**). Compound **32** contains DPP core, which has four quaterfluorene arms, and twofold substitution of the core with quaterfluorenes is represented by **33** and **34** compounds. The absorption spectra of all compounds in dichloromethane give two peaks are attributed to $\pi - \pi^*$ transition of quaterfluorene arms and the DPP unit respectively. The great conjugated length in **32** compared to **34** can be ascribed to the intramolecular charge transfer (ICT) in **32**, which is happened from push of electrons from substituents at the 3,6-positions to the 1,4-carbonyls. In CV experiment, compound **33** exhibits higher of LUMO level compared to other compounds, which is confirmed the different effects of the hexldecyl and phenyl groups. In TGA, compound **33** does not show glass transition temperature contrasted to compounds **32** and **34**, which is proved that the compound **33** crystalline and not amorphous in nature. The two dimensional character of the Star system and the alternating positions of phenylene spacers between the core and the arms generate very strong aggregating propensity in the solid state and also in hexane solutions. The different types of aggregation in the solid phase provided by ICT, the substitution pattern, and the dimensionality of the molecular system must be taken into account during the design of new materials. The DPP unit is clearly an interesting and exciting unit for use as a core in star-shaped conjugated architectures.

In the second section of chapter three, new six of structural isomers of trigonal star-shaped molecules contain quaterfluorene arms with three BT units at each possible position have been synthesised and characterised by cyclic voltammetry, UV-vis and emission spectroscopy. The spectroscopic experiment of compounds **41**-**45** gives

ICT absorption peak, which was hypsochromic shift in compound **41** whereas compound **46** does not show this effect that owing to the decreasing of the overlapping between T4 HOMO and BT LUMO. The emission spectra showed red shift in compounds **42-45** compared to compounds **41** and **46**. The electrochemical behaviour, compounds **41 - 44** exhibited a good agreement between electrochemical and optical HOMO-LUMO gap. While compound **46** gives a significant difference between electrochemical and optical HOMO-LUMO gaps, which is confirmed of the poor HOMO-LUMO overlap in this conjugated system.

In chapter four, novel processing methodology has used for fabrication of multi-layer organic electronic devices by employing electropolymerisation method to form bi-layer. PEDOT was deposited on an ITO glass slide by electropolymerisation with cycling between 0 V and +1.1 V over 150 cycles, and then similar conditions, the bi-layer was fabricated by growing the polyEDTT by cycling over the range +0.3 V to +1.78 V to form **PEDOT/PEDTT** layer. The successful bi-layer has confirmed by use of comparative Raman spectroscopy. the bi-layer has been assessed in a diode configuration to act as a potential candidate as hole injector/transporter in organic light emitting diodes, or organic photovoltaics by using linear-c(**33**) as acceptor on the top of bi-layer. Furthermore, a multi-layer organic diode has been engineered by combining the methodology developed here with conventional spin-coating. The finished device does not exhibit any distinctive photo response, where the current voltage characteristics under dark and illumination, due to inefficient charge separation at the PEDTT- linear-c (**33**) interface.

6. References

1. J. Roncali, *Chemical Reviews*, 1992, **92**, 711-738.
2. D. L. S. I. H. Campbell, *International Journal of High Speed Electronic and System*, 2001, **11**, 585-615.
3. P.J.Skabara, *Chemistry and Industry*, 2001, **12**, 371-372.
4. H. Pang, P. J. Skabara, D. J. Crouch, W. Duffy, M. Heeney, I. McCulloch, S. J. Coles, P. N. Horton and M. B. Hursthouse, *Macromolecules*, 2007, **40**, 6585-6593.
5. P. Leriche, M. Turbiez, V. Monroche, P. Frère, P. Blanchard, P. J. Skabara and J. Roncali, *Tetrahedron Letters*, 2003, **44**, 649-652.
6. I. D. W. Samuel and G. A. Turnbull, *Chemical Reviews*, 2007, **107**, 1272-1295.
7. R. Berridge, S. P. Wright, P. J. Skabara, A. Dyer, T. Steckler, A. A. Argun, J. R. Reynolds, R. W. Harrington and W. Clegg, *Journal of Materials Chemistry*, 2007, **17**, 225-231.
8. F. G. a. L. E. Lyons and . *Organic Semiconductors. John Wiley & Sons, Inc*, 1967.
9. J. O. H. LeBlanc, *The Journal of Chemical Physics*, 1960, **33**, 626-626.
10. R. G. Kepler and D. C. Hoesterey, *Physical Review B*, 1974, **9**, 2743-2745.
11. Akamatu, H., Inokuchi, H. & Matsunaga, Y. , *Nature*, 1954, **173**, 168-169.
12. H. Shirakawa, *Reviews of Modern Physics*, 2001, **73**, 713-718.
13. M. R. Bryce, *Chemical Society Reviews*, 1991, **20**, 355-390.
14. S. Pyo, L. Ma, J. He, Q. Xu, Y. Yang and Y. Gao, *Journal of Applied Physics*, 2005, **98**, 054303-054306.
15. *http://www.nobelprize.org/nobel_prizes/chemistry/laureates/2000/index.html*.
16. C. K. Chiang, C. R. Fincher, Jr., Y. W. Park, A. J. Heeger, H. Shirakawa, E. J. Louis, S. C. Gau and A. G. MacDiarmid, *Physical Review Letters*, 1977, **39**, 1098-1101.
17. *http://perphysics.ph-astr.gsu.edu./hbase/soliss/band.html*.
18. J. K. a. J. Dorak, *Principles of Electrochemistry", John Wiley & Sons Ltd* 1987.
19. A. J. B. a. L. R. Faulkner, *Electrochemical Methods Fundamentals and Applications', John Wiley & Sons, Inc.*, 2001.
20. B. L. R. F. Brovelli, J. C. Bernede, M. A. d. Valle, F. R. Diaz, and Y. Berredjem,, *Polym. Bull.*, 2006, **58**, 521.
21. F. Garnier, *Philosophical Transactions of the Royal Society of London. Series A: Mathematical, Physical and Engineering Sciences*, 1997, **355**, 815-827.
22. A. Pron and P. Rannou, *Progress in Polymer Science*, 2002, **27**, 135-190.
23. R. Berridge, P. J. Skabara, C. Pozo-Gonzalo, A. Kanibolotsky, J. Lohr, J. J. W. McDouall, E. J. L. McInnes, J. Wolowska, C. Winder, N. S. Sariciftci, R. W. Harrington and W. Clegg, *The Journal of Physical Chemistry B*, 2006, **110**, 3140-3152.
24. F. Carpi and D. De Rossi, *Optics & Laser Technology*, 2006, **38**, 292-305.
25. R. H. Friend, R. W. Gymer, A. B. Holmes, J. H. Burroughes, R. N. Marks, C. Taliani, D. D. C. Bradley, D. A. D. Santos, J. L. Bredas, M. Logdlund and W. R. Salaneck, *Nature*, 1999, **397**, 121-128.
26. P. K. M. A. Rahman, Deog-Su. Park and Yoon-Bo. Shim *Sensors* 2008, **8**, 118.
27. J. C. Forgie, A. L. Kanibolotsky, P. J. Skabara, S. J. Coles, M. B. Hursthouse, R. W. Harrington and W. Clegg, *Macromolecules*, 2009, **42**, 2570-2580.
28. P. J. Skabara, R. Berridge, E. J. L. McInnes, D. P. West, S. J. Coles, M. B. Hursthouse and K. Mullen, *Journal of Materials Chemistry*, 2004, **14**, 1964-1969.

29. S.-H. Yang, C.-H. Huang, C.-H. Chen and C.-S. Hsu, *Macromolecular Chemistry and Physics*, 2009, **210**, 37-47.
30. J. Roncali, *Chemical Reviews*, 1997, **97**, 173-206.
31. G. T. a. F. Garnier, *J.Electochem.Soc*, 1983, **130**, 2042-2044.
32. S. Glenis, D. S. Ginley and A. J. Frank, *Journal of Applied Physics*, 1987, **62**, 190-194.
33. P. J. Skabara, D. M. Roberts, I. M. Serebryakov and C. Pozo-Gonzalo, *Chemical Communications*, 2000, 1005-1006.
34. G. Zotti, *Synthetic Metals*, 1992, **51**, 373-382.
35. R. J. Mortimer, A. L. Dyer and J. R. Reynolds, *Displays*, 2006, **27**, 2-18.
36. R. Berridge, P. J. Skabara, R. Andreu, J. Garín, J. Orduna and M. Torra, *Tetrahedron Letters*, 2005, **46**, 7871-7875.
37. T. Anjos, A. Charlton, S. J. Coles, A. K. Croft, M. B. Hursthouse, M. Kalaji, P. J. Murphy and S. J. Roberts-Bleming, *Macromolecules*, 2009, **42**, 2505-2515.
38. D. Zhang, J. Qin and G. Xue, *Synthetic Metals*, 1999, **100**, 285-289.
39. C. R. Mason, P. J. Skabara, D. Cupertino, J. Schofield, F. Meghdadi, B. Ebner and N. S. Sariciftci, *Journal of Materials Chemistry*, 2005, **15**, 1446-1453.
40. D. J. Crouch, P. J. Skabara, J. E. Lohr, J. J. W. McDouall, M. Heeney, I. McCulloch, D. Sparrowe, M. Shkunov, S. J. Coles, P. N. Horton and M. B. Hursthouse, *Chemistry of Materials*, 2005, **17**, 6567-6578.
41. C. Pozo-Gonzalo, T. Khan, J. J. W. McDouall, P. J. Skabara, D. M. Roberts, M. E. Light, S. J. Coles, M. B. Hursthouse, H. Neugebauer, A. Cravino and N. S. Sariciftci, *Journal of Materials Chemistry*, 2002, **12**, 500-510.
42. R. J. Mortimer, *Chemical Society Reviews*, 1997, **26**, 147-156.
43. H. J. Spencer, P. J. Skabara, M. Giles, I. McCulloch, S. J. Coles and M. B. Hursthouse, *Journal of Materials Chemistry*, 2005, **15**, 4783-4792.
44. A. Cravino, H. Neugebauer, A. Petr, P. J. Skabara, H. J. Spencer, J. J. W. McDouall, L. Dunsch and N. S. Sariciftci, *The Journal of Physical Chemistry B*, 2006, **110**, 2662-2667.
45. X.-S. Du, C.-F. Zhou and Y.-W. Mai, *Materials Letters*, 2009, **63**, 1590-1593.
46. X. Hu and L. Xu, *Polymer*, 2000, **41**, 9147-9154.
47. H. Randriamahazaka, G. Sini and F. Tran Van, *The Journal of Physical Chemistry C*, 2007, **111**, 4553-4560.
48. H. Pang, P. J. Skabara, S. Gordeyev, J. J. W. McDouall, S. J. Coles and M. B. Hursthouse, *Chemistry of Materials*, 2006, **19**, 301-307.
49. B. M. W. L.-V. a. E. W. M. Francesca Goldonia, *Synthetic Communications*, 1998, **28**, 2237-2244.
50. S. Akoudad and J. Roncali, *Synthetic Metals*, 1999, **101**, 149.
51. P. K. A.Misra, R. Srivastava, S.K. Dhawan, M. N. Kamalasanan and S. Chandra, *Indain Journal of Applied Physics*, 2005, 921-925.
52. A. Ajayaghosh, *Chemical Society Reviews*, 2003, **32**, 181-191.
53. C.-L. Pai, C.-L. Liu, W.-C. Chen and S. A. Jenekhe, *Polymer*, 2006, **47**, 699-708.
54. A. Durmus, G. E. Gunbas, P. Camurlu and L. Toppare, *Chemical Communications*, 2007, 3246-3248.
55. A. Balan, D. Baran, G. Gunbas, A. Durmus, F. Ozyurt and L. Toppare, *Chemical Communications*, 2009, 6768-6770.
56. J.-M. Raimundo, P. Blanchard, H. Brisset, S. Akoudad and J. Roncali, *Chemical Communications*, 2000, 939-940.
57. B. F. C. Eva, Krebs *Polymer Bulletin*, 2005, **55**, 157-164.

58. E. Bundgaard and F. C. Krebs, *Solar Energy Materials and Solar Cells*, 2007, **91**, 1019-1025.
59. A. J. Moore, P. J. Skabara, M. R. Bryce, A. S. Batsanov, J. A. K. Howard and S. T. A. K. Daley, *Journal of the Chemical Society, Chemical Communications*, 1993, 417-419.
60. P. Frere and P. J. Skabara, *Chemical Society Reviews*, 2005, **34**, 69-98.
61. P. Leriche, J.-M. Raimundo, M. Turbiez, V. Monroche, M. Allain, F.-X. Sauvage, J. Roncali, P. Frere and P. J. Skabara, *Journal of Materials Chemistry*, 2003, **13**, 1324-1332.
62. P. J. Skabara, K. Mullen, M. R. Bryce, J. A. K. Howard and A. S. Batsanov, *Journal of Materials Chemistry*, 1998, **8**, 1719-1724.
63. R. Berridge, I. M. Serebryakov, P. J. Skabara, E. Orti, R. Viruela, R. Pou-Amerigo, S. J. Coles and M. B. Hursthouse, *Journal of Materials Chemistry*, 2004, **14**, 2822-2830.
64. A. L. Kanibolotsky, R. Berridge, P. J. Skabara, I. F. Perepichka, D. D. C. Bradley and M. Koeberg, *Journal of the American Chemical Society*, 2004, **126**, 13695-13702.
65. K. M. Omer, A. L. Kanibolotsky, P. J. Skabara, I. F. Perepichka and A. J. Bard, *The Journal of Physical Chemistry B*, 2007, **111**, 6612-6619.
66. J. Liu, L. Bu, J. Dong, Q. Zhou, Y. Geng, D. Ma, L. Wang, X. Jing and F. Wang, *Journal of Materials Chemistry*, 2007, **17**, 2832-2838.
67. P. T. Kissinger and W. R. Heineman, *Journal of Chemical Education*, 1983, **60**, 702.
68. J. F. Rusling and S. L. Suib, *Advanced Materials*, 1994, **6**, 922-930.
69. A. H. C. H. Hamann, and W. Vielstich, *"Electrochemistry", WILEYVCH*, 2007.
70. *http://www.files.chem.vt.edu/chem-ed/echem/cv.html*.
71. R. G. D.Pletcher, R.Peat, L.M.Peter, J.Robinson, *Instrumental Methods in Electrochemistry, University of Southampton*, 2011.
72. R. S. Nicholson and I. Shain, *Analytical Chemistry*, 1964, **36**, 706-723.
73. P.M.S.Monk, R.J.Mortimer and D.R.Rosseinsky, *Electrochromism and Electrochrmic Devices, Cambridge University Press, Cambridge*, 2007.
74. J. Crank, *The Mathematics of Diffusion, Oxford University Press*, 1980.
75. W. Kemula and Z. Kublik, *Nature*, 1958, **182**, 793-794.
76. T. P. I. Saragi, T. Spehr, A. Siebert, T. Fuhrmann-Lieker and J. Salbeck, *Chemical Reviews*, 2007, **107**, 1011-1065.
77. J. G. Gritzner and J. Kûta, *Pure & Appl. Chem*, 1984, **56**, 462-466.
78. J. Roncali, *Macromolecular Rapid Communications*, 2007, **28**, 1761-1775.
79. *http://teaching.shu.ac.uk/hwb/chemistry/tutorials/molspec/uvvisab1.htm*.
80. D. H. W. a. I. Fleming, *'Spectroscopic Methods in Organic Chemistry', McGraw-Hill*, 1995.
81. D. Cortizo-Lacalle, S. Arumugam, S. E. T. Elmasly, A. L. Kanibolotsky, N. J. Findlay, A. R. Inigo and P. J. Skabara, *Journal of Materials Chemistry*, 2012, **22**, 11310-11315.
82. S. Kaur, N. J. Findlay, A. L. Kanibolotsky, S. E. T. Elmasly, P. J. Skabara, R. Berridge, C. Wilson and S. J. Coles, *Polymer Chemistry*, 2012, **3**, 2277-2286.
83. D. J. Crouch, P. J. Skabara, M. Heeney, I. McCulloch, S. J. Coles and M. B. Hursthouse, *Chemical Communications*, 2005, 1465-1467.
84. I. Schwendeman, J. Hwang, D. M. Welsh, D. B. Tanner and J. R. Reynolds, *Advanced Materials*, 2001, **13**, 634-637.
85. X. Tu, X. Fu, Q. Jiang, Z. Liu and G. Chen, *Dyes and Pigments*, 2011, **88**, 39-43.
86. A. Georg and A. Georg, *Solar Energy Materials and Solar Cells*, 2009, **93**, 1329-1337.

87. H. Shin, Y. Kim, T. Bhuvana, J. Lee, X. Yang, C. Park and E. Kim, *ACS Applied Materials & Interfaces*, 2011, **4**, 185-191.
88. Y. A. Udum, A. Durmus, G. E. Gunbas and L. Toppare, *Organic Electronics*, 2008, **9**, 501-506.
89. V. Jain, H. M. Yochum, R. Montazami and J. R. Heflin, *Applied Physics Letters*, 2008, **92**, 033304-033303.
90. M. M. Payne, S. R. Parkin, J. E. Anthony, C.-C. Kuo and T. N. Jackson, *Journal of the American Chemical Society*, 2005, **127**, 4986-4987.
91. H. E. Katz and J. Huang, *Annual Review of Materials Research*, 2009, **39**, 71-92.
92. M. Mas-Torrent and C. Rovira, *Chemical Society Reviews*, 2008, **37**, 827-838.
93. M. D. Iosip, S. Destri, M. Pasini, W. Porzio, K. P. Pernstich and B. Batlogg, *Synthetic Metals*, 2004, **146**, 251-257.
94. S. Sepeai, M. M. Salleh, M. Yahaya and A. A. Umar, *Thin Solid Films*, 2009, **517**, 4679-4683.
95. Y. Shirota and H. Kageyama, *Chemical Reviews*, 2007, **107**, 953-1010.
96. P. R. Wilson, *Solid-State Electronics*, 1969, **12**, 539-547.
97. K. W. Teng and S. S. Li, *Solid-State Electronics*, 1985, **28**, 277-285.
98. H. Spreitzer, H. Becker, E. Kluge, W. Kreuder, H. Schenk, R. Demandt and H. Schoo, *Advanced Materials*, 1998, **10**, 1340-1343.
99. H. Zhou, L. Yang and W. You, *Macromolecules*, 2012, **45**, 607-632.
100. C. Pozo-Gonzalo, R. Berridge, P. J. Skabara, E. Cerrada, M. Laguna, S. J. Coles and M. B. Hursthouse, *Chemical Communications*, 2002, 2408-2409.
101. W. J. Potscavage, A. Sharma and B. Kippelen, *Accounts of Chemical Research*, 2009, **42**, 1758-1767.
102. Y.-J. Cheng, S.-H. Yang and C.-S. Hsu, *Chemical Reviews*, 2009, **109**, 5868-5923.
103. M. Grätzel, *Accounts of Chemical Research*, 2009, **42**, 1788-1798.
104. S. Günes, H. Neugebauer and N. S. Sariciftci, *Chemical Reviews*, 2007, **107**, 1324-1338.
105. F. He, W. Wang, W. Chen, T. Xu, S. B. Darling, J. Strzalka, Y. Liu and L. Yu, *Journal of the American Chemical Society*, 2011, **133**, 3284-3287.
106. B. Sun, Y. Hao, F. Guo, Y. Cao, Y. Zhang, Y. Li and D. Xu, *The Journal of Physical Chemistry C*, 2011, **116**, 1395-1400.
107. A. Facchetti, *Chemistry of Materials*, 2010, **23**, 733-758.
108. G. S. a. G. Kossmehl, *Springer*, 1997.
109. G. Tourillon, Skotheim, T. A and edited by Marcel Dekker 1986, **1**, 293.
110. M. R. Andersson, O. Thomas, W. Mammo, M. Svensson, M. Theander and O. Inganas, *Journal of Materials Chemistry*, 1999, **9**, 1933-1940.
111. T.-A. Chen and R. D. Rieke, *Synthetic Metals*, 1993, **60**, 175-177.
112. I. Osaka and R. D. McCullough, *Accounts of Chemical Research*, 2008, **41**, 1202-1214.
113. S. Tanaka and Y. Yamashita, *Synthetic Metals*, 1993, **55**, 1251-1254.
114. C. A. Ramsden, *Tetrahedron*, 1977, **33**, 3193-3202.
115. M. Tachibana, S. Tanaka, Y. Yamashita and K. Yoshizawa, *The Journal of Physical Chemistry B*, 2002, **106**, 3549-3556.
116. Y. Yamashita, K. Ono, M. Tomura and S. Tanaka, *Tetrahedron*, 1997, **53**, 10169-10178.
117. M. Karikomi, C. Kitamura, S. Tanaka and Y. Yamashita, *Journal of the American Chemical Society*, 1995, **117**, 6791-6792.
118. T. T. Steckler, K. A. Abboud, M. Craps, A. G. Rinzler and J. R. Reynolds, *Chemical Communications*, 2007, 4904-4906.

119. T. Kono, D. Kumaki, J.-i. Nishida, S. Tokito and Y. Yamashita, *Chemical Communications*, 2010, **46**, 3265-3267.
120. S. Tanaka and Y. Yamashita, *Synthetic Metals*, 1995, **69**, 599-600.
121. J. Roncali, P. Blanchard and P. Frere, *Journal of Materials Chemistry*, 2005, **15**, 1589-1610.
122. R. A. Carboni, J. C. Kauer, J. E. Castle and H. E. Simmons, *Journal of the American Chemical Society*, 1967, **89**, 2618-2625.
123. R. A. Carboni, J. C. Kauer, W. R. Hatchard and R. J. Harder, *Journal of the American Chemical Society*, 1967, **89**, 2626-2633.
124. J. C. Forgie, P. J. Skabara, I. Stibor, F. Vilela and Z. Vobecka, *Chemistry of Materials*, 2009, **21**, 1784-1786.
125. P. M. Beaujuge, S. Ellinger and J. R. Reynolds, *Advanced Materials*, 2008, **20**, 2772-2776.
126. Z. Li, Y. Zhang, A. L. Holt, B. P. Kolasa, J. G. Wehner, A. Hampp, G. C. Bazan, T.-Q. Nguyen and D. E. Morse, *New Journal of Chemistry*, 2011, **35**, 1327-1334.
127. E. N. Esmer, S. Tarkuc, Y. A. Udum and L. Toppare, *Materials Chemistry and Physics*, 2011, **131**, 519-524.
128. D. Baran, G. Oktem, S. Celebi and L. Toppare, *Macromolecular Chemistry and Physics*, 2011, **212**, 799-805.
129. A. A. El-Shehawy, N. I. Abdo, A. A. El-Barbary and J.-S. Lee, *European Journal of Organic Chemistry*, 2011, **2011**, 4841-4852.
130. S. Tarkuc, E. K. Unver, Y. A. Udum and L. Toppare, *European Polymer Journal*, 2010, **46**, 2199-2205.
131. B. Aydogan, G. E. Gunbas, A. Durmus, L. Toppare and Y. Yagci, *Macromolecules*, 2009, **43**, 101-106.
132. A. Durmus, G. E. Gunbas and L. Toppare, *Chemistry of Materials*, 2007, **19**, 6247-6251.
133. P. J. Skabara, R. Berridge, I. M. Serebryakov, A. L. Kanibolotsky, L. Kanibolotskaya, S. Gordeyev, I. F. Perepichka, N. S. Sariciftci and C. Winder, *Journal of Materials Chemistry*, 2007, **17**, 1055-1062.
134. J.-C. Li, S.-J. Kim, S.-H. Lee, Y.-S. Lee, K. Zong and S.-C. Yu, *Macromolecular Research*, 2009, **17**, 356-360.
135. M. Sendur, A. Balan, D. Baran, B. Karabay and L. Toppare, *Organic Electronics*, 2010, **11**, 1877-1885.
136. Y. Zhang, L. Gao, C. He, Q. Sun and Y. Li, *Polymer Chemistry*, 2013.
137. E. Poverenov, M. Li, A. Bitler and M. Bendikov, *Chemistry of Materials*, 2010, **22**, 4019-4025.
138. J. L. Segura, R. Gómez, E. Reinold and P. Bäuerle, *Organic Letters*, 2005, **7**, 2345-2348.
139. H. C. Ko, M. Kang, B. Moon and H. Lee, *Advanced Materials*, 2004, **16**, 1712-1716.
140. J. C. Sharp Norton, M. G. Han, P. Jiang, G. H. Shim, Y. Ying, S. Creager and S. H. Foulger, *Chemistry of Materials*, 2006, **18**, 4570-4575.
141. X. Liu, K. G. Neoh and E. T. Kang, *Langmuir*, 2002, **18**, 9041-9047.
142. K. Araki, H. Endo, G. Masuda and T. Ogawa, *Chemistry – A European Journal*, 2004, **10**, 3331-3340.
143. A. Abbotto, E. H. Calderon, M. S. Dangate, F. De Angelis, N. Manfredi, C. M. Mari, C. Marinzi, E. Mosconi, M. Muccini, R. Ruffo and M. Seri, *Macromolecules*, 2010, **43**, 9698-9713.
144. C. J. DuBois, K. A. Abboud and J. R. Reynolds, *The Journal of Physical Chemistry B*, 2004, **108**, 8550-8557.
145. F. Algı and A. Cihaner, *Organic Electronics*, 2009, **10**, 453-458.

146. A. L. Kanibolotsky, I. F. Perepichka and P. J. Skabara, *Chemical Society Reviews*, 2010, **39**, 2695-2728.
147. T. Beyerlein and B. Tieke, *Macromolecular Rapid Communications*, 2000, **21**, 182-189.
148. L. Huo, J. Hou, H.-Y. Chen, S. Zhang, Y. Jiang, T. L. Chen and Y. Yang, *Macromolecules*, 2009, **42**, 6564-6571.
149. A. B. Tamayo, X.-D. Dang, B. Walker, J. Seo, T. Kent and T.-Q. Nguyen, *Applied Physics Letters*, 2009, **94**, 103301-103303.
150. B. Walker, A. B. Tamayo, X.-D. Dang, P. Zalar, J. H. Seo, A. Garcia, M. Tantiwiwat and T.-Q. Nguyen, *Advanced Functional Materials*, 2009, **19**, 3063-3069.
151. Y. Zou, D. Gendron, R. Neagu-Plesu and M. Leclerc, *Macromolecules*, 2009, **42**, 6361-6365.
152. G.-Y. Chen, C.-M. Chiang, D. Kekuda, S.-C. Lan, C.-W. Chu and K.-H. Wei, *Journal of Polymer Science Part A: Polymer Chemistry*, 2010, **48**, 1669-1675.
153. C. Kanimozhi, P. Balraju, G. D. Sharma and S. Patil, *The Journal of Physical Chemistry B*, 2010, **114**, 3095-3103.
154. S. Qu, W. Wu, J. Hua, C. Kong, Y. Long and H. Tian, *The Journal of Physical Chemistry C*, 2009, **114**, 1343-1349.
155. P. Sonar, G.-M. Ng, T. T. Lin, A. Dodabalapur and Z.-K. Chen, *Journal of Materials Chemistry*, 2010, **20**, 3626-3636.
156. J.-H. Tsai, C.-C. Chueh, W.-C. Chen, C.-Y. Yu, G.-W. Hwang, C. Ting, E.-C. Chen and H.-F. Meng, *Journal of Polymer Science Part A: Polymer Chemistry*, 2010, **48**, 2351-2360.
157. J.-H. Tsai, W.-Y. Lee, W.-C. Chen, C.-Y. Yu, G.-W. Hwang and C. Ting, *Chemistry of Materials*, 2010, **22**, 3290-3299.
158. E. Zhou, Q. Wei, S. Yamakawa, Y. Zhang, K. Tajima, C. Yang and K. Hashimoto, *Macromolecules*, 2009, **43**, 821-826.
159. A. P. Zoombelt, S. G. J. Mathijssen, M. G. R. Turbiez, M. M. Wienk and R. A. J. Janssen, *Journal of Materials Chemistry*, 2010, **20**, 2240-2246.
160. G. Zhang, K. Liu, H. Fan, Y. Li, X. Zhan, Y. Li and M. Yang, *Synthetic Metals*, 2009, **159**, 1991-1995.
161. T. Beyerlein, B. Tieke, S. Forero-Lenger and W. Brütting, *Synthetic Metals*, 2002, **130**, 115-119.
162. D. Cao, Q. Liu, W. Zeng, S. Han, J. Peng and S. Liu, *Journal of Polymer Science Part A: Polymer Chemistry*, 2006, **44**, 2395-2405.
163. A. R. Rabindranath, Y. Zhu, I. Heim and B. Tieke, *Macromolecules*, 2006, **39**, 8250-8256.
164. Y. Zhu, A. R. Rabindranath, T. Beyerlein and B. Tieke, *Macromolecules*, 2007, **40**, 6981-6989.
165. K. Zhang and B. Tieke, *Macromolecules*, 2008, **41**, 7287-7295.
166. A. R. Rabindranath, Y. Zhu, K. Zhang and B. Tieke, *Polymer*, 2009, **50**, 1637-1644.
167. A. K. Palai, S. P. Mishra, A. Kumar, R. Srivastava, M. N. Kamalasanan and M. Patri, *Macromolecular Chemistry and Physics*, 2010, **211**, 1043-1053.
168. K. Zhang, B. Tieke, J. C. Forgie, F. Vilela, J. A. Parkinson and P. J. Skabara, *Polymer*, 2010, **51**, 6107-6114.
169. R. Anemian, J.-C. Mulatier, C. Andraud, O. Stephan and J.-C. Vial, *Chemical Communications*, 2002, 1608-1609.
170. H. Langhals, T. Grundei, T. Potrawa and K. Polborn, *Liebigs Annalen*, 1996, **1996**, 679-682.

171. F. J. M. Hoeben, M. Wolffs, J. Zhang, S. De Feyter, P. Leclère, A. P. H. J. Schenning and E. W. Meijer, *Journal of the American Chemical Society*, 2007, **129**, 9819-9828.
172. Ž. Tomović, J. van Dongen, S. J. George, H. Xu, W. Pisula, P. Leclère, M. M. J. Smulders, S. De Feyter, E. W. Meijer and A. P. H. J. Schenning, *Journal of the American Chemical Society*, 2007, **129**, 16190-16196.
173. V. J. P. Srivatsavoy, M. Eschle, J. E. Moser and M. Gratzel, *Journal of the Chemical Society, Chemical Communications*, 1995, 303-304.
174. K. Liu, Y. Li and M. Yang, *Journal of Applied Polymer Science*, 2009, **111**, 1976-1984.
175. P. Herguth, X. Jiang, M. S. Liu and A. K. Y. Jen, *Macromolecules*, 2002, **35**, 6094-6100.
176. D. Kabra, L. P. Lu, M. H. Song, H. J. Snaith and R. H. Friend, *Advanced Materials*, 2010, **22**, 3194-3198.
177. J. Chen and Y. Cao, *Accounts of Chemical Research*, 2009, **42**, 1709-1718.
178. M. Wang, X. Hu, P. Liu, W. Li, X. Gong, F. Huang and Y. Cao, *Journal of the American Chemical Society*, 2011, **133**, 9638-9641.
179. X. Zhan and D. Zhu, *Polymer Chemistry*, 2010, **1**, 409-419.
180. K.-H. Ong, S.-L. Lim, H.-S. Tan, H.-K. Wong, J. Li, Z. Ma, L. C. H. Moh, S.-H. Lim, J. C. de Mello and Z.-K. Chen, *Advanced Materials*, 2011, **23**, 1409-1413.
181. L. Huo, J. Hou, S. Zhang, H.-Y. Chen and Y. Yang, *Angewandte Chemie International Edition*, 2010, **49**, 1500-1503.
182. F. G. Brunetti, R. Kumar and F. Wudl, *Journal of Materials Chemistry*, 2010, **20**, 2934-2948.
183. H. Zhou, L. Yang, A. C. Stuart, S. C. Price, S. Liu and W. You, *Angewandte Chemie International Edition*, 2011, **50**, 2995-2998.
184. D. H. Lee, M. J. Lee, H. M. Song, B. J. Song, K. D. Seo, M. Pastore, C. Anselmi, S. Fantacci, F. De Angelis, M. K. Nazeeruddin, M. Gräetzel and H. K. Kim, *Dyes and Pigments*, 2011, **91**, 192-198.
185. M. Tange, T. Okazaki and S. Iijima, *Journal of the American Chemical Society*, 2011, **133**, 11908-11911.
186. S. H. Park, A. Roy, S. Beaupre, S. Cho, N. Coates, J. S. Moon, D. Moses, M. Leclerc, K. Lee and A. J. Heeger, *Nat Photon*, 2009, **3**, 297-302.
187. J. Hou, H.-Y. Chen, S. Zhang, G. Li and Y. Yang, *Journal of the American Chemical Society*, 2008, **130**, 16144-16145.
188. K. R. J. Thomas, T.-H. Huang, J. T. Lin, S.-C. Pu, Y.-M. Cheng, C.-C. Hsieh and C. P. Tai, *Chemistry – A European Journal*, 2008, **14**, 11231-11241.
189. J.-L. Wang, Z.-M. Tang, Q. Xiao, Y. Ma and J. Pei, *Organic Letters*, 2008, **10**, 4271-4274.
190. S. W. Thomas, G. D. Joly and T. M. Swager, *Chemical Reviews*, 2007, **107**, 1339-1386.
191. A. Rose, Z. Zhu, C. F. Madigan, T. M. Swager and V. Bulovic, *Nature*, 2005, **434**, 876-879.
192. Y. Yang, G. A. Turnbull and I. D. W. Samuel, *Advanced Functional Materials*, 2010, **20**, 2093-2097.
193. Y. Zhang and P. W. M. Blom, *Applied Physics Letters*, 2011, **98**, 143504-143503.
194. J. Zaumseil, R. H. Friend and H. Sirringhaus, *Nat Mater*, 2006, **5**, 69-74.
195. E. J. Feldmeier and C. Melzer, *Organic Electronics*, 2011, **12**, 1166-1169.
196. C. L. Donley, J. Zaumseil, J. W. Andreasen, M. M. Nielsen, H. Sirringhaus, R. H. Friend and J.-S. Kim, *Journal of the American Chemical Society*, 2005, **127**, 12890-12899.

197. J. M. Winfield, A. Van Vooren, M.-J. Park, D.-H. Hwang, J. Cornil, J.-S. Kim and R. H. Friend, *The Journal of Chemical Physics*, 2009, **131**, 035104-035105.
198. K. G. Jespersen, W. J. D. Beenken, Y. Zaushitsyn, A. Yartsev, M. Andersson, T. Pullerits and V. Sundstrom, *The Journal of Chemical Physics*, 2004, **121**, 12613-12617.
199. R. B. A. L. Kanibolotsky, P. J. Skabara, I. F. Perepichka, D. D. C. Bradley, and M. Koeberg, *J. Am. Chem.Soc*, 2004, **126**, 13695.
200. A. L. K. K. M. Omar, R. Berridge, P. J. Skabara, I. F. Perepichka, and A. J. Brad, *J. Phys. Chem*, 2007, **111**, 6612.
201. E. Menard, M. A. Meitl, Y. Sun, J.-U. Park, D. J.-L. Shir, Y.-S. Nam, S. Jeon and J. A. Rogers, *Chemical Reviews*, 2007, **107**, 1117-1160.
202. E. Tekin, P. J. Smith and U. S. Schubert, *Soft Matter*, 2008, **4**, 703-713.
203. J.-H. Huang, Z.-Y. Ho, T.-H. Kuo, D. Kekuda, C.-W. Chu and K.-C. Ho, *Journal of Materials Chemistry*, 2009, **19**, 4077-4080.
204. L. Duan, L. Hou, T.-W. Lee, J. Qiao, D. Zhang, G. Dong, L. Wang and Y. Qiu, *Journal of Materials Chemistry*, 2010, **20**, 6392-6407.
205. A. A. Zakhidov, J.-K. Lee, H. H. Fong, J. A. DeFranco, M. Chatzichristidi, P. G. Taylor, C. K. Ober and G. G. Malliaras, *Advanced Materials*, 2008, **20**, 3481-3484.
206. J.-K. Lee, M. Chatzichristidi, A. A. Zakhidov, P. G. Taylor, J. A. DeFranco, H. S. Hwang, H. H. Fong, A. B. Holmes, G. G. Malliaras and C. K. Ober, *Journal of the American Chemical Society*, 2008, **130**, 11564-11565.
207. F. Estrany, D. Aradilla, R. Oliver and C. Alemán, *European Polymer Journal*, 2007, **43**, 1876-1882.
208. F. Estrany, D. Aradilla, R. Oliver, E. Armelin and C. Alemán, *European Polymer Journal*, 2008, **44**, 1323-1330.
209. D. Aradilla, F. Estrany and C. Alemán, *The Journal of Physical Chemistry C*, 2011, **115**, 8430-8438.
210. B. M. W. L.-V. F. Goldoni, E. W. Meijer, *Synth. Commun*, 1998, **28**, 2237.
211. S. Garreau, G. Louarn, J. P. Buisson, G. Froyer and S. Lefrant, *Macromolecules*, 1999, **32**, 6807-6812.
212. F. Tran-Van, S. Garreau, G. Louarn, G. Froyer and C. Chevrot, *Journal of Materials Chemistry*, 2001, **11**, 1378-1382.
213. S. Garreau, G. Louarn, G. Froyer, M. Lapkowski and O. Chauvet, *Electrochimica Acta*, 2001, **46**, 1207-1214.
214. M. Kalbáč, L. Kavan and L. Dunsch, *Synthetic Metals*, 2009, **159**, 2245-2248.
215. N. Kocharova, J. Lukkari, A. Viinikanoja, T. Ääritalo and J. Kankare, *The Journal of Physical Chemistry B*, 2002, **106**, 10973-10981.
216. N. J. Everall, *Analyst*, 2010, **135**, 2512-2522.
217. A. L. Kanibolotsky, F. Vilela, J. C. Forgie, S. E. T. Elmasly, P. J. Skabara, K. Zhang, B. Tieke, J. McGurk, C. R. Belton, P. N. Stavrinou and D. D. C. Bradley, *Advanced Materials*, 2011, **23**, 2093-2097.

7. Publications

1- Synthesis and electropolymerisation of a new hetropentalene mesomeric betaine: preparation of a novel low band gap conjugated polymer.
Saadeldin Elmasly, A. Gehre, P.J. Skabara, S.P. Stanforth and F. Vilela,. Tetrahedron Letters, Volume 52, Issue 4, 26 January 2011, Pages 526-529.

2- Well-defined and monodisperse linear and star-shaped quaterfluorene-DPP molecules: the significance of conjugation and dimensionality.
Alexander L. Kanibolotsky, Filipe Vilela, John C. Forgie, Saadeldin E. T. Elmasly, Peter J. Skabara,Kai Zhang , Bernd Tieke, John McGurk, Colin R. Belton, Paul N. Stavrinou, and D. D. C. Bradley. Advanced. Material journal. 2011, 23, 2093–2097.

3- Incorporation of fused tetrathiafulvalene units in a DPP–terthiophene copolymer for air stable solution processable organic field effect transistors
Diego Cortizo-Lacalle, Sasikumar Arumugam, Saadeldin E T Elmasly, Alexander L Kanibolotsky, Neil J Findlay, Anto Regis Inigo and Peter J Skabara. Journal of Material Chemistry, 2012,**22**, 11310-11315.

4- Electrochromic properties of a poly(dithienylfuran) derivative featuring a redox-active dithiin unit.
Kaur Sandeep, Neil Findlay, Alexander L Kanibolotsky, Saadeldin E T Elmasly, Peter J Skabara and R. Berridge, C. Wilson and S. Coles. Journal: Polymer Chemistry, VOL 3 , PAGES 2277-2286, 2012.

5- Location, Location, Location- Strategic Positioning of 2,1,3-benzothiadiazole Units within Trigonal Quaterfl uorene-Truxene Star-Shaped Structures. Colin R. Belton , Alexander L. Kanibolotsky, James Kirkpatrick, Clara Orofino, Saadeldin E. T. Elmasly, Paul N. Stavrinou, Peter J. Skabara, and Donal D. C. Bradley. Advanced functional materials. 2013, DOI: 10.1002/adfm.201202644.

6- Linear oligofluorene-BODIPY structures for fluorescence applications. Neil J. Findlay, Clara Orofino-Peña, Jochen Bruckbauer, Saadeldin E. T. Elmasly, Sasikumar Arumugam, Anto R. Inigo, Alexander L. Kanibolotsky, Robert W. Martin and Peter J. Skabara. J. Mater. Chem. C, 2013,1, 2249-2256. DOI: 10.1039/C3TC00706E.